THE UNIVERSITY OF CHICAGO

REACTIVITY OF METAL ALKYL COMPLEXES WITH CARBON DIOXIDE

A DISSERTATION SUBMITTED TO

THE FACULTY OF THE DIVISION OF THE PHYSICAL SCIENCES

IN CANDIDACY FOR THE DEGREE OF

DOCTOR OF PHILOSOPHY

DEPARTMENT OF CHEMISTRY

BY

KA CHEONG LAU

CHICAGO, ILLINOIS

MARCH 2016

TABLE OF CONTENTS

LIST OF TABLES

CHAPTER TWO

CHAPTER THREE

LIST OF FIGURES

CHAPTER TWO

CHAPTER THREE

LIST OF SCHEMES

CHAPTER THREE

ACKNOWLEDGEMENTS

First, I thank my advisor, Professor Richard Jordan, for his invaluable guidance and instruction throughout my graduate studies. It has been a privilege to learn from his example of both scientific rigor and professionalism. I also thank the other members of my thesis committee, Professor Michael Hopkins and Professor John Anderson, for their helpful advice and discussions.

I have been fortunate to work with many talented and helpful people in the Jordan group. I am especially grateful to Dr. Zhongliang (Ernest) Shen for his training when I first joined the group, and to Dr. Youngmin Kim, Dr. Xiaoyuan (Joe) Zhou, Dr. Benjamin Petro, Dr. Ryan Zarkesh and Dr. Nathan Contrella for their assistance and insightful discussions. Other past and current group members have provided friendship and a great environment, and I thank Dr. Jia Wei, Dr. Ge (David) Feng, Qian Liu, Feng Zhai, Rebecca Black, Erik Reinhart, Alison Johnson, Shinji Wada, Dr. Meagan Evans, Dr. Mingfang Zheng, Dr. Biyun Su, Dr. Hiroshi Terao, Dr. Jacqueline Defoe, and Tabbetha Bohac.

I am grateful to my undergraduate research advisor, Professor Kin Shing Chan at the Chinese University of Hong Kong, for his support during college and beyond, and for providing an ideal opportunity to become involved in research.

The research described in this thesis has relied on many departmental facilities, and I thank Dr. Antoni Jurkiewicz and Dr. Chang-Jin Qin for their assistance with NMR spectroscopy and mass spectrometry, respectively, and Dr. Ian Steele and Dr. Alexander Filatov for their assistance with x-ray crystallography.

I am also grateful to Melinda Moore, Dr. Vera Dragisich, and Laura Baker for their assistance of administrative work.

Many good friends within and outside of the Chemistry Department have provided great memories, and I am grateful to have them throughout graduate school. I thank my family and especially my parents for a lifetime of support and encouragement.

Finally, I thank my wife, Siu Yin (Serena), for her love, support, and patience through the stress and uncertainty of graduate school.

ABSTRACT

This thesis describes the studies of reactions of CO_2 with olefin polymerization catalysts and analogous metal alkyl complexes. These metal alkyl complexes differ by the number of alkyl groups, charges and coordination sites and thus provide insights to how these factors affect the carboxylation of olefin polymerization catalysts.

Chapter One introduces the scope and mechanisms of the reactions of metal alkyl complexes with CO_2. These reactions can occur by a spectrum of mechanisms. Structure/reactivity relationships and mechanistic studies of these reactions are discussed.

Chapter Two describes structure/reactivity and DFT studies of the carboxylation reactions of $Cp_2ZrMe(ClC_6D_5)^+$ and (PO-^{i}Pr)PdMe (PO-^{i}Pr$^-$ = 2-P^{i}Pr$_2$-4-Me-$C_6H_3SO_3^-$) complexes, and their corresponding dimethyl complexes Cp_2ZrMe_2 and (PO-^{i}Pr)PdMe$_2^-$. CO_2 reacts with $Cp_2ZrMe(C_6D_5Cl)^+$ more than 10^4 faster than with Cp_2ZrMe_2, yielding monoacetate products in both cases. These reactions proceed by insertion mechanisms in which Zr---O interactions activate the CO_2, and the electrophilicity of the Zr center controls the reactivity. In contrast, CO_2 reacts readily with anionic [(PO-^{i}Pr)PdMe$_2$]$^-$ to yield [(PO-^{i}Pr)PdMe(OAc)]$^-$ but not with neutral (PO-^{i}Pr)PdMe(L) species. Carboxylation of [(PO-^{i}Pr)PdMe$_2$]$^-$ occurs by direct S_E2 attack of CO_2 at the Pd–Me$_{trans\text{-to-P}}$ group, and the nucleophilicity of the Pd–Me group controls the reactivity. However, the S_E2 process is accelerated by a Li^+---OCO interaction when Li^+ is present.

Chapter Three describes mechanistic studies of reactions of CO_2 with (PDI)FeMe, (PDI)Fe(Me)PMe$_3$ and [(PDI)FeMe][BPh$_4$]. Solvent effects and kinetic studies provide evidence that these reactions occur by an insertion mechanism involving CO_2 pre-coordination to the Fe

center regardless of charge state. CO_2 reacts with neutral (PDI)FeMe 5-fold faster than with cationic [(PDI)FeMe][BPh_4], suggesting that the nucleophilicity of Fe–Me group controls the reactivity.

PREFACE

Each chapter has an independent numbering system for compounds. A given compound may have a different number in different chapters. For each chapter, the relevant experimental information, references, and notes are provided at the end of the chapter.

Chapter One

Introduction

1.1. Use of CO_2 in Metal-Mediated and Metal-Catalyzed Carboxylation Reactions

CO_2 is an attractive green C1 chemical feedstock because it is non-toxic, cheap and readily available. However, the conversion of CO_2 to value-added chemicals has been a longstanding challenge, as CO_2 is thermodynamically stable and kinetically inert. To date, the industrial synthesis of chemicals using CO_2 has largely been stoichiometric, and limited to urea[1] and salicylic acid (Scheme 1.1).[2] In order to advance the use of CO_2 as C1 synthon, catalytic, scalable reactions with CO_2 need to be developed.

Scheme 1.1. Industrial syntheses of urea (top) and salicylic acid (bottom).

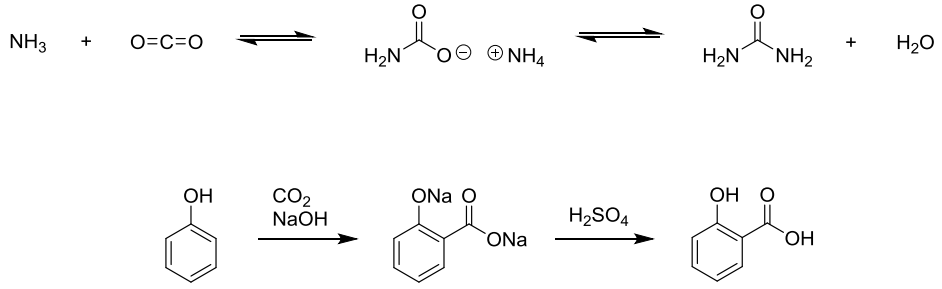

Over the past decades, numerous reports of metal-mediated and metal-catalyzed CO_2 functionalization have emerged. These have been extensively reviewed.[3] One of the major modes of reaction involves cyclometallation of CO_2 and olefins or alkynes to form 5-membered

metallocycles. The metallocycle can be ring-opened to release a carboxylate or carboxylic acid product. For example, Martin and co-workers have reported the Ni-mediated hydrocarboxylation of various aromatic alkynes (Scheme 1.2).[4] It was proposed that a Ni^0 species is generated in situ by the stoichiometric reduction of Ni^{2+} by Mn^0. The Ni^0 species then couples CO_2 and alkynes to form an α,β–unsaturated nickelalactone. The α,β–unsaturated nickelalactone is ring-opened by nucleophilic attack of alcohol at the Ni center. Transmetallation with Mn^{2+} and subsequent acidic workup give a α,β–unsaturated carboxylic acid as the product. The hydrocarboxylation reaction is stoichiometric in Mn and acid.

Scheme 1.2

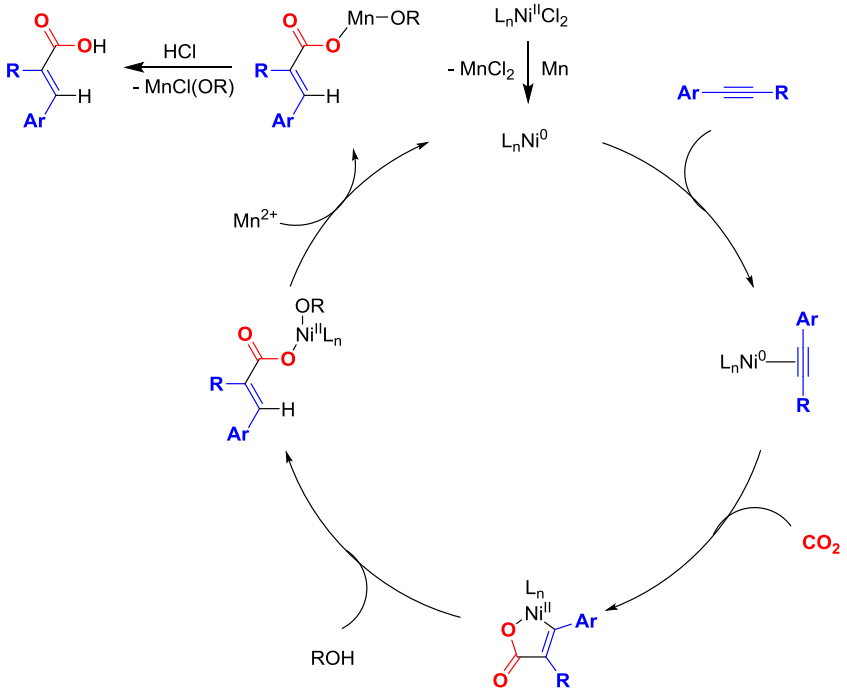

Despite the success of these reactions on the laboratory scale, most require unsaturated compounds with weak π-bonds for metal-mediated cyclization with CO_2. Additionally, the nickelalactone intermediates are usually very robust. Only a few nickelalactones were reported to ring-open and release the carboxylate species using stoichiometric reagents.[5] For example, nickelalactones have been reported to ring-open with stoichiometric amounts of MeI,[5b,c] MX salts[5g] and Lewis acids such as $B(C_6F_5)_3$,[5f] or bases such as NaO^tBu[5d] and phenoxides.[5h] The highest catalytic turnover number (>100) reported to date involving ring-opening of a nickelalactone uses 300 equivalents of Na[O–2–F–C_6H_4] as the base, which presumably abstracts the α–H to form sodium acrylate salt, and 100 equivalents of elemental zinc as the additive (role of Zn is unknown; Scheme 1.3).[5h] Catalytic turnover of nickelalactones to release Ni^0 and carboxylate species is still very challenging.

Another major mode of reaction involves the generation of M–X species and the subsequent addition of CO_2 across the M–X bond. A well-studied reaction of this class is the copolymerization of CO_2 with epoxides.[6] In this case, epoxides are ring-opened by initiators to generate M–OR species. CO_2 is then added across M–OR bond to afford a M–O_2COR carboxylate species, which ring-opens another epoxide molecule. These processes repeat to afford polycarbonate with alternating CO_2 and epoxide units (Scheme 1.4).

Scheme 1.3

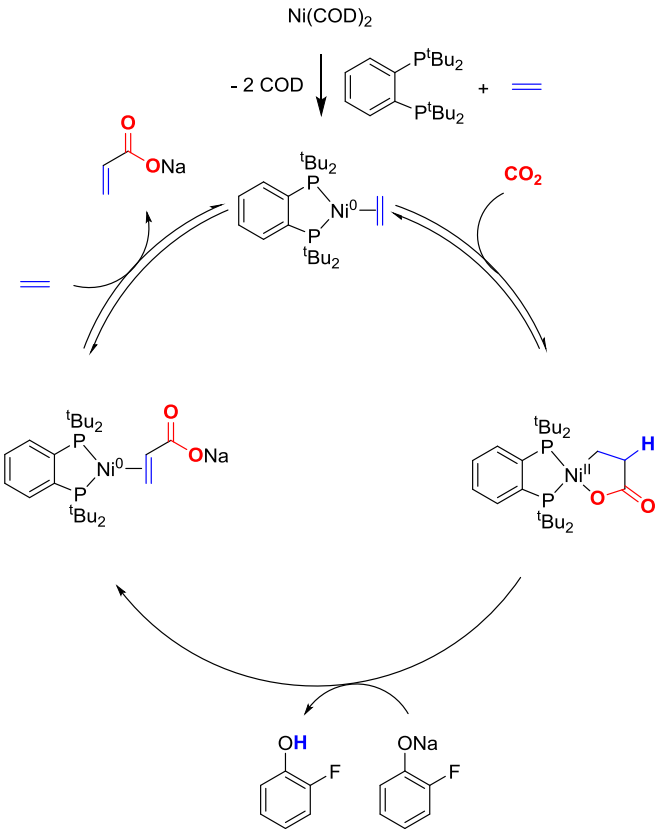

Scheme 1.4

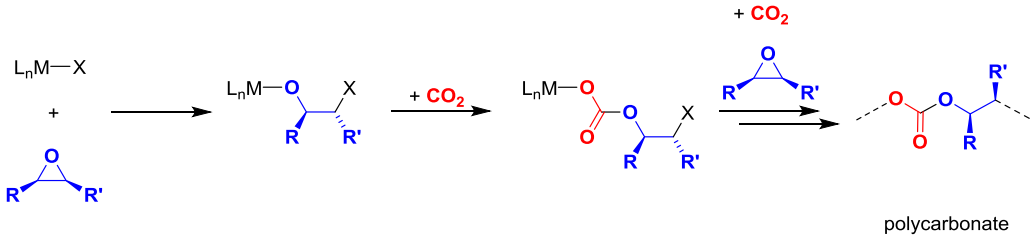

An example of catalytic coupling of CO_2 with olefins that follows this mode of reaction has been reported by Rovis and co-workers.[7] Substituted styrenes were hydrocarboxylated with

the sacrificial hydride donor Et_2Zn to form 2-methyl-2-arylacetic acid products. This conversion was catalytic in Ni using $Ni(acac)_2$ or $Ni(COD)_2$ as the catalyst precursor and stoichiometric in Et_2Zn. The reaction was proposed to proceed via the generation of a Ni^{II}–Et species (Scheme 1.5). β–H elimination forms a Ni^{II}–H species and styrene inserts into the Ni–H bond to form a Ni–benzyl species. CO_2 then inserts into the Ni–benzyl bond to afford a Ni carboxylate species. Transmetallation with Et_2Zn and subsequent β–H elimination yield the carboxylate product and regenerate the Ni^{II}–H species. Overall, the reaction consumes one equivalent each of Et_2Zn, CO_2 and styrene to yield the carboxylate product and ethylene as the by-product.

Scheme 1.5

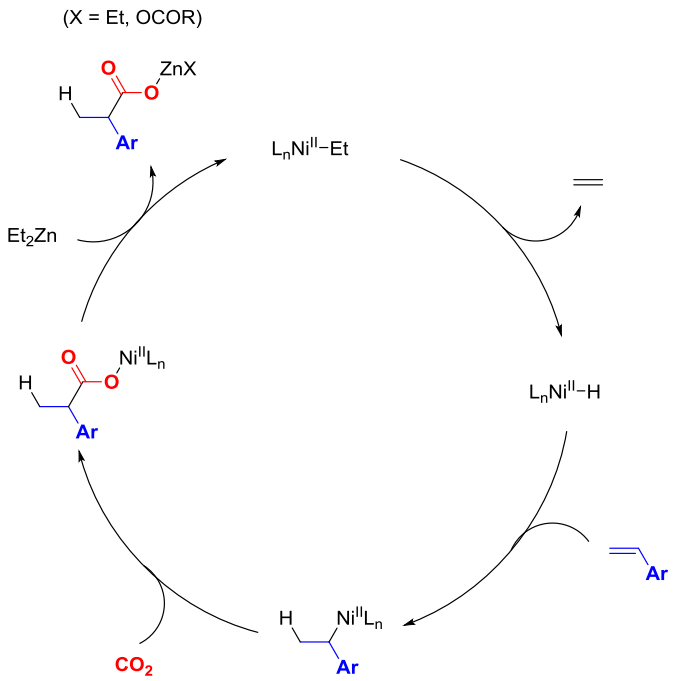

Similarly, catalytic coupling of CO_2 with 1,3–butadiene to afford the lactone 3-ethylidene-6-vinyltetrahydro-2*H*-pyran-2-one was discovered by Inoue and co-workers,[8] and then later optimized by Behr.[9] The reaction was proposed to go through cyclometallation of two butadiene molecules to form a Pd^{II}-bis(allyl) palladacycle. CO_2 insertion into a Pd–C_{allyl} bond occurred and subsequent reductive elimination afforded the lactone species. Recently, Nozaki and co-workers have coupled the conversion of CO_2 and 1,3–butadiene to the lactone with the radical polymerization of the lactone in one pot to give a polymer with approximately 33 mol% CO_2 incorporation (Scheme 1.6).[10]

Scheme 1.6

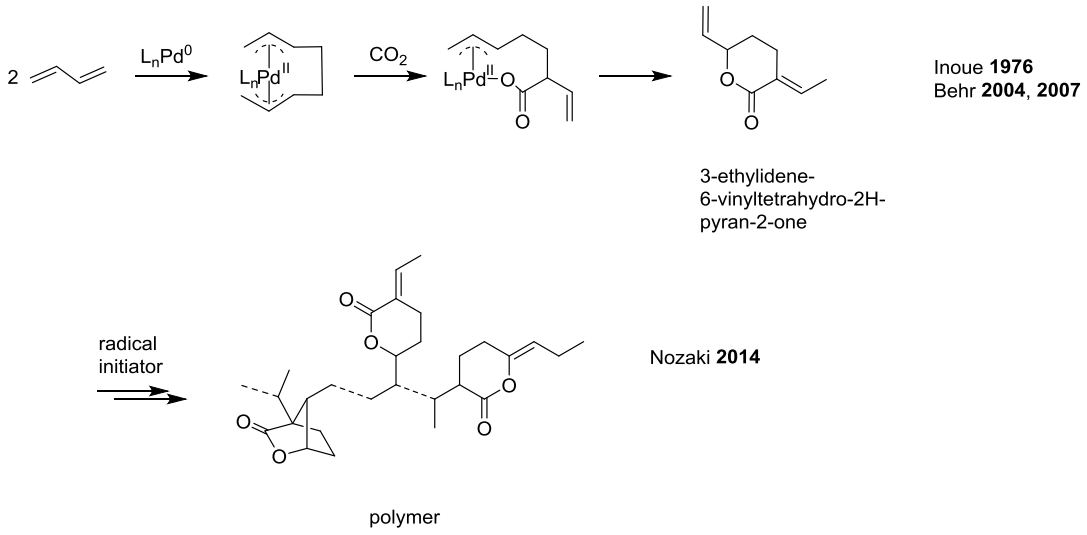

In Scheme 1.5 and Scheme 1.6, CO_2 is inserted into a M–H or M–C(allyl) bond. Developing new catalytic processes that involve CO_2 insertion into a M–C(alkyl) bond is interesting and potentially useful for synthesis of chemicals such as aliphatic polyester. In these

processes, the metal alkyl species can be readily generated from olefin insertion into M–H bond or M–R bond. In order to realize this long term goal, knowledge of the reactivity of CO_2 with metal–alkyl complexes is essential.

1.2. Scope and Mechanisms of Carboxylation of Metal Alkyl Complexes

The reaction of CO_2 with metal alkyl complexes to produce metal carboxylate species could potentially serve as a key step in the catalytic coupling of CO_2 with olefins. CO_2 insertion reactions of metal alkyls have been reported for metals such as Sc,[11a] Zr,[11b-c] Cr,[11d-f] W,[11d-g] Fe,[11h-j] Rh,[11k-l] Ni,[11m-p] and Pd systems.[11q-r] However, none of these reactions are of catalytic use, and only a few reports provide mechanistic insights into the carboxylation reaction. These insights may be useful for designing metal alkyl complexes for catalytic coupling of CO_2 with olefins. This section of the thesis will provide an overview of these studies.

Literature reports suggest that the carboxylation reaction of metal alkyl complexes can occur by a spectrum of mechanisms. The spectrum can be defined by two limiting cases: (i) migratory insertion, in which CO_2 first coordinates to metal center and CO_2 insertion proceeds via a four-membered, cyclic transition state (Scheme 1.7), resulting in *retention* of configuration at the alkyl carbon; and (ii) formal bimolecular electrophilic substitution (S_E2) in which CO_2 does not coordinate to the metal center but rather directly attacks the carbon atom of metal–carbon bond, resulting in *inversion* of configuration at the alkyl carbon. An $[M]^+[OCOR]^-$ ion pair is formed and recombines to afford metal carboxylate species (S_E2; Scheme 1.7).

Scheme 1.7

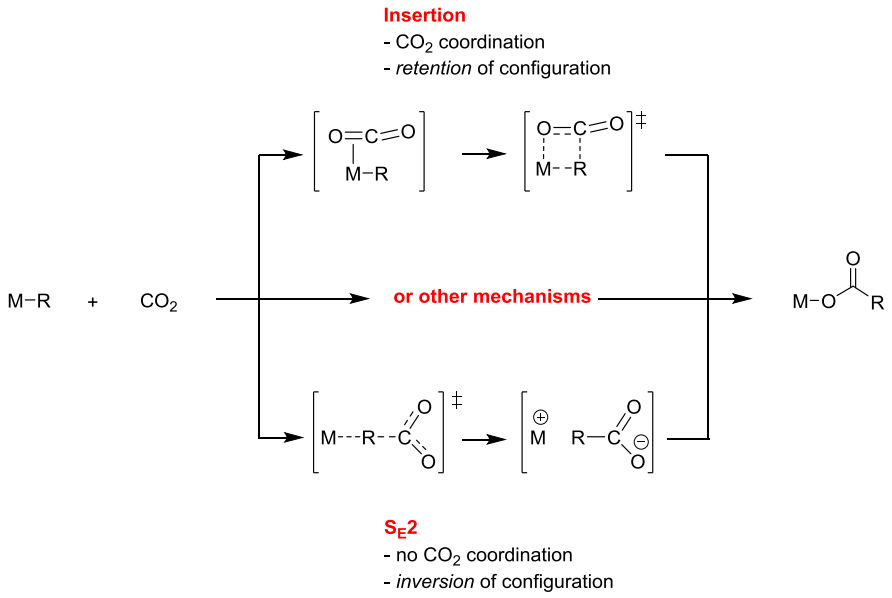

Several carboxylation reactions of metal alkyl complexes have been proposed to proceed via the insertion pathway. For example, [(nacnac)ScMe][MeB(C_6F_5)] (nacnac = κ^2–(2,6–^{i}Pr$_2$–C_6H_3)–N=C(^{t}Bu)HC(^{t}Bu)=N–(2,6–^{i}Pr$_2$–C_6H_3)) and (nacnac)ScMe$_2$ react with CO_2 to afford the corresponding mono- and di-acetate species (Scheme 1.8).[11a] Similarly, [Cp$_2$ZrMe][MeB(C_6F_5)$_3$] was found to react with CO_2 to afford a putative bridging acetate species, which was converted to the monomeric acetate complex Cp$_2$Zr(THF-d_8)OAc in the presence of THF-d_8 (Scheme 1.9).[11b] Insertion mechanisms were proposed for these cases based on the high oxophilicity of Sc^{III} and Zr^{IV}.

Scheme 1.8. Degradation pathways from products are omitted.

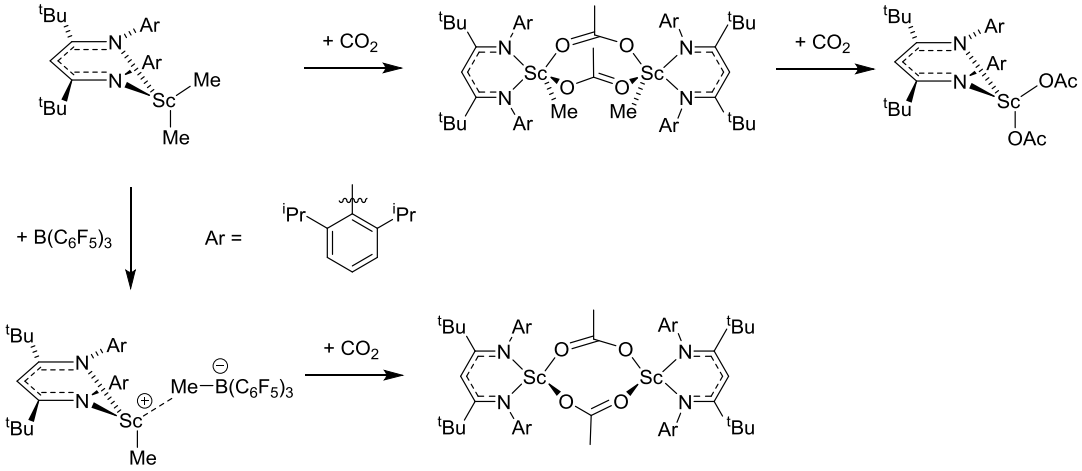

Scheme 1.9

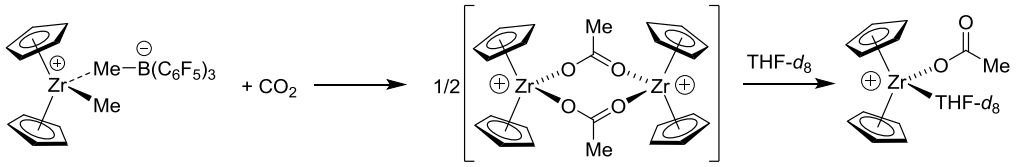

The carboxylation reactions of group 10 (^{tBu}PCP)MMe pincer complexes ([^{tBu}PCP]$^-$ = [2,6–(^{t}Bu$_2$PCH$_2$)$_2$–C$_6$H$_3$]$^-$; M = Pd, Ni) exhibit features of an S_E2 mechanism (Scheme 1.10; top reaction).[11n,q,r] While (^{tBu}PCP)PdMe reacts with CO_2 to form an acetate product, (^{Ph}PCP)PdMe ([^{Ph}PCP]$^-$ = [2,6–(Ph$_2$PCH$_2$)$_2$–C$_6$H$_3$]$^-$) does not. These results suggest that the increased electron-donation from the ^{tBu}PCP ligand compared to the ^{Ph}PCP ligand facilitates the carboxylation reaction. X-ray diffraction results showed that the Pd–Me bond in (^{tBu}PCP)PdMe, which is *trans* to the central carbon donor of the ^{tBu}PCP ligand, is exceptionally long (2.2 Å; Pd–Me bond in (TMEDA)PdMe$_2$: 2.0 Å).[12] The long bond length was attributed to strong *trans*-influence from

the central carbon donor of the ^{tBu}PCP ligand and is indicative of a highly labilized Pd–*Me* group.[11q] Finally, DFT calculations suggested that the reaction of (^{tBu}PCP)MMe with CO_2 proceeds via direct S_E2 attack of CO_2 at the back side of Pd-CH_3 alkyl carbon.[11n,r] These computational results, together with the ligand reactivity trend, long Pd–Me bond and kinetic results, are consistent with a S_E2 mechanism. This mechanism is expected to result in inversion of configuration at the α-carbon. However, this issue was not studied.

Scheme 1.10

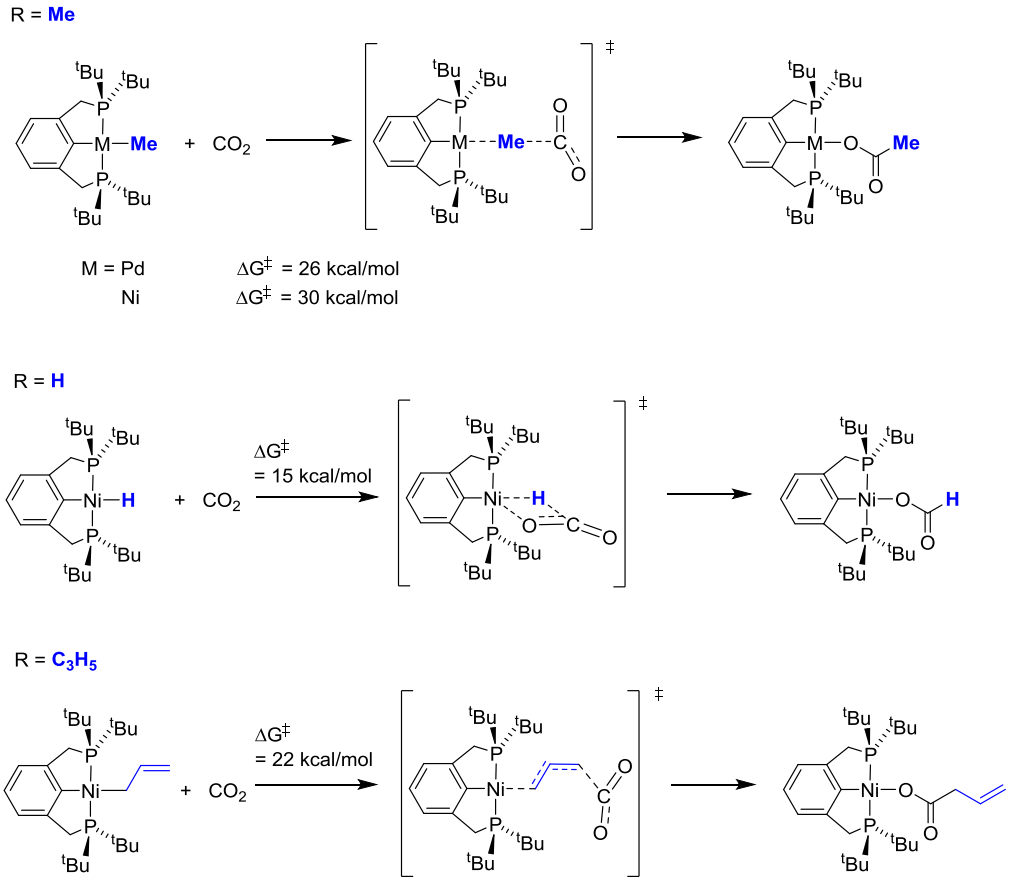

The reactions of the analogous (^{tBu}PCP)NiR (R = H, Me, C_3H_5) have also been studied experimentally and computationally (Scheme 1.10).[11n] These studies showed that the identity of the R group of (^{tBu}PCP)Ni–R had a significant impact on the mechanism and rate of the carboxylation reaction. For R = H, the reaction proceeded through a migratory insertion mechanism and the activation barrier was the lowest ($\Delta G^{\ddagger}$ = 15 kcal/mol). For R = Me and C_3H_5, the reaction proceeded by direct attack of CO_2 at a carbon atom without initial CO_2 coordination. For R = Me, the reaction proceeded by a S_E2 mechanism and the activation barrier was the highest ($\Delta G^{\ddagger}$ = 30 kcal/mol), while for R = C_3H_5, the reaction proceeded by an S_E2' mechanism involving remote CO_2 attack at the γ–carbon atom of the Ni–C_3H_5 group, and the activation barrier was intermediate among the three reactions ($\Delta G^{\ddagger}$ = 22 kcal/mol).

For group 6 *cis*-$M(CO)_4L(R)^-$ complexes (M = Cr, W; L = CO, $P(OMe)_3$, PMe_3; R = Me, Et, Ph), intermediate mechanisms for carboxylation were proposed by Darensbourg and co-workers.[11d-g] Stereochemical studies on the conversion of *threo*-$W(CO)_5CHDCHDPh^-$ to *threo*-$W(CO)_5O_2CCHDCHDPh^-$ and of the conversion of *threo-cis*-$W(CO)_4(PMe_3)CHDCHDPh^-$ to *threo-cis*-$W(CO)_4(PMe_3)O_2CCHDCHDPh^-$ established that the carboxylation reaction proceeded with retention of configuration at the α-carbon atom, consistent with a migratory insertion mechanism (Scheme 1.11).[11g] However, kinetic analyses for the conversion of $W(CO)_5Me^-$ to $W(CO)_5O_2CMe^-$ in the presence of CO showed that the carboxylation reaction does not require dissociation of CO to generate a vacant site. The activation parameters for the reaction ($\Delta H^{\ddagger}$ = +10 kcal/mol and $\Delta S^{\ddagger}$ = –43 e.u.) implied significant bond making and a high degree of organization in the transition state. These results and the 18-electron configuration of $W(CO)_5R^-$ led Darensbourg to propose that the carboxylation reactions proceed via a concerted I_a (associative interchange) process, which may also be categorized as an S_Ei (internal electrophilic

substitution) mechanism. In this mechanism, the carbon atom of CO_2 attacks metal alkyl carbon with the involvement of a M- - -OCO interaction, but a M(OCO) adduct is not formed prior to the transition state (Scheme 1.12). The M- - -OCO interaction forms as the M–R bond is cleaved and no vacant coordination site is required. However, there was no evidence to unambiguously differentiate S_Ei from S_E2 (front), which would also result in retention of configuration. [11f]

Scheme 1.11

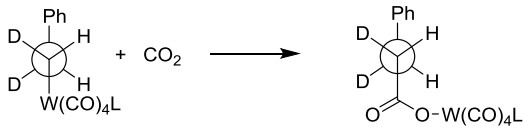

Scheme 1.12

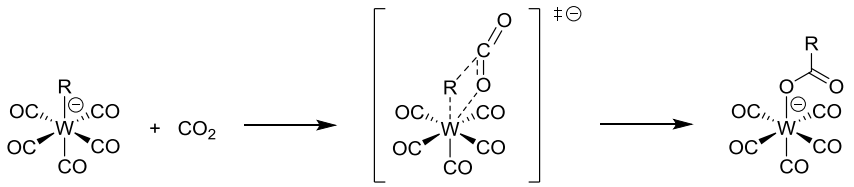

Reactivity studies have provided additional structure/reactivity relationships and mechanistic insights.[11d-f] The reaction in Scheme 1.12 was accelerated 6-fold with the coordinating counter-cation Na^+ compared with the non-coordinating counter-cation $(Ph_3P)_2N^+$ (PPN^+), presumably due to a stronger activation of CO_2 via a Na---OCO vs. W---OCO (if any) interaction. Comparison of the reactions of CO_2 with $Cr(CO)_5Me^-$ versus $W(CO)_5Me^-$ showed that the rate of carboxylation of $W(CO)_5Me^-$ is 6 times higher than that of $Cr(CO)_5Me^-$.

Darensbourg proposed that this difference is consistent with the I_a (S_Ei) mechanism, which involves significant simultaneous C–R and O–M bond formation, presumably because this process is expected to be favored for the larger radius of W versus Cr (covalent radii: W: 1.37 Å; Cr: 1.22 Å).[13] Increasing the electron density of *cis*-$W(CO)_4L(Me)^-$ species by using more electron-donating L ligands also enhanced the rate of carboxylation (k_{rel} for PMe_3: $P(OMe)_3$: CO = 243: 58: 1), suggesting that the nucleophilicity of W–Me group controls the reactivity of *cis*-$W(CO)_4L(Me)^-$ species with CO_2. The identity of the W-*R* group of $W(CO)_5R^-$ had a comparatively minor effect (k_{rel} for Me: Et: Ph = 6: 4: 1).

Leitner and co-workers reported a DFT study on the hypothetical carboxylation reactions of a series of $(L_1L_2L_3)Rh^IEt$ pincer complexes.[11l] The calculated transition state for the carboxylation revealed direct front-side CO_2 attack at the α–carbon of the Rh–Et group, resulting in *retention* of configuration (Scheme 1.13), which may be categorized as an S_E2 (front) process. Calculated ligand reactivity trends are consistent with an S_E2 (front) process. First, Rh^I pincer complexes with anionic ligands are predicted to be more reactive than complexes with neutral ligands. Second, the donor atom *trans* to the Et group is predicted to greatly influence the reactivity of the complex toward CO_2 in the order of $C^- \sim B^- > Si^- > N > C > O$, consistent with the trend of decreasing *trans*-influence on the Et group. Finally, higher basicities of donor atoms *cis* to Et group are also predicted to enhance the reactivity of the complex toward CO_2 ($\Delta G^{\ddagger}$: $N_{amine} < N_{guanidine} < N_{imine} < N_{oxazole} < N_{pyridine} < N_{pyrazole} < N_{triazole}$).

Scheme 1.13. (2-^{t}Bu$_2$P-CH$_2$CH$_2$)$_2$O is shown as an example of a $L_1L_2L_3$ pincer ligand

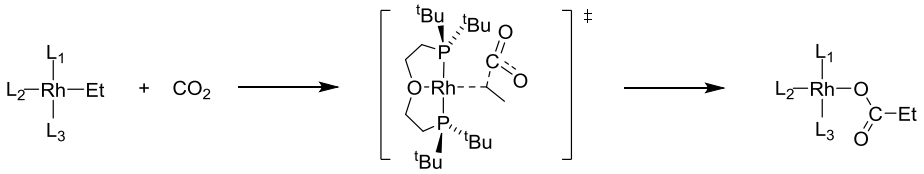

Goff and co-workers reported that (TPP)Fe^{III}–R complexes ([TPP]$^{2-}$ = *meso*-tetraphenylporphyrinato dianion; R = Et, Bu, CH$_2$^{t}Bu) react with CO and CO_2 to form (TPP)Fe^{III}–COR and (TPP)Fe^{III}–OCOR species respectively (Scheme 1.14).[11h] Some mechanistic insights for the carbonylation reaction were revealed but the carboxylation reaction was not studied in detail. In the carbonylation reaction, light was not required, (TPP)Fe^{II}(CO) was observed and an alkyl radical was trapped and observed by ESR. These results suggested that carbonylation proceeds by homolytic cleavage of the (TPP)Fe^{III}–R bond to form solvent-caged R· and (TPP)Fe^{II} radicals. Direct reaction of (TPP)Fe^{II} radical with CO forms (TTP)Fe^{II}(CO), and attack by R· on this species accounts for the formation of (TPP)Fe^{III}–COR. Goff did not elucidate how the carboxylation product was formed, but a similar mechanism may be operative. Given the numerous reports on radical polymerization in supercritical CO_2 that showed no CO_2 incorporation, mechanisms involving direct attack of R· on free CO_2 are highly unlikely.[14]

Scheme 1.14

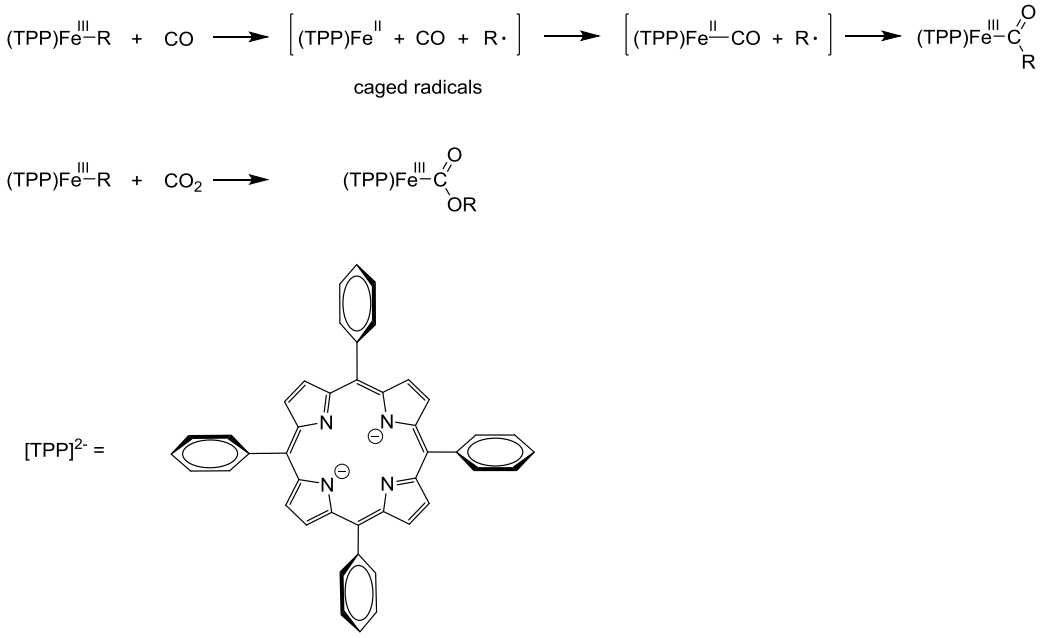

1.3. Thesis Objectives

Despite the reports of carboxylation reactions of several classes of metal alkyl complexes, none of those reactions have been incorporated into a catalytic CO_2 conversion reaction. Our group has a longstanding interest in olefin insertion and polymerization reactions. It is envisioned that incorporating carboxylation steps into olefin oligomerization or polymerization reactions might enable new methods of catalytic coupling of CO_2 with olefins. The objective of this thesis is to understand how olefin polymerization catalysts react with CO_2, which is a key first step toward this goal. This objective has been achieved through studies of reactions of CO_2 with (i) Cp_2ZrMe^+ and (PO)PdMe complexes ($[PO]^-$ = 2−PR_2−4−Me−$C_6H_3SO_3^-$; R = 3,5–$^tBu_2$–C_6H_3, ^{i}Pr), and their corresponding dimethyl complexes Cp_2ZrMe_2 and $(PO)PdMe_2^-$, and (ii)

(PDI)FeMe (PDI = 2,6−(2,6−$^{i}Pr_2$−C_6H_3−N=CMe)$_2$−C_5H_3N) and (PDI)$FeMe^+$, a pair of isocompositional and nearly isostructural complexes with different charge states.

Chapter Two describes structure/reactivity and DFT studies of the carboxylation reactions of $Cp_2ZrMe(ClC_6D_5)^+$ and (PO-^{i}Pr)PdMe ([PO-^{i}Pr]$^-$ = 2−P$^{i}Pr_2$−4−Me−$C_6H_3SO_3^-$) complexes, and their corresponding dimethyl complexes Cp_2ZrMe_2 and (PO-^{i}Pr)$PdMe_2^-$. CO_2 reacts with $Cp_2ZrMe(C_6D_5Cl)^+$ more than 10^4 faster than with Cp_2ZrMe_2, yielding monoacetate products in both cases. These reactions proceed by insertion mechanisms in which Zr---O interactions activate the CO_2, and the electrophilicity of the Zr center controls the reactivity. In contrast, CO_2 reacts readily with anionic [(PO-^{i}Pr)$PdMe_2$]$^-$ to yield [(PO-^{i}Pr)PdMe(OAc)]$^-$ but not with neutral (PO-^{i}Pr)PdMe(L) species. Carboxylation of [(PO-^{i}Pr)$PdMe_2$]$^-$ occurs by direct S_E2 attack of CO_2 at the Pd–Me$_{trans\text{-to-P}}$ group, and the nucleophilicity of the Pd–Me group controls the reactivity. However, the S_E2 process is accelerated by a Li^+---OCO interaction when Li^+ is present.

Chapter Three describes studies of reactions of CO_2 with (PDI)FeMe, (PDI)Fe(Me)PMe_3 and [(PDI)FeMe][BPh_4], which generate the corresponding mono-acetate products. Solvent effects and kinetic studies provide evidence that these reactions occur by an insertion mechanism involving pre-coordination of CO_2 to the Fe center regardless of the charge state. For (PDI)Fe(Me)PMe_3, the reaction occurs by initial dissociation of PMe_3 to generate base-free (PDI)FeMe, which reacts with CO_2 by an insertion mechanism to generate a monoacetate complex; (PDI)Fe(Me)PMe_3 does not react directly with CO_2. Interestingly, and in contrast to the trend observed for Cp_2ZrMe^+ and Cp_2ZrMe, CO_2 reacts with neutral (PDI)FeMe five times faster than with cationic [(PDI)FeMe][BPh_4], suggesting that the nucleophilicity of the Fe–Me group has a strong influence on the reactivity.

1.4. References and Notes

1. (a) The first report was by Bassarov and cited in reference 1b. (b) Clark, K. G.; Gaddy, V. L.; Rist, C. E. *Ind. Eng. Chem.* **1933**, *25*, 1092. (c) Fromm, D.; Lutzov, D. *Chem. Unserer Zeit*. **1979**, *13*, 78.

2. (a) Kolbe, H.; Lautemann, E. *Ann.* **1869**, *113*, 125. (b) Schmitt, R.; Burkard, E. *Ber.* **1877**, *20*, 2699.

3. (a) Darensbourg, D. J.; Kudaroski, R. *Adv. Organomet. Chem.* **1983**, *22*, 129. (b) Braunstein, P.; Matt, D.; Nobel, D. *Chem. Rev.* **1988**, *88*, 747. (c) Behr, A. *Angew. Chem. Int. Ed. Engl.* **1988**, *27*, 661. (d) Leitner, W. *Angew. Chem. Int. Ed. Engl.* **1995**, *34*, 2207. (e) Yin, H.; Moss, J. R. *Coord. Chem. Rev.* **1999**, *181*, 27. (f) Jessop, P. G.; Joó, F.; Tai, C.-C. *Coord. Chem. Rev.* **2004**, *248*, 2425. (g) Louie, J. *Curr. Org. Chem.* **2005**, *9*, 605. (h) Rayner, C. M. *Org. Process Res. Dev.* **2007**, *11*, 121. (i) Sakakura, T.; Choi, J.-C.; Yasuda, H. *Chem. Rev.* **2007**, *107*, 2365. (j) Aresta, M.; Dibenedetto, A. *Dalton Trans.* **2007**, 2975. (k) Correa, A.; Martin, R. *Angew, Chem. Int. Ed.* **2009**, *48*, 6201. (l) Sakakura, T.; Kohno, K. *Chem. Commun.* **2009**, 1312. (m) Mikkelsen, M., Jorgensen, M.; Krebs, F. C. *Energy Environ. Sci.* **2010**, *3*, 43. (n) Zhang, Y.; Riduan, S. N. *Angew. Chem. Int. Ed.* **2011**, *50*, 6210. (o) Martin, R.; Kleij, A. W. *ChemSusChem.* **2011**, *4*, 1259. (p) Huang, K.; Sun, C.-L.; Shi, Z.-J. *Chem. Soc. Rev.* **2011**, *40*, 2435. (q) Wang, W.; Wang, S.; Ma, X.; Gong, J. *Chem. Soc. Rev.* **2011**, *40*, 3703. (r) Fan, T.; Chen, X.; Lin, Z. *Chem. Commun.* **2012**, *48*, 10808. (s) Tsuji, Y.; Fujihara, T. *Chem. Commun.* **2012**, *48*, 9956. (t) Maeda, C.; Miyazaki, Y.; Ema, T. *Catal. Sci. Technol.* **2014**, *4*, 1482. (u) Liu, Q.; Wu, L.; Jackstell, R.; Beller, M. *Nat. Commun.* **2015**, *6*, 1.

4. Wang, X.; Nakajima, M.; Martin, R. *J. Am. Chem. Soc.* **2015**, *137*, 8924.

5. (a) Fischer, R.; Langer, J.; Malassa, G.; Walther, D.; Gorls, H.; Vaughan, G. *Chem. Commun.* **2006**, 2510. (b) Bruckmeier, C.; Lehenmeier, M. W.; Reichardt, R.; Vagin, S.; Rieger, B. *Organometallics* **2010**, *29*, 2199. (c) Lee, S. Y. T.; Cokoja, M.; Drees, M.; Li, Y.; Mink, J.; Herrmann, W. A.; Kuhn, F. E. *ChemSusChem* **2011**, *4*, 1275. (d) Lejkowski, M. L.; Lindner, R.; Kageyama, T.; Bodizs, G. E.; Plessow, P. N.; Muller, I. B.; Schafer, A.; Rominger, F.; Hofmann, P.; Futter, C.; Schunk, S. A.; Limbach, M. *Chem. Eur. J.* **2012**, *18*, 14017. (e) González-Sebastián, L.; Flores-Alamo, M.; García, J. J. *Organometallics* **2012**, *31*, 8200. (f) Jin, D.; Schmeier, T. J.; Williard, P. G.; Hazari, N.; Bernskoetter, W. H. *Organometallics* **2013**, *32*, 2152. (g) Hendriksen, C.; Pidko, E. A.; Yang, G.; Schäffner, B.; Vogt, D. *Chem. Eur. J.* **2014**, *20*, 12037. (h) Huguet, N.; Jevtovikj, I.; Gordillo, A.; Lejkowski, M. L.; Lindner, R.; Bru, M.; Khalimon, A.; Rominger, F.; Schunk, S. A.; Hofmann, P.; Limbach, M. *Chem. Eur. J.* **2014**, *20*, 16858.

6. (a) Inoue, S.; Koinuma, H.; Tsuruta, T. *J. Polym. Sci. Part B* **1969**, *7*, 287. (b) Inoue, S.; Koinuma, H.; Tsuruta, T. *Makromol. Chem.* **1969**, *130*, 210. (c) Coates, G. W.; Moore, D. R. *Angew. Chem. Int. Ed.* **2004**, *43*, 6618. (d) Darensbourg, D. J. *Chem. Rev.* **2007**, *107*, 2388.

7. Williams, C. M.; Johnson, J. B.; Rovis, T. *J. Am. Chem. Soc.* **2008**, *130*, 14936.

8. Sasaki, Y.; Inoue, Y.; Hashimoto, H. *J. Chem. Soc. Chem. Commun.* 1976, 605.

9. Behr, A.; Bahke, P.; Becker, M. *Chem. Ing. Tech.* **2004**, *76*, 1828. (b) Behr, A.; Bahke, P.; Klinger, B.; Becker, M. *J. Mol. Catal. A* **2007**, *267*, 149.

10. Nakano, R.; Ito, S.; Nozaki, K. *Nature Chem.* **2014**, *6*, 325.

11. (a) LeBlanc, F. A.; Berkefeld, A.; Piers, W. E.; Parvez, M. *Organometallics* **2012**, *31*, 810. (b) Hill, M.; Wendt, O. *Organometallics* **2005**, *24*, 5772. (c) Kloppenburg, L.; Petersen, J. L. *Organometallics* **1996**, *15*, 7. (d) Darensbourg, D. J.; Rokicki, A. *J. Am. Chem. Soc.* **1982**, *104*, 349. (e) Darensbourg, D. J.; Kudaroski, R. *J. Am. Chem. Soc.* **1984**, *106*, 3672. (f) Darensbourg, D. J.; Hanckel, R. K.; Bauch, C. G.; Pala, M.; Simmons, D.; White, J. N. *J. Am. Chem. Soc.* **1985**, *107*, 7463. (g) Darensbourg, D. J.; Grotsch, G. *J. Am. Chem. Soc.* **1985**, *107*, 7473. (h) Arafa, I. M.; Shin, K.; Goff, H. M. *J. Am. Chem. Soc.* **1988**, *110*, 5228. (i) Allen, O. R.; Dalgarno, S. J.; Field, L. D.; Jensen, P.; Turnbull, A. J.; Willis, A. C. *Organometallics* **2008**, *27*, 2092. (j) Roth, C. E.; Dibenedetto, A.; Aresta, M. *Eur. J. Inorg. Chem.* **2015**, *30*, 5066. (k) Darensbourg, D. J.; Groetsch, G.; Weigreffe, P.; Rheingold, A. L. *Inorg. Chem.* **1987**, *26*, 3827. (l) Ostapowicz, T. G.; Hölscher, M.; Leitner, W. *Chem. Eur. J.* **2011**, *17*, 10329. (m) Yamamoto, T.; Yamamoto, A. *Chem. Lett.* **1978**, 615. (n) Schmeier, T. J.; Hazari, N.; Incarvito, C. D.; Raskatov, J. A. *Chem. Commun.* **2011**, *47*, 1824. (o) Schmeier, T. J.; Nova, A.; Hazari, N.; Maseras, F. *Chem. Eur. J.* **2012**, *18*, 6915. (p) Jonasson, K. J.; Wendt, O. *Chem. Eur. J.* **2014**, *20*, 11894. (q) Johansson, R.; Jarenmark, M.; Wendt, O. F. *Organometallics* **2005**, *24,* 4500. (r) Johnson, M. T.; Johansson, R.; Kondrashov, M. V.; Steyl, G.; Ahlquist, M.H.G.; Roodt, A.; Wendt, O. F. *Organometallics* **2010**, *29*, 3521.

12. de Graaf, W.; Boersma, J.; Smeets, W. J. J.; Spek, A. J.; van Koten, G. *Organometallics* **1989**, *8*, 2907.

13. Pyykkö, P.; Atsumi, M. *Chem. Eur. J.* **2008**, *15*, 186.

14. (a) Kendall, J. L.; Canelas, D. A.; Young, J. L.; DeSimone, J. M. *Chem. Rev.* **1999**, *99*, 543. (b) Nishi, K.; Morikawa, Y.; Misumi, R.; Kaminoyama, M. *Chem. Eng. Sci.* **2005**, *60*, 2419. (c) Zetterlund, P. B.; Kagawa, Y.; Okubo, M. *Chem. Rev.* **2008**, *108*, 3747. (d) Oh, J. W. *J. Polym. Sci., Part A: Polym. Chem.* **2008**, *46*, 6983. (e) Thurecht, K. J.; Howdle, S. M. *Aust. J. Chem.* **2009**, 62, 786. (f) Zetterlund, P. B.; Thickett, S. C.; Perrier, S.; Bourgeat-Lami, E.; Lansalot, M. *Chem. Rev.* **2015**, *115*, 9745.

Chapter Two

Comparative Reactivity of Zr and Pd–Alkyl Complexes with Carbon Dioxide

2.1. Introduction

The reaction of metal alkyls with CO_2 to yield metal carboxylate products plays a prominent role in strategies for the conversion of CO_2 to value-added chemicals.[1] As discussed in the previous chapter, these reactions can proceed by a spectrum of mechanisms that are defined by two limiting cases: insertion mechanisms involving M---OCO interactions,[1b,c,2] and direct S_E2 attack of CO_2 at the metal alkyl carbon (Scheme 2.1).[1g-j,o] This chapter explores the reactions of CO_2 with two prototypical Zr and Pd L_xMR^{n+} olefin polymerization catalysts and the corresponding $L_xMR_2^{(n-1)+}$ species. These studies provide insight to the mechanistic differences and parallels in the carboxylation of early versus late transition metal alkyls.

Scheme 2.1

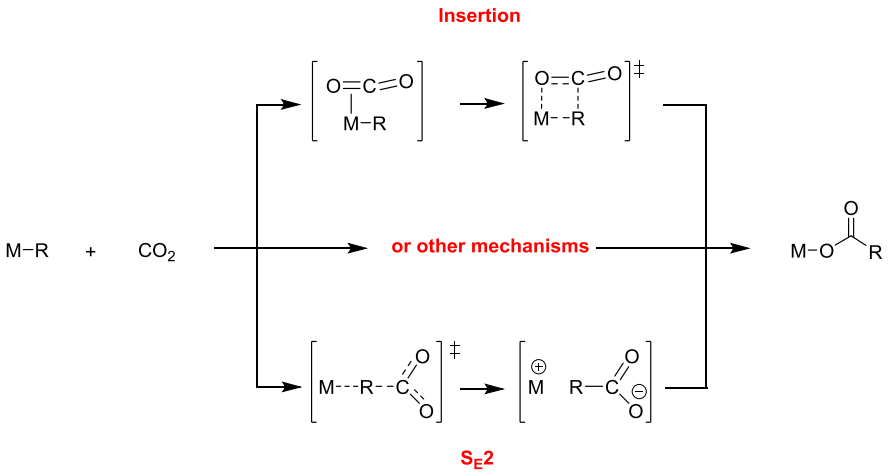

2.2. Results and Discussion

Carboxylation of [Cp_2ZrMe][$B(C_6F_5)_4$]. Cp_2ZrR^+ cations generated from Cp_2ZrR_2 precursors are effective olefin polymerization catalysts. [3] Wendt reported that $Cp_2ZrMe\{MeB(C_6F_5)_3\}$ reacts with CO_2 to form $[\{Cp_2Zr(\mu\text{-}OAc)\}_2][MeB(C_6F_5)_3]_2$, which was characterized by X-ray diffraction and conversion to $[Cp_2Zr(OAc)(THF\text{-}d_8)][MeB(C_6F_5)_3]$.[2] In principle, this reaction could proceed by reaction of CO_2 with the Cp_2ZrMe^+ cation, or with the $MeB(C_6F_5)_3^-$ anion to generate $B(C_6F_5)_3(OAc)^-$,[4] followed by Me/OAc exchange. To probe the reactivity of the Cp_2ZrMe^+ cation more directly, we investigated the carboxylation of $[Cp_2ZrMe(C_6D_5Cl)][B(C_6F_5)_4]$ (**1**).[5] Cationic complex **1** was generated by methyl abstraction of Cp_2ZrMe_2 (**2**) with $[Ph_3C][B(C_6F_5)_4]$ in C_6D_5Cl. The reaction of **1** with 1 atm of CO_2 in C_6D_5Cl at 20 °C occurs within the time of mixing to form a gelatinous product assigned as $[Cp_2Zr(OAc)][B(C_6F_5)_4]$; addition of THF-$d_8$ gives $[Cp_2Zr(OAc)(THF\text{-}d_8)][B(C_6F_5)_4]$ quantitatively (Scheme 2.2). DFT computations show that this reaction proceeds by initial formation of the κ^1-O-bound CO_2 adduct $Cp_2Zr(Me)(CO_2)^+$,[6] followed by insertion via a 4-center transition state with a barrier of 16.4 kcal/mol (Figure 2.1).

Scheme 2.2

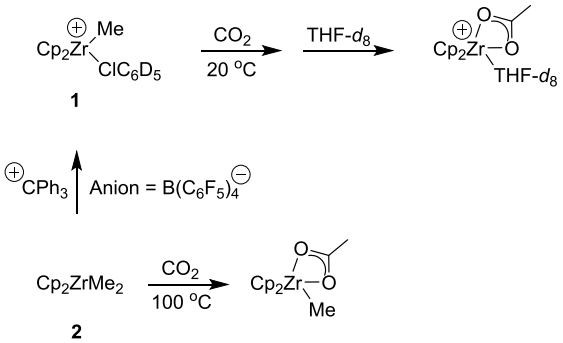

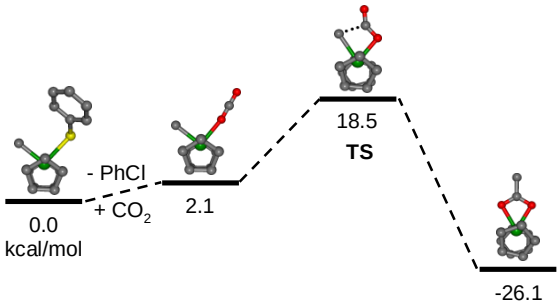

Figure 2.1. Calculated free-energy profile for the reaction of $Cp_2ZrMe(C_6H_5Cl)^+$ with CO_2.

In contrast, neutral complex **2** was reported to react only slowly with CO_2 (50 atm CO_2, 80 °C, 24 h) to yield an insoluble and ill-defined product that liberates acetic acid and methane upon reaction with H_2SO_4.[7] We found that **2** reacts very slowly with CO_2 (1 atm, 100 °C, C_6D_5Cl, $t_{1/2}$ ca. 30 h) to yield $Cp_2Zr(Me)(OAc)$[8] with no NMR-observable intermediates (Scheme 2.2). DFT computations show that this reaction also proceeds by an insertion mechanism, but a stable intermediate CO_2 adduct was not found (Figure 2.2). Lateral attack of CO_2 ($\Delta G^{\ddagger}$ = 33.2 kcal/mol) is preferred over central attack ($\Delta G^{\ddagger}$ = 34.4 kcal/mol).

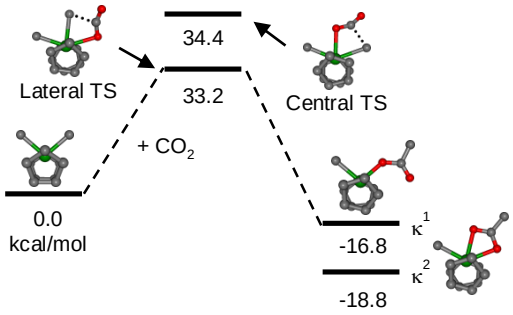

Figure 2.2. Calculated free-energy profile for the reaction of Cp_2ZrMe_2 (**2**) and CO_2.

The $>10^4$ fold difference in the reactivity of **1** and **2** with CO_2 reflects the greater electrophilicity of the Zr center in **1**, which results in a stronger Zr–*O*CO interaction and greater

activation of the CO_2 for nucleophilic attack by the Zr–Me group. The Zr---O distance in the transition state for CO_2 insertion of **1** (2.166 Å; van der Waals radii: Zr: 2.57 Å; O: 1.71 Å)[9] is much shorter than that for **2** (2.464 Å, lateral; 2.357 Å, central), consistent with a stronger Zr–O interaction. In contrast, the Zr–Me bond of **2** (2.283 Å (calculated); van der Waals radius of C = 1.96 Å) is 0.03 Å longer than that of **1** (2.250 Å (calculated)), suggesting that nucleophilicity of the Zr–Me groups in **2** may be greater than that in **1**. This result argues against the role of nucleophilicity of Zr–Me groups in the difference in reactivity.

Carboxylation of Neutral (PO)PdR(L). Neutral (PO)PdR(L) complexes that contain *ortho*-phosphino-arenesulfonate ligands ($[PO]^-$) and their base-free dimeric analogues $\{(PO)PdR\}_2$ catalyze the insertion copolymerization of ethylene and polar monomers.[10] Chain growth in these reactions proceeds by formation of $(PO)PdR(CH_2{=}CH_2)$ or $(PO)PdR(CH_2{=}CHX)$ adducts followed by insertion (Scheme 2.3). In contrast, these species do not react with CO_2 under conditions where they are thermally stable. For example, (PO-^{i}Pr)PdMe(L) species ($[PO\text{-}^i Pr]^-$ = 2–P^{i}Pr$_2$–4–Me–$C_6H_3SO_3^-$; L = py, THF) do not react with CO_2 (23–50 °C, 2.5–5.6 atm) in THF-d_8. Similarly, the dimer $\{(PO\text{-}3,5\text{-}^t Bu)PdMe\}_2$ ($[PO\text{-}3,5\text{-}^t Bu]^-$ = 2–P(3,5–^{t}Bu$_2$–C_6H_3)$_2$–4–Me–$C_6H_3SO_3^-$)[11] is unreactive with CO_2 in CD_2Cl_2 (Scheme 2.4).

Scheme 2.3

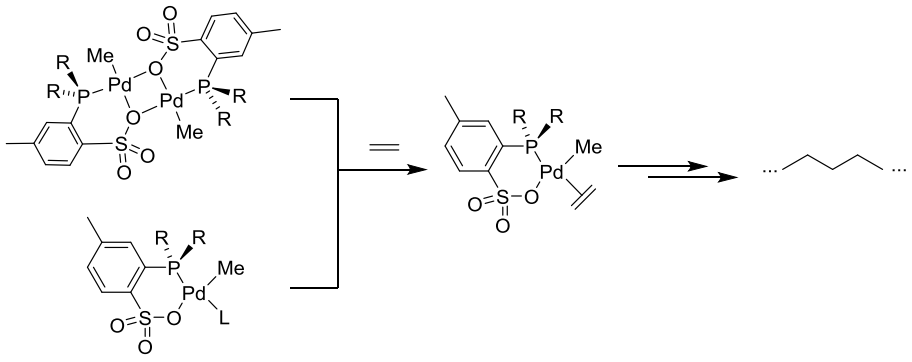

Scheme 2.4

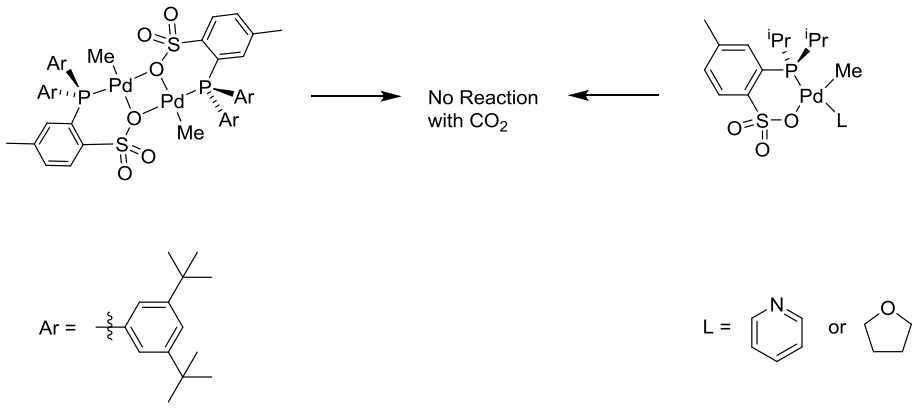

The lack of reactivity of (PO)PdR(L) and {(PO)PdR}$_2$ complexes may reflect an inability of CO_2 to displace the THF, py, or μ–sulfonate ligands, a high barrier to insertion of a putative (PO)PdMe(CO_2) species, or a high barrier to an S_E2 process. DFT calculations show that displacement of THF from (PO-^{i}Pr)PdMe(THF) by CO_2 is endergonic by 10.9 kcal/mol, insertion of (PO-^{i}Pr)PdMe(κ^1–*O*CO) has a high barrier ($\Delta G^{\ddagger}$ = 33.8 kcal/mol), and overall conversion to (PO-^{i}Pr)Pd(OAc)(THF) is endergonic by 9.2 kcal/mol. An S_E2 transition state was not found (Figure 2.3). The lack of reactivity of neutral (PO)PdMe species is consistent with previous reports that L_2PdMe_2 complexes (L_2 = $Me_2NCH_2CH_2NMe_2$, $Ph_2PCH_2CH_2PPh_2$, *cis*–CH_2{*cyclo*–NHCH=CHN(2,4,6–Me_3–C_6H_2)C}$_2$) are unreactive with CO_2,[12] and (PCP)PdR pincer complexes only react with CO_2 at elevated temperature and when the PCP ligand is a very strong donor, i.e. (^{tBu}PCP)PdMe ([^{tBu}PCP]$^-$ = [2,6–(^{t}Bu$_2$PCH$_2$)$_2$–C_6H_3]$^-$).[1g,h,o]

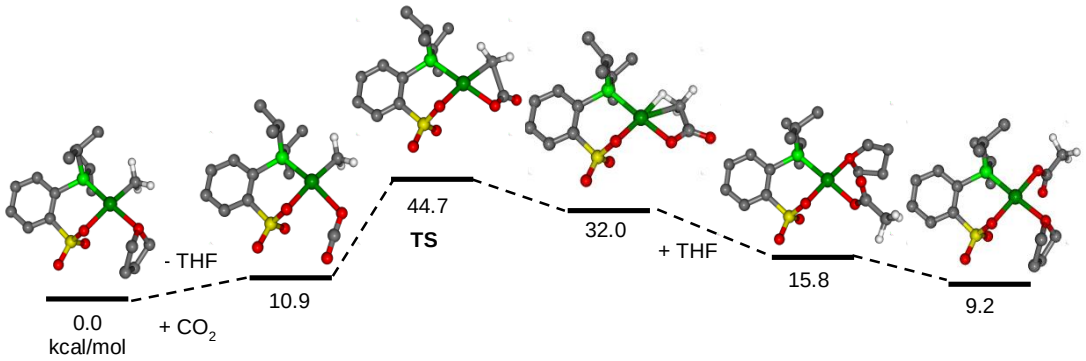

Figure 2.3. Calculated free-energy profile for the reaction of (PO-^{i}Pr)PdMe(THF) and CO_2.

Synthesis of (PO)PdMe$_2^-$. One potential approach to enhancing the reactivity of (PO)PdMe species with CO_2 is to make the complex anionic to increase the nucleophilicity of the Pd–*Me* group.[13] The dimethyl complex {[Li(THF)$_2$][(PO-^{i}Pr)PdMe$_2$]}$_2$ (**3a**) was synthesized from Li[PO-^{i}Pr] and (COD)PdMe$_2$ (Scheme 2.5). The ^{1}H and ^{13}C NMR spectra of **3a** each contain two doublets for the Pd-*Me* groups, which were assigned by HMQC–NMR, taking advantage of the large difference in the $^{2}J_{CP}$ values ($^{2}J_{CP,trans}$ = 112 Hz; $^{2}J_{CP,cis}$ = 6.5 Hz; Figure 2.4). In the solid state, **3a** adopts a dimeric structure in which two (PO-^{i}Pr)PdMe$_2^-$ anions are linked by Li(THF)$_2^+$ ions that bind sulfonate oxygens (Figure 2.5). The Pd–Me$_{trans\text{-}to\text{-}P}$ bond is 0.05 Å longer than Pd–Me$_{cis\text{-}to\text{-}P}$ bond, due to the strong *trans* influence of the phosphine. PGSE-NMR data indicate that **3a** is monomeric in THF-d_8. The ^{7}Li NMR resonance of **3a** in THF-d_8 appears at δ -2.4, outside of the normal range for solvent-separated Li(THF)$_n^+$X$^-$ ion-pairs (δ -0.5 − -1.5; e.g. δ -0.6 for [Li(THF)$_n$][B(C$_6$F$_5$)$_4$]).[14] These results and the previous observation that B(C$_6$F$_5$)$_3$ binds to a sulfonate oxygen of (PO-3,5-^{t}Bu)PdMe(OEt$_2$)[10] suggest that **3a** exists as a tight ion-pair with Li$^+$ binding to a sulfonate oxygen in THF-d_8 solution. **3a** is thermally unstable in the solid state and in THF-d_8, decomposing at 20 °C to ethane, Pd^0 and unidentified products.

Scheme 2.5

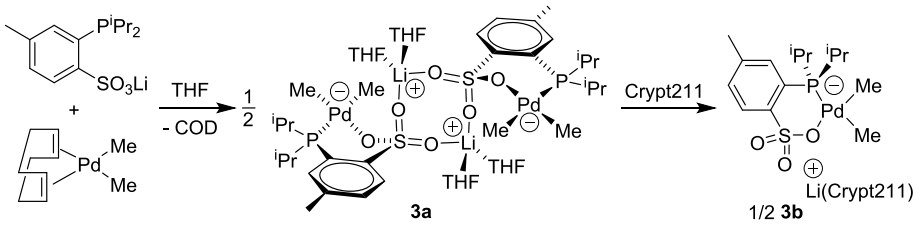

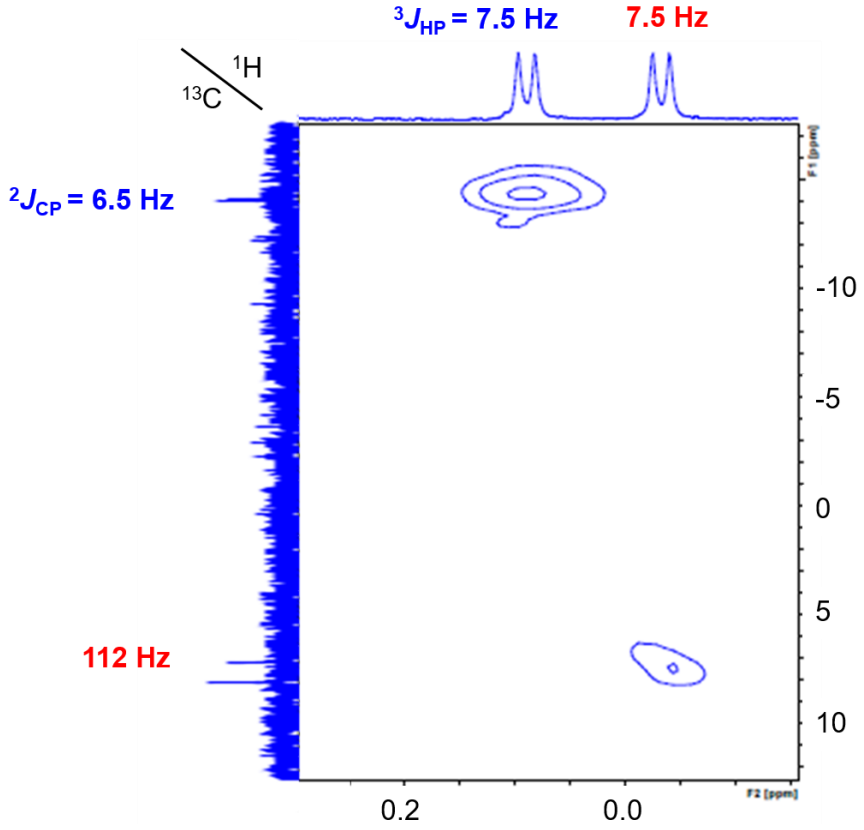

Figure 2.4. HMQC–NMR spectrum of **3a** in THF-d_8. Selected region for Pd–$Me_{\text{trans-to-P}}$ (^{1}H NMR: δ -0.04, $^3J_{HP}$ = 7.5 Hz; ^{13}C NMR: δ 7.7, $^2J_{CP}$ = 112 Hz) and Pd–$Me_{\text{cis-to-P}}$ (^{1}H NMR: δ 0.06, $^3J_{HP}$ = 7.5 Hz; ^{13}C NMR δ -13.9, $^2J_{CP}$ = 6.5 Hz) resonances is shown.

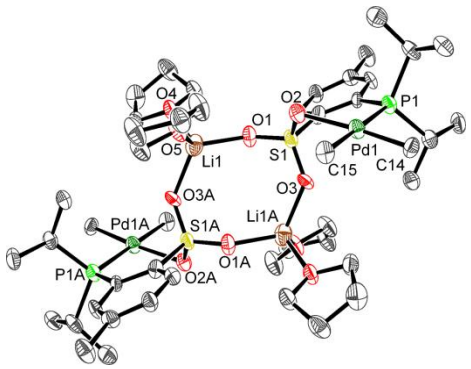

Figure 2.5. Molecular structure of $\{[Li(THF)_2][(PO\text{-}^iPr)PdMe_2]\}_2$ (**3a**). Hydrogen and solvent atoms are omitted. Selected bond lengths (Å) and angles (deg): Pd1–C14 1.986(6), Pd1–C15 2.038(6), Pd1–P1 2.309(2), Pd1–O2 2.197(4), C14–Pd1–C15 85.1(2), O2–Pd1–P1 87.52(12).

Sequestration of Li^+ from **3a** by Crypt211 (1 equiv per Pd) in THF-d_8 solution affords [Li(Crypt211)][(PO-^{i}Pr)PdMe$_2$] (**3b**; Scheme 2.5). The ^{1}H and ^{7}Li NMR (δ -0.7) resonances of **3b** are shifted from those of **3a**, and **3b** is markedly more soluble in THF-d_8 and more thermally stable compared to **3a**.

Reaction of 3a with CO_2. Complex **3a** reacts irreversibly with CO_2 (0.36 – 2.3 atm) in THF-d_8 at 20 °C to afford the acetate complex Li[(PO-^{i}Pr)PdMe(OAc)] (**4a**) in 77 % yield (Scheme 2.6). This reaction also produces small amounts of methane, ethane, Pd^0, and Li[(PO-^{i}Pr)PdMe(κ^1-*P*O-^{i}Pr)] (**5**) from competing thermal decomposition of **3a**. **4a** was independently synthesized by the reaction of **3a** and CH_3CO_2H. The IR ν_{CO} bands for **4a** (1575, 1433 cm^{-1}) were identified by comparison of the IR spectra of **4a** and Li[(PO-^{i}Pr)PdMe(O^{13}C(O)Me)] (**4a-^{13}C$_1$**), which was prepared from **4a** and $CH_3{}^{13}CO_2H$. The $\Delta\nu_{CO}$ value ($\nu_{CO,asym} - \nu_{CO,sym}$ = 142 cm^{-1}) indicates that both oxygen atoms of the OAc unit are bound to metals.[15]

Scheme 2.6

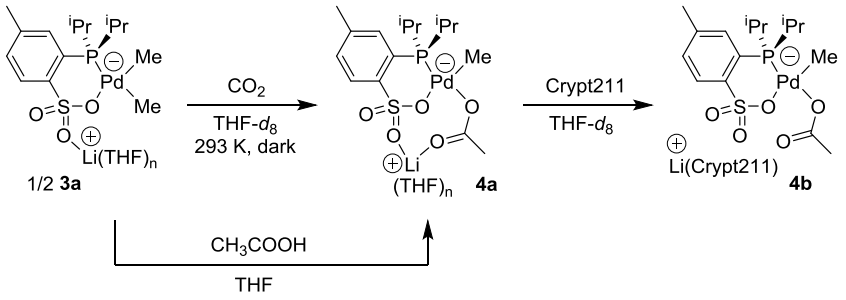

Attempts to obtain crystalline samples of **4a** were unsuccessful. However, the analogous complex {[Li(THF)][(PO-^{i}Pr)Pd(Me)OC(O)An]}$_2$ (**6**; An = 9-anthracenyl), prepared from **3a** and $AnCO_2H$, was characterized by X-ray diffraction (Figure 2.6). **6** crystallizes as a dimer. The anthracenoate units are bound in a κ^1, κ^1 fashion to Pd and a Li^+ ion. Each Li^+ also binds a THF and a sulfonate oxygen from each [(PO-^{i}Pr)Pd(Me)OC(O)An]$^-$ unit, similar to the structure of **3a**. The IR ν_{CO} values for **6** (1595, 1430 cm^{-1}; $\Delta\nu_{CO}$ = 165 cm^{-1}) are similar to those for **4a**, consistent with a similar carboxylate coordination mode for the two species.

The ^{7}Li NMR resonance of **4a** in THF-d_8 appears at δ 0.0. Addition of Crypt211 to **4a** gives [Li(Crypt211)][(PO-^{i}Pr)PdMe(OAc)] (**4b**; Scheme 2.6). The ^{1}H NMR OAc resonance of **4b** is shifted from that of **4a** (**4b**: δ 2.01; **4a**: δ 1.84), and the $\Delta\nu_{CO}$ value for **4b** (237 cm^{-1}) is consistent with κ^1–OAc coordination. Addition of Li^+ to **4b** regenerates **4a**. These results suggest that Li^+ ion-pairs with the sulfonate and acetate oxygens of **4a** in THF-d_8 as shown in Scheme 2.6.

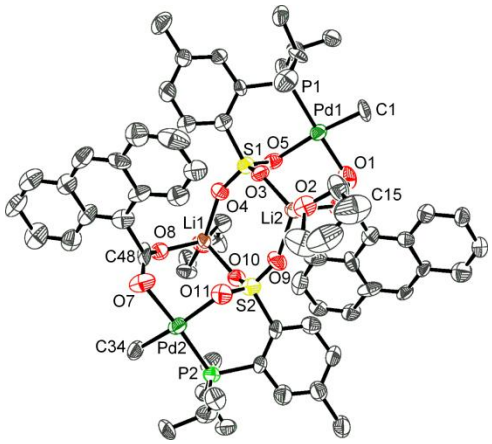

Figure 2.6. Molecular structure of {[Li(THF)][(PO-^{i}Pr)Pd(Me)OC(O)An]}$_2$ (**6**). Hydrogen and solvent atoms are omitted. Selected bond lengths (Å) and angles (deg): Pd2–C34 2.006(6), Pd2–O7 2.062(5), Pd2–O11 2.150(5), Pd2–P2 2.186(2), C48–O7 1.259(8), C48–O8 1.223(8), C34–Pd2–O7 86.2(3).

NMR Monitoring of the Carboxylation of 3a. The reaction of **3a** and CO_2 was monitored by ^{31}P and ^{1}H NMR. No intermediates were observed. Upon exposure to CO_2, the ^{31}P resonance of **3a** decreased in intensity over time and that for **4a** grew in, and only resonances of **4a** and byproduct **5** were observed at the end of the reaction (Figure 2.7). However, the changes in the ^{1}H NMR spectrum that accompany the carboxylation of **3a** are more complex. In the ^{1}H NMR spectrum (Figure 2.8), the Pd–$Me_{\mathbf{3a},\text{cis-to-P}}$ resonance of **3a** initially appeared as a broad singlet and the Pd–$Me_{\mathbf{3a},\text{trans-to-P}}$ resonance appeared as a sharp singlet. As the reaction proceeded, singlets for the Pd-*Me* (broad) and Pd–OC(O)*Me* (sharp) groups of **4a** emerged, and the signals of **3a** disappeared. These results are consistent with the conversion of **3a** to **4a** and concurrent reversible exchange of **3a** and **4a**.

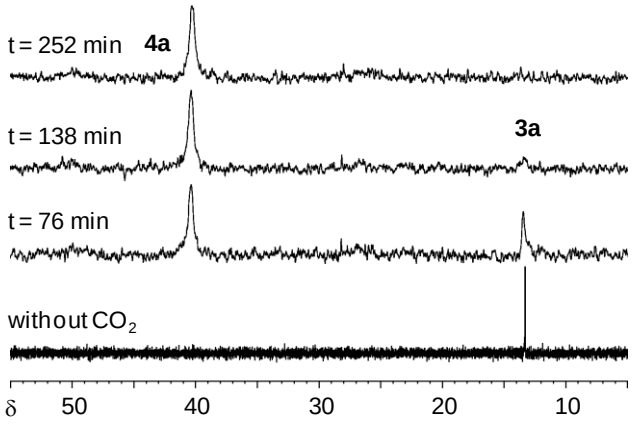

Figure 2.7. ^{31}P NMR monitoring of the reaction of CO_2 (2.3 atm) with **3a** in THF-d_8 at 20 °C. The signal for **5** is at δ 27.9.

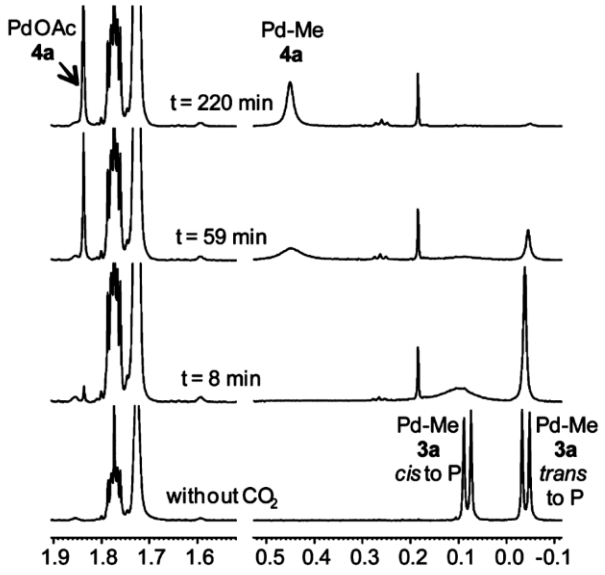

Figure 2.8. ^{1}H NMR monitoring of the reaction of CO_2 (1.1 atm) with **3a** in THF-d_8 at 20 °C. Unlabeled resonances: δ 1.79 (m, THF), 1.72 (s, THF-d_7), 0.25 (t, Pd–*Me* of **5**), 0.19 (s, CH_4).

The **3a**/**4a** exchange can be explained by the mechanism in Scheme 2.7, which involves displacement of OAc^- from **4a** by the nucleophilic Pd–$Me_{trans\text{-}to\text{-}P}$ group of **3a** to generate a

methyl-bridged intermediate, followed by displacement of **3a** from the intermediate by OAc^-. This process permutes the Pd–$Me_{\mathbf{3a},\text{cis-to-P}}$ and Pd–$Me_{\mathbf{4a}}$ groups, resulting in broadening of these ^1H resonances, but simply shuttles the Pd–$Me_{\mathbf{3a},\text{trans-to-P}}$ groups between equivalent positions of different (PO)PdMe units, resulting in collapse of the ^{31}P coupling but no line broadening of the Pd–$Me_{\mathbf{3a},\text{trans-to-P}}$ resonance. The second order rate constant for the **3a**/**4a** exchange estimated by lineshape analysis is $1.5(8) \times 10^4$ $M^{-1}s^{-1}$ at 20 °C (Figure 2.9).

Scheme 2.7

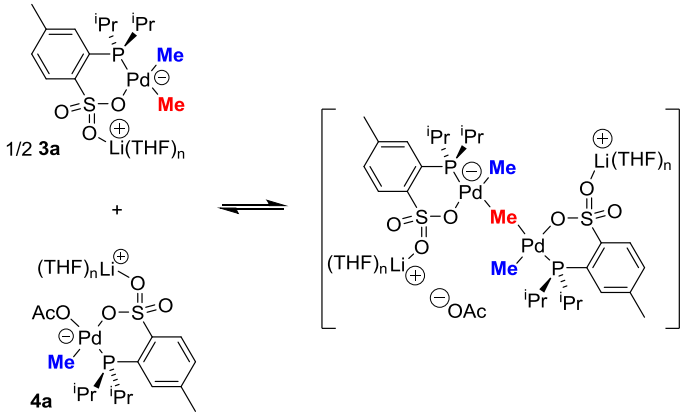

The proposed mechanism for the **3a**/**4a** exchange was further supported by analysis of ^1H NMR spectra of mixtures of **3a** and (PO-^{i}Pr)PdMe(THF)-Li^+, generated by reaction of **3a** with $[Ph_3C][B(C_6F_5)_4]$ (Figure 2.10). In the ^1H NMR spectrum, at 226 K, separate Pd–Me resonances for (PO-^{i}Pr)PdMe(THF)-Li^+ and **3a** were observed. As the temperature was raised, the Pd-Me resonance for (PO-^{i}Pr)PdMe(THF)-Li^+ and the resonance of the Pd–Me group *cis* to P for **3a** (Pd-$Me_{\mathbf{3a},\text{cis-to-P}}$) broadened and coalesced (at 273 K), and the Pd–$Me_{\mathbf{3a},\text{trans-to-P}}$ collapsed to a singlet. As the temperature was raised above 273 K, the coalesced Pd–Me resonance for (PO-^{i}Pr)PdMe(THF)-Li^+/**3a** (*cis* to P) sharpened and the Pd–$Me_{\mathbf{3a},\text{trans-to-P}}$ resonance remained sharp.

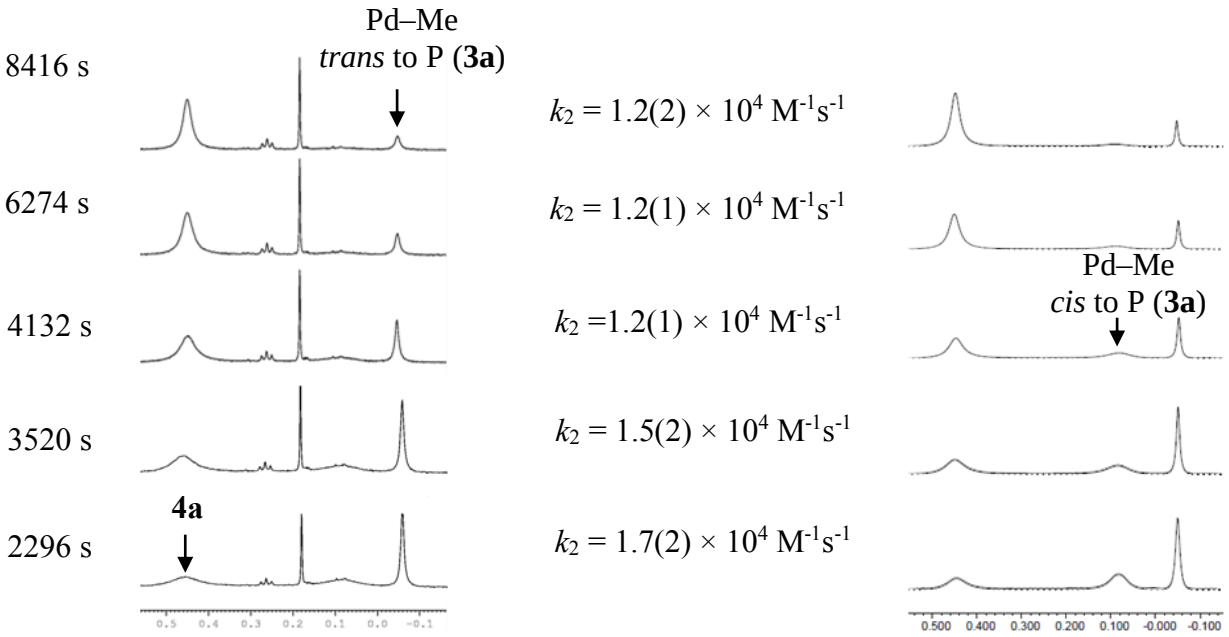

Figure 2.9. Representative ^{1}H NMR spectra for the exchange between **3a** and **4a** during the reaction of **3a** with CO_2 (1.06 atm) in THF-d_8 at 20 °C. The Pd–Me region is shown. Experimental spectra are shown on the left and simulated spectra and k_2 values are shown on the right. Other resonances: δ 0.25 (t, Pd–Me, **5**), 0.19 (s, CH_4).

These lineshape changes were reversed when the temperature was lowered. These results are consistent with reversible exchange of the Pd–$Me_{\text{trans-to-P}}$ methyl group between **3a** and(PO-^{i}Pr)PdMe(THF)-Li$^+$, which permutes the Pd–Me group for (PO-^{i}Pr)PdMe(THF)-Li$^+$ and Pd–$Me_{\mathbf{3a},\text{cis-to-P}}$ (Scheme 2.8). The second order rate constant for the **3a**/(PO-^{i}Pr)PdMe(THF)-Li$^+$ exchange determined from lineshape analysis is 5.4 × 10^5 M^{-1}s^{-1} at 20 °C. Therefore, the **3a**/(PO-^{i}Pr)PdMe(THF)-Li$^+$ exchange is 36-fold faster than **3a**/**4a** exchange at 20 °C. This difference likely reflects the lower Coulombic barrier to bringing a neutral and an anionic species (versus two anionic species) together and the greater leaving group ability of THF versus OAc$^-$.

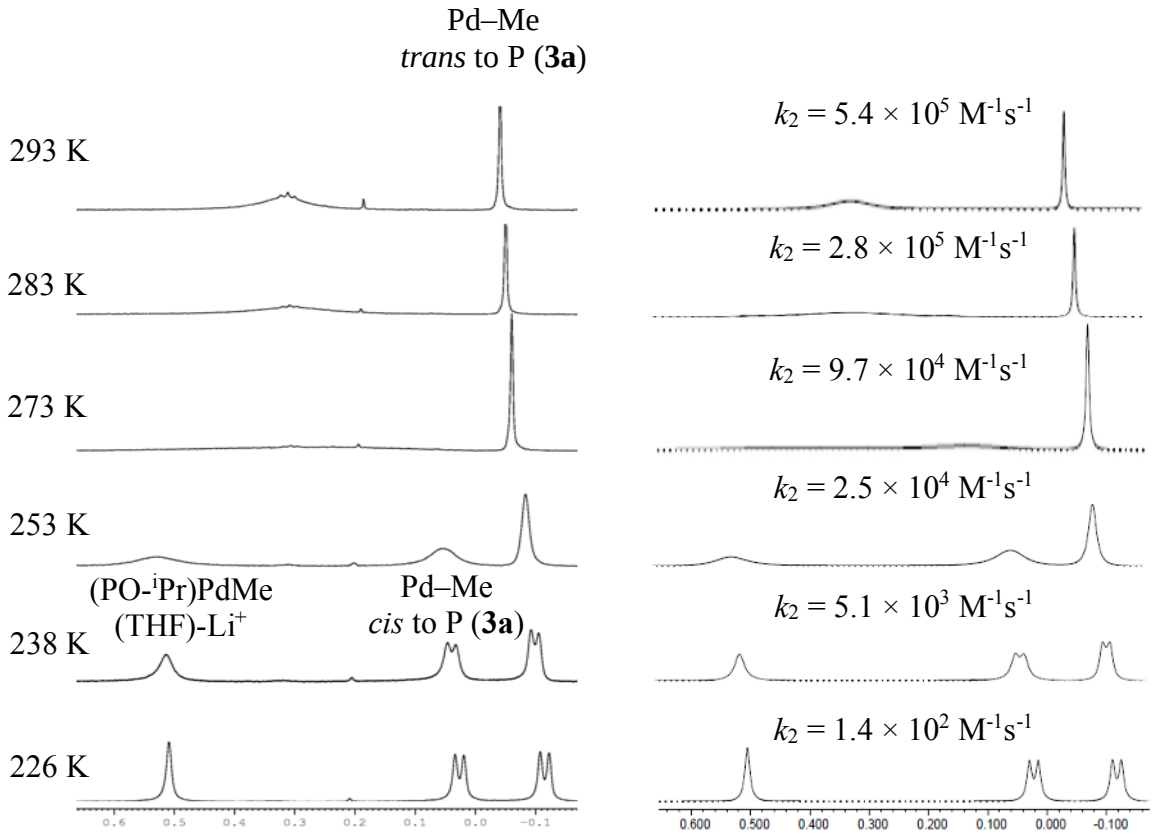

Figure 2.10. Representative variable temperature ^{1}H NMR spectra of a solution of **3a** and (PO-^{i}Pr)PdMe(THF)-Li^{+} in THF-d_8. Experimental spectra are shown on the left and simulated spectra are shown on the right. The Pd–Me region of the spectra and second-order rate constants for the exchange at each temperature are shown.

Scheme 2.8

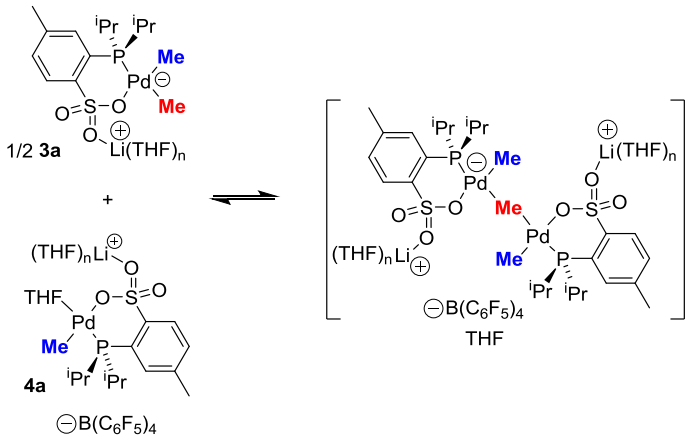

Kinetics of Carboxylation of 3a. Due to the presence of the competing minor formation of CH_4, C_2H_6, **5** and Pd^0, the kinetics of the reaction of **3a** with CO_2 were measured by ^1H NMR by monitoring the appearance of the OAc resonance of **4a.** Kinetic studies were conducted at 20 °C over the range of CO_2 pressure of 0.36 atm to 2.0 atm. The reaction is first order in **3a** and in CO_2; i.e. Rate = k_2[**3a**]P_{CO2} with k_2 = 2.2(1) × 10^{-4} $atm^{-1}s^{-1}$ at 20 °C (Figure 2.11).

In classic work, Darensbourg reported that Na^+ accelerates the insertion of CO_2 into the W–R bond of *cis*-$W(CO)_4LR^-$ (R= Me, Et, Ph; L = CO, PMe_3, $P(OMe)_3$).[1b] The observation of significant Li^+ ion-pairing for **3a**, **4a** and **6** suggests that Li^+ might play a role in the carboxylation of **3a**. Indeed, **3b**, in which the Li^+ is sequestered by Crypt211, reacts irreversibly with CO_2 to afford **4b** at a rate that is ca. 6 times *slower* than the reaction of **3a** under similar conditions (red dot in Figure 2.12).[16] Interestingly, the exchange between **3b** and **4b** is also much slower than the corresponding **3a**/**4a** exchange, indicating that Li^+ plays a role in the latter process.

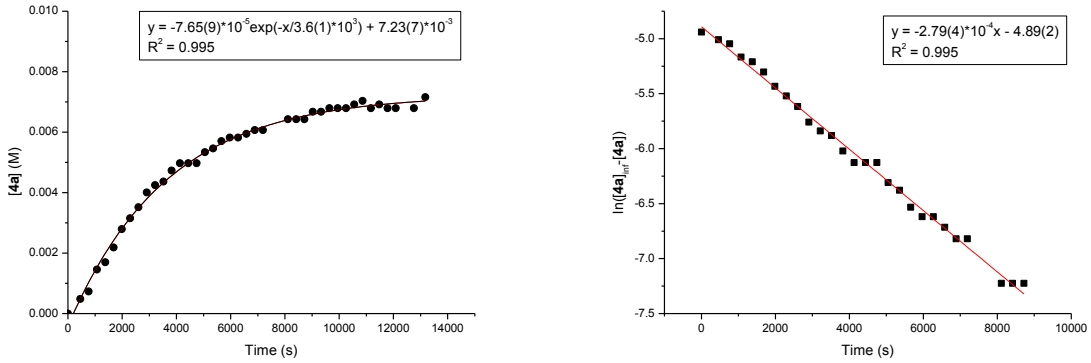

Figure 2.11. Representative first-order kinetic plots for the formation of **4a** in the reaction of **3a** with CO_2 (1.1 atm) in THF-d_8 at 20 °C. The exponential form is shown on the left (k_{obs} = 2.75(9) × 10^{-4} s^{-1}) and the logarithmic form is shown on the right (k_{obs} = 2.79(4) × 10^{-4} s^{-1}).

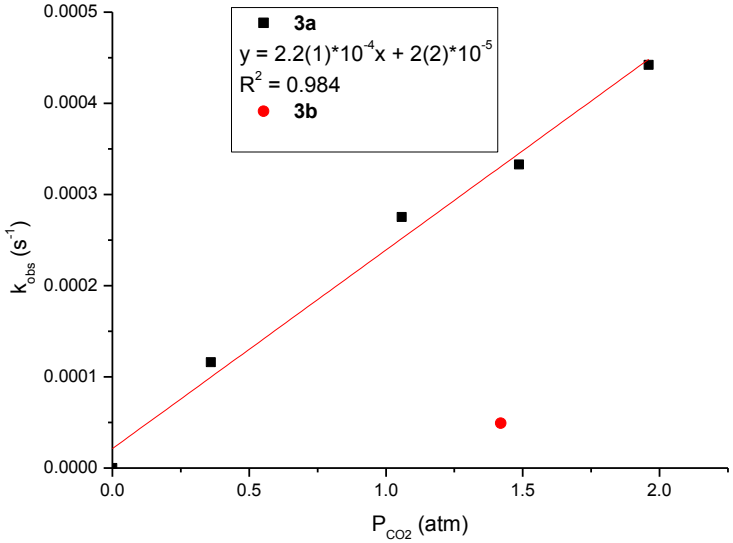

Figure 2.12. Plot of k_{obs} vs CO_2 pressure for the formation of **4a** from the reaction of **3a** with CO_2 in THF-d_8 at 20 °C. ■ = Data for **3a**. ● = Data for **3b**.

DFT Studies on Reactions of CO_2 with 3a and 3b. The observations that anionic **3a** reacts readily with CO_2 while neutral (PO)PdMe(L) species do not and that Li^+ accelerates the carboxylation of **3a** are consistent with an S_E2 mechanism in which Li^+ can play a role. To probe the mechanism further, DFT studies with implicit THF solvation (IEF-PCM) were carried out on (PO-^{i}Pr)$PdMe_2^-$ with and without Li^+. For the free (PO-^{i}Pr)$PdMe_2^-$ anion, the lowest-energy pathway involves S_E2 attack of the CO_2 carbon at the Pd–$Me_{trans\text{-to-P}}$ group with $\Delta G^{\ddagger}$ = 31.3 kcal/mol, to generate a C–H-σ-bound acetate intermediate that relaxes to the O-bound acetate product (Figure 2.13). The lowest-energy pathway with inclusion of Li^+ involves a Li^+-assisted S_E2 transition state, in which a sulfonate oxygen anchors Li^+ in a position where it can bind a CO_2 oxygen with a Li^+---*O*CO distance of 1.981 Å, activating the CO_2 for nucleophilic attack by the Pd–$Me_{trans\text{-to-P}}$ group (Figure 2.14). The initial product is again a C–H-σ-complex, which rearranges to an O-bound acetate product in which Li^+ binds sulfonate and acetate oxygens, similar to the structure of **6**. The presence of Li^+ lowers the barrier by 5.2 kcal/mol and increases the exergonicity by 13.1 kcal/mol. Similar energies (difference < 2 kcal/mol) were obtained for this pathway with explicit THF coordination (2 per Li^+). The $Me_{trans\text{-to-P}}$---*C*O_2 distance (2.118 Å) is longer, the Pd–$Me_{trans\text{-to-P}}$ distance is shorter (2.171 Å) and the C–O distances (1.208, 1.185 Å) are less perturbed overall from those in free CO_2, in the Li^+-assisted transition state than in the non-Li^+-assisted transition state ($Me_{trans\text{-to-P}}$---*C*O_2: 2.027 Å; Pd–$Me_{trans\text{-to-P}}$: 2.215 Å; C–O: 1.202 Å). These results show that the Li^+-assisted transition state is earlier than the non-Li^+-assisted transition state, as expected given the greater exergonicity of the former process. While further work is needed to fully elucidate the role of Li^+, these results show that Li^+ accelerates this carboxylation reaction by binding a CO_2 oxygen.

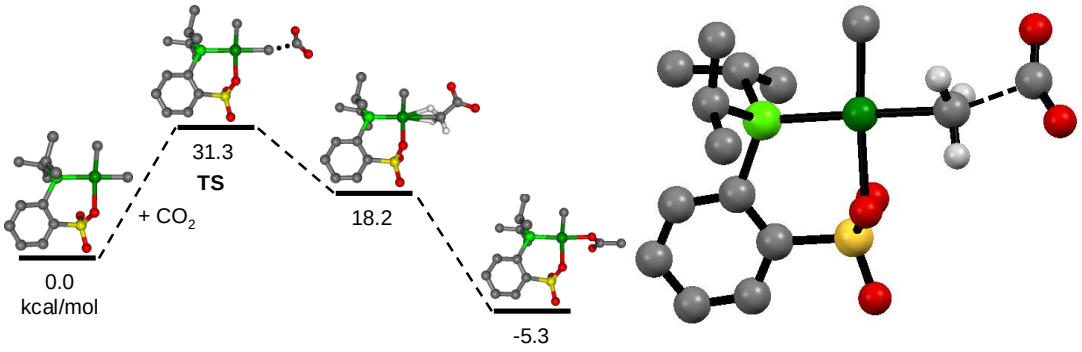

Figure 2.13. Calculated free-energy profile for the reaction of (PO-^{i}Pr)PdMe$_2^-$ and CO_2 with implicit THF solvation (left). A view of the transition state for S_E2 attack at Pd–*Me*$_{trans\text{-to-P}}$ that includes the methyl hydrogen atoms is shown (right).

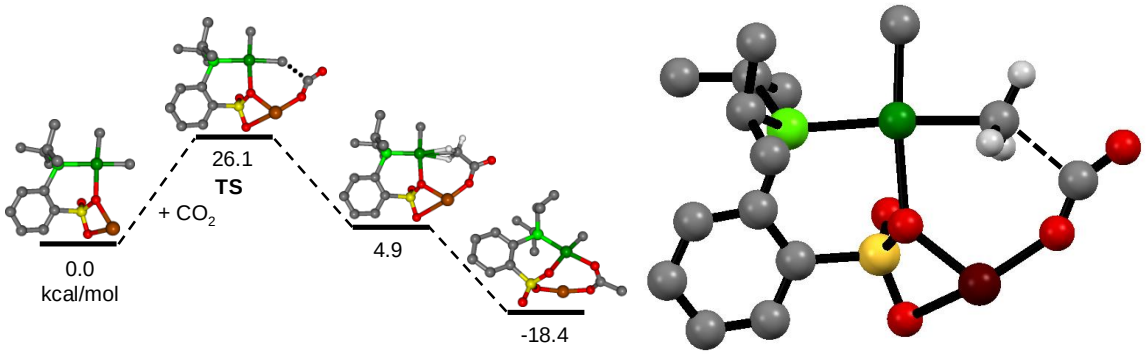

Figure 2.14. Calculated free-energy profile for the reaction of Li[(PO-^{i}Pr)PdMe$_2$] and CO_2 with implicit THF solvation (left). A view of the the transition state for S_E2 attack at Pd–*Me*$_{trans\text{-to-P}}$ that includes the methyl hydrogen atoms is shown (right).

Mechanistic Considerations. Other mechanisms for the reaction of **3a** with CO_2 besides S_E2 attack of CO_2 at Pd–Me$_{trans\text{-to-P}}$ have been considered and ruled out. For example, mechanisms for the reaction of **3a** with CO_2 involving S_E2 attack at Pd–*Me*$_{cis\text{-to-P}}$ ($\Delta G^{\ddagger}$ = 38.9 kcal/mol) or insertion of CO_2 with sulfonate group dissociation ($\Delta G^{\ddagger}$ = 39.6 kcal/mol) have

higher barriers (Figure 2.15). An insertion mechanism with a Pd---*O*CO interaction without displacement of the sulfonate is ruled out as the transition state could not be located. Mechanisms involving dissociation of MeLi from **3a** followed by reaction with CO_2 and coordination of the resulting OAc^- to Pd were ruled out by the observation that pyridine does not react with or influence the decomposition of **3a**. In contrast, pyridine reacts rapidly with MeLi to afford 1–lithio–2–methyl–1,2–dihydropyridine.[17]

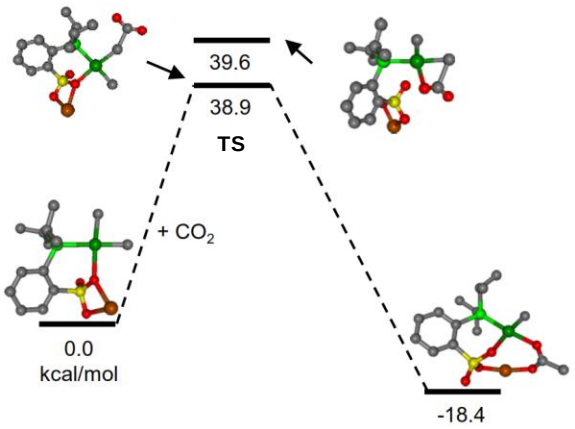

Figure 2.15. Calculated free-energy profile for the reaction of Li[(PO-^{i}Pr)PdMe$_2$] and CO_2 with implicit THF solvation. Transition states involving a S_E2 attack at Pd–*Me*$_{cis\text{-to-P}}$ (bottom) and an insertion of CO_2 with sulfonate group dissociation (top) are shown.

Carboxylation of Group 4 and 10 Metal Alkyls. The reactions of CO_2 with **1**, **2**, **3a** and **3b** represent unusual examples of carboxylation of group 4 and 10 metal alkyls. To the best of our knowledge, the only other reported examples of group 4 metal alkyls that react with CO_2 are Cp$_2$TiMe$_2$,[1r] Cp*$_2$TiCH$_2$CMe$_3$,[1s] (C$_8$Me$_6$)TiMe$_2$,[1t] and {(C$_5$Me$_4$)SiMe$_2$(N)^{t}Bu}ZrMe$_2$.[1q] Only

two examples of discrete group 10 metal alkyls that undergo carboxylation have been reported previously, namely (^{tBu}PCP)PdMe ([^{tBu}PCP]$^-$ = [2,6–(^{t}Bu$_2$PCH$_2$)$_2$–C$_6$H$_3$]$^-$),[1g,o] and (^{tBu}POCOP)NiMe ([^{tBu}POCOP]$^-$ = [2,6–(^{t}Bu$_2$PO)$_2$–C$_6$H$_9$]$^-$).[1u]

2.3. Conclusions

Previously Wendt proposed that insertion of CO_2 by zirconocene alkyls is promoted by the presence of an open coordination site and an electrophilic metal center, implicating the importance of initial coordination of the CO_2 to Zr, whereas (^{tBu}PCP)PdMe reacts by an S_E2 process that is promoted by the electron-rich Pd center.[1g,o,2] The results reported here support this general picture, clarify several aspects of the carboxylation of zirconocene alkyls, and show that the presence of an anionic charge dramatically promotes the S_E2 carboxylation of Pd alkyls. Furthermore, in parallel to the Zr system, the S_E2 process can be accelerated by a Li^+---OCO interaction when a suitably positioned Li^+ counter-ion is present.

2.4. Experimental Section

General Procedures. All experiments were performed using dry box or Schlenk techniques under a nitrogen atmosphere. Nitrogen was purified by passage through activated molecular sieves and Q-5 oxygen scavenger. Deuterated solvents were purchased from Cambridge Isotope Laboratories. C_6D_5Cl was distilled from and stored over P_2O_5. C_6D_6 was dried over CaH_2 and stored over 3 Å molecule sieves. CD_2Cl_2 was distilled from P_2O_5. Toluene-d_8 and THF-d_8 were distilled from Na/benzophenone or NaK. Pentane, hexanes and toluene were purified by passage through activated alumina and BASF R3-11 oxygen scavenger. THF,

CH_2Cl_2, and Et_2O were purified by passage through activated alumina. Ferrocene was purified by sublimation. CO_2 (99.999%) was purchased from Airgas and passed through a column of P_2O_5 (to remove water), condensed at -196 °C, warmed to -78 °C (to remove O_2) and condensed at -196 °C and stored over P_2O_5. Cp_2ZrMe_2 (**2**)[18] was freshly sublimed before use (85 °C, 0.001 mmHg), and stored at -35 °C. (TMEDA)$PdMe_2$ (TMEDA = $Me_2N(CH_2)_2NMe_2$), [19] (COD)PdMeCl (COD = 1,5–cyclooctadiene)[20] and $\{(PO\text{-}3,5\text{-}^tBu_2)PdMe\}_2$ ($[PO\text{-}3,5\text{-}^tBu_2]^-$ = *o*–{(3,5–^{t}Bu$_2$–Ph)$_2$P}–*p*–toluenesulfonate) [21] were synthesized by literature procedures. NMR spectra were recorded on Bruker DMX-500 or DRX-400 spectrometers in Teflon-valved J. Young tubes at ambient temperature unless otherwise indicated. Valved J. Young tubes were silylated by neat TMSCl, washed with acetone and dried in an oven overnight for reactions with CO_2. ^1H and $^{13}C\{^1H\}$ chemical shifts are reported relative to $SiMe_4$ and were determined by reference to the residual ^1H and ^{13}C solvent resonances. Assignments were made with the aid of ^{31}P decoupling experiments, COSY, NOESY, HMQC and HMBC NMR. $^{31}P\{^1H\}$ NMR spectra were referenced externally to 85 % H_3PO_4 (δ 0). $^7Li\{^1H\}$ NMR spectra were referenced externally to 1 M LiCl/D_2O (δ 0). Coupling constants are given in Hz. The numbering scheme for NMR assignment is given in Figure 2.16.

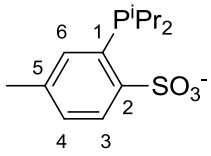

Figure 2.16. Numbering scheme used for NMR assignments.

X-Ray Crystallography. Crystallographic data are summarized in Table 2.1. Full details (CIF files and reports) are also provided in the accompanying information. Data were collected on a Bruker Smart Apex diffractometer using Mo K_α radiation (0.71073 Å). Direct methods were used to locate many atoms from the E-map. Repeated difference Fourier maps allowed location of all expected non-hydrogen atoms. Following anisotropic refinement of all non-H atoms, ideal H-atom positions were calculated. Final refinement was anisotropic for all non-H atoms, and isotropic-riding for H atoms. ORTEP diagrams are drawn with 50 % probability ellipsoids. Specific comments for each structure are as follows. **H[PO-^{i}Pr] ([PO-^{i}Pr]- = 2–P^{i}Pr$_2$–4–Me–C$_6$H$_3$SO$_3^-$):** Crystals of H[PO-^{i}Pr] were obtained by crystallization from saturated THF/CH_2Cl_2 solution at room temperature. No anomalous bond lengths or thermal parameters were noted. **3a**: Crystals of **3a** were obtained by layering pentane onto a solution of **3a** in THF at -35 ℃. No anomalous bond lengths or thermal parameters were noted. Because of the small crystal size, intensities were rather weak. The largest residual electron density is associated with the Pd atom. **(PO-^{i}Pr)PdMe(py):** Crystals of (PO-^{i}Pr)PdMe(py) were obtained by crystallization from saturated toluene solution at room temperature. No anomalous bond lengths or thermal parameters were noted. ***Trans*–P,P–(PO-^{i}Pr)$_2$Pd:** Crystals of *trans*–P,P–(PO-^{i}Pr)$_2$Pd were obtained by crystallization from CD_2Cl_2 at -78 ℃. No anomalous bond lengths or thermal parameters were noted although the solvent showed slight disorder. **6**: Crystals of **6** were obtained by slow diffusion of hexanes into a solution of **6** in THF/toluene (ca. 1/10 v/v) at -40 ℃. There were two slightly disordered toluene molecules and another disordered solvent cluster in the unit cell. The solvent atoms were removed and the program SQUEEZE used to obtain solvent-free intensities. This calculation gave 677 e^-/cell. No anomalous bond lengths or thermal parameters were noted.

Table 2.1. Summary of X-ray Diffraction Data for H[PO-^{i}Pr], **3a**, (PO-^{i}Pr)PdMe(py)**,** *trans*–P,P–(PO-^{i}Pr)$_2$Pd and **6**.

	H[(PO-^{i}Pr)]	**3a**	(PO-^{i}Pr) PdMe(py)	*trans*–P,P–(PO-^{i}Pr)$_2$Pd	**6**
Formula	$C_{13}H_{21}O_3PS$	$C_{46}H_{84}Li_2O_{10}P_2Pd_2S_2$	$C_{19}H_{28}NO_3PPdS$	$C_{26}H_{40}O_6P_2PdS_2$ + 2 CH_2Cl_2	$C_{66}H_{80}Li_2O_{12}P_2Pd_2S_2$
Formula weight	288.33	1149.87	487.85	850.89	1418.04
Crystal system	Monoclinic	Monoclinic	Monoclinic	Monoclinic	Orthorhombic
Space group	$P2_1/c$	$P2_1/c$	$C2/c$	$P2_1/c$	$P2_12_12_1$
a (Å)	7.6417(5)	11.064(5)	29.166(8)	11.564(11)	13.976(4)
b (Å)	15.5087(10)	17.858(8)	9.204(2)	11.102(10)	21.636(7)
c (Å)	13.6509(7)	14.970(5)	15.971(4)	16.492(11)	26.011(8)
β (deg)	118.792(3)	117.41(2)	102.135(4)	122.57(5)	90.0
V (Å^3)	1417.80(15)	2625.7(19)	4191.4(19)	1784(3)	7865(4)
Z	4	2	8	2	4
T (K)	100	100	100	100	100
Color, habit	clear, plate	clear, rhomb	clear, fragment	pale yellow, fragment	clear, fragment

Table 2.1. (Continued)

GOF on F^2	1.028	0.715	0.953	0.984	0.778
R indices ($I > 2\sigma(I)$)[a]	R1 = 0.0324 wR2 = 0.0869	R1 = 0.0546 wR2 = 0.0970	R1 = 0.0352, wR2 = 0.0731	R1 = 0.0601 wR2 = 0.1267	R1 = 0.0548 wR2 = 0.0924
R indices (all data)[a]	R1 = 0.0341 wR2 = 0.0882	R1 = 0.0861 wR2 = 0.1154	R1 = 0.0475 wR2 = 0.0759	R1 = 0.0855 wR2 = 0.1414	R1 = 0.0994 wR2 = 0.1015

[a] $R1 = \Sigma||F_o| - |F_c|| / \Sigma|F_o|$; $wR2 = [\Sigma[w(F_o^2 - F_c^2)^2] / \Sigma[w(F_o^2)^2]]^{1/2}$, where $w = q[\sigma^2(F_o^2) + (aP)^2 + bP]^{-1}$

Synthesis, Reactions and Characterization of Compounds

Reaction of $[Cp_2ZrMe(C_6D_5Cl)][B(C_6F_5)_4]$ (1) and CO_2. A J. Young NMR tube was charged with Cp_2ZrMe_2 (**2**) (0.0131 g, 0.0521 mmol) and $[Ph_3C][B(C_6F_5)_4]$ (0.0480 g, 0.0520 mmol), and C_6D_5Cl (0.5 mL) was added by vacuum transfer at -196 °C. The tube was immediately protected from light, vigorously shaken and then maintained at room temperature for 1.5 h. NMR analysis showed that formation of $[Cp_2ZrMe(C_6D_5Cl)][B(C_6F_5)_4]$ (**1**) was complete. The tube was exposed to CO_2 (1 atm, 0.1 mmol) at room temperature, sealed, and shaken. An orange-yellow gelatinous material formed immediately, which coated the tube, and a

small amount of red solution remained. The tube was re-exposed to CO_2 until completely consuming the red solution and leaving only the gel. A small amount of THF-d_8 was vacuum transferred into the tube, at -196 °C. The tube was warmed to room temperature and the gel immediately dissolved to afford an orange-yellow solution. ^{1}H NMR analysis showed that complete conversion to Ph_3CMe and $[Cp_2Zr(OAc)(THF\text{-}d_8)][B(C_6F_5)_4]$ had occurred. Data for **2**: ^{1}H NMR (C_6D_5Cl): δ 5.86 (s, Cp, 10 H), -0.23 (s, Me, 6 H). $^{13}C\{^1H\}$ NMR (C_6D_5Cl): δ 110.4 (Cp), 30.3 (Me). Data for **1**: ^{1}H NMR (C_6D_5Cl): δ 5.88 (s, Cp, 10 H), 0.67 (s, Me, 3 H). Data for Ph_3CMe: ^{1}H NMR (C_6D_5Cl; before reaction of **1** with CO_2): δ 7.09 (m), 2.01 (s, 3 H). ^{1}H NMR (THF-d_8): δ 7.14 (m, 15 H, *Ph*$_3$CMe), 2.16 (s, 3 H, Ph_3C*Me*). ^{1}H NMR (C_6D_5Cl; after reaction of **1** with CO_2): δ 7.13 (m), 2.08 (s, 3 H). $^{13}C\{^1H\}$ NMR (C_6D_5Cl; after reaction of **1** with CO_2): δ 149.4 (*Ph*$_3$CMe), 129.0 (*Ph*$_3$CMe), 128.1 (*Ph*$_3$CMe), 126.2 (*Ph*$_3$CMe), 52.8 (Ph_3*C*Me), 30.5 (Ph_3C*Me*). Data for $[Cp_2Zr(OAc)(THF\text{-}d_8)][B(C_6F_5)_4]$. ^{1}H NMR (THF-$d_8$): δ 6.50 (s, Cp, 10 H), 2.07 (s, OAc, 3 H). ^{1}H NMR (C_6D_5Cl): δ 6.09 (s, Cp, 10 H), 1.90 (s, OAc, 3 H). $^{13}C\{^1H\}$ NMR (THF-d_8): δ 188.5 (O*C*(O)Me), 149.0 (d, $^1J_{CF}$ = 236, $B(C_6F_5)_4^-$), 138.9 (d, $^1J_{CF}$ = 244, $B(C_6F_5)_4^-$), 137.0 (d, $^1J_{CF}$ = 242, $B(C_6F_5)_4^-$), 125.0 (br s, *ipso*-$B(C_6F_5)_4^-$), 117.1 (Cp), 22.4 (OC(O)*Me*). $^{13}C\{^1H\}$ NMR (C_6D_5Cl): δ 187.9 (O*C*(O)Me), 148.8 (d, $^1J_{CF}$ = 240, $B(C_6F_5)_4^-$), 138.7 (d, $^1J_{CF}$ = 242, $B(C_6F_5)_4^-$), 136.8 (d, $^1J_{CF}$ = 243, $B(C_6F_5)_4^-$), 125.0 (br s, *ipso*-$B(C_6F_5)_4^-$), 115.9 (Cp), 22.1 (OC(O)*Me*). These data agree with the data reported by Wendt in ref 2 in the text.

Reaction of Cp_2ZrMe_2 (2) with CO_2. A J. Young NMR tube was charged with **2** (0.0118 g, 0.0469 mmol) and C_6D_5Cl (0.66 mL) was added by vacuum transfer at -196 °C. The tube was warmed to room temperature, exposed to CO_2 (1 atm, 0.087 mmol), and heated to 100 °C in an oil bath. Periodically, the tube was removed from the oil bath and NMR spectra were

recorded at room temperature. After 6 d at 100 °C, 75 % conversion to the known $Cp_2ZrMeOAc$ was observed. Data for $Cp_2ZrMeOAc$: ^1H NMR (C_6D_5Cl): δ 5.83 (s, Cp, 10 H), 1.73 (s, OAc, 3 H), 0.32 (s, Me, 3 H). These data agree with the data in ref 8 in the text. $^{13}C\{^1H\}$ NMR (C_6D_5Cl): δ 187.6 (O*C*(O)Me), 111.0 (Cp), 31.9 (Me), 22.8 (OC(O)*Me*).

2–P^{i}Pr$_2$–4–Me–C$_6$H$_3$SO$_3$Li (Li[PO-^{i}Pr]). Anhydrous *p*-toluenesulfonic acid (1.05 g, 6.09 mmol) was dissolved in THF (40 mL) and the solution was stirred at 0 °C. A solution of BuLi in THF (2.5 M, 4.7 mL, 12 mmol) was added dropwise giving a white suspension. The mixture was warmed to room temperature and stirred for 15 min. (^{i}Pr)$_2$PCl (0.91 mL, 5.7 mmol) was added dropwise forming a clear yellow solution. The mixture was stirred at room temperature for 1 d. The volatiles were removed under vacuum to give a pale yellow solid. The solid was taken up in CH_2Cl_2 and the mixture was filtered through Celite. The filtrate was evaporated under vacuum. The residue was taken up in Et_2O and filtered to afford a pale yellow solid. The solid was washed with Et_2O and THF and dried under vacuum, yielding a white solid (1.17 g, 65% vs. *p*–toluenesulfonic acid). ^1H NMR analysis showed that this material contained 0.2 equiv of THF. ^1H NMR (THF-d_8): δ 7.97 (dd, $^3J_{HH}$ = 8, $^4J_{PH}$ = 4, 1 H, H^3), 7.38 (br s, 1 H, H^6), 7.07 (dd, $^3J_{HH}$ = 8, $^5J_{PH}$ = 2, 1 H, H^4), 2.34 (s, 3 H, C*H*$_3$-ArSO$_3$), 2.12 (d of septets, $^2J_{PH}$ = 7, $^3J_{HH}$ = 4, 2 H, C*H*Me$_2$), 1.15 (dd, $^4J_{PH}$ = 14, $^3J_{HH}$ = 7, 6 H, CH*Me*$_2$), 0.93 (dd, $^4J_{PH}$ = 13, $^3J_{HH}$ = 7, 6 H, CH*Me*$_2$). $^{31}P\{^1H\}$ NMR (THF-d_8): δ 1.0. ESI–MS (CH_2Cl_2, negative ion mode) *m*/*z* 287.0 (M – Li$^+$)$^-$, 581.0 (M$_2$ – Li$^+$)$^-$.

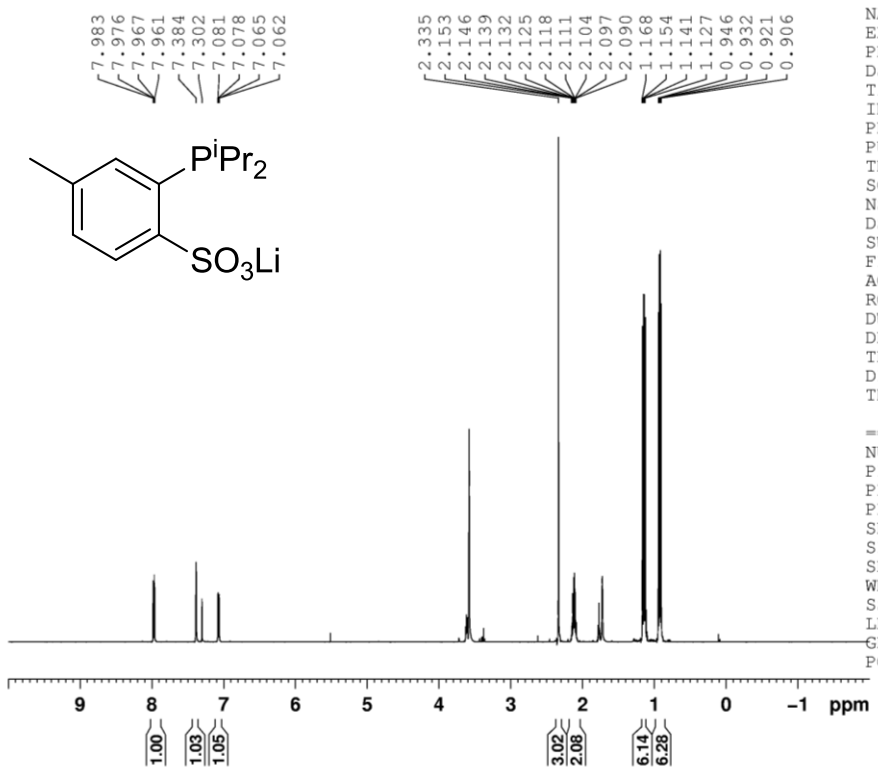

NAME	KCL1022
EXPNO	22
PROCNO	1
Date_	20110802
Time	17.03
INSTRUM	spect
PROBHD	5 mm PAQNP 1H/
PULPROG	zg
TD	44998
SOLVENT	THF
NS	8
DS	0
SWH	10000.000 Hz
FIDRES	0.222232 Hz
AQ	2.2499499 sec
RG	456
DW	50.000 usec
DE	71.43 usec
TE	295.2 K
D1	10.00000000 sec
TD0	1
======== CHANNEL f1 ========	
NUC1	1H
P1	12.00 usec
PL1	0.00 dB
PL1W	24.54113007 W
SFO1	500.1330008 MHz
SI	16384
SF	500.1300143 MHz
WDW	no
SSB	0
LB	0.00 Hz
GB	0
PC	1.00

^{31}P

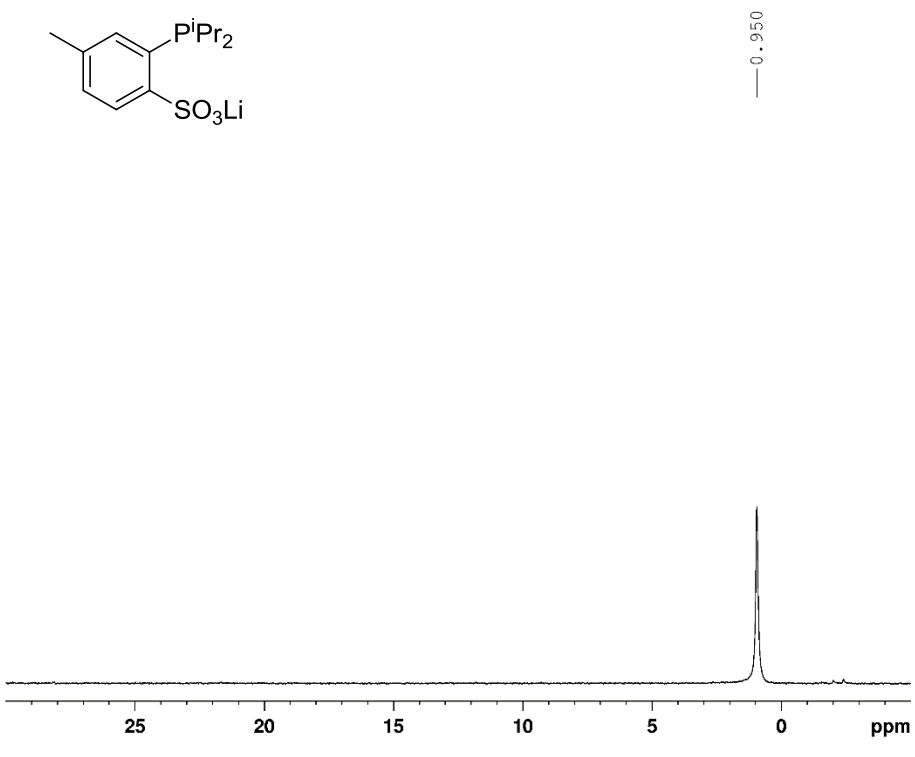

NAME	KCL1045
EXPNO	2
PROCNO	1
Date_	20120118
Time	13.54
INSTRUM	spect
PROBHD	5 mm PAQNP 1H/
PULPROG	zgpg
TD	244560
SOLVENT	THF
NS	38
DS	4
SWH	40760.871 Hz
FIDRES	0.166670 Hz
AQ	2.9999859 sec
RG	2890
DW	12.267 usec
DE	6.00 usec
TE	295.5 K
D1	3.00000000 sec
D11	0.03000000 sec
TD0	1
======== CHANNEL f1 ========	
NUC1	31P
P1	11.00 usec
PL1	3.00 dB
PL1W	41.92221451 W
SFO1	202.4745561 MHz
======== CHANNEL f2 ========	
CPDPRG2	waltz16
NUC2	1H
PCPD2	100.00 usec
PL2	120.00 dB
PL12	16.50 dB
PL13	17.00 dB
PL2W	0.00000000 W
PL12W	0.54940748 W
PL13W	0.48965994 W
SFO2	500.1325000 MHz
SI	32768
SF	202.4558035 MHz
WDW	EM
SSB	0
LB	3.00 Hz
GB	0
PC	1.40

H[PO-^{i}Pr]. This species was synthesized for use in the synthesis of (PO-^{i}Pr)PdMe(THF) and **5**. Anhydrous *p*-toluenesulfonic acid (1.09 g, 6.33 mmol) was dissolved in THF (40 mL) and stirred at 0 °C. A solution of ^{n}Hexyl-lithium (5.5 mL, 6.8 mmol, 2.3 M in hexane) was added dropwise giving a white suspension. The mixture was warmed to room temperature and stirred for 15 min. (^{i}Pr)$_2$PCl (1.0 mL, 6.3 mmol) was added dropwise forming a clear yellow solution. The mixture was stirred at room temperature for 1 d. After 1 d, the volatiles were removed under vacuum to give a pale yellow solid. The solid was taken up in HCl/H_2O solution and the pH was adjusted to ~2 using HCl or $NaHCO_3$. The mixture was extracted with CH_2Cl_2 three times (40 mL total) and the combined extract was dried over $MgSO_4$ and taken to dryness under vacuum overnight to give a pale yellow solid. The solid was taken up in Et_2O to give a white suspension, which was filtered to afford an off-white solid. The solid was washed with Et_2O and THF and dried under vacuum to yield a white solid (0.936 g, 51 % vs. *p*–toluenesulfonic acid). ^{1}H NMR (THF-d_8): δ 8.02 (apparent br t, 1 H, H^{3}; this resonance collapses to a doublet with $^{3}J_{HH}$ = 8 in the {^{31}P} spectrum), 7.63 (d, $^{3}J_{HH}$ = 8, 1 H, H^{4}), 7.34 (d, $^{3}J_{PH}$ = 16, 1 H, H^{6}), 5.15 (br d, $^{1}J_{PH}$ = 365, 1 H, H-P) 3.40 (br s, 2 H, C*H*Me$_2$), 2.45 (s, 3 H, C*H*$_3$-ArSO$_3$), 1.48 (dd, $^{4}J_{PH}$ = 19, $^{3}J_{HH}$ = 7, 6 H, CH*Me$_2$*), 1.22 (br dd, $^{4}J_{PH}$ = 21, $^{3}J_{HH}$ = 7, 6 H, CH*Me$_2$*). ^{31}P{^{1}H} NMR (THF-d_8): δ 65.5. ESI–MS (CH_2Cl_2/MeOH, positive ion mode): *m*/*z* 289.0 $(M + H^+)^+$, 577.2 $(M_2 + H^+)^+$. Mp: 177–178 ° C.

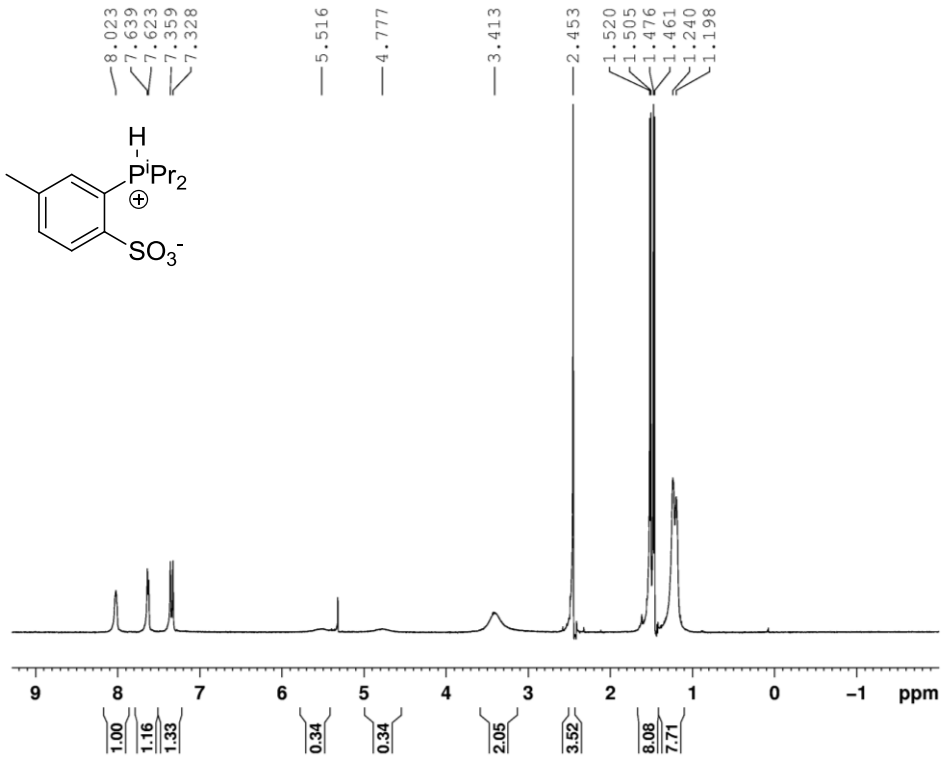


```
NAME              KCL1065
EXPNO                   1
PROCNO                  1
Date_            20110825
Time                 9.56
INSTRUM             spect
PROBHD   5 mm PAQNP 1H/
PULPROG                zg
TD                  59998
SOLVENT            CD2Cl2
NS                      8
DS                      0
SWH             10000.000
FIDRES          0.166672
AQ              2.9999499
RG                    406
DW                 50.000
DE                  71.43
TE                  294.9
D1             10.00000000
TD0                     1

======== CHANNEL f1 ===
NUC1                   1H
P1                  12.00
PL1                  0.00
PL1W         24.54113007
SFO1         500.1330008
SI                  16384
SF           500.1300175
WDW                   no
SSB                    0
LB                  0.00
GB                     0
PC                  1.00
```

$^{31}P\{^{1}H\}$

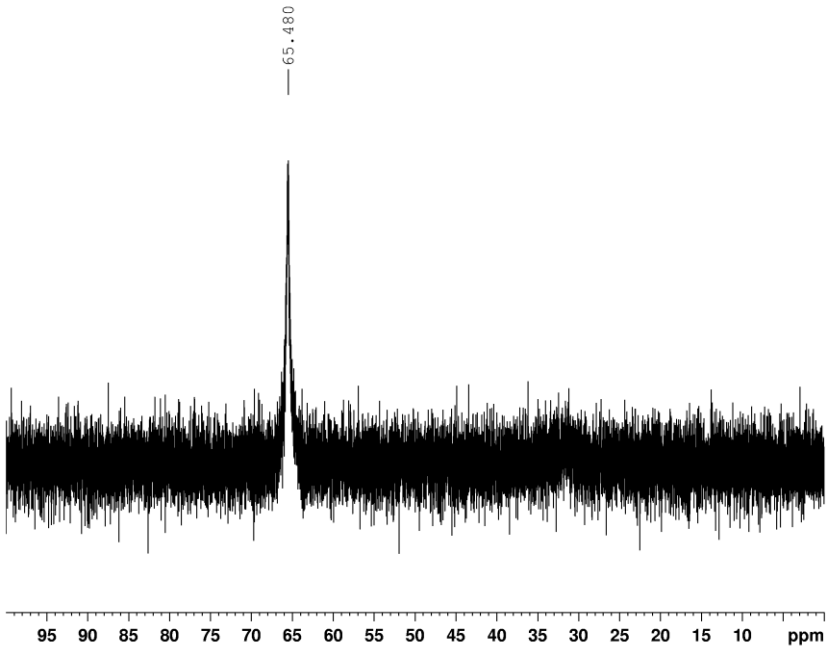


```
NAME              KCL1065
EXPNO                   2
PROCNO                  1
Date_            20110825
Time                10.00
INSTRUM             spect
PROBHD   5 mm PAQNP 1H/
PULPROG             zgpg
TD                 244560
SOLVENT           CD2Cl2
NS                     21
DS                      4
SWH           40760.871 Hz
FIDRES         0.166670 Hz
AQ             2.9999859 sec
RG                  2890
DW                12.267 use
DE                  6.00 use
TE                 295.4 K
D1           3.00000000 sec
D11          0.03000000 sec
TD0                     1

======== CHANNEL f1 =======
NUC1                  31P
P1                 11.00 use
PL1                 3.00 dB
PL1W        41.92221451 W
SFO1       202.4705069 MHz

======== CHANNEL f2 =======
CPDPRG2          waltz16
NUC2                  1H
PCPD2              100.00 use
PL2                120.00 dB
PL12                16.50 dB
PL13                17.00 dB
PL2W         0.00000000 W
PL12W        0.54940748 W
PL13W        0.48965994 W
SFO2       500.1325000 MHz
SI                  32768
SF         202.4558604 MHz
WDW                   no
SSB                    0
LB                  0.00 Hz
GB                     0
PC                  1.40
```

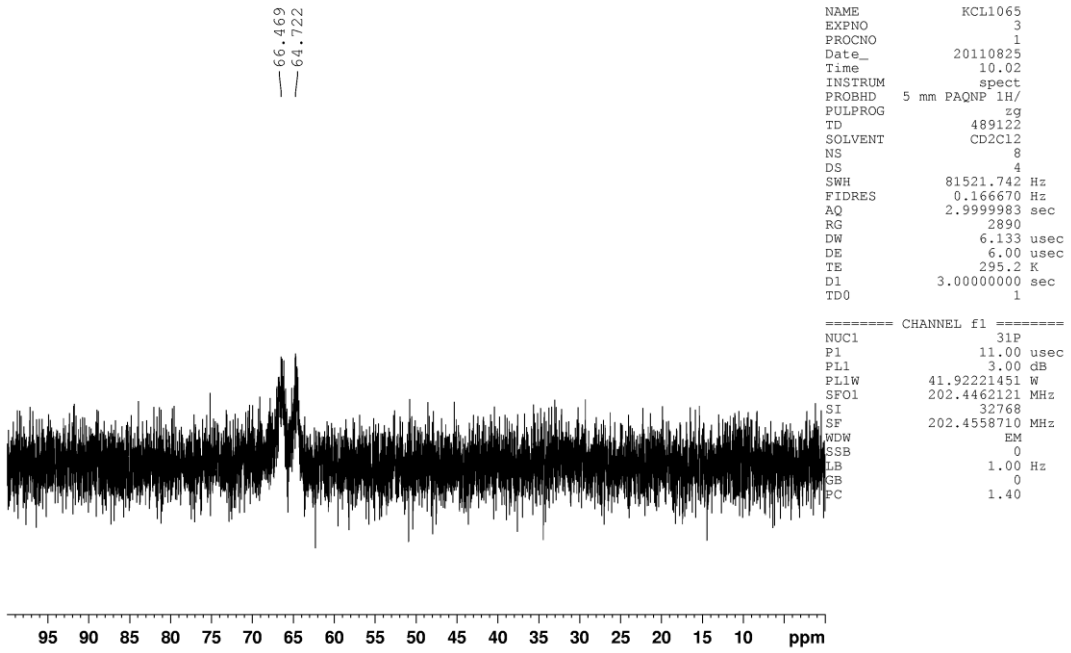
66.469
64.722
NAME KCL1065
EXPNO 3
PROCNO 1
Date_ 20110825
Time 10.02
INSTRUM spect
PROBHD 5 mm PAQNP 1H/
PULPROG zg
TD 489122
SOLVENT CD2Cl2
NS 8
DS 4
SWH 81521.742 Hz
FIDRES 0.166670 Hz
AQ 2.9999983 sec
RG 2890
DW 6.133 usec
DE 6.00 usec
TE 295.2 K
D1 3.00000000 sec
TD0 1
======== CHANNEL f1 ========
NUC1 31P
P1 11.00 usec
PL1 3.00 dB
PL1W 41.92221451 W
SFO1 202.4462121 MHz
SI 32768
SF 202.4558710 MHz
WDW EM
SSB 0
LB 1.00 Hz
GB 0
PC 1.40
95 90 85 80 75 70 65 60 55 50 45 40 35 30 25 20 15 10 ppm

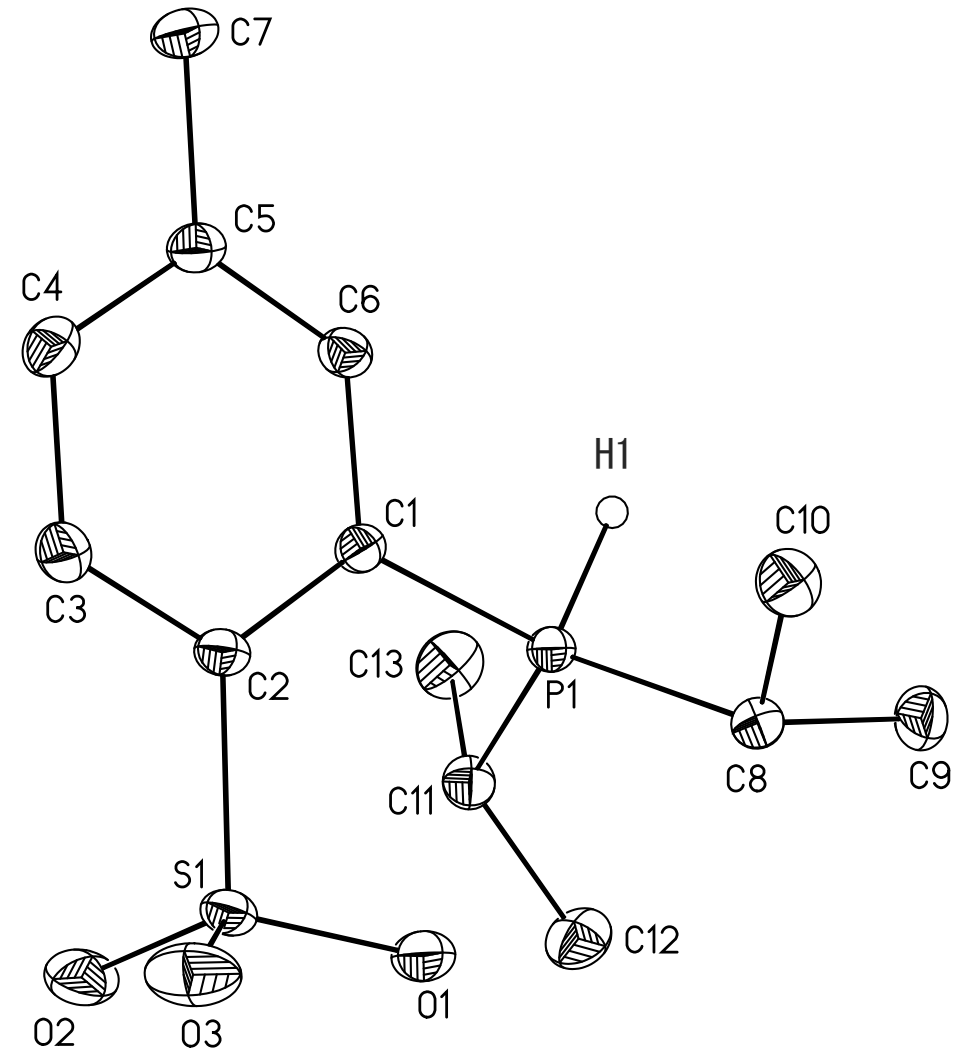

Figure 2.17. Molecular structure of H[(PO-^{i}Pr)]. Hydrogen and solvent atoms are omitted except the hydrogen atom bonded to the P atom. Selected bond lengths (Å) and angles (deg): P1–H1 1.28(2), P1–C8 1.827(1), P1–C11 1.834(1), P1–C1 1.805(1), C8–P1–C11 121.05(6), C1–P1–C11 110.95(6), C8–P1–C1 115.56(6).

(COD)PdMe$_2$.[22] Et_2O (40 mL) was added to (COD)$PdCl_2$ (972 mg, 3.40 mmol) and the mixture was stirred at -78 °C to give a yellow suspension. A solution of MeMgCl in THF (3.0 M, 2.2 mL, 6.6 mmol) was added dropwise and the mixture was stirred at -40 °C for 5.5 h. The

volatiles were removed under vacuum at 0 °C to yield a dark grey solid. The solid was extracted with pentane (80 mL) at 0 °C. The extract was taken to dryness under vacuum at 0 °C to yield a white solid (393 mg, 47 %). **2** is stable in the solid state or in solution for 1 h at 0 °C but decomposes readily at higher temperatures. **2** was stored as a solid below -30 °C. ^{1}H NMR (CD_2Cl_2): δ 5.39 (br s, 4 H, =CH), 2.45 (m, 8 H, CH_2), 0.25 (s, 6 H, CH_3).

{[Li(THF)$_2$][(PO-^{i}Pr)PdMe$_2$]}$_2$ (3a). Li[PO-^{i}Pr] (183 mg, 0.621 mmol) and (COD)$PdMe_2$ (157 mg, 0.645 mmol) were dissolved in THF (9 mL) that was pre-cooled at -35 °C. Pentane (11 mL) that was pre-cooled at -35 °C was layered on top and the mixture was cooled to -35 °C for 1 d to produce a slurry of a white solid in a yellowish green supernatant. The supernatant was removed by pipette and the white solid was washed with pentane and dried under vacuum (195 mg, 55 %). In the ^{1}H NMR spectrum, H^6 was assigned by a $^1H\{^{31}P\}$ experiment that collapsed H^3 and H^4 to doublets and H^6 to a singlet, and H^3 and H^4 were assigned by comparing their chemical shifts to those for other phosphine-sulfonate palladium(II) analogues. The C*H*Me_2, C*H*$_3$–$ArSO_3$, C*H*Me_2, and Pd–C*H*$_3$ resonances were assigned by peak integration and resolving the coupling patterns with the aid of a $^1H\{^{31}P\}$ spectrum. In the $^{13}C\{^1H\}$ NMR spectrum, C^3, C^4, C^6, *C*HMe_2, *C*H_3–$ArSO_3$, CH*Me*$_2$, and the two Pd–*C*H_3 carbons were assigned by a HMQC-NMR experiment. The Pd–*C*H_3 carbons (*cis* and *trans* to P) were assigned based on $^2J_{PC}$ values; these assignments enabled assignment of the Pd–C*H*$_3$ resonances in the ^{1}H NMR spectrum via HMQC–NMR. C^1, C^2, C^5 were assigned by HMBC–NMR and comparing their chemical shifts to values for model compounds. ^{1}H NMR (THF-d_8): δ 7.98 (dd, $^3J_{HH}$ = 8, $^4J_{HP}$ = 4, 1 H, H^3), 7.45 (d, $^3J_{PH}$ = 5, 1 H, H^6), 7.20 (d, $^3J_{HH}$ = 8, 1 H, H^4), 2.40 (m, partly obscured by C*H*$_3$–$ArSO_3$, 2 H, C*H*Me_2), 2.36 (s, 3 H, C*H*$_3$–$ArSO_3$), 1.22 (dd, $^4J_{PH}$ = 16, $^3J_{HH}$ = 8, 6 H, CH*Me*$_2$), 1.13 (dd, $^4J_{PH}$ =

15, $^{3}J_{HH}$ = 7, 6 H, CH*Me*$_2$), 0.06 (d, $^{3}J_{PH}$ = 8, 3 H, Pd-C*H*$_3$ *cis* to P), -0.04 (d, $^{3}J_{PH}$ = 8, 3 H, Pd–C*H*$_3$ *trans* to P). ^{31}P{^{1}H} NMR (THF-d_8): δ 13.3. ^{13}C{^{1}H} NMR (THF-d_8): δ 148.8 (d, J_{PC} = 15, C^{2}), 139.9 (C^{5}), 134.9 (C^{6}), 132.3 (d, J_{PC} = 5, C^{1}), 130.2 (C^{4}), 128.6 (d, J_{PC} = 6, C^{3}), 25.6 (d, J_{PC} = 10, *C*HMe$_2$), 21.0 (s, *C*H$_3$-ArSO$_3$), 19.5 (d, J_{PC} = 9, CH*Me*$_2$), 18.9 (d, J_{PC} = 4, CH*Me*$_2$), 7.7 (d, $^{2}J_{PC}$ = 112, Pd–*C*H$_3$ *trans* to P), -13.9 (d, $^{2}J_{PC}$ = 7, Pd–*C*H$_3$ *cis* to P). ^{7}Li{^{1}H} NMR (THF-d_8): δ -2.4. ESI–MS (THF, positive ion mode) *m*/*z* 723.0 (M – (PO)PdMe$_2^-$)$^+$, 867.0 (M + Li$^+$ – 4 THF)$^+$. Crystals suitable for X-ray diffraction analysis were obtained by layering pentane onto THF solution at -35 °C. The complex is too thermally unstable for elemental analysis.

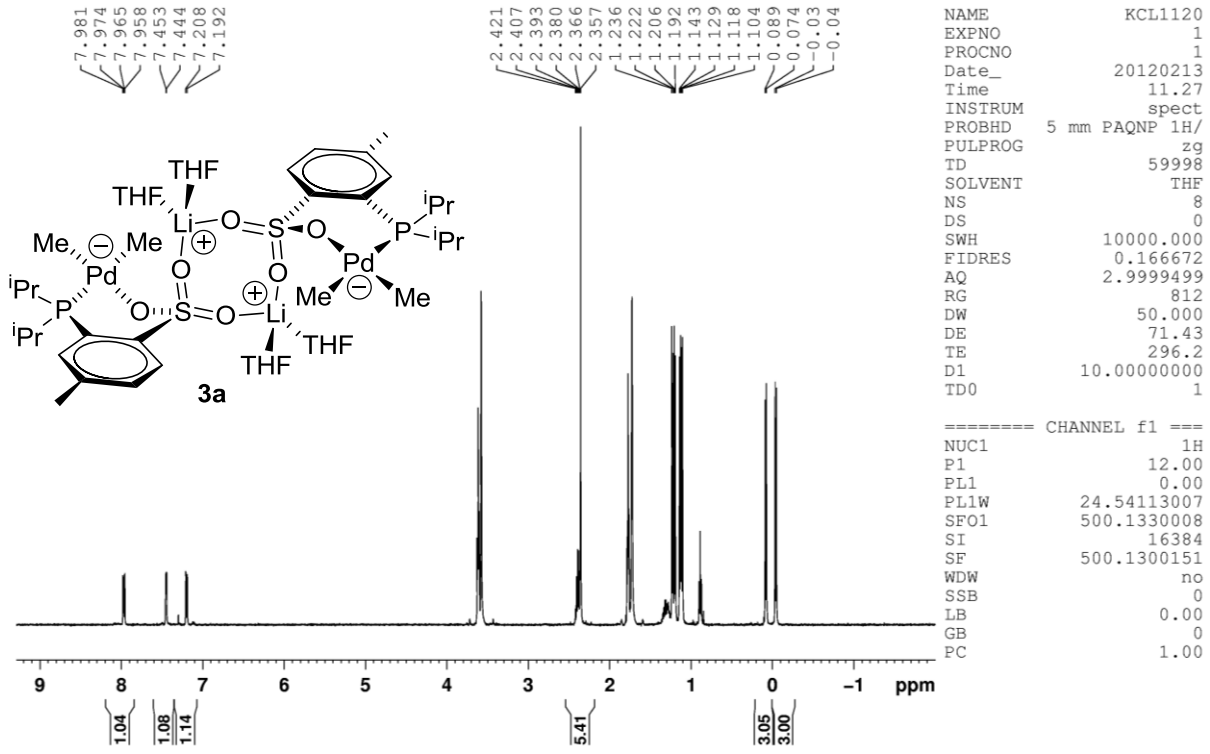

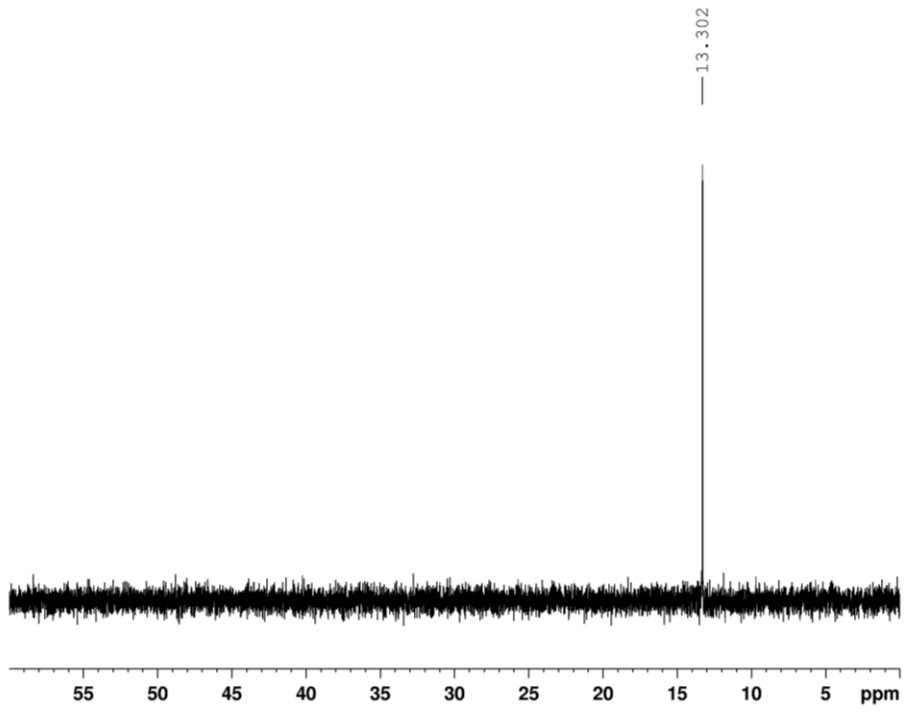


```
NAME            KCL1120
EXPNO                 2
PROCNO                1
Date_          20120213
Time              11.31
INSTRUM           spect
PROBHD   5 mm PAQNP 1H/
PULPROG            zgpg
TD                244560
SOLVENT              THF
NS                    26
DS                     4
SWH            40760.871 Hz
FIDRES         0.166670 Hz
AQ             2.9999859 sec
RG                  2890
DW                12.267 use
DE                 6.00 use
TE                297.1 K
D1            3.00000000 sec
D11           0.03000000 sec
TD0                   1

======== CHANNEL f1 =======
NUC1                31P
P1                11.00 use
PL1                3.00 dB
PL1W         41.92221451 W
SFO1        202.4705069 MHz

======== CHANNEL f2 =======
CPDPRG2          waltz16
NUC2                1H
PCPD2             100.00 use
PL2               120.00 dB
PL12               16.50 dB
PL13               17.00 dB
PL2W          0.00000000 W
PL12W         0.54940748 W
PL13W         0.48965994 W
SFO2        500.1325000 MHz
SI                 32768
SF          202.4557845 MHz
WDW                   no
SSB                    0
LB                 0.00 Hz
GB                     0
PC                  1.40
```

^{13}C

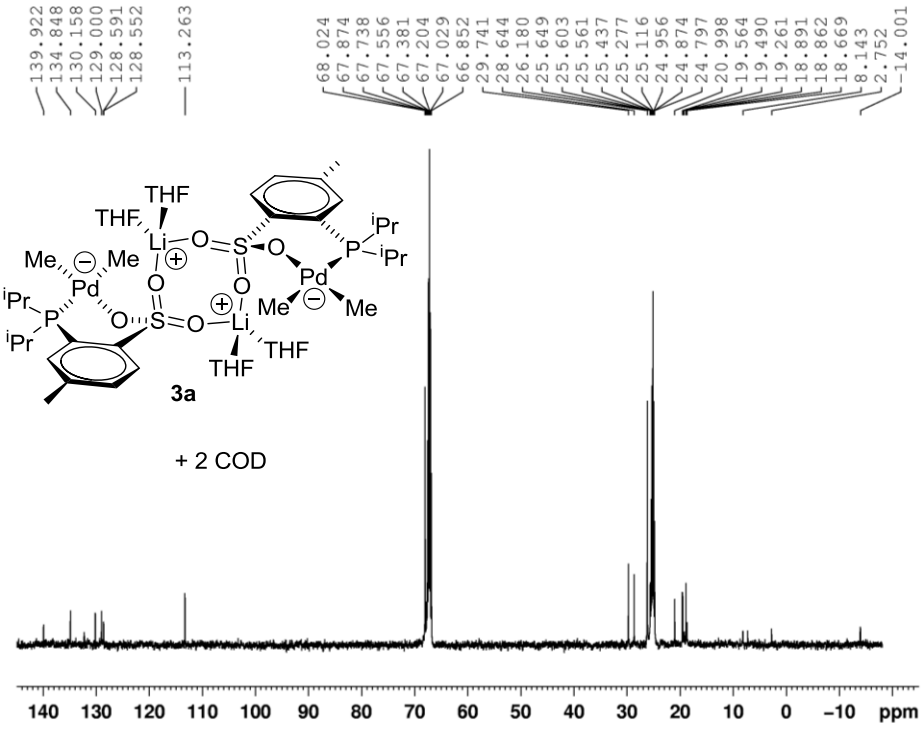


```
NAME      Li[PO-iPr2]PdMe2
EXPNO                   2
PROCNO                  1
Date_            20110601
Time                17.13
INSTRUM             spect
PROBHD   5 mm PAQNP 1H/
PULPROG              zgpg
TD                 197364
SOLVENT               THF
NS                     93
DS                      4
SWH             32894.738 Hz
FIDRES          0.166670 Hz
AQ              2.9999828 sec
RG                   2050
DW                 15.200 use
DE                  6.00 use
TE                 296.7 K
D1             5.00000000 sec
D11            0.03000000 sec
TD0                    1

======== CHANNEL f1 =======
NUC1                  13C
P1                  8.00 use
PL1                 1.00 dB
PL1W          72.42802429 W
SFO1         125.7716224 MHz

======== CHANNEL f2 =======
CPDPRG2           waltz16
NUC2                  1H
PCPD2              80.00 use
PL2                 0.00 dB
PL12               16.50 dB
PL13               17.00 dB
PL2W          24.54113007 W
PL12W          0.54940748 W
PL13W          0.48965994 W
SFO2         500.1325006 MHz
SI              131072
SF           125.7574554 MHz
WDW                   EM
SSB                    0
LB                 3.00 Hz
GB                     0
PC                  1.40
```

^{7}Li

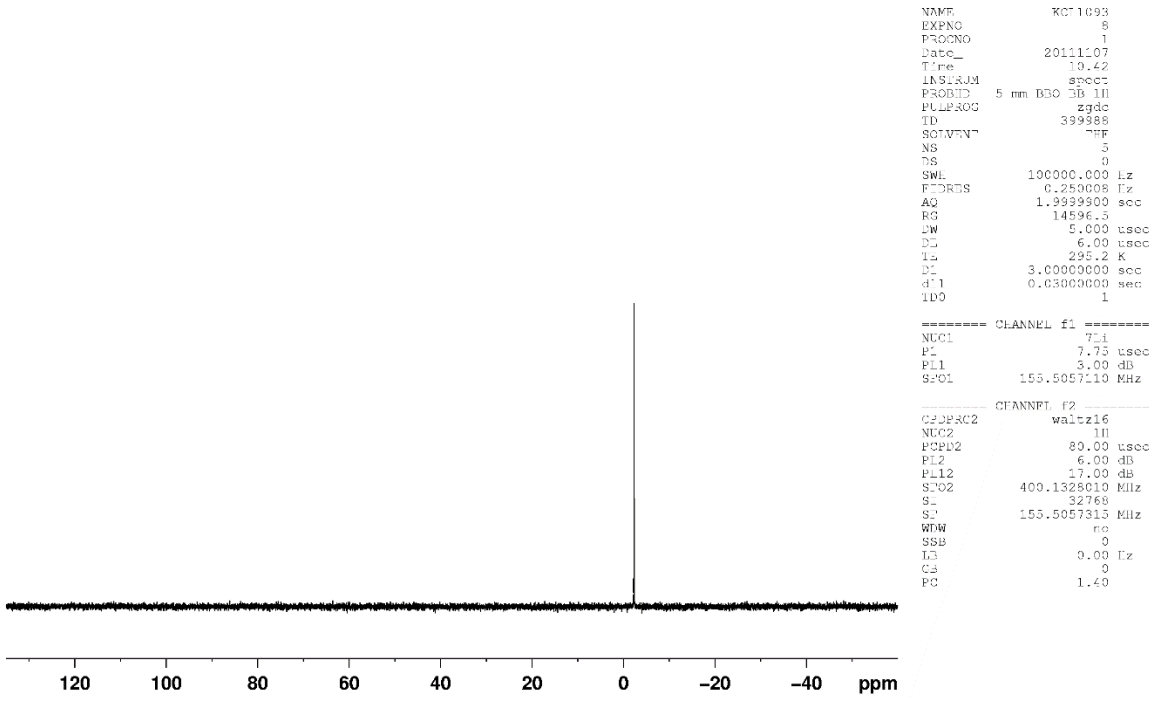

Generation of [Li(Crypt211)][(PO-^{i}Pr)PdMe$_2$] (Crypt211 = 4,7,13,18–tetraoxa–1,10–diazabicyclo[8.5.5]eicosane, 3b). A valved J. Young NMR tube was charged with **3a** (2.5 mg, 0.0022 mmol) and Crypt211 (0.0045 mmol). THF-d_8 (0.50 mL) was added by vacuum transfer at -196 ˚C. The reaction mixture was thawed at room temperature and NMR spectra were recorded. ^{1}H NMR (THF-d_8): δ 7.96 (dd, $^{3}J_{HH}$ = 8, $^{4}J_{PH}$ = 4, 1 H, H^{3}), 7.33 (d, $^{3}J_{PH}$ = 5, 1 H, H^{6}), 7.08 (d, $^{3}J_{HH}$ = 8, 1 H, H^{4}), 3.91 (m, 4 H, Crypt), 3.57 (m, 38 H, Crypt), 3.42 (t, J_{HH} = 5, 6 H, Crypt), 3.09 (m, 4 H, Crypt), 2.67 (m, 24 H, Crypt), 2.53 (m, 5 H, Crypt), 2.40 (octet, $^{2}J_{PH}$ = $^{3}J_{HH}$ = 7, 2 H, C*H*Me$_2$), 2.31 (s, 3 H, C*H*$_3$–ArSO$_3$), 1.21 (dd, $^{4}J_{PH}$ = 14, $^{3}J_{HH}$ = 7, 6 H, CH*Me$_2$*), 1.13 (dd, $^{4}J_{PH}$ = 13, $^{3}J_{HH}$ = 7, 6 H, CH*Me$_2$*), 0.01 (d, $^{3}J_{PH}$ = 8, 3 H, Pd–C*H*$_3$ *trans* to P), -0.07 (d, $^{3}J_{PH}$ = 8, 3 H, Pd–C*H*$_3$ *cis* to P). ^{31}P{^{1}H} NMR (THF-d_8): δ 12.4. ^{13}C{^{1}H} NMR (THF-d_8): δ 152.3 (d, J_{PC} = 19, C^{2}), 137.6 (d, J_{PC} = 2, C^{5}), 133.7 (d, J_{PC} = 2, C^{6}), 131.9 (d, J_{PC} = 7, C^{1}), 129.3 (d, J_{PC} = 2, C^{4}),

128.8 (d, J_{PC} = 5, C^3), 69.4 (Crypt), 67.8 (Crypt), 66.7 (Crypt), 52.5 (Crypt), 51.5 (Crypt), 25.6 (d, J_{PC} = 7, CHMe$_2$), 21.0 (s, CH$_3$–ArSO$_3$), 19.6 (d, J_{PC} = 8, CHMe_2), 19.4 (d, J_{PC} = 3, CHMe_2), 8.3 (d, $^2J_{PC}$ = 115, Pd–CH$_3$ *trans* to P), -14.9 (d, $^2J_{PC}$ = 6, Pd–CH$_3$ *cis* to P). ^{7}Li{^{1}H} NMR (THF-d_8): δ -0.7. ESI–MS (CH_2Cl_2, positive ion mode) *m*/*z* 295.2 (Li(Crypt211))$^+$. The complex is too thermally unstable for elemental analysis.

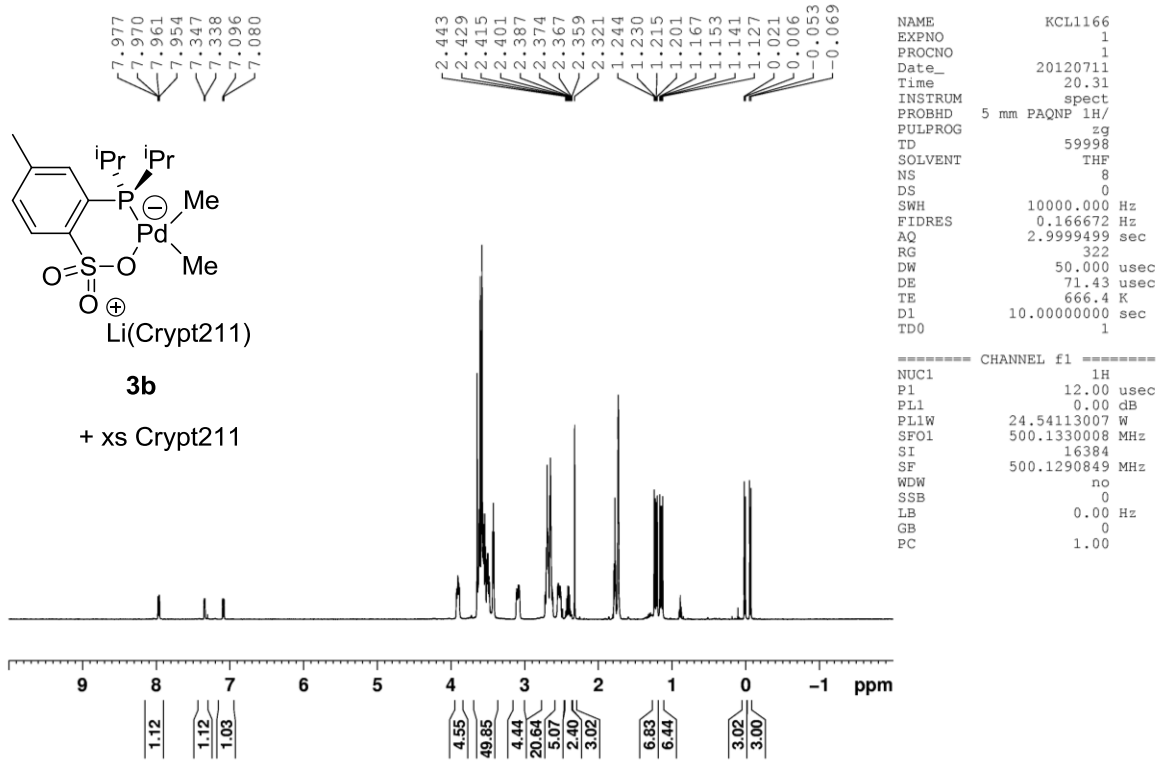

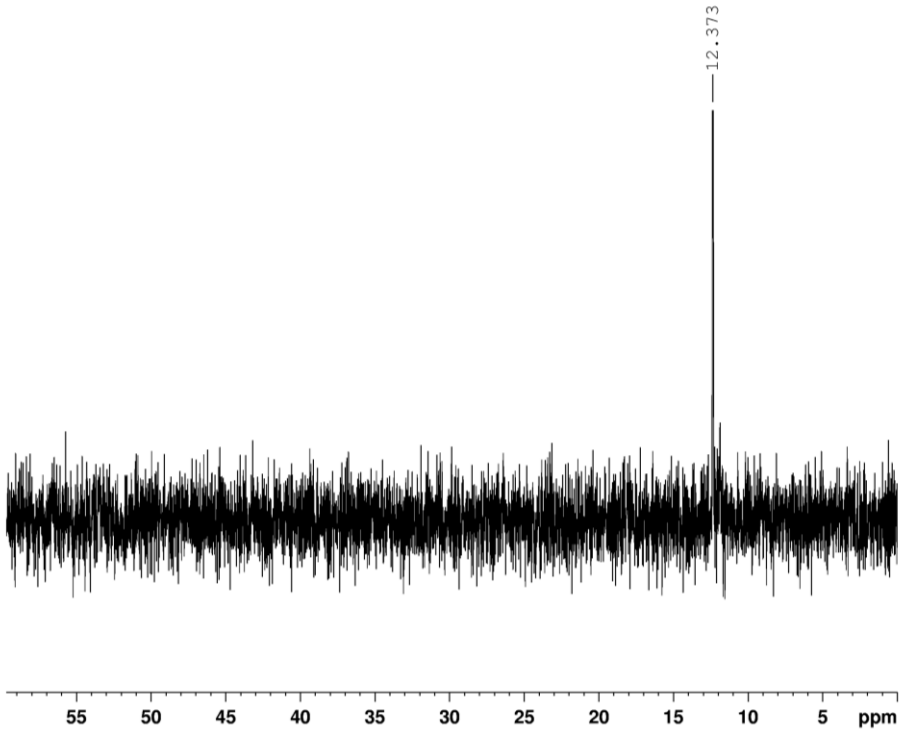


```
NAME              KCL1124
EXPNO                   2
PROCNO                  1
Date_            20120216
Time                16.59
INSTRUM             spect
PROBHD    5 mm PAQNP 1H/
PULPROG              zgpg
TD                 489122
SOLVENT               THF
NS                     33
DS                      4
SWH             81521.742 Hz
FIDRES          0.166670 Hz
AQ              2.9999983 se
RG                   2890
DW                6.133 us
DE                6.00 us
TE                297.0 K
D1           3.00000000 se
D11          0.03000000 se
TD0                     1

======== CHANNEL f1 ======
NUC1                  31P
P1                 11.00 us
PL1                3.00 dB
PL1W        41.92221451 W
SFO1       202.4462121 MH

======== CHANNEL f2 ======
CPDPRG2           waltz16
NUC2                   1H
PCPD2             100.00 us
PL2               120.00 dB
PL12               16.50 dB
PL13               17.00 dB
PL2W         0.00000000 W
PL12W        0.54940748 W
PL13W        0.48965994 W
SFO2       500.1325000 MH
SI               32768
SF         202.4561695 MH
WDW                   no
SSB                    0
LB                0.00 Hz
GB                     0
PC                1.40
```

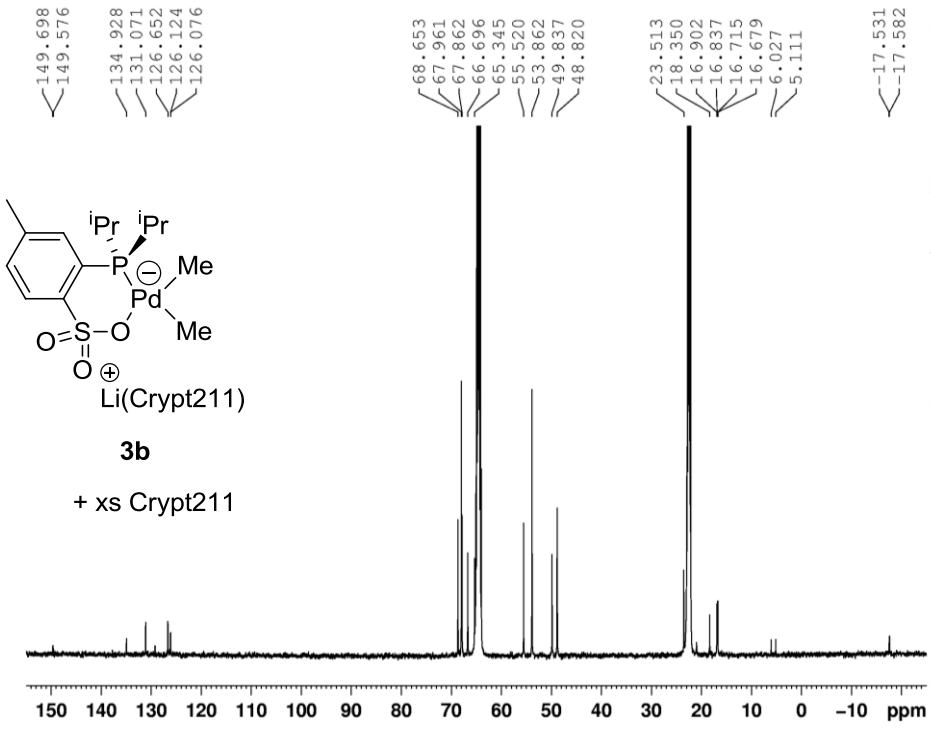


```
NAME              KCL1166
EXPNO                   4
PROCNO                  1
Date_            20120712
Time                9.07
INSTRUM             spect
PROBHD    5 mm PAQNP 1H/
PULPROG              zgpg
TD                 197364
SOLVENT               THF
NS                   7360
DS                      4
SWH             32894.738 Hz
FIDRES          0.166670 Hz
AQ              2.9999828 sec
RG                   2050
DW               15.200 usec
DE                6.00 usec
TE                666.2 K
D1           3.00000000 sec
D11          0.03000000 sec
TD0                     1

======== CHANNEL f1 ========
NUC1                  13C
P1                 8.00 usec
PL1                1.00 dB
PL1W        72.42802429 W
SFO1       125.7703648 MHz

======== CHANNEL f2 ========
CPDPRG2           waltz16
NUC2                   1H
PCPD2             80.00 usec
PL2                0.00 dB
PL12               16.50 dB
PL13               17.00 dB
PL2W        24.54113007 W
PL12W        0.54940748 W
PL13W        0.48965994 W
SFO2       500.1325006 MHz
SI               131072
SF         125.7577890 MHz
WDW                   EM
SSB                    0
LB                0.30 Hz
GB                     0
PC                1.00
```

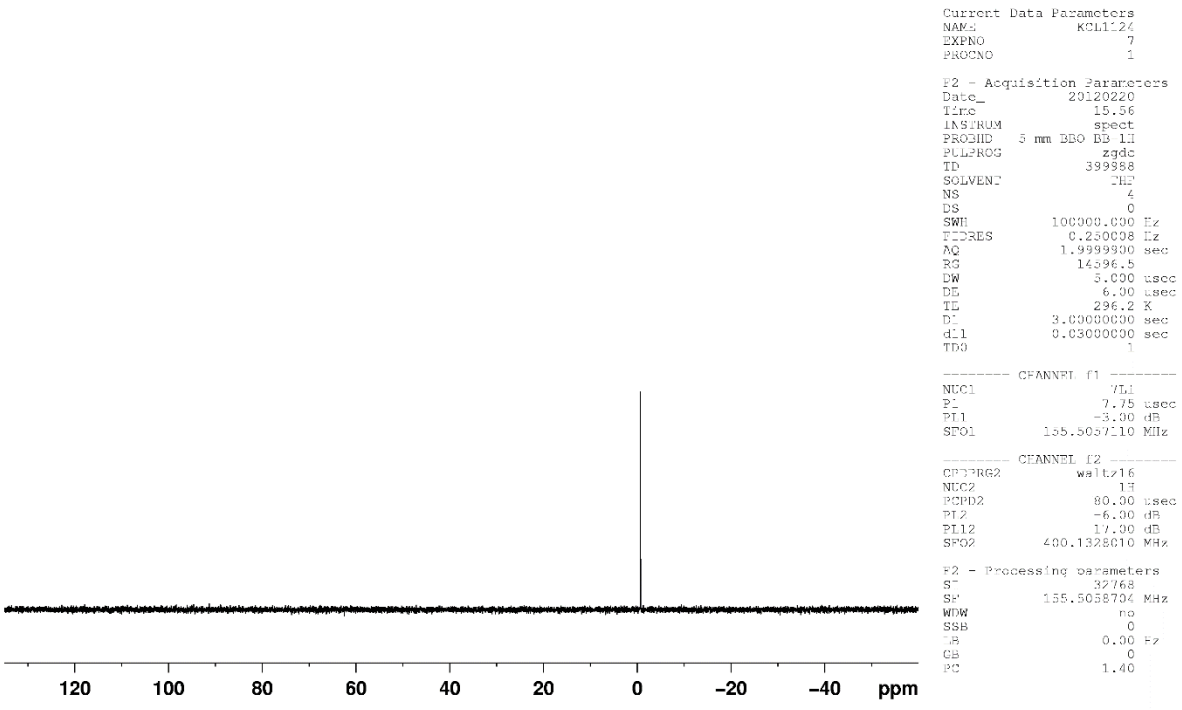

Thermal decomposition of 3a. A valved J. Young NMR tube was charged with **3a** (2.4 mg, 0.0021 mmol, i.e. 0.0042 mmol of (PO)PdMe$_2$ units) and Cp_2Fe (2.8 mg, 0.015 mmol, internal standard). THF-d_8 (0.50 mL) was added by vacuum transfer at -196 ˚C. The reaction mixture was thawed at room temperature and inserted in an NMR probe that had been pre-cooled at 293.0 K. NMR spectra were acquired over time. These spectra showed that **3a** decomposes to ethane, Pd^0 and unidentified products. The ^{1}H NMR spectrum of the reaction mixture contains 5 sets of apparent PO-^{i}Pr resonances (A-E), and the $^{31}P\{^1H\}$ spectrum contains 6 peaks.[23]

The concentration of **3a** was determined by integration of Pd–CH_3 resonance relative to the Cp_2Fe internal standard and ln[**3a**] was fitted against time (t) using the program Origin 8 (eq 1). A first-order kinetic plot is shown in Figure 2.18. The first-order rate constant for thermal decomposition of **3a** to unidentified products is $3.24(9) \times 10^{-5}$ s^{-1}. The logarithmic form of eq 1 is given by eq 2, and the corresponding plot is shown in Figure 2.10. $k = 2.95(7) \times 10^{-5}$ s^{-1}.

$$[\mathbf{3a}] = [\mathbf{3a}]_0 \exp(-kt)\} \quad (1)$$

where $[\mathbf{3a}]_0 = [\mathbf{3a}]$ at t = 0

$$\ln[\mathbf{3a}] = -kt + \ln[\mathbf{3a}]_0 \quad (2)$$

where k = first-order rate constant

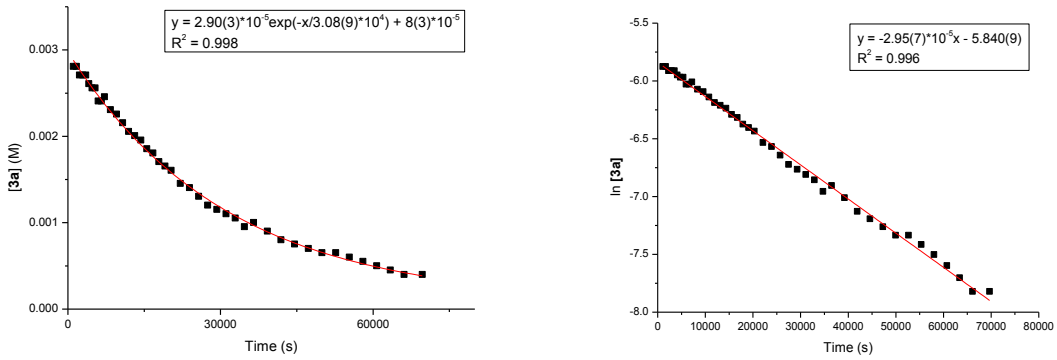

Figure 2.18. First-order kinetic plots for the thermal decomposition of **3a** in THF-d_8 at 20 °C. The exponential form is shown on the left (k = 3.24(9) × 10^{-5} s^{-1}) and the logarithmic form is shown on the right (k = 2.95(7) × 10^{-5} s^{-1}).

(PO-^{i}Pr)PdMe(py). This species was synthesized to investigate the reactivity of neutral (PO)PdMe species with CO_2. ^{n}Hexyl-lithium (2.3 M in hexane, 3.0 mL, 6.8 mmol) was added to a solution of *p*–toluenesulfonic acid (0.592 g, 3.40 mmol) in THF (20 mL) at 0°C. The mixture was warmed to room temperature, stirred for 15 min, and $(^i\text{Pr})_2\text{PCl}$ (0.55 ml, 3.4 mmol) was added dropwise. The mixture was stirred for 1 h at room temperature. The mixture was cooled to -78 °C and added to a suspension of (COD)PdMeCl (0.866 g, 3.30 mmol) in THF (15 mL) at -78

°C. The mixture was warmed to room temperature and one equiv of pyridine (267 μL, 3.30 mmol) was added. The mixture was stirred for 15 min and the volatiles were removed under vacuum. The resulting solid was extracted with CH_2Cl_2 (30 mL) and the extract was filtered through Celite. The solvent was removed from the filtrate under vacuum. The resulting yellow powder was recrystallized from a saturated toluene solution at room temperature to afford colorless crystals (950 mg, 61 %). ^{1}H NMR (CD_2Cl_2): δ 8.82 (d, 2 H, $^3J_{HH}$ = 5, *o*–py), 8.08 (dd, 1 H, $^3J_{HH}$ = 8, $^4J_{HP}$ = 4, H^3), 7.89 (tt, 1 H, $^3J_{HH}$ = 8, $^4J_{HH}$ = 2, *p*–py), 7.50 (t, 2 H, $^3J_{HH}$ = 7, *m*–py), 7.39 (d, 1 H, $^3J_{PH}$ = 8, H^6), 7.36 (d, 1 H, $^3J_{HH}$ = 8, H^4), 2.57 (d of septets, 2 H, $^3J_{HH}$ = 7, $^2J_{PH}$ = 22, C*H*Me$_2$), 2.42 (s, 3 H, C*H*$_3$–ArSO$_3$), 1.28 (dd, 6 H, $^4J_{PH}$ = 17, $^3J_{HH}$ = 7, CH*Me*$_2$), 1.25 (dd, 6 H, $^4J_{PH}$ = 15, $^3J_{HH}$ = 7, CH*Me*$_2$), 0.56 (d, 3 H, $^3J_{PH}$ = 2, Pd–C*H*$_3$). ^{1}H NMR (THF-*d*$_8$): δ 8.89 (d, 2 H, $^3J_{HH}$ = 5, *o*-py), 8.06 (dd, 1 H, $^3J_{HH}$ = 8, $^4J_{HP}$ = 4, H^3), 7.93 (tt, 1 H, $^3J_{HH}$ = 8, $^4J_{HH}$ = 2, *p*-py), 7.54 (t, 2 H, $^3J_{HH}$ = 7, *m*-py), 7.49 (d, 1 H, $^3J_{PH}$ = 8, H^6), 7.33 (d, 1 H, $^3J_{HH}$ = 8, H^4), 2.66 (octets, 2 H, $^2J_{PH}$ = $^3J_{HH}$ = 7, C*H*Me$_2$), 2.40 (s, 3 H, C*H*$_3$–ArSO$_3$), 1.29 (dd, 6 H, $^4J_{PH}$ = 17, $^3J_{HH}$ = 7, CH*Me*$_2$), 1.24 (dd, 6 H, $^4J_{PH}$ = 15, $^3J_{HH}$ = 7, CH*Me*$_2$), 0.49 (d, 3 H, $^3J_{PH}$ = 2, Pd–C*H*$_3$). ^{31}P{^{1}H} NMR (CD_2Cl_2): δ 40.1. ^{31}P{^{1}H} NMR (THF-*d*$_8$): δ 41.5. ^{13}C{^{1}H} NMR (CD_2Cl_2): δ 150.5 (*o*–py), 146.5 (d, $^2J_{PC}$ = 11, C^2), 139.9 (d, $^3J_{PC}$ = 6, C^5), 138.6 (*p*–py), 133.3 (C^4), 131.8 (d, $^3J_{PC}$ = 2, C^3), 128.8 (d, $^2J_{PC}$ = 7, C^6), 125.5 (*m*–py), 124.1 (d, $^1J_{PC}$ = 36, C^1), 25.8 (d, $^1J_{PC}$ = 27, *C*HMe$_2$), 21.4 (*C*H$_3$–ArSO$_3$), 19.2 (d, $^2J_{PC}$ = 5, CH*Me*$_2$), 18.6 (CH*Me*$_2$), -5.9 (d, $^2J_{PC}$ = 6, Pd–*C*H$_3$). Mp: 153–155 °C. Anal. Calcd. For $C_{19}H_{28}NO_3PPdS$: C, 46.77; H, 5.78; N, 2.87. Found: C, 46.84; H, 5.66; N, 2.71.

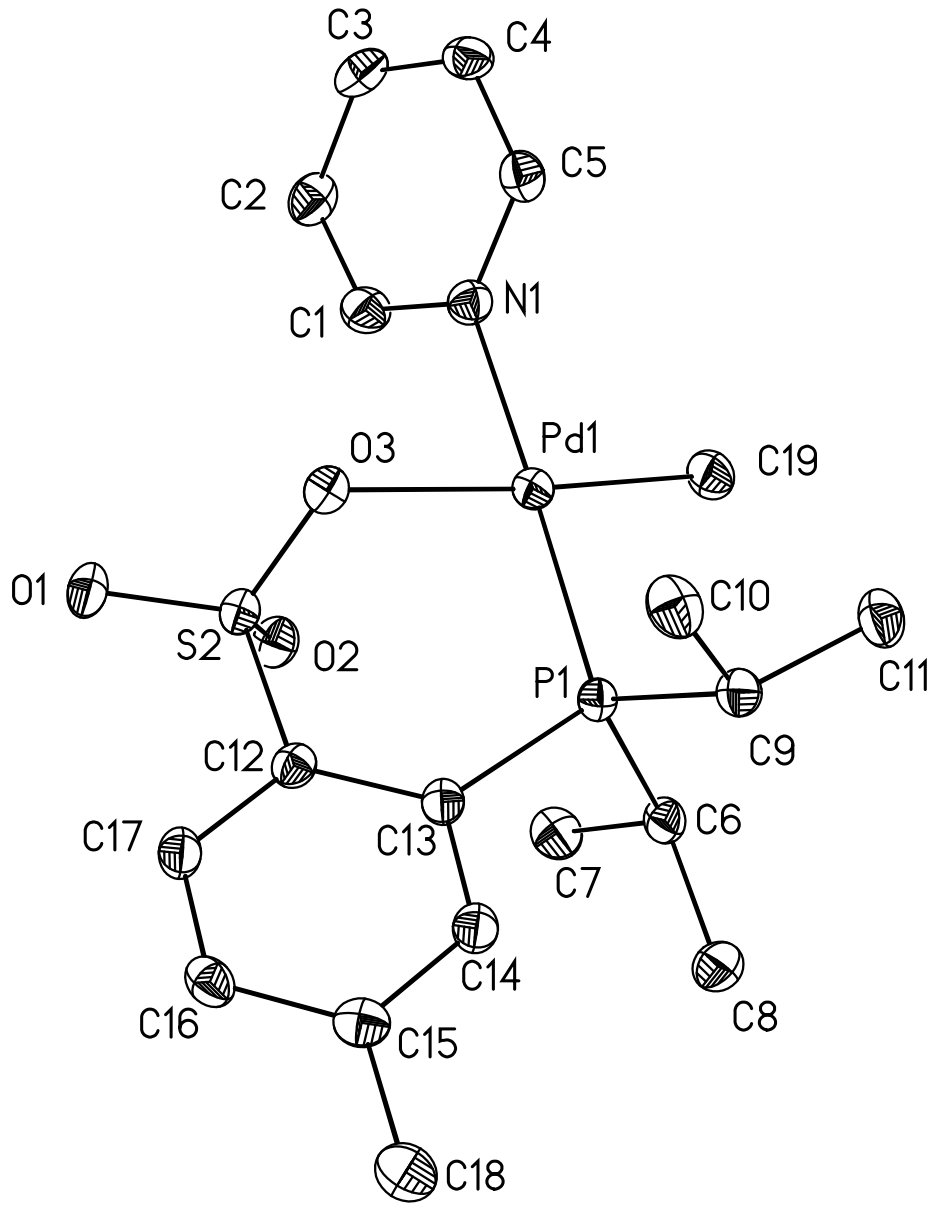

Figure 2.19. Molecular structure of (PO-^{i}Pr)PdMe(py). Hydrogen and solvent atoms are omitted. Selected bond lengths (Å) and angle (deg): Pd1–C19 2.037(3), Pd1–O3 2.151(2), Pd1–N1 2.114(2), Pd1–P1 2.2349(9), C19–Pd2–O3 175.0(1).

Generation of "(PO-^{i}Pr)PdMe(py)-Li^{+}". This species was generated to investigate the role of Li^+ in the reactivity of neutral (PO)PdMe species with CO_2. A valved J. Young NMR tube was charged with (PO-^{i}Pr)PdMe(py) (3.0 mg, 0.0061 mmol) and $[Li(Et_2O)_{2.8}][B(C_6F_5)_4]$ (6.0 mg, 0.0067 mmol). THF-d_8 (0.50 mL) was added by vacuum transfer at -196 °C. The reaction mixture was thawed at room temperature. ^{1}H NMR spectrum of (PO-^{i}Pr)PdMe(py)-Li$^+$ is shifted from that of (PO-^{i}Pr)PdMe(py), indicative of Li^+ ion-pairing. ^{1}H NMR (THF-d_8): δ 8.83 (d, $^3J_{HH}$ = 5, 2 H, *o*–py), 7.99 (dd, 1 H, $^3J_{HH}$ = 8, $^4J_{HP}$ = 4, H^3), 7.97 (tt, 1 H, $^3J_{HH}$ = 8, $^4J_{HH}$ = 2, *p*–py) 7.60 (d, $^3J_{HH}$ = 8, H^6), 7.56 (t, 2 H, $^3J_{HH}$ = 7, *m*–py), 7.40 (d, $^3J_{HH}$ = 8, H^4), 2.70 (octet, $^2J_{PH}$ = $^3J_{HH}$ = 7, C*H*Me$_2$), 2.43 (s, 3 H, C*H*$_3$–ArSO$_3$), 1.29 (dd, $^4J_{PH}$ = 18, $^3J_{HH}$ = 7, 6 H, CH*Me$_2$*), 1.25 (dd, $^4J_{PH}$ = 15, $^3J_{HH}$ = 7, 6 H, CH*Me$_2$*), 0.59 (d, $^3J_{PH}$ = 2, Pd–C*H*$_3$). ^{31}P{^{1}H} NMR (THF-d_8): δ 41.5.

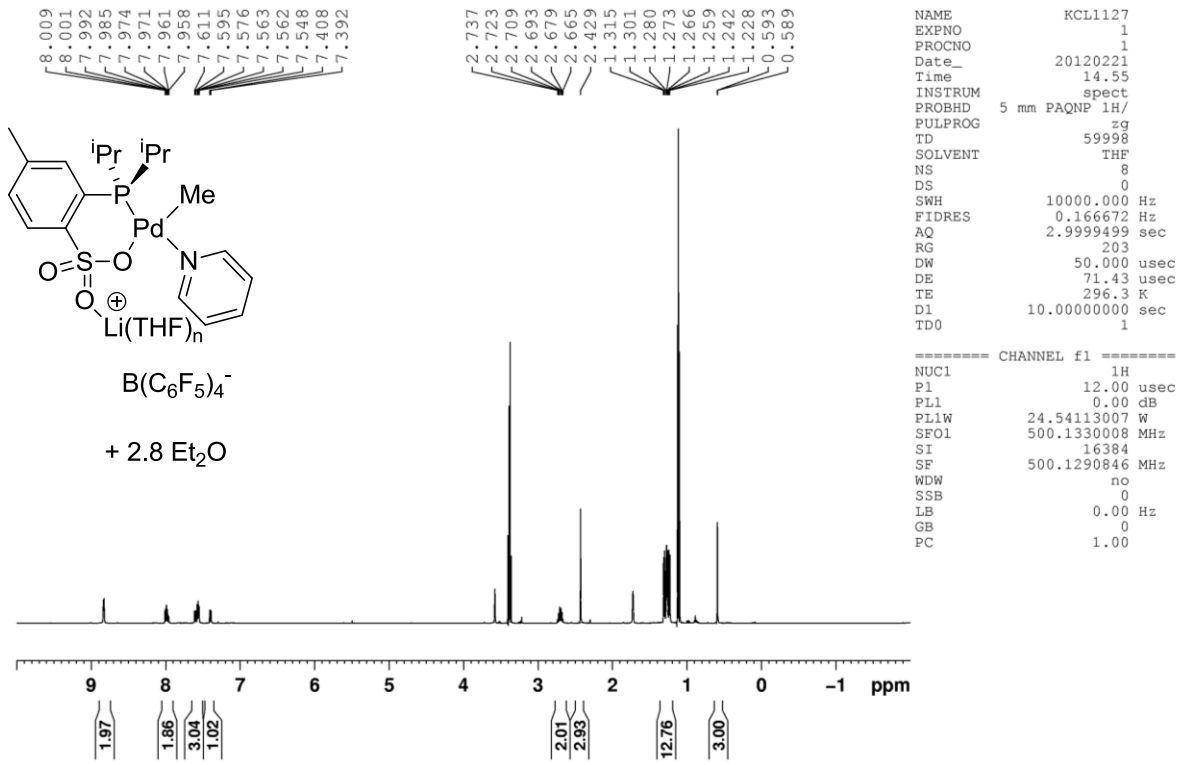

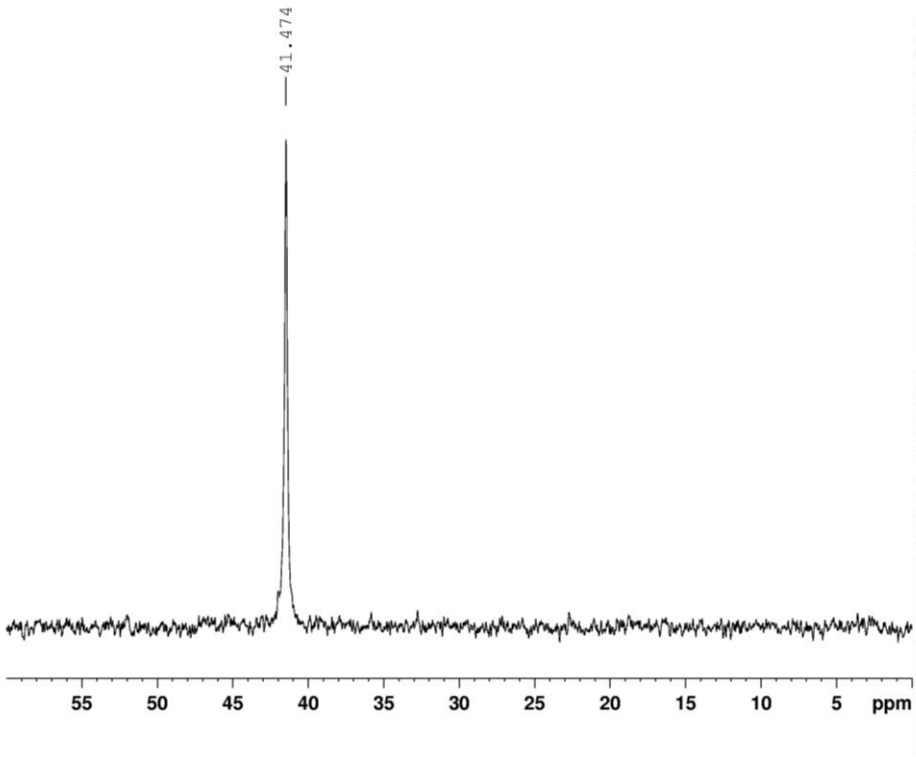

(PO-^{i}Pr)PdMe(THF) and *trans*–P,P–(PO-^{i}Pr)$_2$Pd. (PO-^{i}Pr)PdMe(THF) was synthesized to investigate the reactivity of neutral (PO)PdMe species with CO_2. *Trans*–P,P–(PO-^{i}Pr)$_2$Pd was formed as a side-product. A vial was charged with H[PO-^{i}Pr] (100 mg, 0.347 mmol) and (TMEDA)PdMe$_2$ (88.0 mg, 0.348 mmol). THF (8 mL) was added to form a colorless solution. Gas evolution (CH_4) was observed in 5 min. The solution was stirred for 1 h at room temperature to afford {(PO-^{i}Pr)PdMe}$_2$(TMEDA) (See below). $BF_3(Et_2O)$ (90 μL, 0.726 mmol) was added dropwise to give a turbid pale yellow solution. The mixture was stirred for 30 min and filtered through Celite. The filtrate was evaporated under vacuum for 48 h to give a pale yellow solid. The solid was dissolved in C_6H_6, precipitated with pentane, collected by filtration and dried under vacuum to afford a pale yellow solid that was shown by NMR to be a 16/1 mixture of (PO-^{i}Pr)PdMe(THF) and *trans*–P,P–(PO-^{i}Pr)$_2$Pd. Attempts to purify (PO-^{i}Pr)PdMe(THF) further were

unsuccessful. However, recrystallization of the mixture from CD_2Cl_2 at -78 °C afforded crystals of *trans*-P,P-(PO-^{i}Pr)$_2$Pd, which was characterized by X-ray diffraction. (PO-^{i}Pr)PdMe(THF) was also generated by the reaction of (PO-^{i}Pr)PdMe(py) with $B(C_6F_5)_3$ in THF-d_8 (See below). Data for (PO-^{i}Pr)PdMe(THF): ^{1}H NMR (THF-d_8): δ 8.04 (dd, $^3J_{HH}$ = 8, $^4J_{PH}$ = 4, 1 H, H^3), 7.45 (d, $^3J_{PH}$ = 8, 1 H, H^6), 7.33 (d, $^3J_{HH}$ = 8, 1 H, H^4), 2.59 (d of septets, $^2J_{PH}$ = 8, $^3J_{HH}$ = 6, 2 H, C*H*Me$_2$), 2.39 (s, 3 H, C*H*$_3$–ArSO$_3$), 1.23 (dd, $^4J_{PH}$ = 17, $^3J_{HH}$ = 6, 6 H, CH*Me$_2$*), 1.20 (dd, $^4J_{PH}$ = 15, $^3J_{HH}$ = 6, 6 H, CH*Me$_2$*), 0.46 (s, Pd–C*H*$_3$). ^{31}P{^{1}H}NMR (THF-d_8): δ 50.9. *trans*–P,P–(PO-^{i}Pr)$_2$Pd exists as a 2/1 mixture of *trans*–P,P and *cis*–P,P isomers in THF-d_8 solution. Data for *trans*–P,P–(PO-^{i}Pr)$_2$Pd: ^{1}H NMR (THF-d_8, both isomers): δ 8.04 (dt, $^3J_{HH}$ = 8, $^4J_{PH}$ = $^6J_{PH}$ = 4, 2 H, H^3), 7.60 (br d, $^3J_{HH}$ = 9, H^4 of *cis*–P,P isomer), 7.56 (br s, 2 H, H^6), 7.45 (d, $^3J_{HH}$ = 8, H^4 of *trans*-P,P isomer; the δ 7.60 and 7.45 signals integrate for 2 H total), 2.82 (m, 4 H, C*H*Me$_2$), 2.44 (s, C*H*$_3$–ArSO$_3$ of *trans*–P,P isomer), 2.42 (s, C*H*$_3$-ArSO$_3$ of *cis*–P,P isomer; the δ 2.44 and 2.42 signals integrate for 6 H total), 1.46 (m, 24 H, CH*Me$_2$*). ^{31}P{^{1}H}NMR (THF-d_8): δ 58.1 (*cis*–P,P isomer), 9.3 (*trans*–P,P isomer).

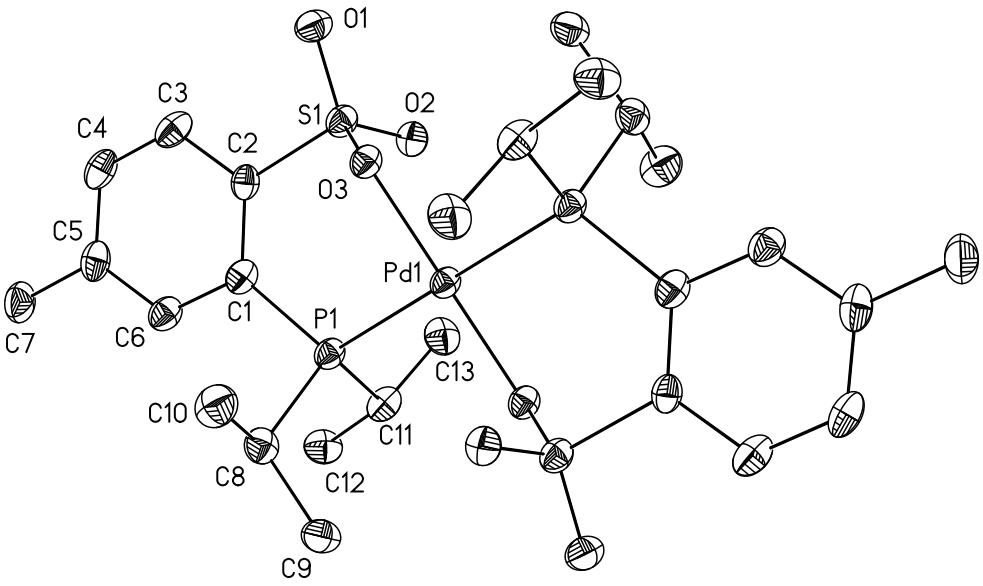

Figure 2.20. Molecular structure of *trans*-P,P-(PO-^{i}Pr)$_2$Pd. Hydrogen and solvent atoms are omitted. Selected bond lengths (Å) and angle (deg): Pd1–O3 2.016(3), Pd1–P1 2.322(2), P1–Pd2–O3 90.81(9).

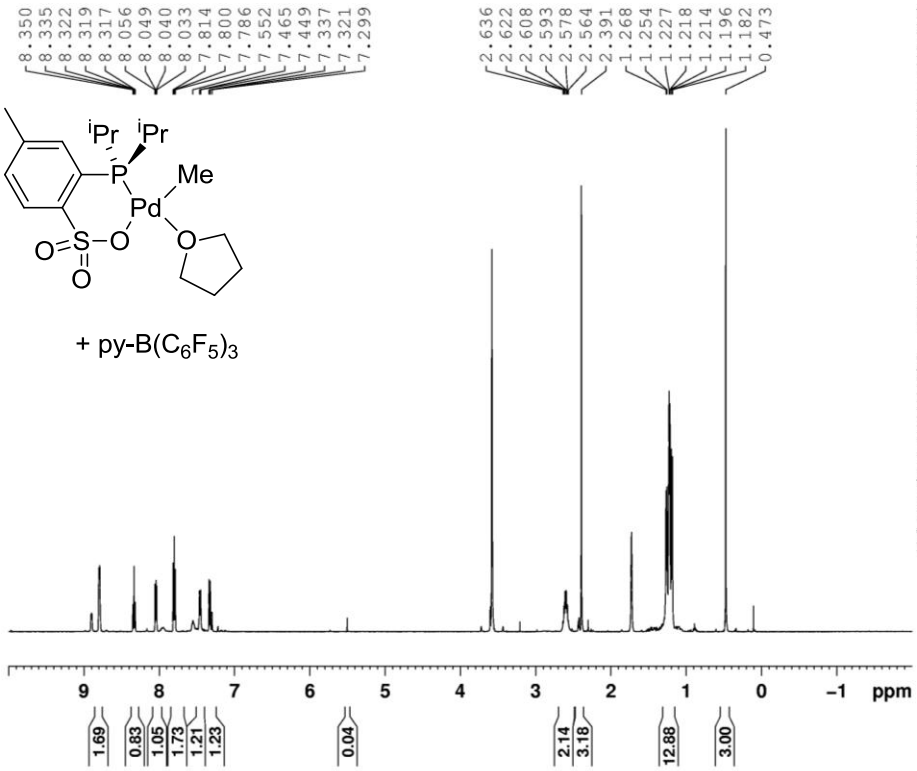


```
NAME            KCL1112
EXPNO                 1
PROCNO                1
Date_          20120126
Time              16.36
INSTRUM           spect
PROBHD   5 mm PAQNP 1H/
PULPROG              zg
TD                44998
SOLVENT             THF
NS                    8
DS                    0
SWH           10000.000 Hz
FIDRES            0.222232 Hz
AQ             2.2499499 sec
RG                  406
DW               50.000 usec
DE               71.43 usec
TE                294.7 K
D1           10.00000000 sec
TD0                   1

======== CHANNEL f1 ========
NUC1                 1H
P1                12.00 usec
PL1                0.00 dB
PL1W        24.54113007 W
SFO1         500.1330008 MHz
SI                16384
SF           500.1290848 MHz
WDW                  no
SSB                   0
LB                 0.00 Hz
GB                    0
PC                 1.00
```

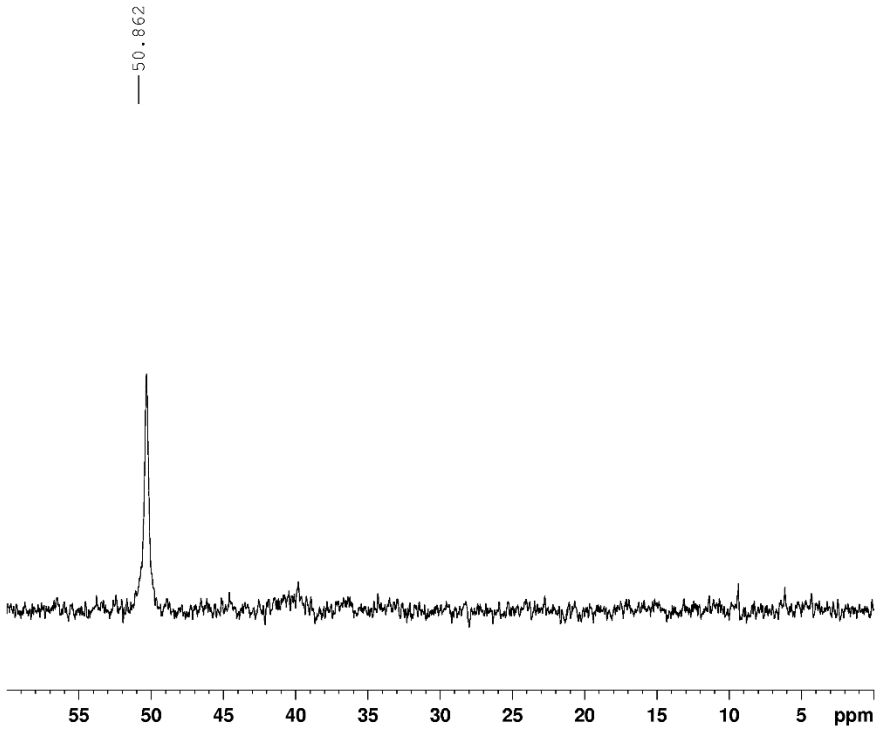


```
NAME            KCL1112
EXPNO                 2
PROCNO                1
Date_          20120126
Time              16.39
INSTRUM           spect
PROBHD   5 mm PAQNP 1H/
PULPROG           zgpg
TD               244560
SOLVENT             THF
NS                   15
DS                    4
SWH           40760.871 Hz
FIDRES            0.166670 Hz
AQ             2.9999859 sec
RG                 2890
DW               12.267 usec
DE                6.00 usec
TE                295.4 K
D1           3.00000000 sec
D11          0.03000000 sec
TD0                   1

======== CHANNEL f1 ========
NUC1                31P
P1                11.00 usec
PL1                3.00 dB
PL1W        41.92221451 W
SFO1         202.4705069 MHz

======== CHANNEL f2 ========
CPDPRG2         waltz16
NUC2                 1H
PCPD2            100.00 usec
PL2               120.00 dB
PL12               16.50 dB
PL13               17.00 dB
PL2W         0.00000000 W
PL12W        0.54940748 W
PL13W        0.48965994 W
SFO2         500.1325000 MHz
SI                32768
SF           202.4557845 MHz
WDW                  EM
SSB                   0
LB                10.00 Hz
GB                    0
PC                 1.40
```

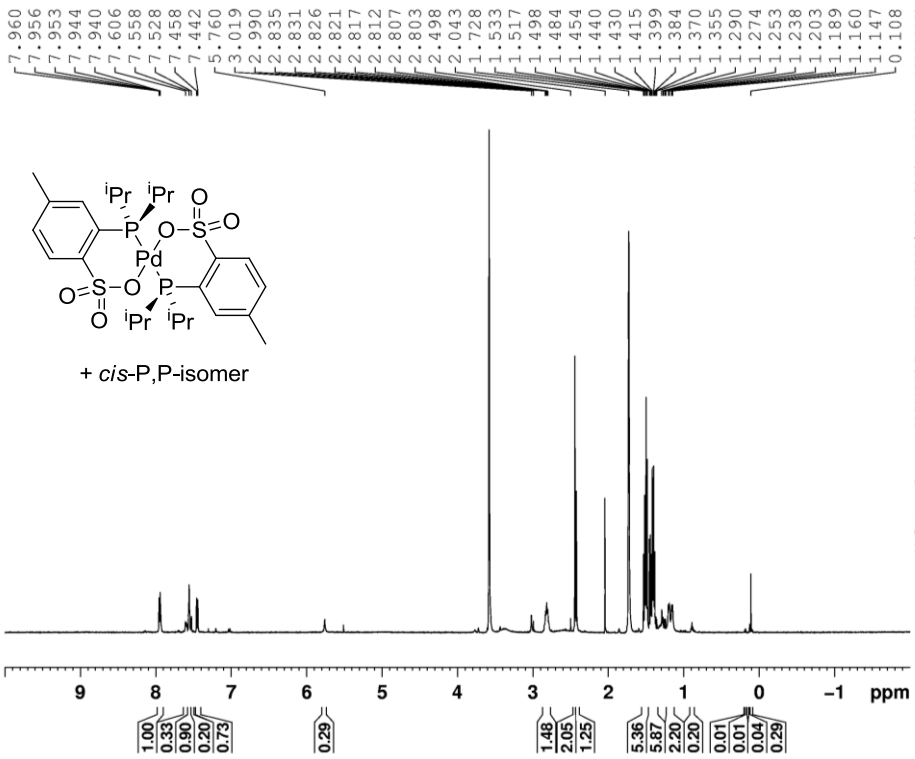
7.960 7.956 7.953 7.944 7.940 7.606 7.558 7.528 7.458 7.442 5.760 3.019 2.990 2.835 2.831 2.826 2.821 2.817 2.812 2.807 2.803 2.498 2.043 1.728 1.533 1.517 1.498 1.484 1.454 1.440 1.430 1.415 1.399 1.384 1.370 1.355 1.290 1.274 1.253 1.238 1.203 1.189 1.160 1.147 0.108
NAME KCL1086
EXPNO 5
PROCNO 1
Date_ 20120327
Time 17.07
INSTRUM spect
PROBHD 5 mm PAQNP 1H/
PULPROG zg
TD 44998
SOLVENT THF
NS 8
DS 0
SWH 10000.000 Hz
FIDRES 0.222232 Hz
AQ 2.2499499 sec
RG 645
DW 50.000 usec
DE 71.43 usec
TE 296.5 K
D1 10.00000000 sec
TD0 1
======== CHANNEL f1 ========
NUC1 1H
P1 12.00 usec
PL1 0.00 dB
PL1W 24.54113007 W
SFO1 500.1330008 MHz
SI 16384
SF 500.1290848 MHz
WDW no
SSB 0
LB 0.00 Hz
GB 0
PC 1.00
iPr iPr
iPr iPr
+ cis-P,P-isomer
9 8 7 6 5 4 3 2 1 0 −1 ppm
1.00 0.33 0.90 0.20 0.73 0.29 1.48 2.05 1.25 5.36 5.87 2.20 0.20 0.01 0.01 0.04 0.29

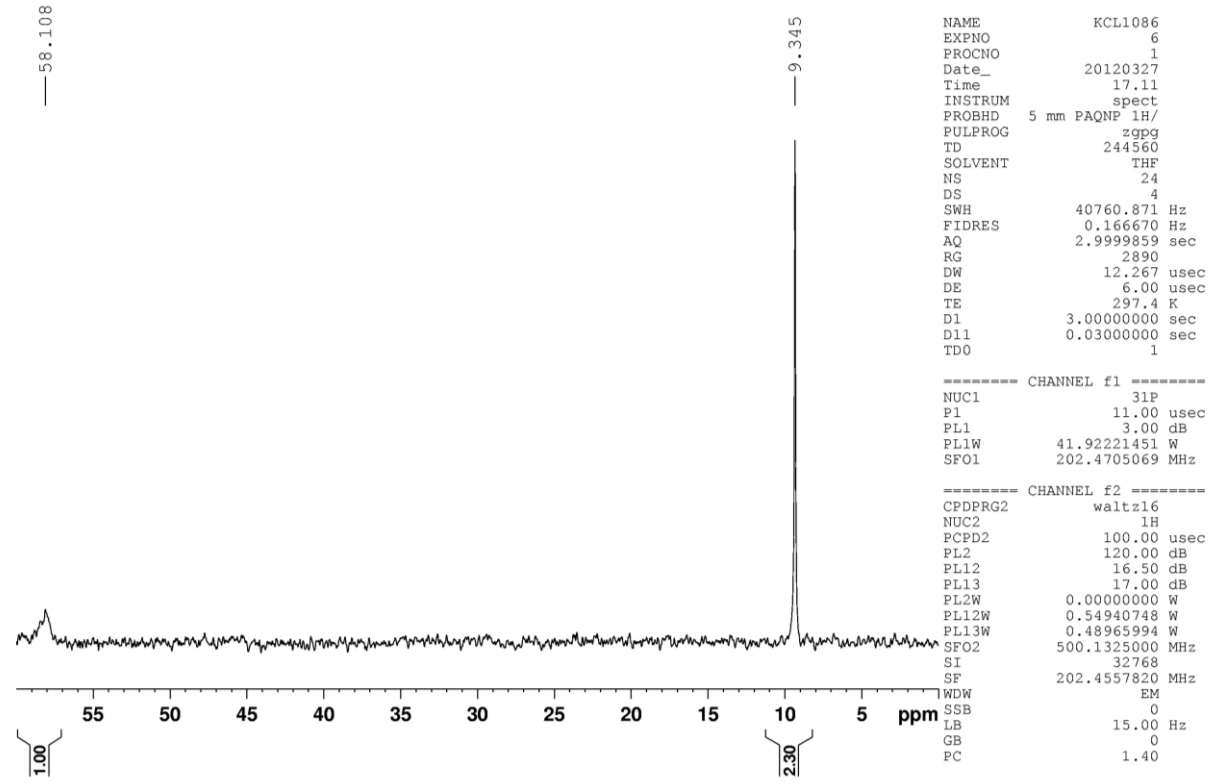
58.108
9.345
NAME KCL1086
EXPNO 6
PROCNO 1
Date_ 20120327
Time 17.11
INSTRUM spect
PROBHD 5 mm PAQNP 1H/
PULPROG zgpg
TD 244560
SOLVENT THF
NS 24
DS 4
SWH 40760.871 Hz
FIDRES 0.166670 Hz
AQ 2.9999859 sec
RG 2890
DW 12.267 usec
DE 6.00 usec
TE 297.4 K
D1 3.00000000 sec
D11 0.03000000 sec
TD0 1
======== CHANNEL f1 ========
NUC1 31P
P1 11.00 usec
PL1 3.00 dB
PL1W 41.92221451 W
SFO1 202.4705069 MHz
======== CHANNEL f2 ========
CPDPRG2 waltz16
NUC2 1H
PCPD2 100.00 usec
PL2 120.00 dB
PL12 16.50 dB
PL13 17.00 dB
PL2W 0.00000000 W
PL12W 0.54940748 W
PL13W 0.48965994 W
SFO2 500.1325000 MHz
SI 32768
SF 202.4557820 MHz
WDW EM
SSB 0
LB 15.00 Hz
GB 0
PC 1.40
55 50 45 40 35 30 25 20 15 10 5 ppm
1.00 2.30

{(PO-^{i}Pr)PdMe}$_2$(TMEDA). This species was synthesized to support the identity of the intermediate in the synthesis of (PO-^{i}Pr)PdMe(THF). (TMEDA)PdMe$_2$ (99.8 mg, 0.394 mmol) was dissolved in CH_2Cl_2 (5 mL) to form a colorless solution. H[PO-^{i}Pr] (110 mg, 0.381 mmol) was dissolved in CH_2Cl_2 (5 mL) to form a colorless solution which was added to the solution of (TMEDA)PdMe$_2$ dropwise at -40 ˚C. The mixture was warmed to room temperature and stirred for 45 min to afford a pale yellow solution. The volatiles were removed under vacuum to give a pale yellow solid. The solid was taken up in pentane and the mixture was filtered to give a pale yellow powder (131 mg). The yellow powder was washed with Et_2O to yield {(PO-^{i}Pr)PdMe}$_2$(TMEDA). ^{1}H NMR (CD_2Cl_2): δ 8.04 (dd, $^3J_{HH}$ = 8, $^4J_{PH}$ = 4, 2 H, H^3), 7.35 (m, 4 H, H^4 & H^6), 3.45 (s, 4 H, N(C*H*$_2$)$_2$N), 2.61 (s, 12 H, NC*H*$_3$), 2.57 (octet, partly obscured by NC*H*$_3$, $^2J_{PH}$ = $^3J_{HH}$ = 8, 4 H, C*H*Me$_2$), 2.41 (s, 6 H, C*H*$_3$–ArSO$_3$), 1.22 (dd, $^4J_{PH}$ = 16, $^3J_{HH}$ = 7, 12 H, CH*Me*$_2$), 1.21 (dd, $^4J_{PH}$ = 16, $^3J_{HH}$ = 7, 12 H, CH*Me*$_2$), 0.37 (d, $^3J_{PH}$ = 1, 6 H, Pd–C*H*$_3$). ^{31}P{^{1}H} NMR (CD_2Cl_2): δ 42.7.

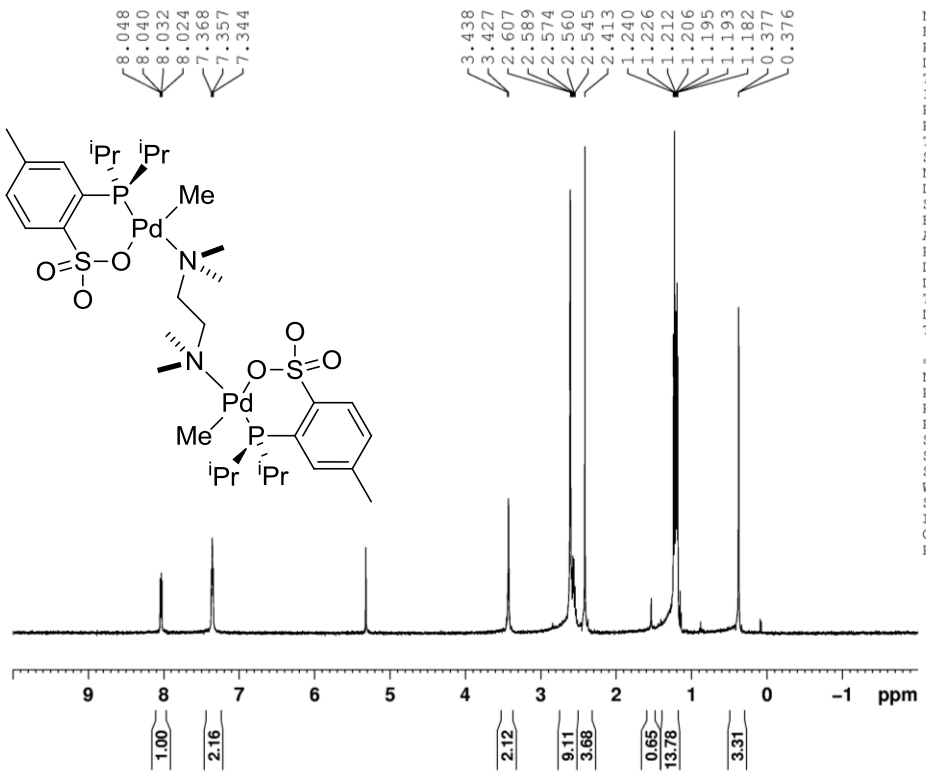


```
NAME              KCL1088
EXPNO                   3
PROCNO                  1
Date_            20111019
Time                17.02
INSTRUM             spect
PROBHD   5 mm PAQNP 1H/
PULPROG                zg
TD                  44998
SOLVENT           CD2Cl2
NS                      8
DS                      0
SWH          10000.000 Hz
FIDRES        0.222232 Hz
AQ            2.2499499 sec
RG                    724
DW               50.000 usec
DE               71.43 usec
TE                294.8 K
D1           10.00000000 sec
TD0                     1

======== CHANNEL f1 ========
NUC1                   1H
P1                 12.00 usec
PL1                 0.00 dB
PL1W         24.54113007 W
SFO1        500.1330008 MHz
SI                  16384
SF          500.1300175 MHz
WDW                    no
SSB                     0
LB                 0.00 Hz
GB                      0
PC                   1.00
```

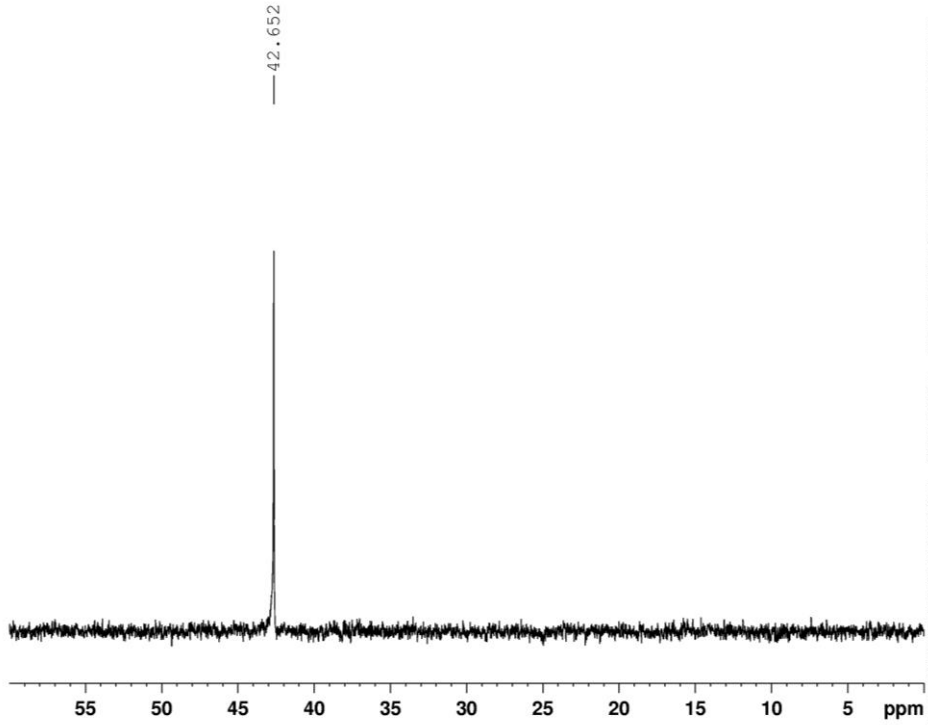


```
NAME              KCL1088
EXPNO                   4
PROCNO                  1
Date_            20111019
Time                17.07
INSTRUM             spect
PROBHD   5 mm PAQNP 1H/
PULPROG             zgpg
TD                 244560
SOLVENT           CD2Cl2
NS                     25
DS                      4
SWH          40760.871 Hz
FIDRES        0.166670 Hz
AQ            2.9999859 sec
RG                   2890
DW               12.267 usec
DE                6.00 usec
TE                295.7 K
D1           3.00000000 sec
D11          0.03000000 sec
TD0                     1

======== CHANNEL f1 ========
NUC1                  31P
P1                 11.00 usec
PL1                 3.00 dB
PL1W        41.92221451 W
SFO1       202.4705069 MHz

======== CHANNEL f2 ========
CPDPRG2          waltz16
NUC2                   1H
PCPD2             100.00 usec
PL2               120.00 dB
PL12               16.50 dB
PL13               17.00 dB
PL2W         0.00000000 W
PL12W        0.54940748 W
PL13W        0.48965994 W
SFO2       500.1325000 MHz
SI                  32768
SF         202.4558604 MHz
WDW                    EM
SSB                     0
LB                 3.00 Hz
GB                      0
PC                   1.40
```

Generation of "(PO-^{i}Pr)PdMe(THF)-Li^{+}". This species was generated to investigate the role of Li^+ in the reactivity of neutral (PO)PdMe species with CO_2. A valved J. Young NMR tube was charged with (PO-^{i}Pr)PdMe(py) (3.8 mg, 0.0078 mmol), $B(C_6F_5)_3$ (5.2 mg, 0.010 mmol) and $[Li(Et_2O)_{2.8}][B(C_6F_5)_4]$ (5.7 mg, 0.0064 mmol). THF-d_8 (0.50 mL) was added by vacuum transfer at -196 ˚C. The reaction mixture was thawed at room temperature. NMR analysis showed that complete conversion to (PO-^{i}Pr)PdMe(THF)-Li^{+} and the known compound py–$B(C_6F_5)_3$ had occurred.[24] ^{1}H NMR spectrum of (PO-^{i}Pr)PdMe(THF)-Li^{+} is shifted from that of (PO-^{i}Pr)PdMe(THF), indicative of Li^+ ion-pairing. Data for py–$B(C_6F_5)_3$: ^{1}H NMR (THF-d_8): δ 8.79 (br d, $^3J_{HH}$ = 6, 2 H, *o*–py–$B(C_6F_5)_3$), 8.33 (tt, $^3J_{HH}$ = 8, $^4J_{HH}$ = 2, 1 H, *p*–py–$B(C_6F_5)_3$), 7.79 (t, $^3J_{HH}$ = 7, 2 H, *m*–py–$B(C_6F_5)_3$). Data for (PO-^{i}Pr)PdMe(THF)-Li^{+}: ^{1}H NMR (THF-d_8): δ8.01 (dd, $^3J_{HH}$ = 8, $^4J_{PH}$ = 4, 1 H, H^3), 7.55 (d, $^3J_{PH}$ = 8, 1 H, H^6), 7.39 (d, $^3J_{HH}$ = 8, 1 H, H^4), 2.65 (octet, $^2J_{PH}$ = $^3J_{HH}$ = 7, 2 H, C*H*Me$_2$), 2.41 (s, 3 H, C*H*$_3$–$ArSO_3$), 1.24 (dd, $^4J_{PH}$ = 16, $^3J_{HH}$ = 7, 6 H, CH*Me$_2$*), 1.21 (dd, $^4J_{PH}$ = 14, $^3J_{HH}$ = 7, 6 H, CH*Me$_2$*), 0.57 (s, Pd–C*H*$_3$). ^{31}P{^{1}H}NMR (THF-d_8): δ 51.3.

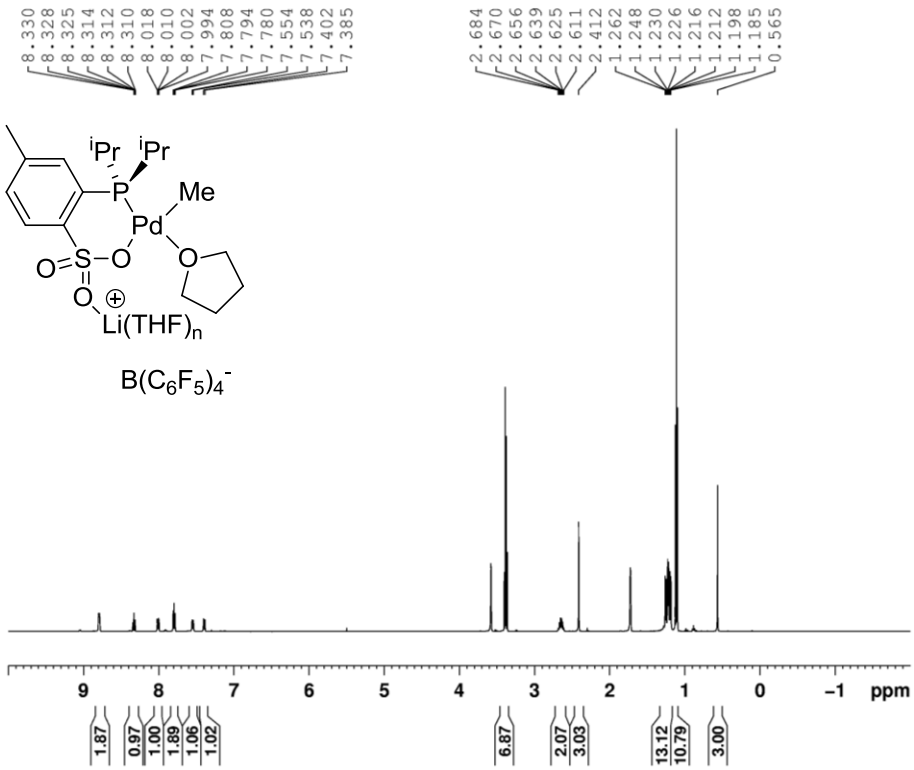


```
NAME              KCL1127
EXPNO                   3
PROCNO                  1
Date_            20120221
Time                15.04
INSTRUM             spect
PROBHD   5 mm PAQNP 1H/
PULPROG                 zg
TD                  59998
SOLVENT               THF
NS                      8
DS                      0
SWH             10000.000 Hz
FIDRES              0.166672 Hz
AQ                2.9999499 sec
RG                      203
DW                 50.000 usec
DE                 71.43 usec
TE                 296.3 K
D1              10.00000000 sec
TD0                     1

======== CHANNEL f1 ========
NUC1                   1H
P1                 12.00 usec
PL1                 0.00 dB
PL1W          24.54113007 W
SFO1          500.1330008 MHz
SI                  16384
SF            500.1290851 MHz
WDW                    no
SSB                     0
LB                 0.00 Hz
GB                      0
PC                   1.00
```

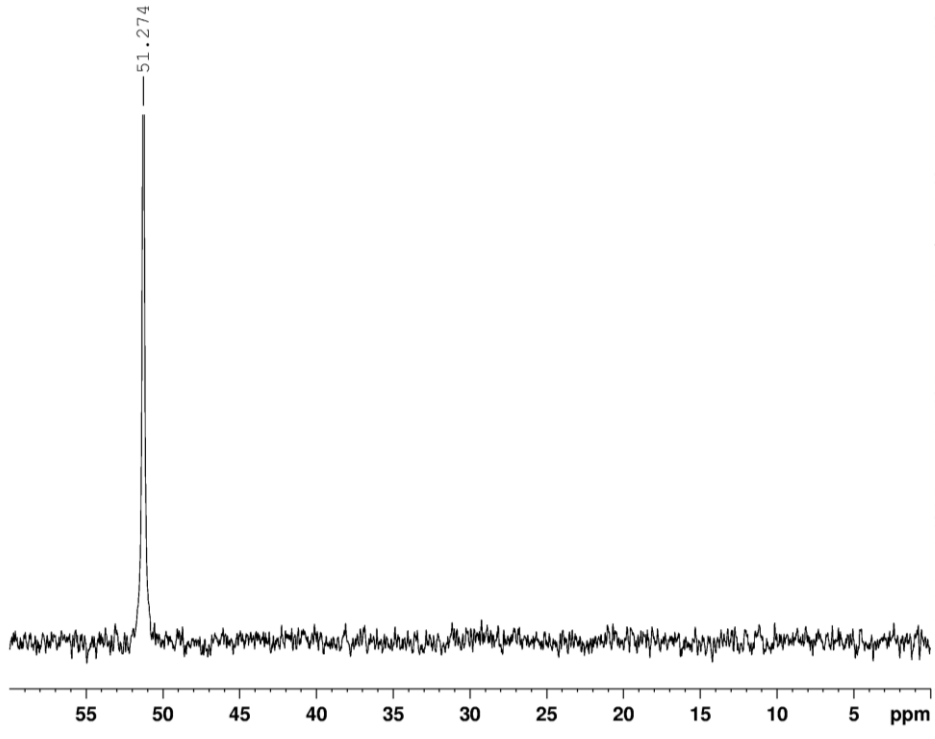


```
NAME              KCL1127
EXPNO                   4
PROCNO                  1
Date_            20120221
Time                15.07
INSTRUM             spect
PROBHD   5 mm PAQNP 1H/
PULPROG              zgpg
TD                 489122
SOLVENT               THF
NS                     14
DS                      4
SWH             81521.742 Hz
FIDRES              0.166670 Hz
AQ                2.9999983 sec
RG                   2890
DW                 6.133 usec
DE                 6.00 usec
TE                 297.0 K
D1              3.00000000 sec
D11             0.03000000 sec
TD0                     1

======== CHANNEL f1 ========
NUC1                  31P
P1                 11.00 usec
PL1                 3.00 dB
PL1W          41.92221451 W
SFO1          202.4462121 MHz

======== CHANNEL f2 ========
CPDPRG2          waltz16
NUC2                   1H
PCPD2             100.00 usec
PL2               120.00 dB
PL12               16.50 dB
PL13               17.00 dB
PL2W           0.00000000 W
PL12W          0.54940748 W
PL13W          0.48965994 W
SFO2          500.1325000 MHz
SI                  32768
SF            202.4557843 MHz
WDW                    EM
SSB                     0
LB                 10.00 Hz
GB                      0
PC                   1.40
```

Li[(PO-^{i}Pr)PdMe(OAc)] (4a). A solution of acetic acid in THF (0.289 M, 1.05 mL, 0.303 mmol) was added to solid **3a** (167 mg, 0.145 mmol, i.e. 0.290 mmol of (PO)$PdMe_2^-$ units) dropwise to form a deep yellow solution. Gas evolution (CH_4) was observed. After 15 min, the solution was evaporated under vacuum to 1/3 of the original volume. Pentane was added slowly to precipitate a white solid. The white solid was collected by filtration, washed with pentane and dried under vacuum (126 mg, 0.266 mmol, 92 %). ^{1}H NMR (THF-d_8): δ 8.03 (dd, $^3J_{HH}$ = 8, $^4J_{HP}$ = 4, 1 H, H^3), 7.47 (d, $^3J_{PH}$ = 7, 1 H, H^6), 7.33 (d, $^3J_{HH}$ = 8, 1 H, H^4), 2.52 (octet, $^2J_{PH}$ = $^3J_{HH}$ = 8, 2 H, C*H*Me_2), 2.40 (s, 3 H, CH_3–$ArSO_3$), 1.84 (s, 3 H, OC(O)CH_3), 1.22 (dd, $^4J_{PH}$ = 16, $^3J_{HH}$ = 7, 6 H, CH*Me*$_2$), 1.19 (dd, $^4J_{PH}$ = 16, $^3J_{HH}$ = 7, 6 H, CH*Me*$_2$), 0.45 (s 3 H, Pd–CH_3). ^{31}P{^{1}H} NMR (THF-d_8): δ 40.5. ^{13}C{^{1}H} NMR (THF-d_8): δ 177.2 (O*C*(O)Me), 149.3 (d, J_{PC} = 11, C^2), 139.8 (d, J_{PC} = 5, C^5), 133.5 (C^6), 131.5 (C^4), 129.5 (d, J_{PC} = 7, C^3), 126.0 (d, J_{PC} = 28, C^1), 26.3 (d, J_{PC} = 27, *C*HMe_2), 21.0 (s, *C*H_3–$ArSO_3$), 19.3 (d, J_{PC} = 5, CH*Me*$_2$), 18.5 (s, CH*Me*$_2$), -7.0 (d, $^2J_{PC}$ = 5, Pd–*C*H_3). The Pd–OC(O)*Me* is obscured by the THF-d_8 resonance at δ 25.1 but was detected by HMQC. ^{7}Li{^{1}H} NMR (THF-d_8): δ 0.0. The presence of an OAc group in **4a** was confirmed by reaction with $B(C_6F_5)_3$, which yields the known $B(C_6F_5)_3(OAc)^-$, characterized by ESI–MS.[25] IR (KBr): 1575, 1433 cm^{-1}. Anal. Calcd. for $C_{16}H_{26}LiO_5PPdS$: C, 40.48; H, 5.52. Found: C, 40.38; H, 5.67.

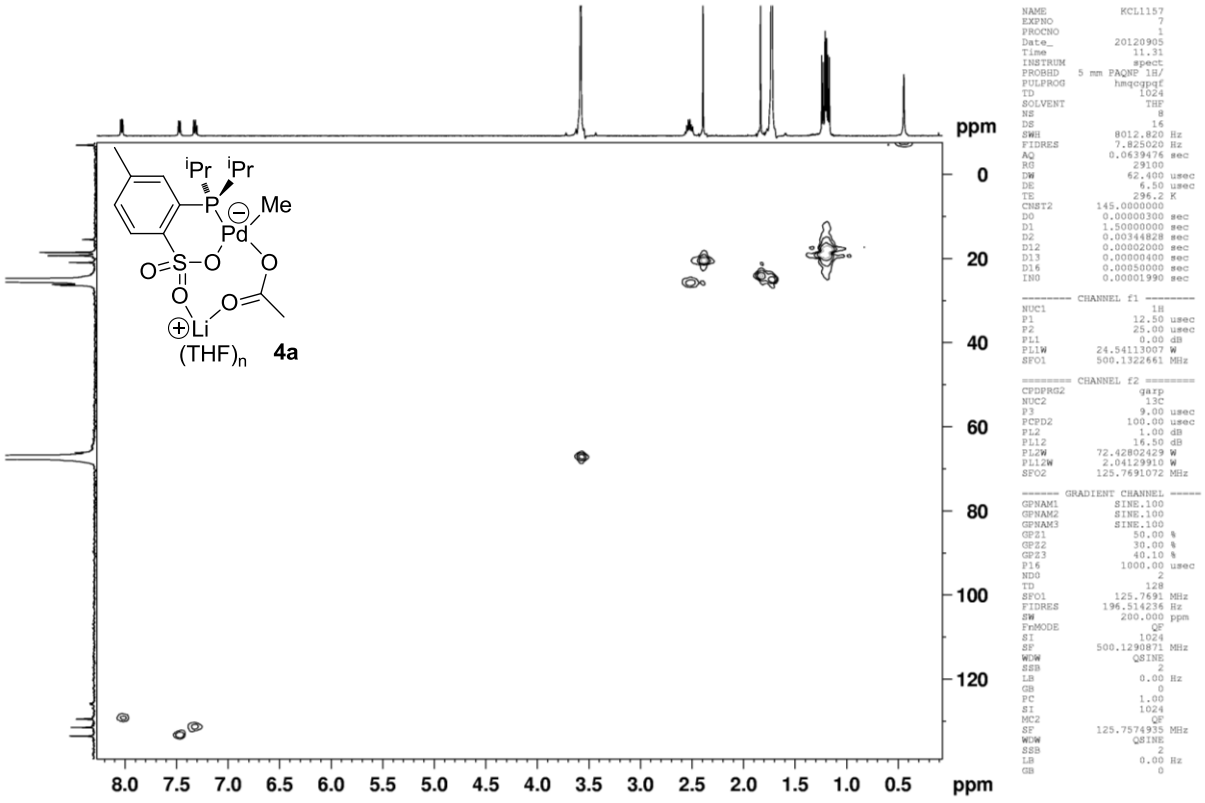


```
NAME            KCL1157
EXPNO                 7
PROCNO                1
Date_          20120905
Time              11.31
INSTRUM           spect
PROBHD   5 mm PAQNP 1H/
PULPROG       hmqcgpqf
TD                 1024
SOLVENT             THF
NS                    8
DS                   16
SWH           8012.820 Hz
FIDRES        7.825020 Hz
AQ            0.0639476 sec
RG                29100
DW               62.400 usec
DE                6.50 usec
TE              296.2 K
CNST2       145.00000000
D0            0.00000300 sec
D1            1.50000000 sec
D2            0.00344828 sec
D12           0.00002000 sec
D13           0.00000400 sec
D16           0.00050000 sec
IN0           0.00001990 sec

======== CHANNEL f1 ========
NUC1                1H
P1                12.50 usec
P2                25.00 usec
PL1                0.00 dB
PL1W        24.54113007 W
SFO1       500.1322661 MHz

======== CHANNEL f2 ========
CPDPRG2           garp
NUC2               13C
P3                9.00 usec
PCPD2           100.00 usec
PL2                1.00 dB
PL12              16.50 dB
PL2W        72.42802429 W
PL12W        2.04129910 W
SFO2       125.7691072 MHz

======= GRADIENT CHANNEL =====
GPNAM1          SINE.100
GPNAM2          SINE.100
GPNAM3          SINE.100
GPZ1              50.00 %
GPZ2              30.00 %
GPZ3              40.10 %
P16             1000.00 usec
ND0                   2
TD                  128
SFO1       125.7691 MHz
FIDRES     196.514236 Hz
SW            200.000 ppm
FnMODE              QF
SI                1024
SF         500.1290871 MHz
WDW             QSINE
SSB                   2
LB                0.00 Hz
GB                    0
PC                1.00
SI                1024
MC2                 QF
SF         125.7574935 MHz
WDW             QSINE
SSB                   2
LB                0.00 Hz
GB                    0
```

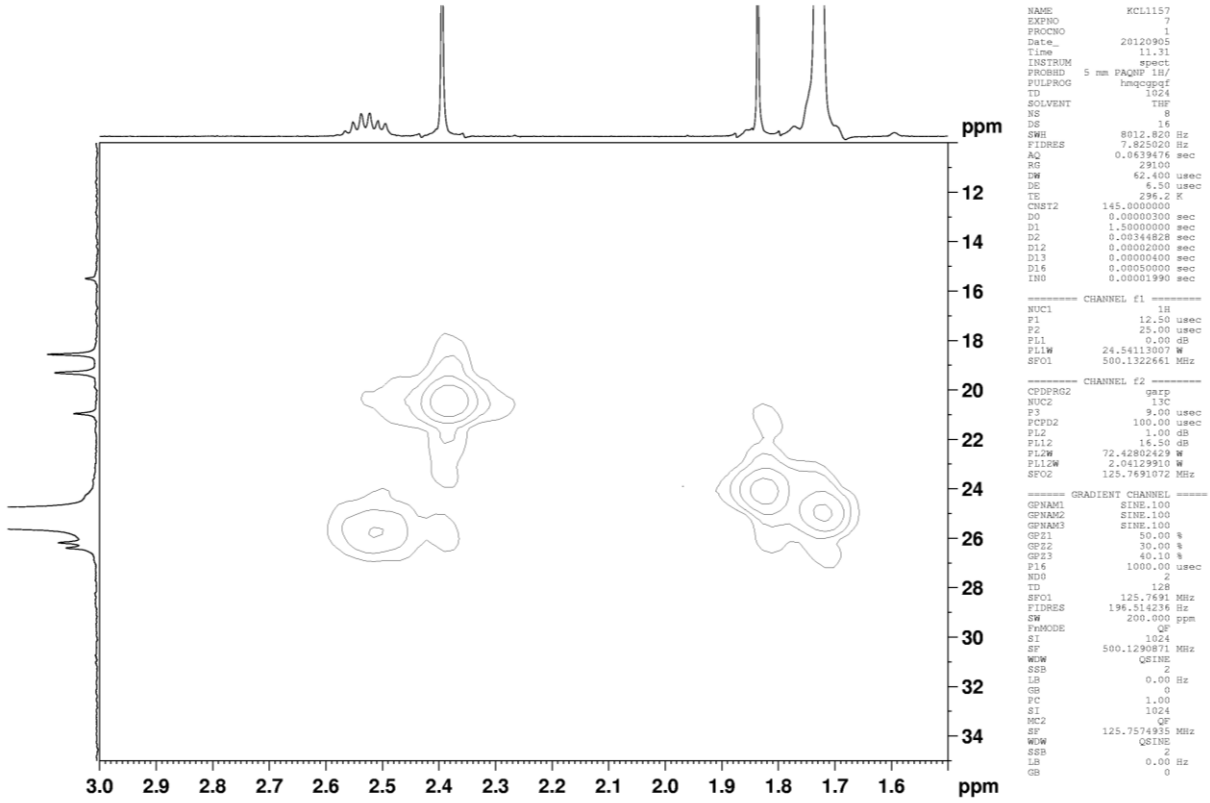


```
NAME            KCL1157
EXPNO                 7
PROCNO                1
Date_          20120905
Time              11.31
INSTRUM           spect
PROBHD   5 mm PAQNP 1H/
PULPROG       hmqcgpqf
TD                 1024
SOLVENT             THF
NS                    8
DS                   16
SWH           8012.820 Hz
FIDRES        7.825020 Hz
AQ            0.0639476 sec
RG                29100
DW               62.400 usec
DE                6.50 usec
TE              296.2 K
CNST2       145.00000000
D0            0.00000300 sec
D1            1.50000000 sec
D2            0.00344828 sec
D12           0.00002000 sec
D13           0.00000400 sec
D16           0.00050000 sec
IN0           0.00001990 sec

======== CHANNEL f1 ========
NUC1                1H
P1                12.50 usec
P2                25.00 usec
PL1                0.00 dB
PL1W        24.54113007 W
SFO1       500.1322661 MHz

======== CHANNEL f2 ========
CPDPRG2           garp
NUC2               13C
P3                9.00 usec
PCPD2           100.00 usec
PL2                1.00 dB
PL12              16.50 dB
PL2W        72.42802429 W
PL12W        2.04129910 W
SFO2       125.7691072 MHz

======= GRADIENT CHANNEL =====
GPNAM1          SINE.100
GPNAM2          SINE.100
GPNAM3          SINE.100
GPZ1              50.00 %
GPZ2              30.00 %
GPZ3              40.10 %
P16             1000.00 usec
ND0                   2
TD                  128
SFO1       125.7691 MHz
FIDRES     196.514236 Hz
SW            200.000 ppm
FnMODE              QF
SI                1024
SF         500.1290871 MHz
WDW             QSINE
SSB                   2
LB                0.00 Hz
GB                    0
PC                1.00
SI                1024
MC2                 QF
SF         125.7574935 MHz
WDW             QSINE
SSB                   2
LB                0.00 Hz
GB                    0
```

Li[(PO-^{i}Pr)PdMe(OAc-$^{13}C_1$)] (4a-$^{13}C_1$). This compound was made using the procedure for **4a** with acetic acid-1-^{13}C and isolated in 75 % yield (99 mg, 0.21 mmol). The NMR data are identical to those of **4a** except that the ^{1}H NMR spectrum exhibited C–H coupling for Pd–O^{13}C(O)CH_3. ^{1}H NMR (THF-d_8): δ 1.84 (d, $^{2}J_{CH}$ = 7, 3 H, O^{13}C(O)CH_3). IR (KBr): 1535, 1401 cm^{-1}.

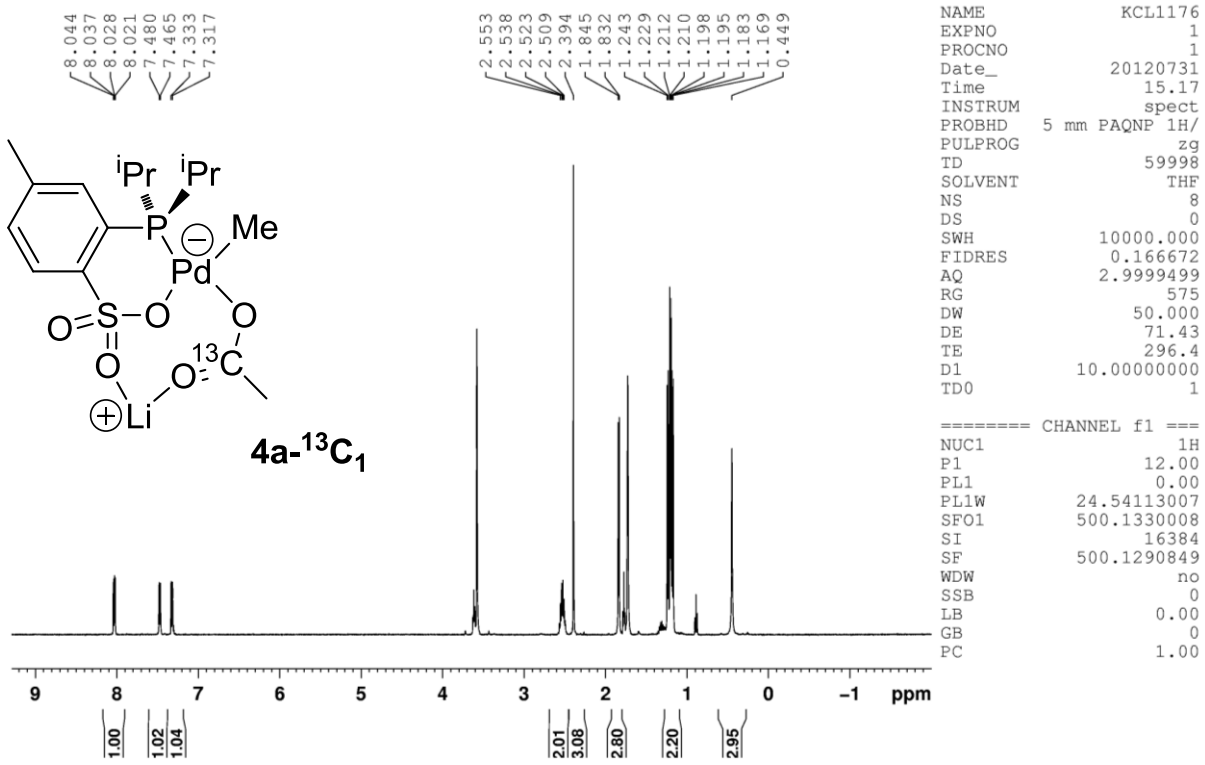

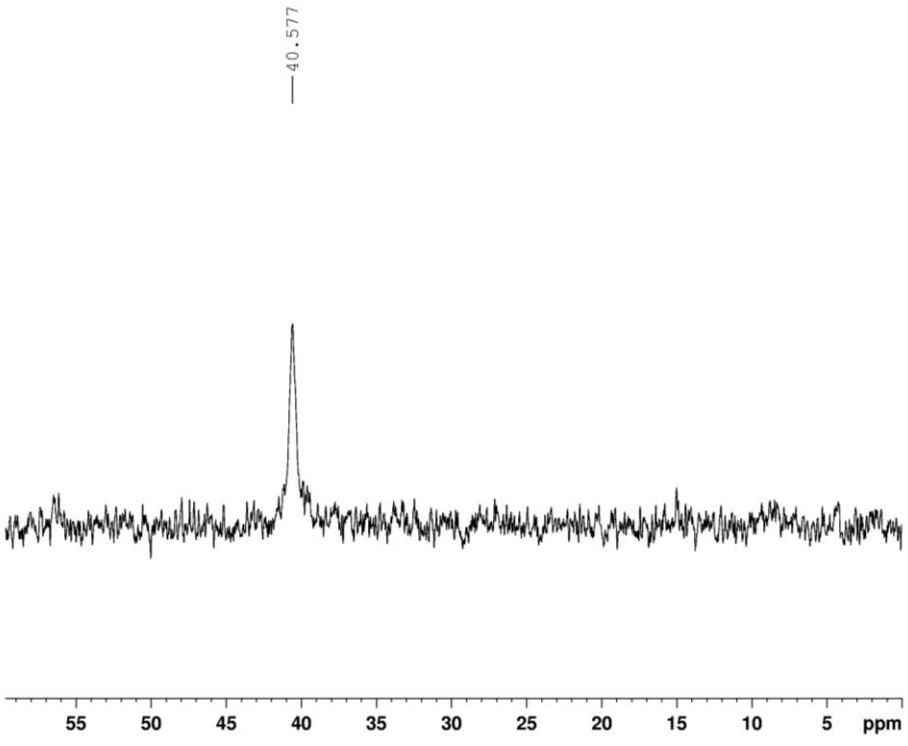

[Li(Crypt211)][(PO-^{i}Pr)PdMe(OAc)] (4b). A solution of Crypt211 in THF (0.0189 M, 1.37 mL, 0.0259 mmol) was added to **4a** (12.3 mg, 0.0259 mmol) to form a colorless solution. After 5 min, hexanes (0.5 mL) were added to the solution. The volatiles were removed under vacuum to afford a white solid (18.0 mg, 0.0236 mmol, 91 %). ^{1}H NMR (THF-d_8): δ 7.99 (dd, $^{3}J_{HH}$ = 8, $^{4}J_{PH}$ = 4, 1 H, H^{3}), 7.41 (d, $^{3}J_{PH}$ = 7, 1 H, H^{6}), 7.22 (d, $^{3}J_{HH}$ = 8, 1 H, H^{4}), 4.01 (br s, 4 H, Crypt), 3.52 (m, 29 H, Crypt), 3.19 (br s, 4 H, Crypt), 2.57 (m, 26 H, C*H*Me$_2$, Crypt), 2.35 (s, 3 H, C*H*$_3$–ArSO$_3$), 2.01 (br s, 3 H, OC(O)C*H*$_3$), 1.23 (dd, $^{4}J_{PH}$ = 17, $^{3}J_{HH}$ = 7, 6 H, CH*Me*$_2$), 1.19 (dd, $^{4}J_{PH}$ = 15, $^{3}J_{HH}$ = 7, 6 H, CH*Me*$_2$), 0.41 (d, $^{3}J_{PH}$ = 2, 3 H, Pd–C*H*$_3$). ^{31}P{^{1}H} NMR (THF-d_8): δ 39.0. ^{13}C{^{1}H} NMR (THF-d_8): δ 175.2 (O*C*(O)Me), 151.9 (d, J_{PC} = 9, C^{2}), 138.2 (C^{5}), 133.3 (C^{6}), 130.9 (C^{4}), 128.8 (d, J_{PC} = 7, C^{3}), 126.3 (d, J_{PC} = 32, C^{1}), 69.4 (Crypt), 52.8 (Crypt), 51.8 (Crypt), 26.3 (d, J_{PC} = 26, *C*HMe$_2$), 21.0 (s, *C*H$_3$–ArSO$_3$), 19.5 (d, J_{PC} = 5, CH*Me*$_2$), 18.9 (s,

CH*Me*$_2$), -8.1 (Pd–*C*H$_3$). Three Crypt211 signals are obscured by the THF-d_8 resonance at δ 67.2. The Pd–OC(O)*Me* resonance is obscured by the THF-d_8 resonance at δ 25.1 but that of **4b-^{13}C$_1$** was detected by HMQC (See below). ^{7}Li{^{1}H} NMR (THF-d_8): δ -0.2. IR (KBr): 1606, 1369 cm^{-1}. Addition of [Li(Et$_2$O)$_{2.8}$][B(C$_6$F$_5$)$_4$] to a solution of **4b** in THF-d_8 regenerates **4a**.

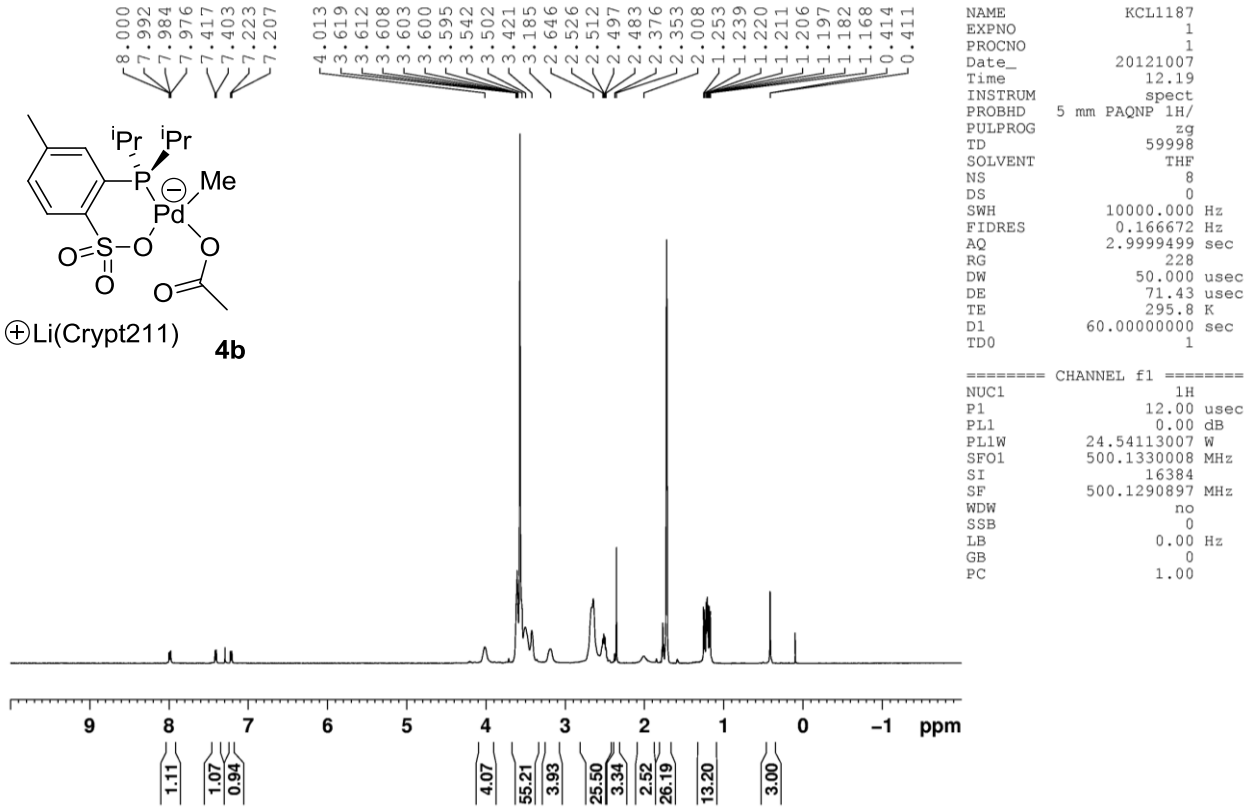

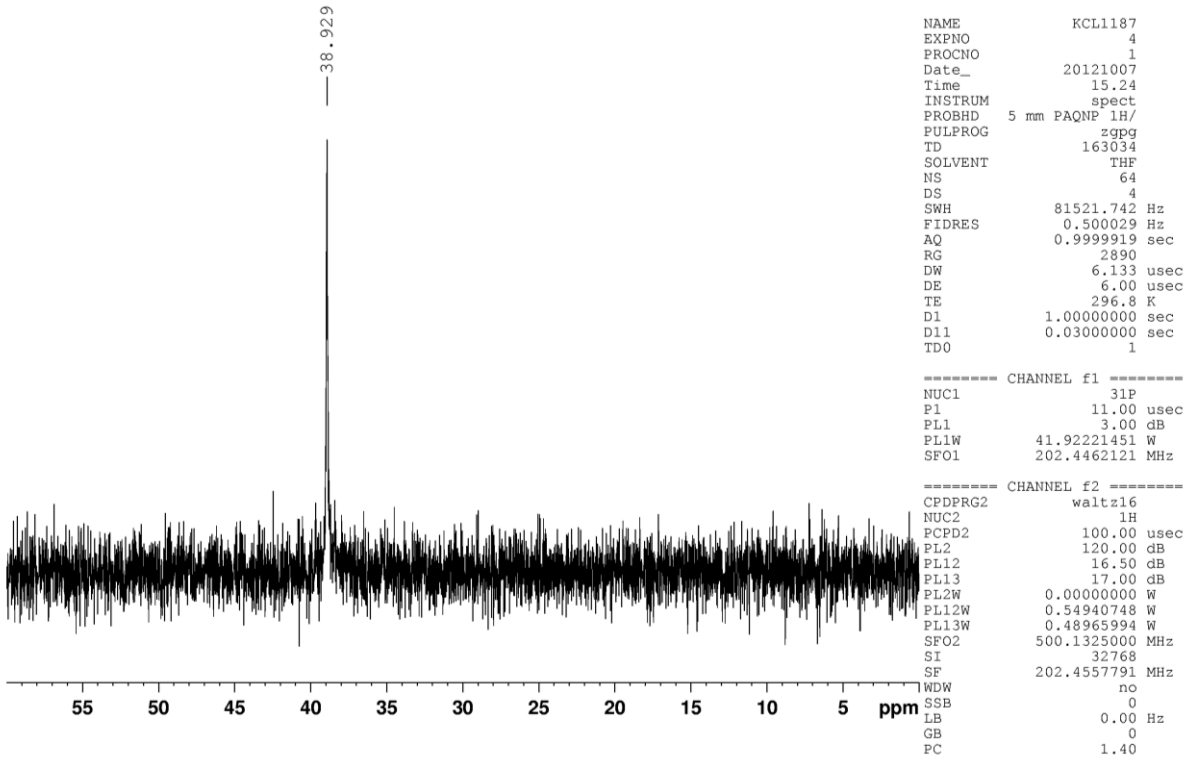
38.929
55 50 45 40 35 30 25 20 15 10 5 ppm
NAME KCL1187
EXPNO 4
PROCNO 1
Date_ 20121007
Time 15.24
INSTRUM spect
PROBHD 5 mm PAQNP 1H/
PULPROG zgpg
TD 163034
SOLVENT THF
NS 64
DS 4
SWH 81521.742 Hz
FIDRES 0.500029 Hz
AQ 0.9999919 sec
RG 2890
DW 6.133 usec
DE 6.00 usec
TE 296.8 K
D1 1.00000000 sec
D11 0.03000000 sec
TD0 1
======== CHANNEL f1 ========
NUC1 31P
P1 11.00 usec
PL1 3.00 dB
PL1W 41.92221451 W
SFO1 202.4462121 MHz
======== CHANNEL f2 ========
CPDPRG2 waltz16
NUC2 1H
PCPD2 100.00 usec
PL2 120.00 dB
PL12 16.50 dB
PL13 17.00 dB
PL2W 0.00000000 W
PL12W 0.54940748 W
PL13W 0.48965994 W
SFO2 500.1325000 MHz
SI 32768
SF 202.4557791 MHz
WDW no
SSB 0
LB 0.00 Hz
GB 0
PC 1.40

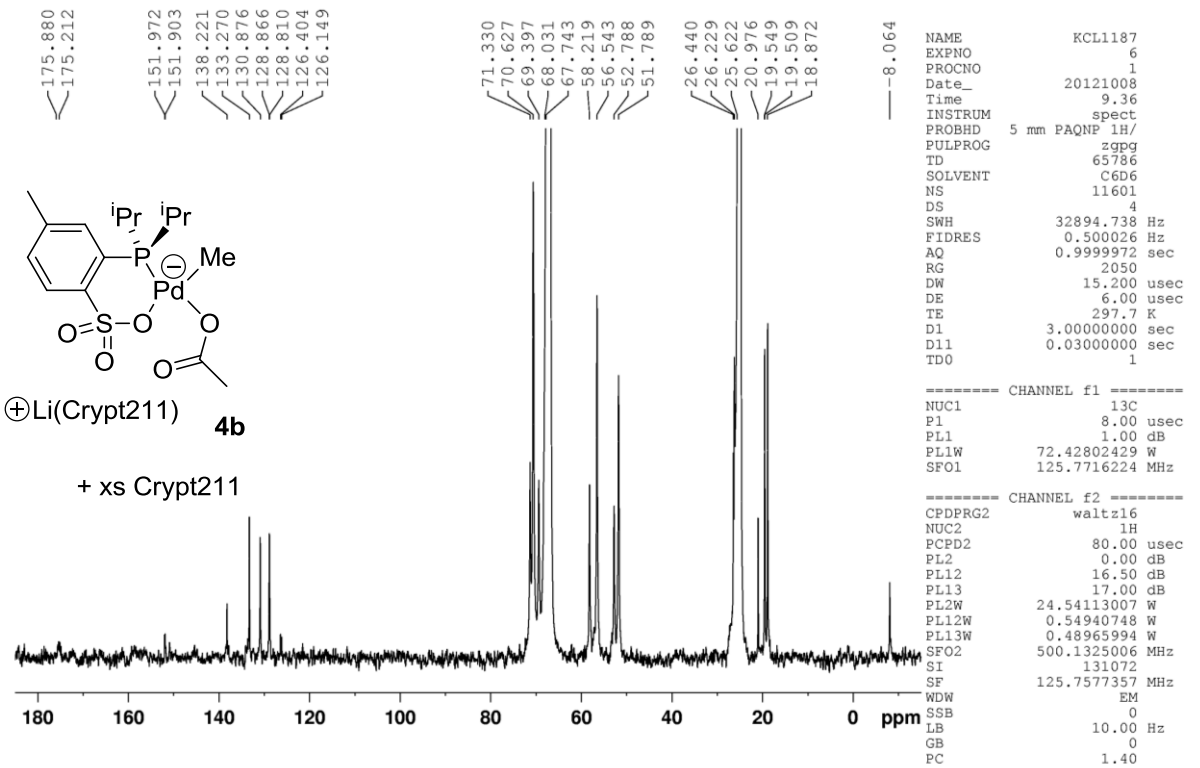
175.880
175.212
151.972
151.903
138.221
133.270
130.876
128.866
128.810
126.404
126.149
71.330
70.627
69.397
68.031
67.743
58.219
56.543
52.788
51.789
26.440
26.229
25.622
20.976
19.549
19.509
18.872
8.064
iPr iPr
P
Me
Pd
S
O
O
O
O
O
⊕Li(Crypt211)
4b
+ xs Crypt211
180 160 140 120 100 80 60 40 20 0 ppm
NAME KCL1187
EXPNO 6
PROCNO 1
Date_ 20121008
Time 9.36
INSTRUM spect
PROBHD 5 mm PAQNP 1H/
PULPROG zgpg
TD 65786
SOLVENT C6D6
NS 11601
DS 4
SWH 32894.738 Hz
FIDRES 0.500026 Hz
AQ 0.9999972 sec
RG 2050
DW 15.200 usec
DE 6.00 usec
TE 297.7 K
D1 3.00000000 sec
D11 0.03000000 sec
TD0 1
======== CHANNEL f1 ========
NUC1 13C
P1 8.00 usec
PL1 1.00 dB
PL1W 72.42802429 W
SFO1 125.7716224 MHz
======== CHANNEL f2 ========
CPDPRG2 waltz16
NUC2 1H
PCPD2 80.00 usec
PL2 0.00 dB
PL12 16.50 dB
PL13 17.00 dB
PL2W 24.54113007 W
PL12W 0.54940748 W
PL13W 0.48965994 W
SFO2 500.1325006 MHz
SI 131072
SF 125.7577357 MHz
WDW EM
SSB 0
LB 10.00 Hz
GB 0
PC 1.40

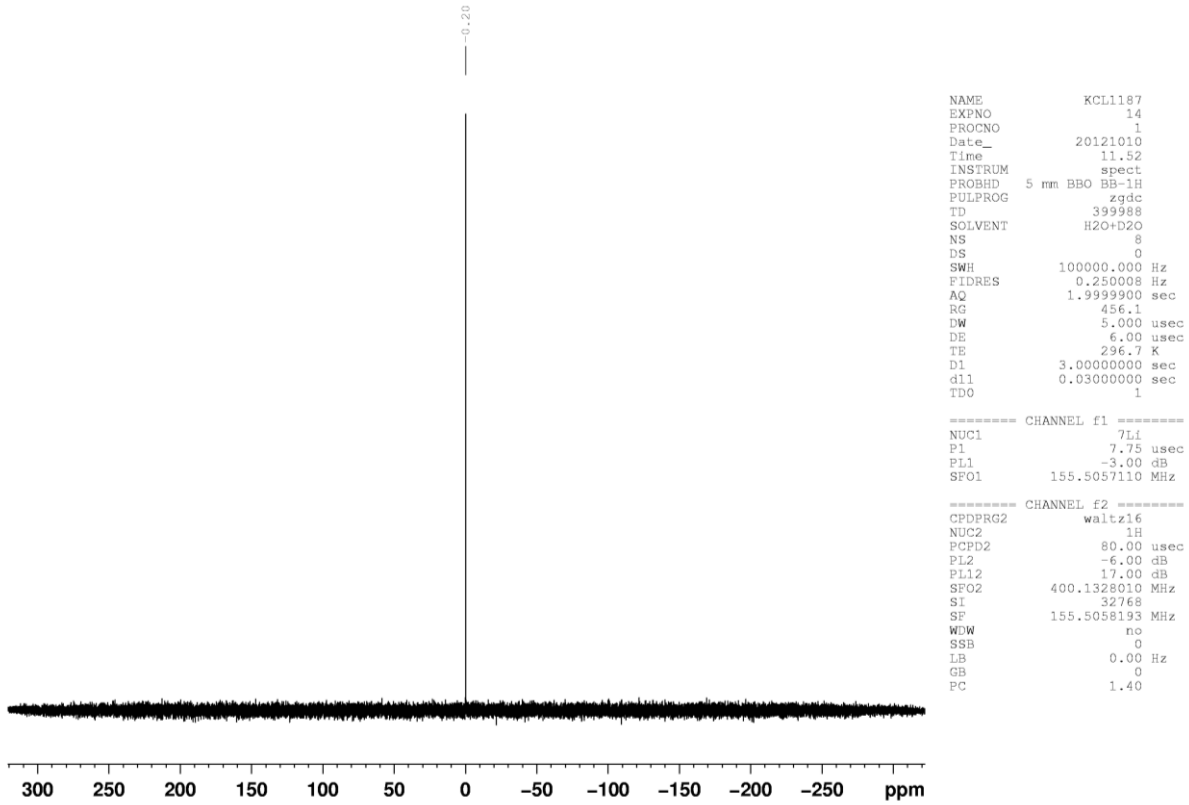

[**Li(Crypt211)][(PO-^{i}Pr)PdMe(OAc-$^{13}C_1$)] (4b-$^{13}C_1$).** This compound was made from **4a-$^{13}C_1$** using the procedure for **4b** and isolated in 82 % yield (50 mg, 0.66 mmol). The NMR data are identical to those of **4b** and showed that this product contains 0.28 equiv excess Crypt211. IR (KBr): 1558, 1359 cm^{-1}. Anal. Calcd. for $C_{30}H_{54}LiN_2O_9PPdS$ + 0.28 $C_{14}H_{28}N_2O_4$: C, 47.08; H, 7.15; N, 4.14. Found: C, 47.16; H, 7.08; N, 3.95.

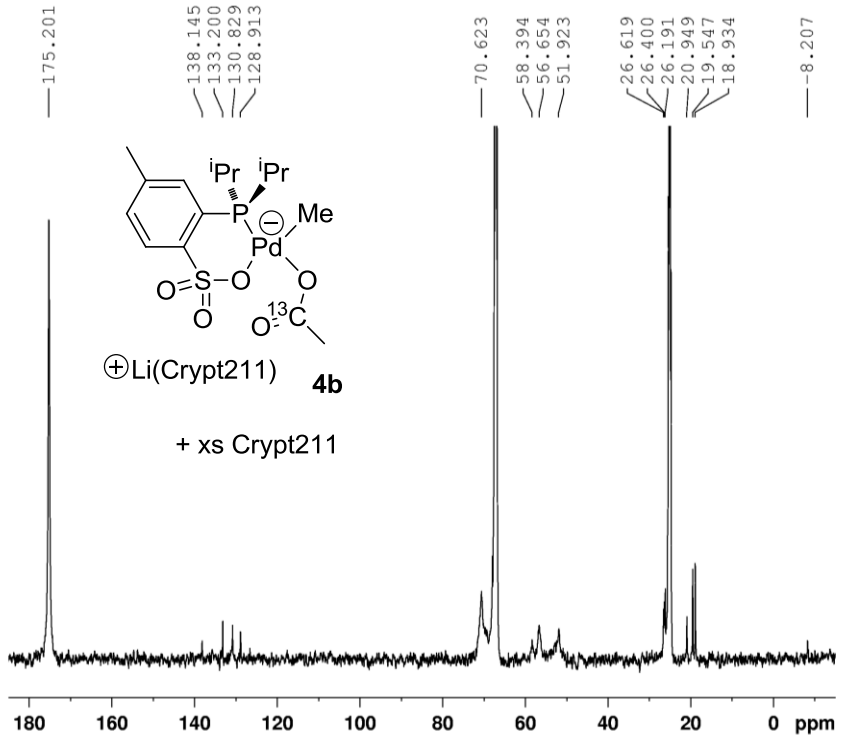


```
NAME                KCL1187
EXPNO                    10
PROCNO                    1
Date_              20121020
Time                  19.01
INSTRUM               spect
PROBHD    5 mm PAQNP 1H/
PULPROG                zgpg
TD                    32890
SOLVENT                 THF
NS                      858
DS                        4
SWH              32894.738 Hz
FIDRES            1.000144 Hz
AQ               0.4999780 sec
RG                     2050
DW                   15.200 usec
DE                    6.00 usec
TE                   323.0 K
D1             3.00000000 sec
D11            0.03000000 sec
TD0                       1

======== CHANNEL f1 ========
NUC1                    13C
P1                    8.00 usec
PL1                   1.00 dB
PL1W          72.42802429 W
SFO1         125.7716224 MHz

======== CHANNEL f2 ========
CPDPRG2             waltz16
NUC2                    1H
PCPD2                80.00 usec
PL2                   0.00 dB
PL12                 16.50 dB
```

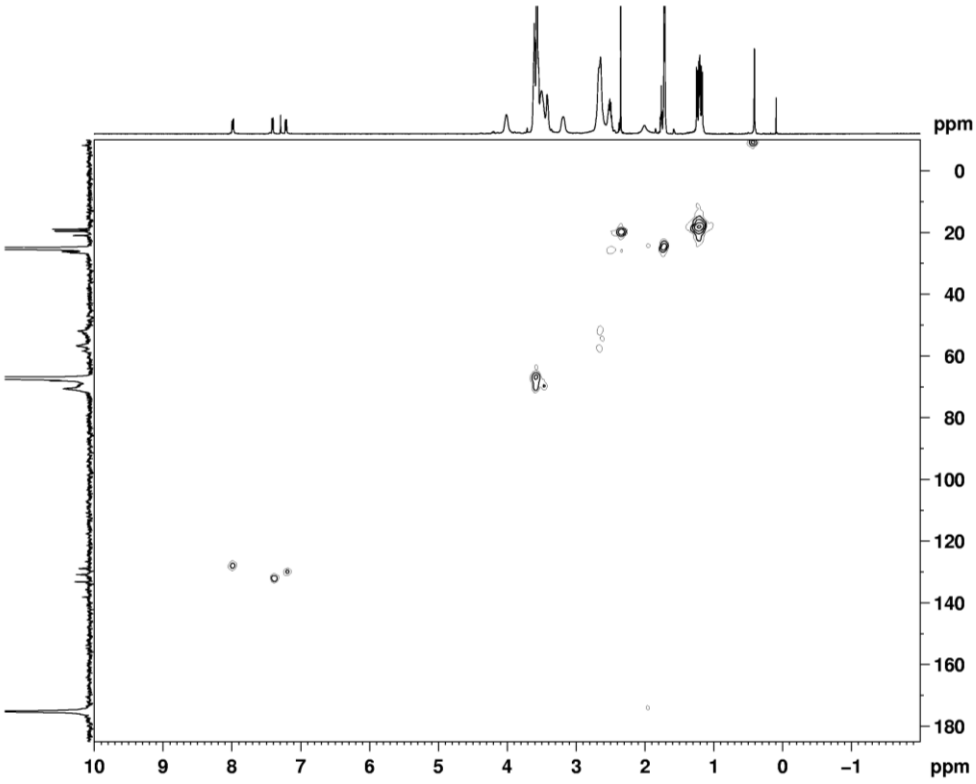


```
NAME                KCL1187
EXPNO                    13
PROCNO                    1
Date_              20121020
Time                  19.32
INSTRUM               spect
PROBHD    5 mm PAQNP 1H/
PULPROG             hmqcgpqf
TD                      1024
SOLVENT                 THF
NS                        8
DS                       16
SWH              10000.000 Hz
FIDRES            9.765625 Hz
AQ               0.0512500 sec
RG                     29100
DW                   50.000 usec
DE                    6.50 usec
TE                   329.9 K
CNST2          145.0000000
D0             0.00000300 sec
D1             2.50000000 sec
D2             0.00344828 sec
D12            0.00002000 sec
D13            0.00000400 sec
D16            0.00050000 sec
IN0            0.00001530 sec

======== CHANNEL f1 ========
NUC1                    1H
P1                   12.50 usec
P2                   25.00 usec
PL1                   0.00 dB
PL1W          24.54113007 W
SFO1         500.1320005 MHz

======== CHANNEL f2 ========
CPDPRG2              garp
NUC2                    13C
P3                   11.80 usec
PCPD2               100.00 usec
PL2                   1.00 dB
PL12                 16.50 dB
PL2W          72.42802429 W
PL12W          2.04129910 W
SFO2         125.7703648 MHz

====== GRADIENT CHANNEL =====
GPNAM1            SINE.100
GPNAM2            SINE.100
GPNAM3            SINE.100
GPZ1                 50.00 %
GPZ2                 30.00 %
GPZ3                 40.10 %
P16                1000.00 usec
NDS                       2
TD                      115
SFO1             125.7704 MHz
FIDRES           284.350403 Hz
SW                 260.000 ppm
FnMODE                   QF
SI                     1024
SF           500.1290894 MHz
WDW                  QSINE
SSB                       2
LB                    0.00 Hz
GB                        0
PC                    1.00
SI                     1024
MC2                      QF
SF           125.7575788 MHz
WDW                  QSINE
SSB                       2
LB                    0.00 Hz
GB                        0
```

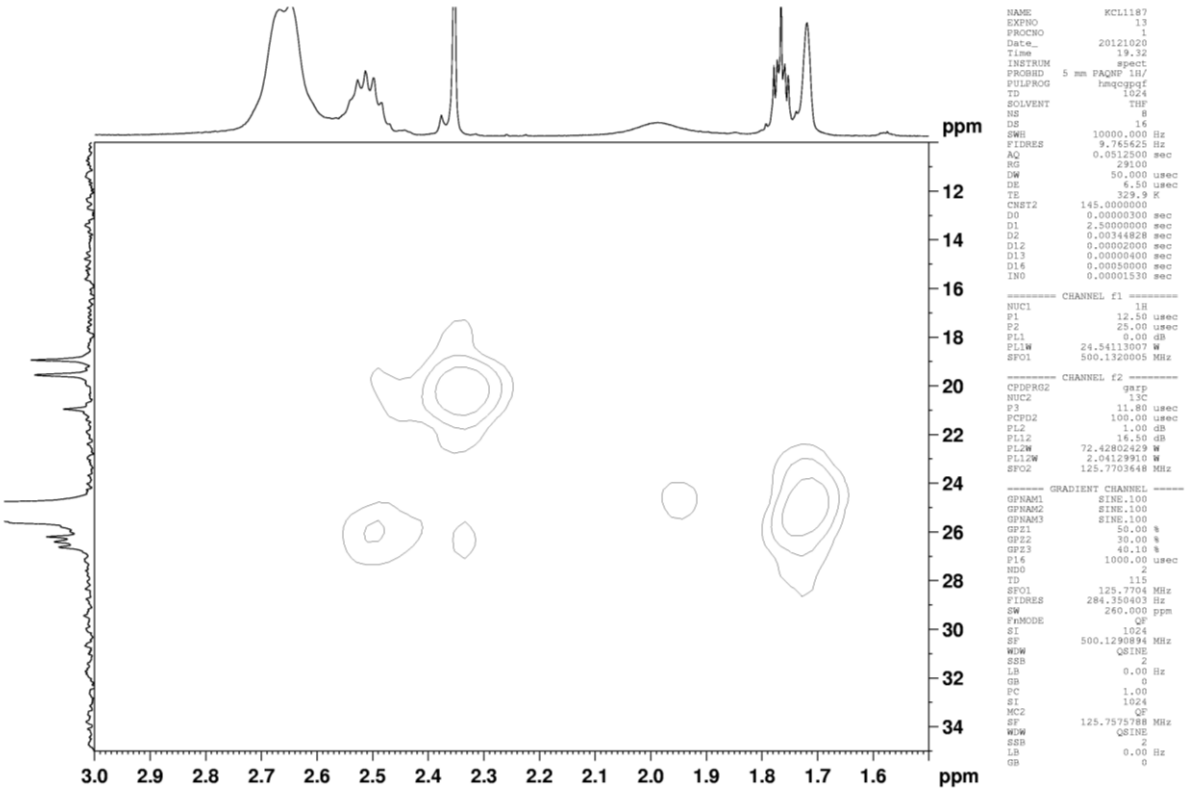

Generation of Li[(PO-^{i}Pr)PdMe(κ^{1}–PO-^{i}Pr)] (5). This species was generated to support the identity of the side-product in the reaction of **3a** with CO_2. A valved J. Young NMR tube was charged with H[PO-^{i}Pr] (2.3 mg, 0.0080 mmol) and **3a** (4.7 mg, 0.0041 mmol, i.e. 0.0082 mmol of (PO)PdMe$_2^-$ units). THF-d_8 (0.60 mL) was added by vacuum transfer at -196 ˚C. The reaction mixture was thawed at room temperature and a colorless solution was formed. Exchange of the two sulfonate rings is fast on the NMR time scale at room temperature but slow at -80 ˚C. ^{1}H NMR (THF-d_8): δ 8.07 (br d, $^{3}J_{HH}$ = 8, 2 H, H^{3}), 7.46 (br s, 2 H, H^{6}), 7.29 (br d, $^{3}J_{HH}$ = 8, 2 H, H^{4}), 2.80 (br s, 4 H, C*H*Me$_2$), 2.39 (s, 6 H, C*H*$_3$–ArSO$_3$), 1.31 (m, 24 H, CH*Me$_2$*), 0.25 (t, $^{3}J_{PH}$ = 6, 3 H, Pd–C*H*$_3$). ^{1}H NMR (THF-d_8, -80 ˚C): δ 7.98 (br d, *J* = 12, 2 H, H^{3}), 7.77 (br s, 1 H, H^{6}), 7.50 (br d, $^{3}J_{HH}$ = 8, 1 H, H^{4}), 7.45 (br s, 1 H, H^{6}), 7.37 (br d, $^{3}J_{HH}$ = 10, 1 H, H^{4}), 2.87 (m, 4 H,

C*H*Me$_2$), 2.45 (s, 3 H, C*H*$_3$–ArSO$_3$), 2.41 (s, 3 H, C*H*$_3$–ArSO$_3$'), 1.6 – 1.0 (m, 24 H, CH*Me$_2$*), 0.29 (br s, 3 H, Pd–C*H*$_3$). ^{31}P{^{1}H} NMR (THF-d_8): δ 27.9 (br s). ^{31}P{^{1}H} NMR (-90 ˚C, THF-d_8): δ 31.9 (d, J_{PP} = 388), 19.9 (d, J_{PP} = 388). ^{13}C{^{1}H} NMR (THF-d_8): δ 149.4 (t, J_{PC} = 5, C^2), 139.2 (br s, C^5), 134.2 (br s, C^6), 130.9 (C^4), 130.5 (br s, C^3), 126.2 (t, J_{PC} = 15, C^1), 25.9 (br s, *C*HMe$_2$), 21.0 (br s, *C*H$_3$–ArSO$_3$), 19.9 (br s, CH*Me$_2$*), -7.1 (br s, Pd–*C*H$_3$). ESI–MS (THF/MeOH, negative ion mode): *m*/*z* 695.0 (M – Li$^+$)$^-$.

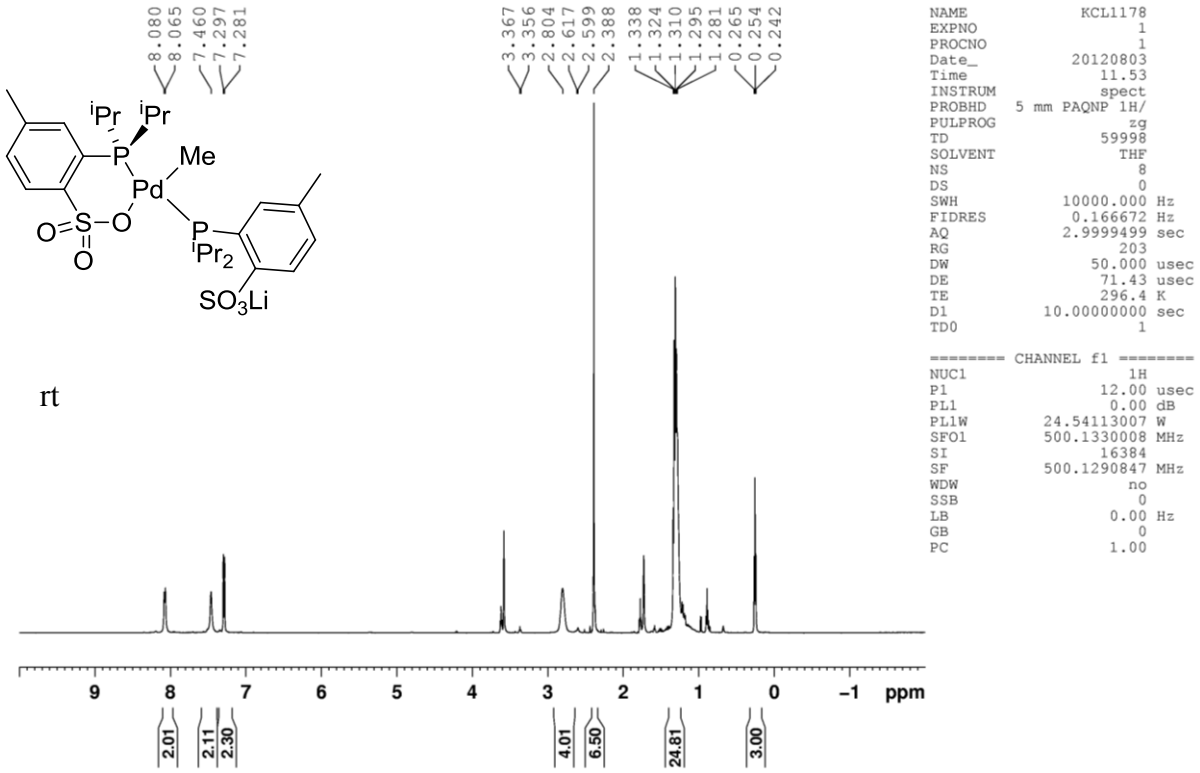

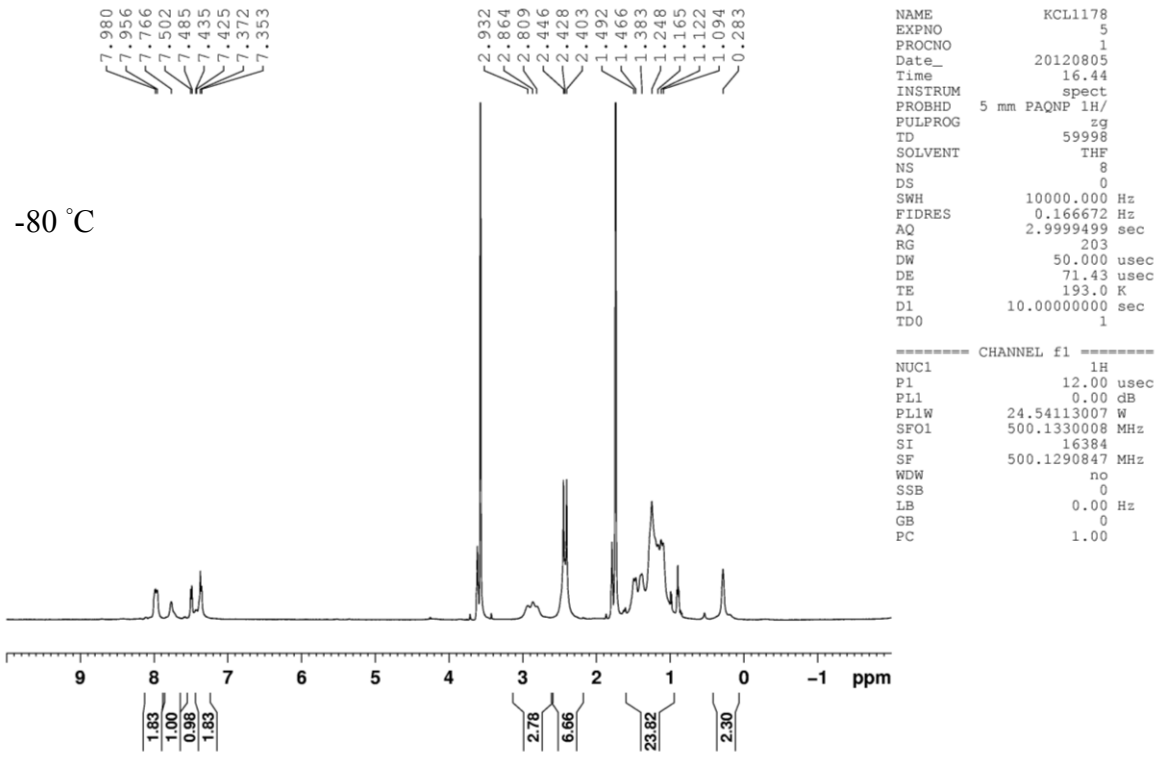
-80 ℃
7.980
7.956
7.766
7.502
7.485
7.435
7.425
7.372
7.353
2.932
2.864
2.809
2.446
2.428
2.403
1.492
1.466
1.383
1.248
1.165
1.122
1.094
0.283
9 8 7 6 5 4 3 2 1 0 −1 ppm
1.83
1.00
0.98
1.83
2.78
6.66
23.82
2.30
NAME KCL1178
EXPNO 5
PROCNO 1
Date_ 20120805
Time 16.44
INSTRUM spect
PROBHD 5 mm PAQNP 1H/
PULPROG zg
TD 59998
SOLVENT THF
NS 8
DS 0
SWH 10000.000 Hz
FIDRES 0.166672 Hz
AQ 2.9999499 sec
RG 203
DW 50.000 usec
DE 71.43 usec
TE 193.0 K
D1 10.00000000 sec
TD0 1
======== CHANNEL f1 ========
NUC1 1H
P1 12.00 usec
PL1 0.00 dB
PL1W 24.54113007 W
SFO1 500.1330008 MHz
SI 16384
SF 500.1290847 MHz
WDW no
SSB 0
LB 0.00 Hz
GB 0
PC 1.00

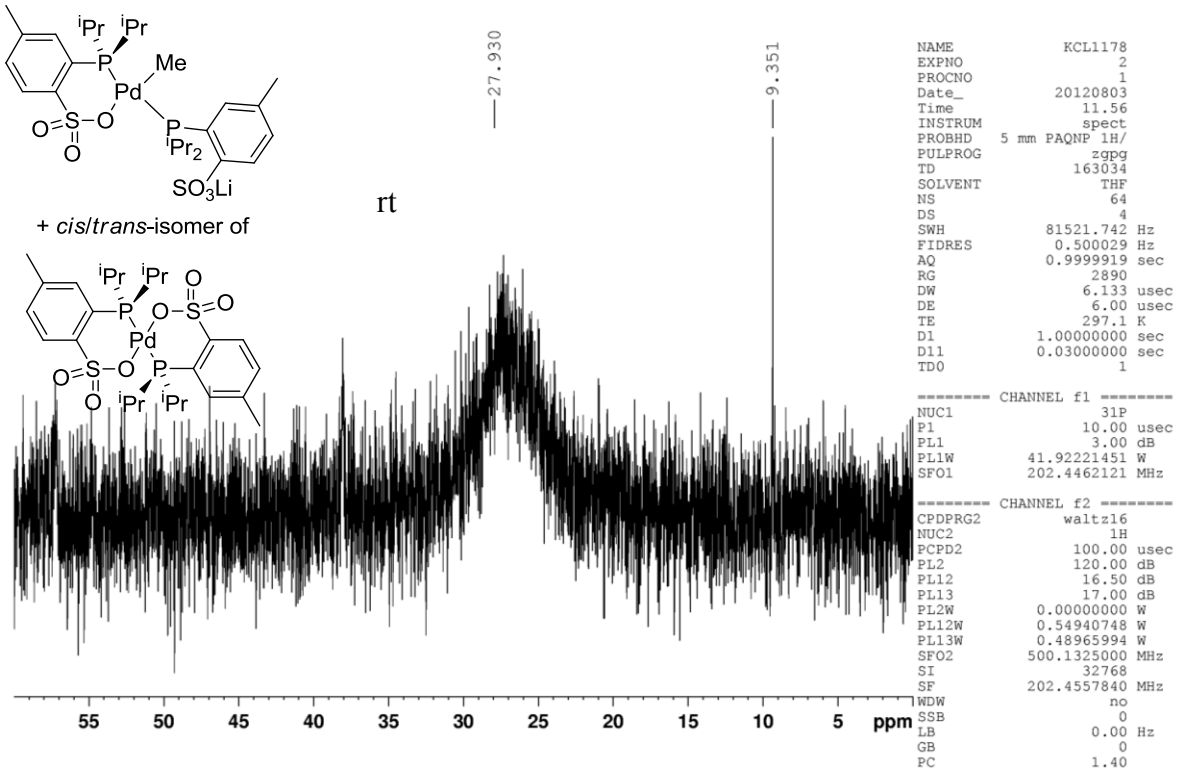
iPr iPr
P
Me
Pd
O
S
O
O
P
iPr2
SO3Li
+ cis/trans-isomer of
rt
27.930
9.351
55 50 45 40 35 30 25 20 15 10 5 ppm
NAME KCL1178
EXPNO 2
PROCNO 1
Date_ 20120803
Time 11.56
INSTRUM spect
PROBHD 5 mm PAQNP 1H/
PULPROG zgpg
TD 163034
SOLVENT THF
NS 64
DS 4
SWH 81521.742 Hz
FIDRES 0.500029 Hz
AQ 0.9999919 sec
RG 2890
DW 6.133 usec
DE 6.00 usec
TE 297.1 K
D1 1.00000000 sec
D11 0.03000000 sec
TD0 1
======== CHANNEL f1 ========
NUC1 31P
P1 10.00 usec
PL1 3.00 dB
PL1W 41.92221451 W
SFO1 202.4462121 MHz
======== CHANNEL f2 ========
CPDPRG2 waltz16
NUC2 1H
PCPD2 100.00 usec
PL2 120.00 dB
PL12 16.50 dB
PL13 17.00 dB
PL2W 0.00000000 W
PL12W 0.54940748 W
PL13W 0.48965994 W
SFO2 500.1325000 MHz
SI 32768
SF 202.4557840 MHz
WDW no
SSB 0
LB 0.00 Hz
GB 0
PC 1.40

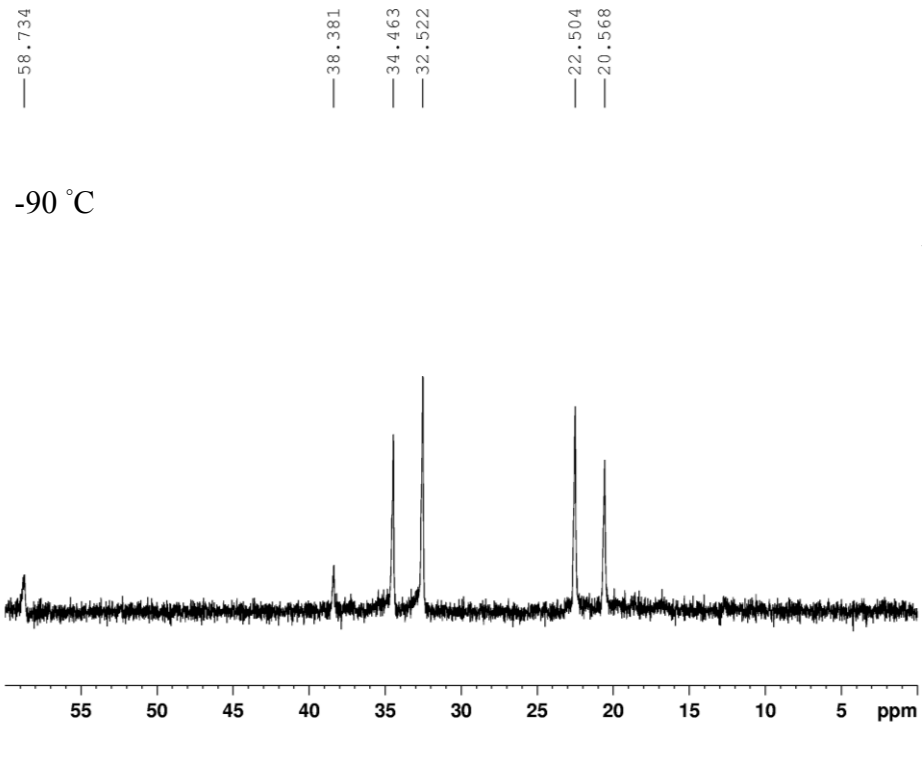

NAME	KCL1178
EXPNO	20
PROCNO	1
Date_	20120807
Time	20.04
INSTRUM	spect
PROBHD	5 mm PAQNP 1H/
PULPROG	zgpg
TD	163034
SOLVENT	CDCl3
NS	64
DS	4
SWH	81521.742 Hz
FIDRES	0.500029 Hz
AQ	0.9999919 sec
RG	2890
DW	6.133 usec
DE	6.00 usec
TE	182.7 K
D1	1.00000000 sec
D11	0.03000000 sec
TD0	1
======== CHANNEL f1 ========	
NUC1	31P
P1	10.00 usec
PL1	3.00 dB
PL1W	41.92221451 W
SFO1	202.4462121 MHz
======== CHANNEL f2 ========	
CPDPRG2	waltz16
NUC2	1H
PCPD2	100.00 usec
PL2	120.00 dB
PL12	16.50 dB
PL13	17.00 dB
PL2W	0.00000000 W
PL12W	0.54940748 W
PL13W	0.48965994 W
SFO2	500.1325000 MHz
SI	32768
SF	202.4557840 MHz
WDW	no
SSB	0
LB	0.00 Hz
GB	0
PC	1.40

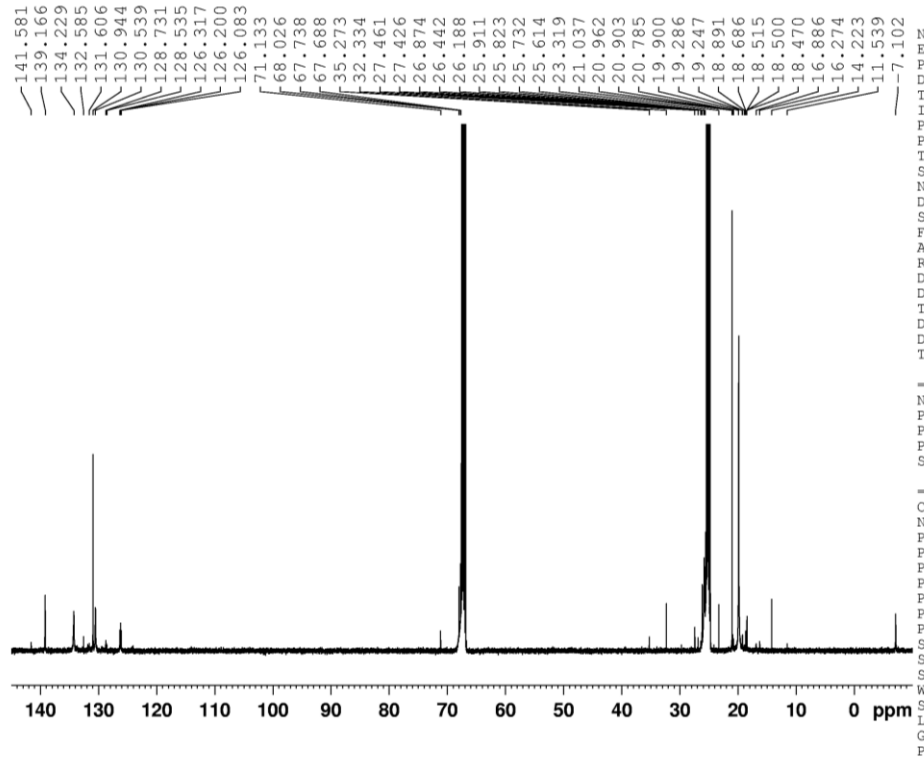

NAME	KCL1178
EXPNO	21
PROCNO	1
Date_	20120910
Time	9.06
INSTRUM	spect
PROBHD	5 mm PAQNP 1H/
PULPROG	zgpg
TD	65786
SOLVENT	DMSO
NS	15600
DS	4
SWH	32894.738 Hz
FIDRES	0.500026 Hz
AQ	0.9999972 sec
RG	2050
DW	15.200 usec
DE	6.00 usec
TE	297.6 K
D1	3.00000000 sec
D11	0.03000000 sec
TD0	1
======== CHANNEL f1 ========	
NUC1	13C
P1	8.00 usec
PL1	1.00 dB
PL1W	72.42802429 W
SFO1	125.7716224 MHz
======== CHANNEL f2 ========	
CPDPRG2	waltz16
NUC2	1H
PCPD2	80.00 usec
PL2	0.00 dB
PL12	16.50 dB
PL13	17.00 dB
PL2W	24.54113007 W
PL12W	0.54940748 W
PL13W	0.48965994 W
SFO2	500.1325006 MHz
SI	131072
SF	125.7576677 MHz
WDW	EM
SSB	0
LB	0.30 Hz
GB	0
PC	1.40

Dynamics of Exchange of 5. A valved J. Young NMR tube was charged with **5** (10.8 mg, 0.0154 mmol) and THF-d_8 (0.51 mL) was added by vacuum transfer at -196 °C. The reaction mixture was thawed at room temperature. The NMR tube was then inserted into an NMR probe that had been pre-cooled to 183 K and spectra were recorded over the temperature range of 183 K – 296 K. In the $^{31}P\{^1H\}$ spectrum, at 183 K, an AB pattern indicative of the presence of two inequivalent phosphine-sulfonate ligands was observed. As the temperature was raised, the doublets broadened and eventually coalesced. Representative experimental and simulated $^{31}P\{^1H\}$ spectra (gNMR) are shown in Figure 2.21.

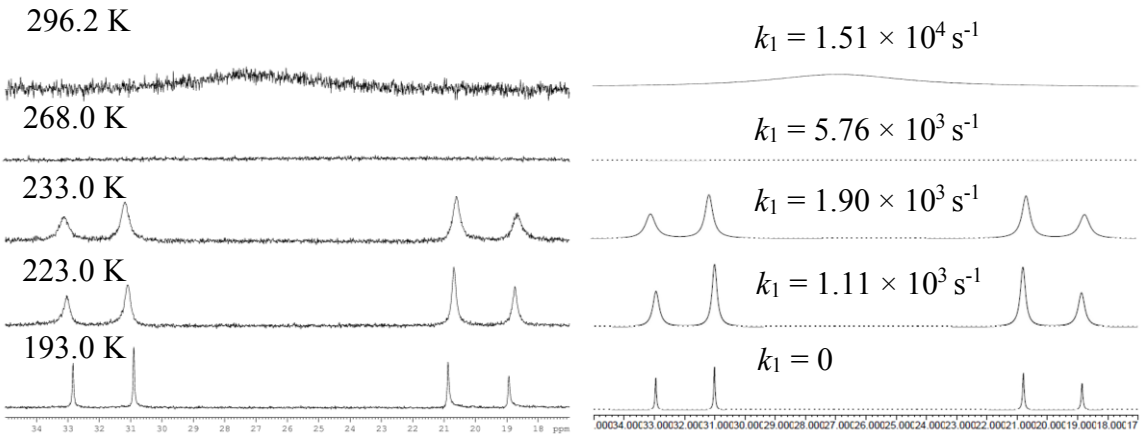

Figure 2.21. Representative variable temperature $^{31}P\{^1H\}$ NMR spectra of **5** in THF-d_8. Experimental spectra are shown on the left and simulated spectra are shown on the right. The first-order rate constants for the exchange of the two phosphine-sulfonate ligands are shown for each temperature.

The rate law for this dynamic process is given in eq 3. From the $^{31}P\{^1H\}$ NMR spectra, the first-order rate constants for the exchange (k_1) were obtained from the line broadening of the

two inequivalent resonances of **5** using eq 4 over the temperature range of 193 K – 263 K, from the coalescence of the two inequivalent resonances of **5** using eq 5 at 268 K, and from the sharpening of the coalesced ^{31}P resonance using eq 6 in the range of 273 K – 296 K. Additionally, rate constants at all temperatures were obtained by total lineshape simulation using the program gNMR. As expected, these two approaches gave similar values for k_1; the values for k_1 determined using gNMR are shown in Figure 2.21.

Exchange rate = k_2[**5**] (3)

Slow exchange: $k_1 = \pi\Delta\nu_{\frac{1}{2}\text{excess}}$ (4)

where $\Delta\nu_{\frac{1}{2}\text{excess}}$ = full-width half-maximum excess linewidth

Coalescence: $k_1 = \frac{\pi\Delta\nu_{\text{AB}}}{\sqrt{2}}$ (5)

where $\Delta\nu_{\text{AB}}$ = chemical shift difference of resonances A and B in Hz

Fast exchange: $k_1 = \frac{\pi\Delta{\nu_{\text{AB}}}^2}{2\Delta\nu_{\frac{1}{2}}}$ (6)

The Eyring plot for the dynamic exchange was generated using the program Origin 8 and is shown in Figure 2.22. The activation parameters for the exchange are as follows: $\Delta G^{\ddagger}$ = 11.5 ± 0.4 kcal/mol at 293 K; $\Delta H^{\ddagger}$ = 8.9 ± 0.4 kcal/mol; $\Delta S^{\ddagger}$ = -8.9 ± 0.4 e.u.

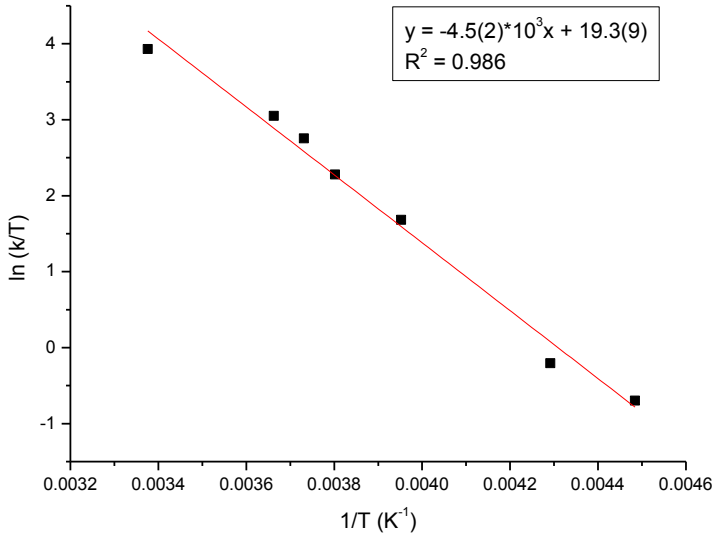

Figure 2.22. Eyring plot for the exchange of phosphine-sulfonate ligands of **8** in THF-d_8.

{[Li(THF)][(PO-^{i}Pr)Pd(Me)OC(O)An]}$_2$ (6, An = 9-anthracenyl). This species was generated to provide structural data to the analogous compound **4a**. A vial was charged with **3a** (56.4 mg, 0.0490 mmol, i.e. 0.098 mmol of (PO)PdMe$_2^-$ units) and 9-anthracenecarboxylic acid (22.3 mg, 0.100 mmol). THF (0.50 mL) was added dropwise at room temperature to form a orange yellow solution. Gas evolution (CH_4) was observed. After 15 min, the solution was evaporated under vacuum to 1/3 of the original volume. Pentane was added slowly to precipitate a yellow solid. The yellow solid was collected by filtration, washed with pentane and dried under vacuum. The solid was recrystallized by slow diffusion of hexanes into THF/toluene solution

(*ca*. 1/10 v/v) at -40 °C to afford colorless crystals. ^{1}H NMR (THF-d_8): δ 8.45 (m, 2 H, An–H^{1} & An–H^{8}), 8.31 (s, 1 H, An–H^{10}), 8.13 (dd, $^{3}J_{HH}$ = 8, $^{4}J_{PH}$ = 4, 1 H, H^{3}), 7.93 (m, 2 H, An–H^{4} & An–H^{5}), 7.55 (d, $^{3}J_{PH}$ = 8, 1 H, H^{6}), 7.37 (m, 5 H, H^{4} & An–H^{2} & An–H^{3} & An–H^{6} & An–H^{7}), 2.63 (octet, $^{2}J_{PH}$ = $^{3}J_{HH}$ = 8, 2 H, C*H*Me$_2$), 2.43 (s, 3 H, C*H*$_3$–ArSO$_3$), 1.31 (dd, $^{4}J_{PH}$ = 17, $^{3}J_{HH}$ = 7, 6 H, CH*Me$_2$*), 1.25 (dd, $^{4}J_{PH}$ = 15, $^{3}J_{HH}$ = 7, 6 H, CH*Me$_2$*), 0.73 (s, 3 H, Pd–C*H*$_3$). ^{31}P{^{1}H} NMR (THF-d_8): δ 41.5. ^{13}C{^{1}H} NMR (THF-d_8): δ 175.5 (O*C*(O)Ar), 149.1 (d, J_{PC} = 11, C^{2}), 140.1 (d, J_{PC} = 5, C^{5}), 138.8 (br s, An–C^{9}), 133.7 (C^{6}), 132.3 (An–C$^{11\text{-}14}$), 131.7 (d, J_{PC} = 2, C^{4}), 129.6 (d, J_{PC} = 7, C^{3}), 128.3 (An–C^{1} & An–C^{8}), 127.9 (An–C^{4} & An–C^{5}), 126.0 (d, J_{PC} = 34, C^{1}), 125.5 (An–C^{2} & An–C^{7}, or An–C^{3} & An–C^{6}), 125.4 (An–C^{10}), 125.2 (An–C^{2} & An–C^{7}, or An–C^{3} & An–C^{6}), 26.5 (d, J_{PC} = 27, *C*HMe$_2$), 21.0 (*C*H$_3$–ArSO$_3$), 19.4 (d, J_{PC} = 5, CH*Me$_2$*) 18.6 (CH*Me$_2$*) -6.8 (d, $^{2}J_{PC}$ = 5, Pd–*C*H$_3$). One An carbon was not observed. ^{7}Li{^{1}H} NMR (THF-d_8): δ 0.3. IR (KBr): 1595, 1430 cm^{-1}. ESI–MS (CH_2Cl_2/CH_3OH, positive ion mode) *m*/*z* 803.0 (M – 2 THF – (PO)Pd(Me)OC(O)An^{-} + 2 THF-d_8)$^{+}$, 821.1 (M – 2 THF – (PO)Pd(Me)OC(O)An^{-} + 2 THF-d_8 + H_2O)$^{+}$. Elemental analysis on a spectroscopically pure sample failed.

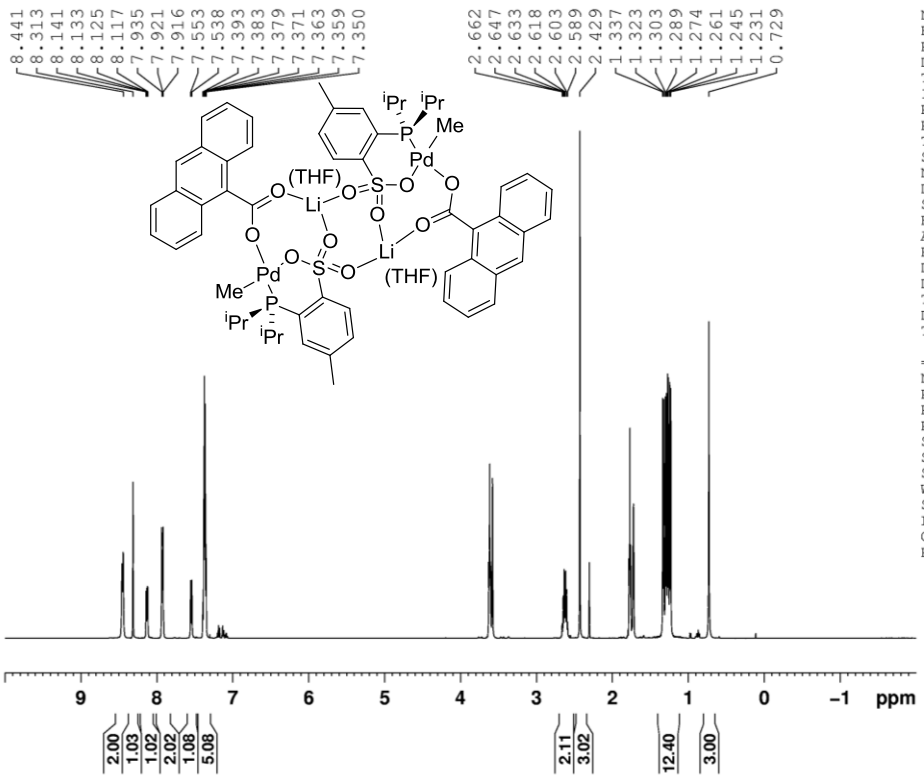


```
NAME            KCL1179
EXPNO                 1
PROCNO                1
Date_          20120913
Time              11.17
INSTRUM           spect
PROBHD   5 mm PAQNP 1H/
PULPROG              zg
TD                59998
SOLVENT             THF
NS                    8
DS                    0
SWH           10000.000 Hz
FIDRES        0.166672 Hz
AQ            2.9999499 sec
RG                  144
DW               50.000 usec
DE               71.43 usec
TE               296.2 K
D1           10.00000000 sec
TD0                   1

======== CHANNEL f1 ========
NUC1                 1H
P1                12.00 usec
PL1                0.00 dB
PL1W        24.54113007 W
SFO1       500.1330008 MHz
SI                16384
SF         500.1290850 MHz
WDW                  no
SSB                   0
LB                 0.00 Hz
GB                    0
PC                 1.00
```

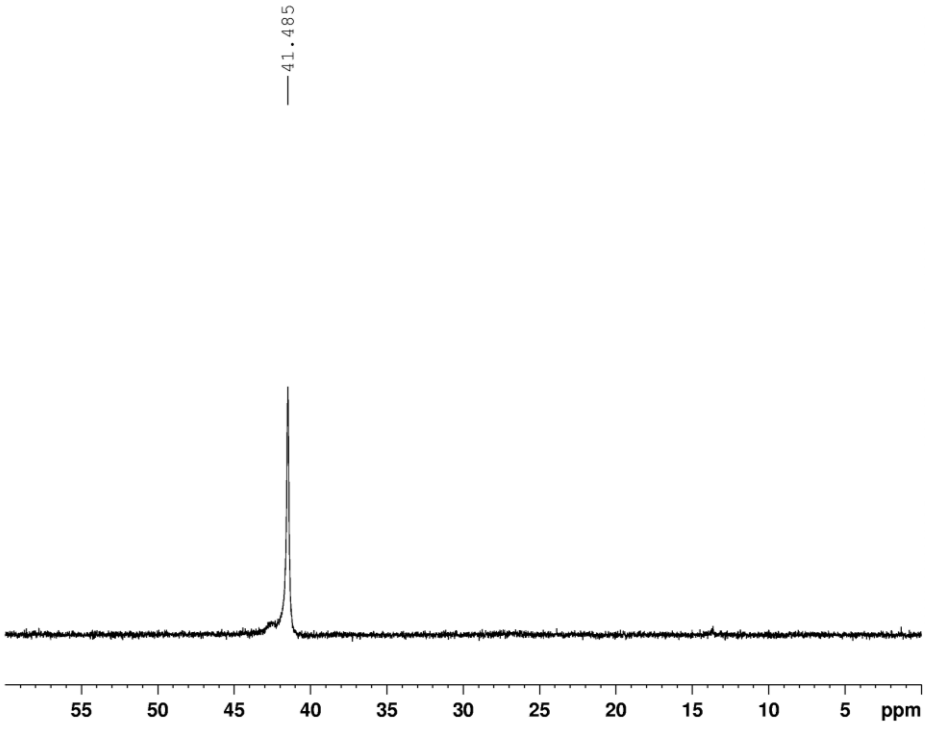


```
NAME            KCL1153
EXPNO                 2
PROCNO                1
Date_          20120605
Time              15.44
INSTRUM           spect
PROBHD   5 mm PAQNP 1H/
PULPROG           zgpg
TD               489122
SOLVENT             THF
NS                  128
DS                    4
SWH           81521.742 Hz
FIDRES        0.166670 Hz
AQ            2.9999983 sec
RG                 2890
DW                6.133 usec
DE                 6.00 usec
TE                298.0 K
D1           3.00000000 sec
D11          0.03000000 sec
TD0                   1

======== CHANNEL f1 ========
NUC1                31P
P1                11.00 usec
PL1                3.00 dB
PL1W        41.92221451 W
SFO1       202.4462121 MHz

======== CHANNEL f2 ========
CPDPRG2         waltz16
NUC2                 1H
PCPD2            100.00 usec
PL2              120.00 dB
PL12              16.50 dB
PL13              17.00 dB
PL2W         0.00000000 W
PL12W        0.54940748 W
PL13W        0.48965994 W
SFO2       500.1325000 MHz
SI                32768
SF         202.4557840 MHz
WDW                  no
SSB                   0
LB                 0.00 Hz
GB                    0
PC                 1.40
```

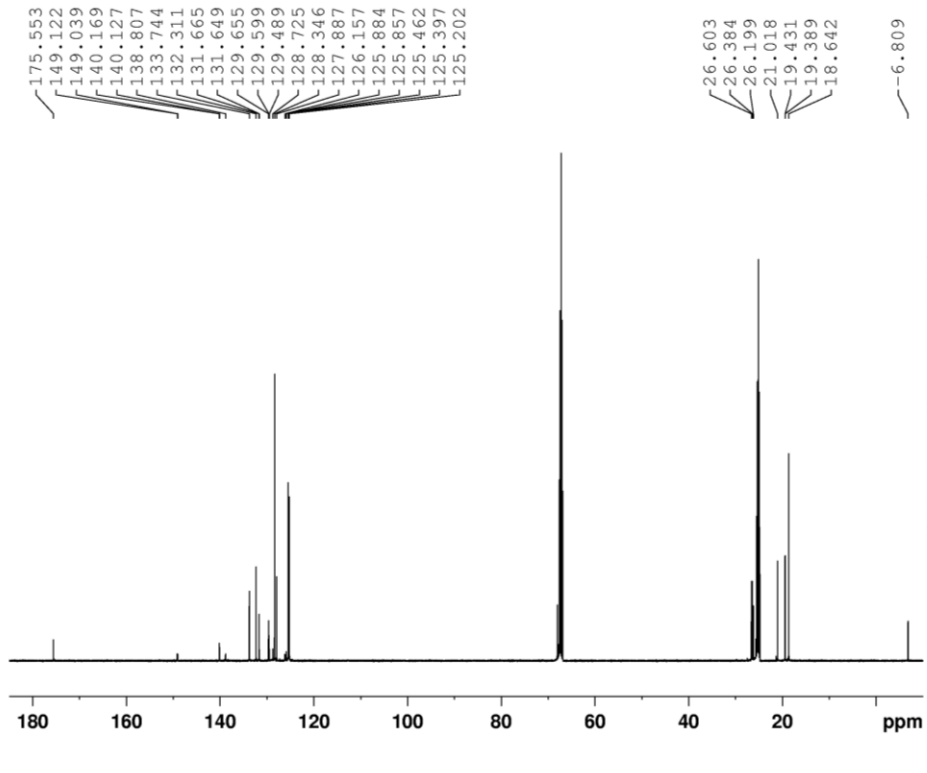

NAME	KCL1179
EXPNO	5
PROCNO	1
Date_	20120916
Time	15.57
INSTRUM	spect
PROBHD	5 mm PAQNP 1H/
PULPROG	zgpg
TD	65786
SOLVENT	Tol
NS	15200
DS	4
SWH	32894.738 Hz
FIDRES	0.500026 Hz
AQ	0.9999972 sec
RG	2050
DW	15.200 usec
DE	6.00 usec
TE	296.6 K
D1	3.00000000 sec
D11	0.03000000 sec
TD0	1
======== CHANNEL f1 ========	
NUC1	13C
P1	8.00 usec
PL1	1.00 dB
PL1W	72.42802429 W
SFO1	125.7716224 MHz
======== CHANNEL f2 ========	
CPDPRG2	waltz16
NUC2	1H
PCPD2	80.00 usec
PL2	0.00 dB
PL12	16.50 dB
PL13	17.00 dB
PL2W	24.54113007 W
PL12W	0.54940748 W
PL13W	0.48965994 W
SFO2	500.1325006 MHz
SI	131072
SF	125.7576965 MHz
WDW	no
SSB	0
LB	0.00 Hz
GB	0
PC	1.00

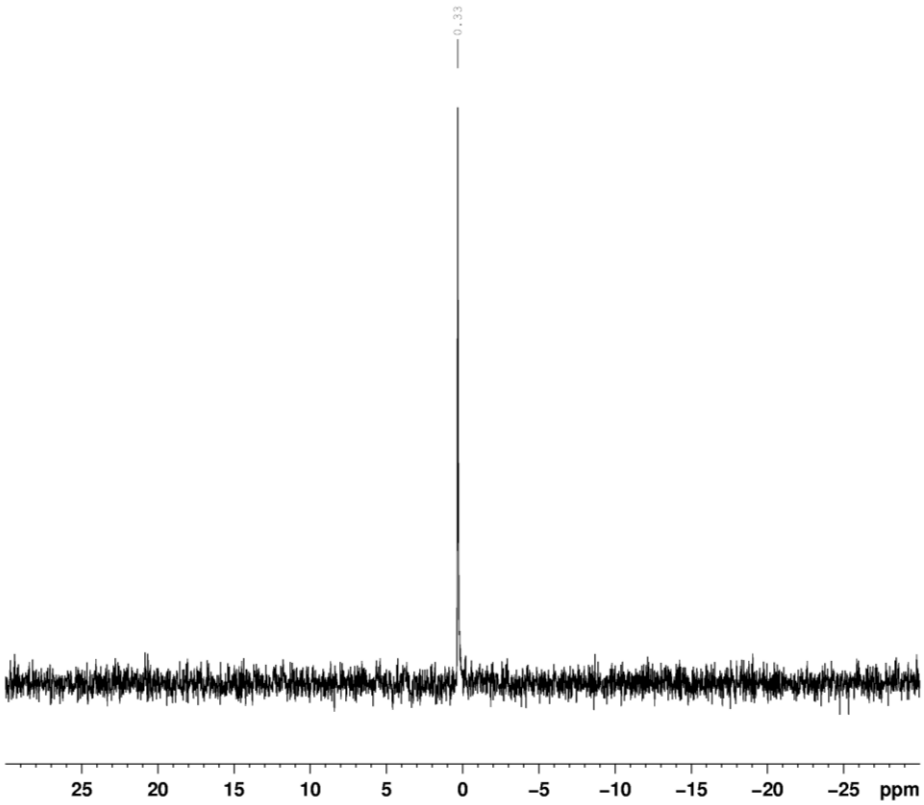

NAME	KCL1179
EXPNO	14
PROCNO	1
Date_	20131002
Time	18.25
INSTRUM	spect
PROBHD	5 mm BBO BB-1H
PULPROG	zgdc
TD	399988
SOLVENT	H2O+D2O
NS	4
DS	0
SWH	100000.000 Hz
FIDRES	0.250008 Hz
AQ	1.9999900 sec
RG	16384
DW	5.000 usec
DE	6.00 usec
TE	295.9 K
D1	3.00000000 sec
d11	0.03000000 sec
TD0	1
======== CHANNEL f1 ========	
NUC1	7Li
P1	7.75 usec
PL1	-3.00 dB
SFO1	155.5057110 MHz
======== CHANNEL f2 ========	
CPDPRG2	waltz16
NUC2	1H
PCPD2	80.00 usec
PL2	-6.00 dB
PL12	17.00 dB
SFO2	400.1328010 MHz
SI	32768
SF	155.5057888 MHz
WDW	no
SSB	0
LB	0.00 Hz
GB	0
PC	1.40

Dynamics of Exchange of 3a with (PO-^{i}Pr)PdMe(THF)-Li^{+}. A valved J. Young NMR tube was charged with **3a** (3.4 mg, 0.0030 mmol, i.e. 0.0060 mmol of (PO)PdMe$_2^-$ units) and [Ph$_3$C][B(C$_6$F$_5$)$_4$] (2.3 mg, 0.0025 mmol). THF-d_8 (0.55 mL) was added by vacuum transfer at -196 °C. The NMR tube was thawed at room temperature to generate Ph$_3$CMe and a 1.4/1 mixture of **3a** and (PO-^{i}Pr)PdMe(THF)-Li^{+}. The tube was inserted into an NMR probe that had been pre-cooled to 226 K. ^{1}H spectra were recorded over the temperature range of 226 K – 293 K. Representative experimental and simulated ^{1}H NMR spectra (gNMR) are shown in Figure 2.10. In the ^{1}H NMR spectrum, at 226 K, separate Pd–Me resonances for (PO-^{i}Pr)PdMe(THF)-Li^{+} and **3a** were observed. As the temperature was raised, the Pd-Me resonance for (PO-^{i}Pr)PdMe(THF)-Li^{+} and the resonance of the Pd–Me group *cis* to P for **3a** (Pd-Me$_{\mathbf{3a},\text{cis-to-P}}$) broadened and coalesced (at 273 K), and the Pd–Me$_{\mathbf{3a},\text{trans-to-P}}$ collapsed to a singlet. As the temperature was raised above 273 K, the coalesced Pd–Me resonance for (PO-^{i}Pr)PdMe(THF)-Li^{+}/**3a** (*cis* to P) sharpened and the Pd–Me$_{\mathbf{3a},\text{trans-to-P}}$ resonance remained sharp. These lineshape changes were reversed when the temperature was lowered. These lineshape changes are consistent with reversible exchange of the Pd–*Me*$_{\text{trans-to-P}}$ methyl group between **3a** and(PO-^{i}Pr)PdMe(THF)-Li^{+}, which permutes the Pd–Me group for (PO-^{i}Pr)PdMe(THF)-Li^{+} and Pd–Me$_{\mathbf{3a},\text{cis-to-P}}$.

In a similar experiment, a valved J. Young NMR tube was charged with **3a** (7.5 mg, 0.0065 mmol, i.e. 0.013 mmol of (PO)PdMe$_2^-$ units) and [Ph$_3$C][B(C$_6$F$_5$)$_4$] (5.3 mg, 0.0057 mmol). THF-d_8 (0.55 mL) was added by vacuum transfer at -196 °C. The NMR tube was thawed at room temperature to generate Ph$_3$CMe and a 1.3/1 mixture of **3a** and (PO-^{i}Pr)PdMe(THF)-Li^{+}. The tube was inserted into an NMR probe that had been pre-cooled to 226 K. ^{31}P{^{1}H} NMR spectra were recorded over the temperature range of 226 K – 293 K. Representative experimental

and simulated $^{31}P\{^{1}H\}$ NMR spectra (gNMR) are shown in Figure 2.23. In the $^{31}P\{^{1}H\}$ NMR spectrum, at 226 K, sharp signals were observed for (PO-^{i}Pr)PdMe(THF)-Li^{+} and **3a**. As the temperature was raised, these resonances broadened and coalesced (at 293 K), consistent with reversible exchange of (PO-^{i}Pr)PdMe(THF)-Li^{+} and **3a**.

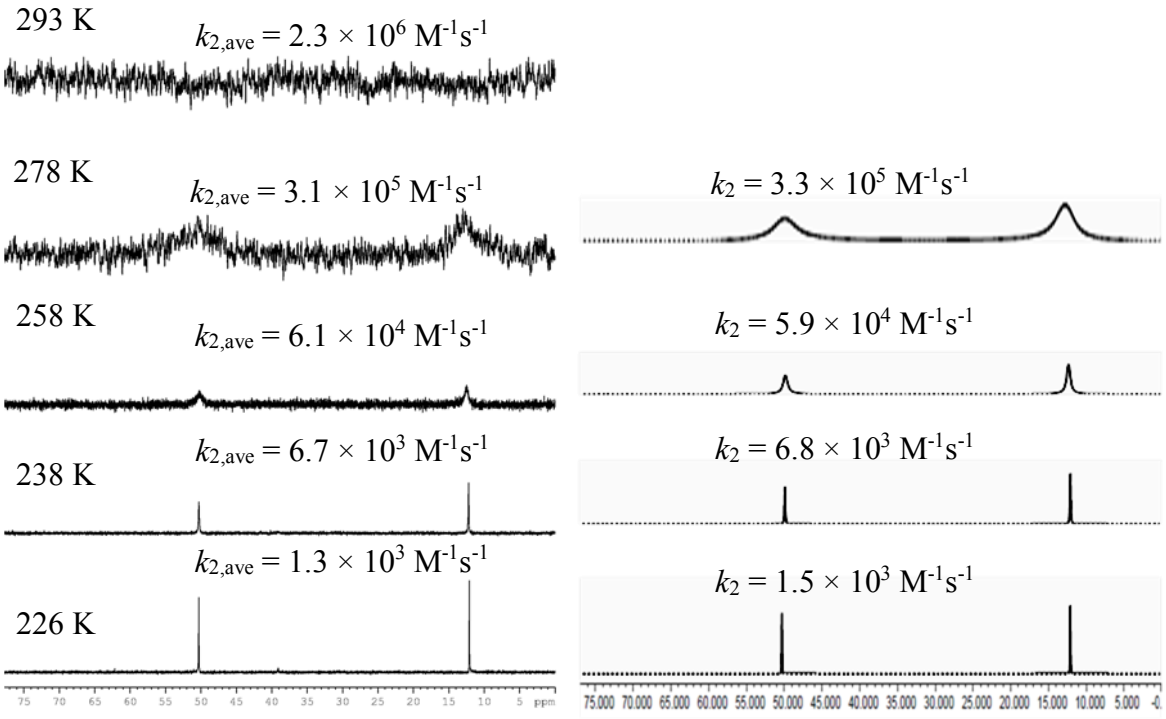

Figure 2.23. Representative variable temperature $^{31}P\{^{1}H\}$ NMR spectra of a solution of **3a** and (PO-^{i}Pr)PdMe(THF)-Li^{+} in THF-d_8. Experimental spectra are shown on the left and simulated spectra are shown on the right. The second-order rate constants for the exchange at each temperature are shown.

The rate law for this dynamic process is given in eq 7. From the ^{1}H NMR spectra, the first-order rate constants for (PO-^{i}Pr)PdMe(THF)-Li^{+} → **3a** ($k_1 = k_2$[**3a**]) were obtained from the

line broadening of the Pd–Me resonance for (PO-^{i}Pr)PdMe(THF)-Li^{+} using eq 4 over the temperature range of 226 K – 268 K, from the coalescence of the Pd–Me group of (PO-^{i}Pr)PdMe(THF)-Li^{+} and Pd–Me$_{\mathbf{3a},\text{cis-to-P}}$ resonances using eq 5 at 273 K, and from the sharpening of the coalesced Pd–Me resonance using eq 6 in the range of 283 K – 293 K. Second-order rate constants (k_2) were obtained by dividing k_1 by the concentration of **3a**. From the ^{31}P{^{1}H} NMR spectra, the first-order rate constants for (PO-^{i}Pr)PdMe(THF)-Li^{+} → **3a** ($k_1 = k_2$[**3a**]) and for **3a** → (PO-^{i}Pr)PdMe(THF)-Li^{+} ($k_1 = k_2$[(PO-^{i}Pr)PdMe(THF)-Li^{+}]) were obtained from line broadening of the resonances of **3a** and (PO-^{i}Pr)PdMe(THF)-Li^{+}. The second-order rate constants (k_2) were obtained by dividing these k_1 by the appropriate concentration ([**3a**] or [(PO-^{i}Pr)PdMe(THF)-Li^{+}]); average values ($k_{2,\text{ave}}$) are shown in Figure 2.23. Additionally, rate constants at all temperatures were obtained by total lineshape simulation using the program gNMR. As expected, these two approaches gave similar values for k_2; the values for k_2 determined using gNMR are shown in Figure 2.10 and 2.23.

$$\text{Exchange rate} = k_2[\mathbf{3a}][(\text{PO-}^{i}\text{Pr})\text{PdMe(THF)-Li}^{+}] \qquad (7)$$

The Eyring plot for the dynamic exchange was generated using the program Origin 8 and is shown in Figure 2.24. The activation parameters for the exchange are as follows: ^{1}H NMR: $\Delta G^{\ddagger}$ = 9.5(4) kcal/mol at 293 K; $\Delta H^{\ddagger}$ = 10.8(4) kcal/mol; $\Delta S^{\ddagger}$ = +4.4(1) e.u. ^{31}P{^{1}H} NMR: $\Delta G^{\ddagger}$ = 9(1) kcal/mol at 293 K; $\Delta H^{\ddagger}$ = 13(1) kcal/mol; $\Delta S^{\ddagger}$ = +12.5(8) e.u.

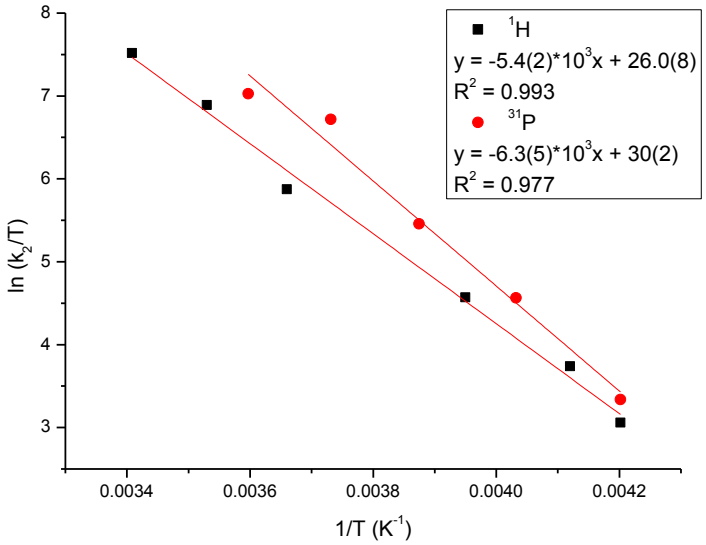

Figure 2.24. Eyring plot for the exchange of methyl group between **3a** and (PO-^{i}Pr)PdMe(THF)-Li^{+} in THF-d_8.

Reaction of 3a with pyridine. A valved J. Young NMR tube was charged with **3a** (3.6 mg, 0.0031 mmol, i.e. 0.0062 mmol of (PO)PdMe$_2^-$ units). A solution of pyridine in THF-d_8 (8.7 mM, 0.73 mL, 0.0063 mmol) was added and the tube was maintained at room temperature and monitored by NMR spectroscopy. **3a** decomposed in the same manner and at approximately the same rate as in the absence of pyridine and there was no change in the pyridine resonances.

Reaction of {(PO-3,5-^{t}Bu$_2$)PdMe}$_2$ with CO$_2$. A valved J. Young NMR tube was charged with {(PO-3,5-^{t}Bu$_2$)PdMe}$_2$ (10 mg, 0.0073 mmol). CD_2Cl_2 (0.50 mL) and CO_2 (equivalent to 2.5 atm at room temperature) were added by vacuum transfer at -196 °C. The reaction mixture was thawed and allowed to stand at room temperature for 2 d and 45 °C for 6 d. NMR spectra were recorded and showed that {(PO-3,5-^{t}Bu$_2$)PdMe}$_2$ had partially decomposed to the same

unidentified products at approximately the same rate as in the absence of CO_2.

Reaction of (PO-^{i}Pr)PdMe(py) with CO_2. A valved J. Young NMR tube was charged with (PO-^{i}Pr)PdMe(py) (4.0 mg, 0.0082 mmol). THF-d_8 (0.50 mL) and CO_2 (equivalent to 5.6 atm at room temperature) were added by vacuum transfer at -196 °C. The reaction mixture was thawed and allowed to stand at room temperature for 1 d and 50 °C for 4 d. NMR spectra were recorded and showed that (PO-^{i}Pr)PdMe(py) had partially decomposed to the same unidentified products at approximately the same rate as in the absence of CO_2.

Reaction of (PO-^{i}Pr)PdMe(THF) with CO_2. A valved J. Young NMR tube was charged with (PO-^{i}Pr)PdMe(py) (3.0 mg, 0.0061 mmol) and $B(C_6F_5)_3$ (3.3 mg, 0.0064 mmol). THF-d_8 (0.40 mL) and CO_2 (equivalent to 5.6 atm at room temperature) were added by vacuum transfer at -196 °C. The reaction mixture was thawed and allowed to stand at room temperature for 1 d and 50 °C for 4 d. NMR spectra were recorded and showed that **6** had partially decomposed to the same unidentified products at approximately the same rate as in the absence of CO_2.

Reaction of (PO-^{i}Pr)PdMe(py)-Li^+ and CO_2. A valved J. Young NMR tube was charged with (PO-^{i}Pr)PdMe(py) (3.0 mg, 0.0061 mmol) and $[Li(Et_2O)_{2.8}][B(C_6F_5)_4]$ (6.0 mg, 0.0067 mmol). THF-d_8 (0.50 mL) and CO_2 (equivalent to 5 atm at room temperature) were added by vacuum transfer at -196 °C. The reaction mixture was thawed and monitored by NMR spectroscopy at room temperature. NMR spectra showed that (PO-^{i}Pr)PdMe(py)-Li^+ had partially decomposed to the same unidentified products at approximately the same rate as in the absence of CO_2.

Reaction of (PO-^{i}Pr)PdMe(THF)-Li^+ and CO_2. A valved J. Young NMR tube was charged with (PO-^{i}Pr)PdMe(py) (3.8 mg, 0.0078 mmol), $B(C_6F_5)_3$ (5.2 mg, 0.010 mmol) and

$[Li(Et_2O)_{2.8}][B(C_6F_5)_4]$ (5.7 mg, 0.0064 mmol). THF-d_8 (0.50 mL) and CO_2 (equivalent to 5 atm at room temperature) were added by vacuum transfer at -196 °C. The reaction mixture was thawed and monitored by NMR spectroscopy at room temperature. NMR spectra showed that (PO-^{i}Pr)PdMe(THF)-Li^+ had partially decomposed to the same unidentified products at approximately the same rate as in the absence of CO_2.

Representative Reaction of 3a with CO_2. A valved J. Young NMR tube was charged with **3a** (3.0 mg, 0.0026 mmol, i.e. 0.0052 mmol of (PO)$PdMe_2^-$ units). THF-d_8 (0.8 mL) and CO_2 (equivalent to 2.27 atm and 141 equiv relative to (PO)$PdMe_2^-$ units at 20 °C; pseudo first order in CO_2) were added by vacuum transfer at -196 °C. The tube was taken out of the liquid N_2 bath, allowed to warm until the mixture thawed, and then rapidly inserted into an NMR probe that had been pre-cooled to 20 °C. $^{31}P\{^1H\}$ NMR spectra were recorded periodically. Representative spectra are shown in Figure 2.25. Initially, the ^{31}P resonance of **3a** decreased in intensity over time and the resonance for **4a** grew in, and only resonances of **4a** and **5** were observed at the end of the reaction. These results are consistent with the conversion of **3a** to **4a**.

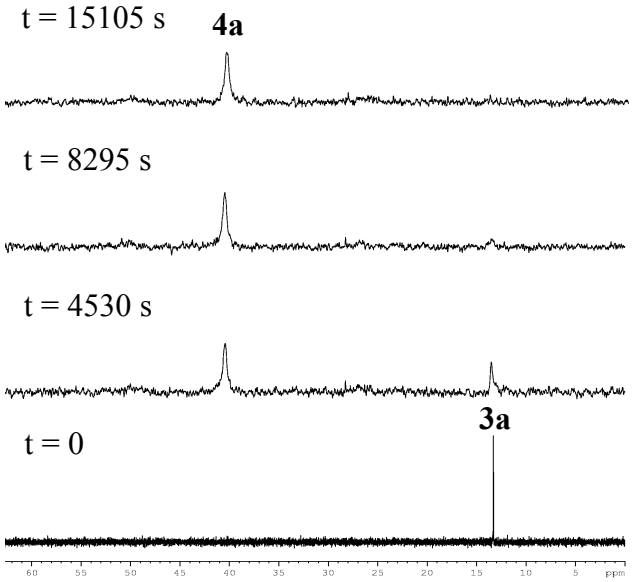

Figure 2.25. $^{31}P\{1H\}$ NMR spectra of the reaction of **3a** with CO_2 (2.27 atm) in THF-d_8 at 20 °C. Key resonances: δ 40.5 (**4a**), 13.3 (**3a**). Other resonance: δ 27.9 (**5**).

In a similar experiment, a valved J. Young NMR tube was charged with **3a** (3.0 mg, 0.0026 mmol, i.e. 0.0052 mmol of (PO)PdMe$_2^-$ units) and Cp_2Fe (4.4 mg, 0.024 mmol, internal standard). THF-d_8 (0.65 mL) and CO_2 (equivalent to 1.06 atm at 20 °C; pseudo first order in CO_2) were added by vacuum transfer at -196 °C. The tube was taken out of the liquid N_2 bath, allowed to warm until the mixture thawed, and then rapidly inserted into an NMR probe that had been pre-cooled to 20 °C. ^1H NMR spectra were recorded periodically. Representative spectra are shown in Figure 2.26. Initially, the Pd–Me$_{\mathbf{3a},\text{cis-to-P}}$ resonance appeared as a broad singlet and the Pd–Me$_{\mathbf{3a},\text{trans-to-P}}$ resonance appeared as a sharp singlet. As the reaction proceeded, a broad singlet for the Pd–Me$_{\mathbf{4a}}$ group and a sharp singlet for the Pd–OC(O)*Me* group of **4a** emerged, while the Pd–Me$_{\mathbf{3a}}$ signals decreased in intensity. These results are consistent with the conversion of **3a** to **4a** with concomitant exchange between these two species in a manner similar to that between **3a** and (PO-^{i}Pr)PdMe(THF)-Li$^+$ but at a lower rate (see below for details).

Small amounts of CH_4, C_2H_6, **5** and Pd black were also observed. The average yield of **4a** was 77 % over 4 runs. As the reaction neared completion, the resonances for **4a** (except the Pd–OC(O)*Me* resonance) sharpened as expected, since the concentration of **3a**, which exchanges with **4a**, decreased.

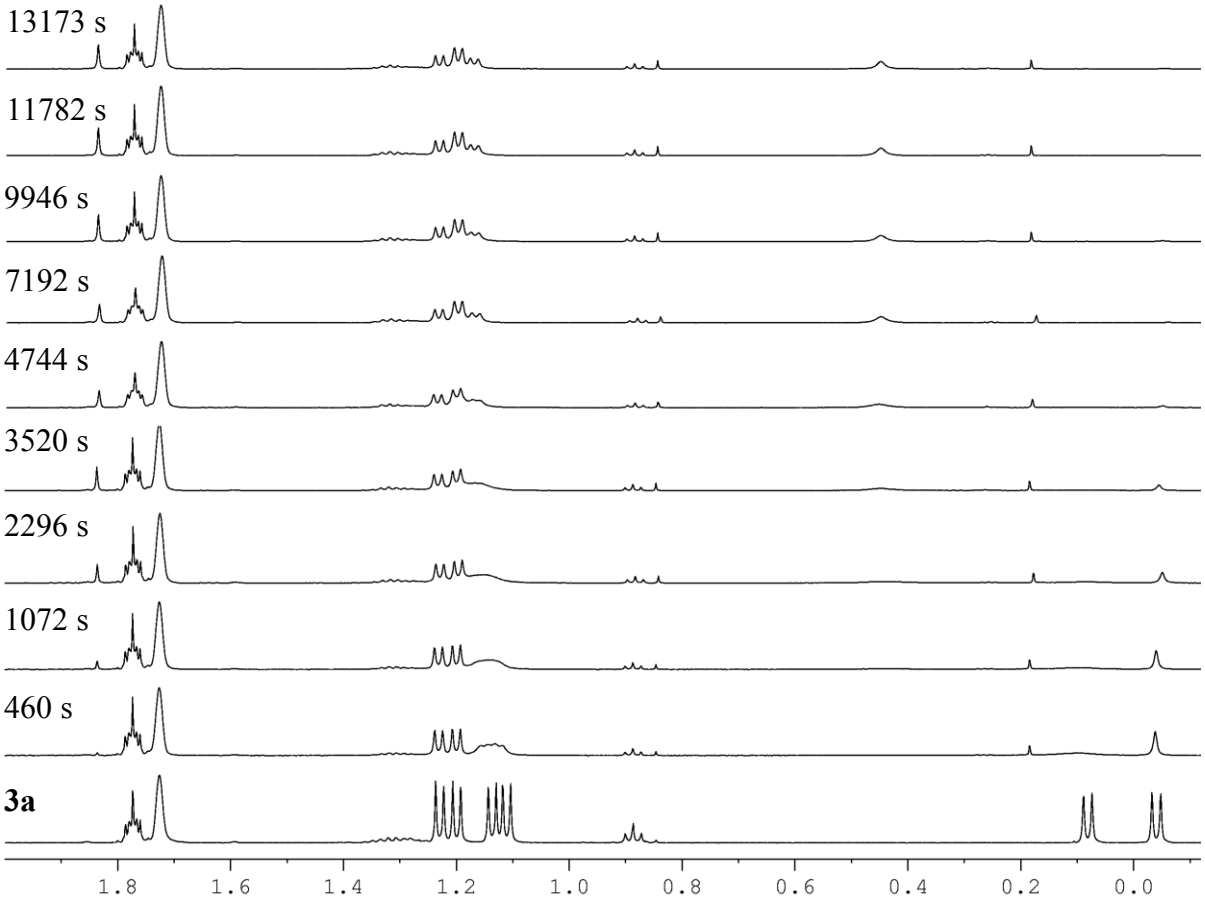

Figure 2.26. ^{1}H NMR spectra of the reaction of **3a** with CO_2 (1.06 atm) in THF-d_8 at 20 ˚C. Key resonances: δ 1.84 (s, Pd–OC(O)CH_3, **4a**), 1.22 (dd, CHMe_2, **3a** & **4a**), 1.19 (dd, CHMe_2, **4a**), 1.13 (dd, CHMe_2, **3a**), 0.45 (s, Pd–Me, **4a**), 0.06 (br s, Pd–Me *cis* to P, **3a**), -0.04 (s, Pd–Me *trans* to P, **3a**). Other resonances: δ 1.79 (m, THF), 1.72 (s, THF-d_7), 1.31 (m, pentane), 0.89 (t, pentane), 0.85 (s, C_2H_6), 0.25 (t, Pd–Me, **5**), 0.19 (s, CH_4).

The rate law for the exchange of **3a** and **4a** is Rate = k_2[**3a**][**4a**]. The second-order rate constant (k_2) for this exchange was obtained by total lineshape simulation of representative spectra from different points during the reaction using the program gNMR. Representative ^{1}H NMR spectra are shown in Figure 2.9. This analysis gave k_2 = 1.5(8) × 10^4 $M^{-1}s^{-1}$; $\Delta G^{\ddagger}$ = 12 kcal/mol at 293 K.

The rate equation for the conversion of **3a** to **4a** is given by eq 8.

Rate = k_2[**3a**]P_{CO2} = k_{obs}[**3a**] (8)

where k_2 = Second-order rate constant; k_{obs} = kP_{CO2} = observed first-order rate constant; P_{CO2} = CO_2 pressure

Due to the presence of the competing minor formation of CH_4, C_2H_6, **5** and Pd^0, the kinetics were evaluated by analyzing the appearance of product **4a**. The first-order rate equation for the appearance of **4a** (exponential form) is given by eq 9. The concentration of **4a** was determined by integration of the Pd–OC(O)*Me* resonance relative to the internal standard resonance. The first-order kinetic plot was generated using the program Origin 8 and is shown in Figure 2.11. k_{obs} = 2.75(9) × 10^{-4} s^{-1}. The logarithmic form of eq 9 is given by eq 10, and the corresponding plot is shown in Figure 2.11. k_{obs} = 2.79(4) × 10^{-4} s^{-1}.

$$[\mathbf{4a}] = -\{[\mathbf{4a}]_\infty \exp(-k_{obs}t)\} + [\mathbf{4a}]_\infty \quad (9)$$

where $[\mathbf{4a}]_\infty$ = [**4a**] at the end of the reaction

$$\ln ([\mathbf{4a}]_\infty - [\mathbf{4a}]) = -k_{obs}t + \ln [\mathbf{4a}]_\infty \quad (10)$$

A plot of k_{obs} vs P_{CO2} is shown in Figure 2.12. The slope of this plot = k_2 = 2.2(1) × 10^{-4} $atm^{-1}s^{-1}$.

Representative Reaction of 3b with CO_2. A valved J. Young NMR tube was charged with **3a** (2.6 mg, 0.0023 mmol, i.e. 0.0046 mmol of (PO)$PdMe_2^-$ units) and Crypt211 (0.0045 mmol). THF-d_8 (0.68 mL) and CO_2 (equivalent to 1.42 atm and 87 equiv relative to (PO)$PdMe_2^-$ units at room temperature; pseudo first order in CO_2) were added by vacuum transfer at -196 °C. The reaction mixture was thawed and monitored by NMR spectroscopy at 296 K. Representative ^{1}H NMR spectra are shown in Figure 2.27. Over time, the Pd-$Me_{\mathbf{3b}}$ resonances decreased in intensity while the Pd–$Me_{\mathbf{4b}}$ and Pd–OC(O)*Me* resonances emerged. These results are consistent with the conversion of **3b** to **4b** without observable exchange between those species. Small amounts of CH_4, C_2H_6, and unidentified compounds[26] were observed. The yield of **4b** was 89 %. The half-life for the formation of **4b** is 235 min. This value corresponds to $k_{obs} = k_2P_{CO2}$ = 4.92 × 10^{-5} s^{-1} and k_2 = 3.46 × 10^{-5} $atm^{-1}s^{-1}$ (see Figure 2.12).

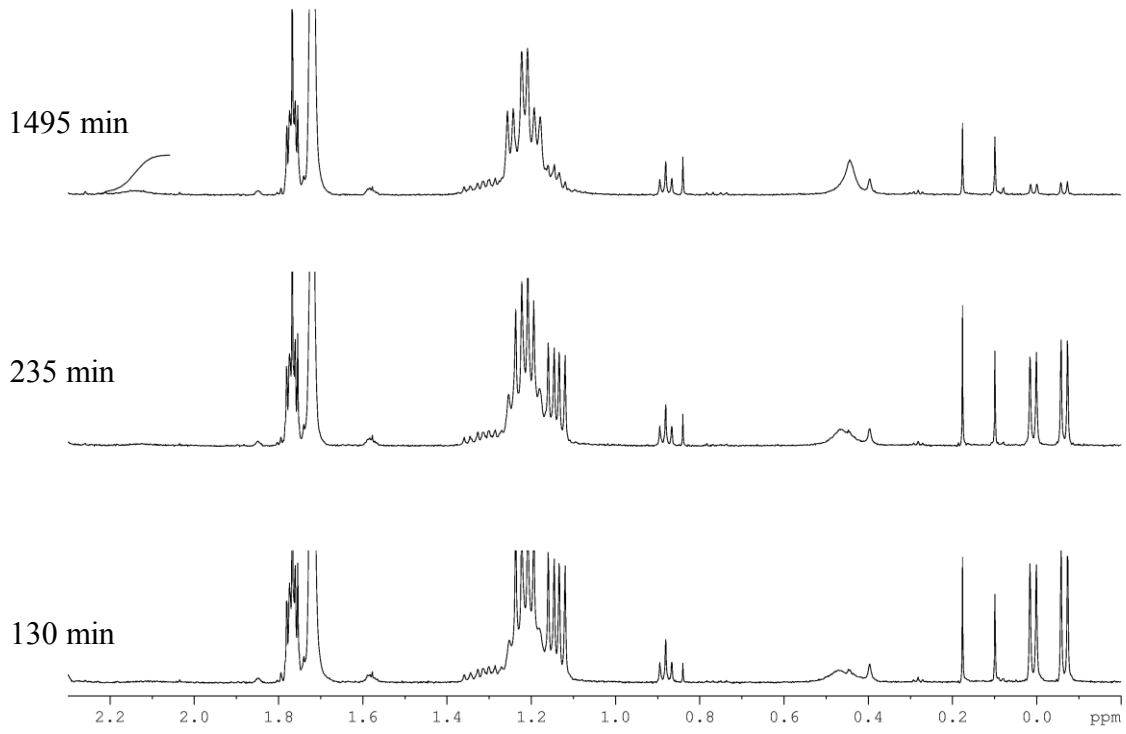

Figure 2.27. ^{1}H NMR spectra of the reaction of **3b** with CO_2 (1.42 atm) in THF-d_8 at 296 K. The aliphatic region is shown. Key resonances: δ 2.01 (br s, Pd–OC(O)*Me*, **4b**), 1.23 (dd, CH*Me*$_2$, **4b**), 1.22 (dd, CH*Me*$_2$, **3b**), 1.19 (dd, CH*Me*$_2$, **4b**), 1.13 (dd, CH*Me*$_2$, **3b**), 0.41 (br s, Pd–Me, **4b**), 0.01 (d, Pd–Me *cis* to P, **3b**), -0.07 (d, Pd–Me *trans* to P, **3b**). Other resonances: δ 1.79 (m, THF), 1.72 (s, THF-d_7), 1.31 (m, pentane), 0.89 (t, pentane), 0.85 (s, C_2H_6), 0.19 (s, CH_4), 0.10 (s, silicone grease).

Reaction of 4a-$^{13}C_1$ with CO_2. A valved J. Young NMR tube was charged with **4a-$^{13}C_1$** (13 mg, 0.027 mmol). THF-d_8 (0.5 mL) was added by vacuum transfer at -196 °C. The mixture was thawed at room temperature, exposed to CO_2 (1 atm, 8 equiv) and allowed to stand at room

temperature for 4 d. The mixture was transferred to a vial and hexanes (0.5 mL) were added to the mixture. The volatiles were removed under vacuum to afford a white solid which was analyzed by IR spectroscopy. Only **4a-$^{13}C_1$** was observed.

Reaction of 4b-$^{13}C_1$ with CO_2. A valved J. Young NMR tube was charged with **4b-$^{13}C_1$** (5.8 mg, 0.0076 mmol). THF-d_8 (0.5 mL) was added by vacuum transfer at -196 °C. The mixture was thawed at room temperature, exposed to CO_2 (1 atm, 29 equiv) and allowed to stand at room temperature for 26 d. The mixture was transferred to a vial and hexanes (0.5 mL) were added to the mixture. The volatiles were removed under vacuum to afford a white solid which was analyzed by IR spectroscopy. Only **4b-$^{13}C_1$** was observed.

Representative Pulsed-Gradient Spin-Echo NMR Results.

Pulsed-Gradient Spin-Echo (PGSE) NMR. All PGSE measurements were performed on a Bruker 500 MHz spectrometer using the Stejskal-Tanner method.[27] Two identical pulsed field gradients with duration δ = 0.004 s separated by a delay time Δ = 0.0151 s were incorporated into a spin-echo sequence, one before and the other after the 180° pulse. ^{1}H NMR spectra were recorded in THF-d_8 at room temperature or 190 K without sample spinning. During an experiment, the gradient strength (G) was varied between 0 and 26 G/cm while keeping all other factors constant. The gradient was calibrated using 2% H_2O in D_2O. In all studies, the integral of the Pd-*Me* resonance was used to evaluate signal intensity. A linear plot of $\ln(I/I_0)$ (I = integral of a peak in the presence of G; I_0 = integral of the peak without a gradient) versus G^2 was generated. According to eq 11, the slope of this line is proportional to the diffusion coefficient

and thus inversely proportional to the hydrodynamic radius of the molecule according to the Stokes-Einstein equation (eq 12). Hydrodynamic volumes were estimated by eq 13.

$$\ln(I/I_0) = -\gamma_H^2\delta^2G^2(\Delta - \delta/3)D \qquad (11)$$

where I = integral of a peak in the presence of G (gradient strength); I_0 = integral of the peak without a gradient; γ_H = magnetogyric ratio of ^1H; δ = length of the gradient pulse; Δ = delay between the midpoints of the gradients; D = diffusion coefficient

$$r_H = k_BT/(6\pi\eta D) \qquad (12)$$

where r_H = hydrodynamic radius, k_B = Boltzmann constant; T = temperature; η = viscosity of the solvent

$$V_H = 4\pi r_H^3/3 \qquad (13)$$

Linear plots of PGSE results for (PO-^{i}Pr)PdMe(THF), **3a** (Figure 2.28) and **4a** (Figure 2.29) relative to model monomer (PO-^{i}Pr)PdMe(py) are generated using eq 11.

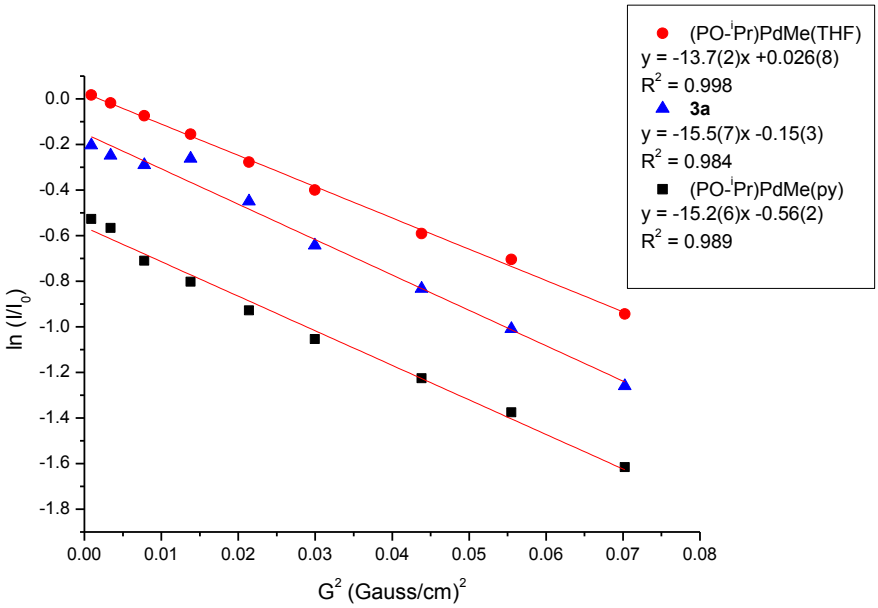

Figure 2.28. Linear plots of PGSE results for (PO-^{i}Pr)PdMe(THF) and **3a** relative to model monomer (PO-^{i}Pr)PdMe(py).

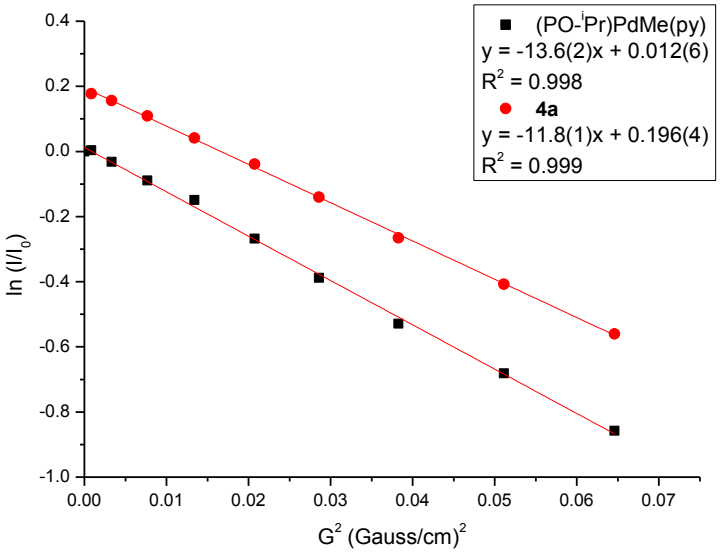

Figure 2.29. Linear plots of PGSE results for **4a** relative to model monomer (PO-^{i}Pr)PdMe(py).

Table 2.2. Estimated relative hydrodynamic volumes for (PO)Pd species determined by PGSE-NMR using eq 12 and 13.

Entry	Compound	Relative hydrodynamic volume
1	(PO-^{i}Pr)PdMe(py)	1
2	**3a**	0.932
3	(PO-^{i}Pr)PdMe(THF)	1.35
4	**4a**	1.55

Computational Details

Computational Methods. The Gaussian 09 computational software package[28] was used for all calculations. All computations were performed using tight convergence criteria (opt=tight), a pruned (99,590) grid (int=ultrafine), and SCF convergence of 10^{-8}. The M06 functional of Zhao and Truhlar[29] was used for all optimizations. Ground-state geometries were verified as true minima by the absence of negative frequencies. Transition-state structures were confirmed by the presence of a single, large, negative frequency corresponding to the bond-forming/bond-breaking step necessary for product formation. All energies reported are Gibbs free energies which include translational, rotational, vibrational, and solvation energy contributions (IEF-PCM), as noted below for individual complexes. Zero-point vibrational contributions are not included in the reported energies. Transition-states were linked to reactants and products using linear transit (LT) calculations with small step-size near the transition state or through the use of intrinsic reaction coordinate (IRC) computations. Structural drawings were produced with Molekel 5.4.[30]

Considerations for Zr systems. For geometry optimizations and transition-state structures the QZVP basis set of Weigand and Ahlrichs[31] with the ECP of Preuss and Stoll[32] was used for Zr; all other atoms were modeled with the TZVP basis set also by Weigand and Ahlrichs.[33] Solvation energies were determined by single-point calculation of the gas-phase, geometry-optimized structures using the PCM model for chlorobenzene solvent. Optimization using PCM solvation essentially gave the same structures as the gas-phase computations, and therefore optimizations were not carried out with the continuum model.

Considerations for Pd systems. Geometry optimizations and transition-state structures utilized a 6-31G** basis set on all atoms except for Pd, for which, the TZVPPD basis set and ECP recommended by Rappoport and Furche[34] was used. Structures were optimized with PCM solvent (THF) correction. Very similar results were obtained for the Li^+-assisted S_E2 mechanism using a discrete $Li(THF)_2^+$ unit under gas-phase conditions.

Functional Selection for DFT Computations. For computations containing Zr, the following functional/basis sets were considered: BP86//6-31G* (H, C, O)/LANL2DZ (Zr), BP86//6-31G** (H, C, O)/LANL2DZ (Zr), and M06//TZVP (H, C, O)/QZVP (Zr). Calculated bond lengths, angles were compared to reported crystal structure for Cp_2ZrMe_2[35] and the M06 functional with TZVP/QZVP performed best based on percent error.

The following functionals were considered for Pd computations: BP86, B3P86, PBEPBE, M06, and TPSSh. The crystal structure of the complex (PO^iPr)PdMe(py) (Figure 2.30) was used as the basis of comparison for the performance of the functionals above based on the percent error of select bond lengths, angles, and dihedrals. In general, TPSSh//6-31G** (H, C, N, O, P, S)/TZVPPD (Pd) was found to perform best for bond distances and angles but was time

consuming. BP86//6-31G** (H, C, N, O, P, S)/TZVPPD (Pd) was found to give the best performance for cost of computational time. The M06 functional was ultimately selected for its performance in modeling weak interactions as well as accuracy for reaction barrier heights and was found to perform well for bond distances, angles, and dihedrals, similar to that for BP86 albeit at a cost of computational time.

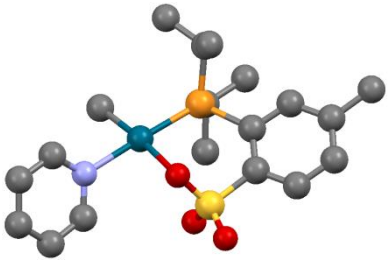

Figure 2.30. Crystal structure of (PO-^{i}Pr)PdMe(py).

Notes on DFT Computational Results. The reaction of $Cp_2ZrMe(C_6H_5Cl)^+$ with CO_2 to yield $Cp_2Zr(\kappa^2\text{-}OAc)^+$ is exergonic by 26.1 kcal/mol. The reaction of Cp_2ZrMe_2 with CO_2 to yield $Cp_2Zr(Me)(OAc)$ is exergonic by 18.8 kcal/mol and lateral attack of the CO_2 ($\Delta G^{\ddagger}$ = 33.2 kcal/mol) is preferred over central attack ($\Delta G^{\ddagger}$ = 34.4 kcal/mol), similar to the selectivity of the reaction of **2** with CO.[36] The DFT results show that both reactions feature early transition states, as expected for exothermic processes, with only minor perturbations in the Zr-CH_3 distances and long Zr*C*H_3---*C*O_2 distances (Table 2.3). The reaction of (PO)PdMe(THF) with CO_2 to yield (PO)Pd(OAc)THF (which was not observed experimentally) is endergonic by 9.2 kcal/mol. The free-energy profile for this reaction is shown in Figure 2.3. The reaction of $(PO)PdMe_2^-$ with CO_2 without Li^+ to yield $(PO)PdMe(OAc)^-$ is exergonic by 5.3 kcal/mol.

Table 2.3. Comparison of select calculated bond lengths (angstroms) and angles (degrees).

	$Cp_2ZrMe(OCO)^+$	$Cp_2ZrMe(OCO)^‡$	Cp_2ZrOAc^+	Cp_2ZrMe_2	$Cp_2ZrMe_2(OCO)^‡$ (lateral)	$Cp_2ZrMe_2(OCO)^‡$ (central)	$Cp_2ZrMe(\kappa^2\text{-OAc})$
Zr–C	2.250	2.370	--	2.283	2.331, 2.475	2.330, 2.543	2.304
Zr–O	2.353	2.166	2.195, 2.196	--	2.464	2.357	2.313, 2.338
C–C	4.083	1.953	1.477	--	2.163	2.152	1.493
C–O	1.168, 1.139	1.239, 1.168	1.274	--	1.198, 1.166	1.200, 1.164	1.260, 1.261
∠ O–C–O	179.67	142.35	117.66	--	152.56	151.83	118.82

Note: The C–O distance of free CO_2 is calculated to be 1.164 Å. For comparison, Zr-O distances[37] of select mononuclear, η^1 Zr–alkoxide complexes range from 1.984-2.075 Å.

Atomic Coordinates for Calculated Structures

Cp_2ZrMe_2

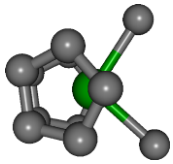

Zr	0.000000	0.252902	0.000000
C	2.213494	-0.279336	-1.141054
C	2.540426	0.477715	0.000000
C	2.213495	-0.279335	1.141054
C	1.659794	-1.498993	0.707843
C	1.659794	-1.498994	-0.707842
C	-2.540426	0.477715	0.000000
C	-2.213494	-0.279336	-1.141054
C	-1.659794	-1.498993	-0.707843
C	-1.659794	-1.498993	0.707843
C	-2.213494	-0.279336	1.141054
C	0.000000	1.739074	-1.733103
C	0.000000	1.739074	1.733103
H	-2.338485	0.035018	-2.166233
H	-2.946990	1.478994	0.000000
H	-1.318561	-2.303504	-1.342614
H	-1.318560	-2.303504	1.342614
H	-2.338485	0.035018	2.166233
H	2.338484	0.035017	-2.166234
H	2.946990	1.478994	-0.000001
H	2.338485	0.035019	2.166233
H	1.318561	-2.303504	1.342614
H	1.318560	-2.303505	-1.342613
H	0.000000	1.279222	2.727657
H	0.887184	2.379964	1.672261
H	-0.887184	2.379963	1.672261
H	0.887184	2.379964	-1.672261
H	0.000000	1.279222	-2.727657
H	-0.887184	2.379964	-1.672261

$Cp_2Zr(Me)_2(OCO)$ Lateral TS

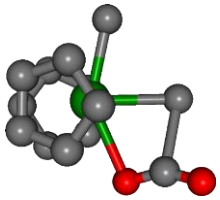

Zr	0.182546	0.046054	0.176555
C	2.092348	-1.642996	0.455771
H	2.124940	-2.232025	1.360517
C	2.693739	-0.377695	0.273441
H	3.275362	0.156861	1.008775
C	2.398580	0.056585	-1.029381
H	2.726639	0.983156	-1.477266
C	1.584183	-0.920214	-1.644225
H	1.172912	-0.876443	-2.642247
C	1.420900	-1.981956	-0.726112
H	0.830944	-2.871547	-0.889196
C	-0.601849	2.393187	0.764592
H	-0.524475	2.710764	1.791597
C	0.404084	2.511962	-0.211470
H	1.382864	2.945571	-0.061870
C	-0.104734	1.992009	-1.426718
H	0.415213	1.954243	-2.372849
C	-1.408736	1.541781	-1.188551
H	-2.056075	1.076380	-1.916031
C	-1.712211	1.759857	0.175475
H	-2.643242	1.516001	0.667041
C	0.834573	0.534851	2.359977
H	1.355782	-0.302597	2.834537
H	1.506507	1.400559	2.401568
H	-0.039671	0.765651	2.977742
C	-1.231191	-1.468672	1.531070
H	-1.919872	-0.932789	2.186397
H	-1.607770	-2.488322	1.409264
H	-0.288115	-1.605453	2.073769
O	-1.367574	-1.288016	-1.198597
C	-2.238908	-1.380937	-0.381013
O	-3.357230	-1.480578	-0.067786

$Cp_2Zr(Me)_2(OCO)$ Central TS

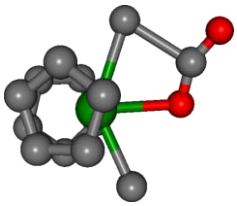

Zr	-0.146355	0.008646	0.102980
C	-0.436710	2.404601	0.909682
H	-0.322882	2.603005	1.962825
C	-1.631378	2.018314	0.271013
H	-2.590047	1.886959	0.751934
C	-1.359885	1.876304	-1.110674
H	-2.074197	1.609426	-1.876086
C	0.001637	2.133447	-1.311125
H	0.521122	2.095960	-2.255691
C	0.582180	2.439362	-0.056541
H	1.621618	2.681632	0.115631
C	-1.905579	-1.721242	0.725744
H	-2.362568	-1.654581	1.700304
C	-2.344955	-1.074901	-0.441244
H	-3.218203	-0.445049	-0.526855
C	-1.453437	-1.407097	-1.488535
H	-1.526621	-1.080531	-2.516064
C	-0.480917	-2.282714	-0.962193
H	0.343843	-2.712722	-1.509560
C	-0.746372	-2.458736	0.405035
H	-0.152500	-3.033528	1.100831
C	-0.354211	-0.002748	2.423769
H	0.406440	0.646380	2.867469
H	-1.336075	0.334656	2.774987
H	-0.179082	-1.011276	2.810056
C	1.703812	-0.288762	-1.616705
H	2.355406	0.538085	-1.902543
H	2.200748	-1.223017	-1.888059
H	0.820264	-0.234394	-2.265437
O	1.883432	-0.600716	1.133470
C	2.712900	-0.482258	0.274716
O	3.819619	-0.432818	-0.083548

$Cp_2ZrMe(\kappa^1\text{-}OAc)$

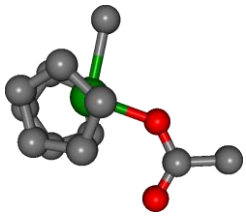

Zr	0.370552	0.003229	0.256690
C	1.840054	-2.063880	0.329933
C	0.517745	-2.524283	0.514861
C	-0.197283	-2.293278	-0.672804
C	0.665442	-1.659990	-1.586520
C	1.933994	-1.532191	-0.968871
C	0.042809	2.515166	0.231677
C	1.396158	2.311462	0.561839
C	2.028246	1.716973	-0.547696
C	1.064425	1.577654	-1.574013
C	-0.161095	2.071031	-1.091921
C	1.086045	0.020076	2.420085
O	-1.664443	-0.029710	0.614590
H	1.862906	2.546641	1.505701
H	-0.717311	2.911420	0.889405
H	3.070749	1.439463	-0.610419
H	1.239135	1.165877	-2.557202
H	-1.102965	2.049215	-1.621332
H	2.630292	-2.099494	1.064833
H	0.121761	-2.959058	1.421003
H	-1.242515	-2.502505	-0.844157
H	0.401447	-1.343978	-2.585209
H	2.818281	-1.106955	-1.420947
H	0.800323	-0.912652	2.916961
H	2.165251	0.148024	2.552274
H	0.590847	0.847798	2.940978
C	-2.748788	-0.037735	-0.119140
O	-2.734883	-0.052846	-1.332198
C	-4.017107	-0.029345	0.687865
H	-4.885898	-0.032858	0.033054
H	-4.043118	-0.901115	1.344369
H	-4.040545	0.851496	1.332166

$Cp_2ZrMe(\kappa^2\text{-}OAc)$

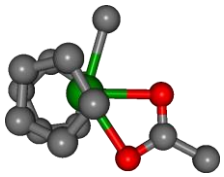

Zr	-0.204531	0.002957	0.146488
C	-1.524557	2.115422	0.627116
C	-0.193299	2.540454	0.424002
C	0.142866	2.294302	-0.916768
C	-0.961058	1.682956	-1.543178
C	-2.001374	1.591901	-0.587302
C	-1.126520	-2.271035	0.804354
C	-2.114053	-1.626723	0.034702
C	-1.630999	-1.518179	-1.291364
C	-0.339661	-2.060116	-1.327964
C	-0.016854	-2.510862	-0.025987
C	-0.525357	0.042777	2.427693
O	1.766969	-0.103637	-1.106071
H	-3.080219	-1.299540	0.391870
H	-1.199017	-2.505112	1.854195
H	-2.159405	-1.080636	-2.125856
H	0.318301	-2.078390	-2.183281
H	0.917277	-2.962617	0.275513
H	-2.071040	2.171969	1.555611
H	0.459791	2.952014	1.179686
H	1.101469	2.477117	-1.377792
H	-1.009083	1.365327	-2.574496
H	-2.990478	1.193937	-0.761831
H	-0.119018	0.972810	2.836194
H	-1.572126	-0.044155	2.741152
H	0.037969	-0.781443	2.875026
C	2.483941	-0.066879	-0.070187
O	1.921846	0.009825	1.055453
C	3.973254	-0.111879	-0.162865
H	4.347805	-0.957190	0.416556
H	4.299793	-0.195403	-1.197356
H	4.390715	0.790705	0.286716

$Cp_2ZrMe(ClPh)^+$

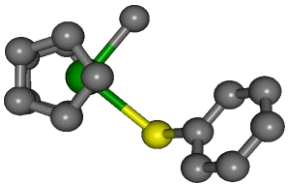

Zr	1.058686	0.077863	0.130450
C	-0.165418	1.866914	-1.142446
C	-0.633555	1.935243	0.190298
C	0.436106	2.346218	1.007795
C	1.575578	2.498181	0.188756
C	1.196597	2.213076	-1.146726
C	2.373483	-2.071837	0.193193
C	2.396930	-1.631646	-1.151697
C	3.104159	-0.418482	-1.202204
C	3.521739	-0.104967	0.115603
C	3.086062	-1.141963	0.970343
C	0.552259	-0.321801	2.292149
H	1.958514	-2.145647	-1.996417
H	1.900722	-2.972841	0.558718
H	3.318510	0.155864	-2.090953
H	4.126587	0.742487	0.402859
H	3.259657	-1.205176	2.033600
H	-0.753469	1.596882	-2.008895
H	-1.641596	1.720665	0.520557
H	0.395061	2.506026	2.074274
H	2.549690	2.834308	0.512482
H	1.834169	2.277761	-2.015707
H	1.235052	0.123711	3.022210
H	-0.448108	0.062978	2.518390
H	0.564989	-1.404490	2.466556
Cl	-0.860393	-1.560167	-0.834789
C	-2.444230	-0.848530	-0.351127
C	-3.184465	-0.206227	-1.319341
C	-2.840498	-0.990266	0.960595
C	-4.394263	0.349710	-0.930639
H	-2.838644	-0.146034	-2.343849
C	-4.054678	-0.425773	1.322558
H	-2.227477	-1.520958	1.678677
C	-4.822802	0.245247	0.383672
H	-5.003937	0.861083	-1.665309
H	-4.398962	-0.518911	2.345202
H	-5.769532	0.682051	0.676322

$Cp_2ZrMe(OCO)^+$ ground state adduct

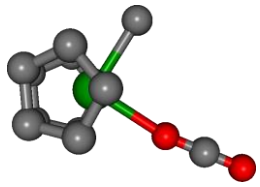

Zr	-0.204659	0.000002	0.126374
C	-1.184514	2.191666	0.851593
C	0.033122	2.497475	0.215696
C	-0.087792	2.159918	-1.152785
C	-1.370543	1.624692	-1.359044
C	-2.047708	1.628460	-0.113507
C	0.033003	-2.497482	0.215634
C	-1.184585	-2.191628	0.851600
C	-2.047803	-1.628361	-0.113443
C	-1.370705	-1.624603	-1.359015
C	-0.087967	-2.159892	-1.152835
C	0.134853	-0.000009	2.350235
H	-1.413133	-2.350279	1.894354
H	0.899748	-2.935955	0.690617
H	-3.069513	-1.319224	0.052029
H	-1.778415	-1.295089	-2.302972
H	0.671022	-2.295029	-1.911493
H	-1.413108	2.350305	1.894339
H	0.899864	2.935896	0.690735
H	0.671244	2.295033	-1.911400
H	-1.778219	1.295218	-2.303029
H	-3.069442	1.319369	0.051904
H	0.708110	0.891466	2.628914
H	-0.767181	0.000001	2.969353
H	0.708082	-0.891507	2.628904
O	2.115555	-0.000068	-0.266502
C	3.283283	-0.000077	-0.248926
O	4.422125	-0.000086	-0.238303

$Cp_2ZrMe(OCO)^+$
TS

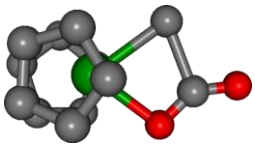

Zr	0.125315	0.006469	0.035916
C	1.188990	-1.944268	1.168018
H	1.227224	-1.989145	2.248217
C	2.165025	-1.377225	0.327535
H	3.089353	-0.916461	0.644136
C	1.738198	-1.548199	-1.013596
H	2.284149	-1.245998	-1.896213
C	0.511424	-2.246007	-0.993374
H	-0.075534	-2.521853	-1.857702
C	0.158934	-2.473912	0.349623
H	-0.724654	-2.990856	0.695936
C	-0.353174	2.461359	-0.100694
H	-1.378064	2.800732	-0.157674
C	0.393584	2.270001	1.080451
H	0.042996	2.447413	2.087941
C	1.678547	1.810364	0.718621
H	2.494341	1.603425	1.396310
C	1.731248	1.741970	-0.695510
H	2.592077	1.457692	-1.283595
C	0.476093	2.143668	-1.197922
H	0.188839	2.187474	-2.239415
C	-1.759143	-0.143836	1.465813
H	-2.329631	0.719077	1.804871
H	-2.235267	-1.055894	1.819386
H	-0.791101	-0.094132	2.043789
O	-1.621797	-0.155552	-1.234348
C	-2.483879	-0.211091	-0.346111
O	-3.637254	-0.289098	-0.180622

$Cp_2Zr(\kappa^2\text{-}OAc)^+$

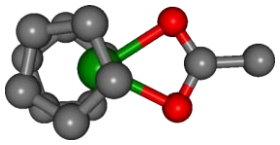

Zr	0.162542	0.002965	0.022580
C	0.929682	-2.025234	1.247314
C	-0.025683	-2.472778	0.304220
C	0.497225	-2.255462	-0.984296
C	1.771249	-1.656810	-0.845087
C	2.043919	-1.533450	0.538587
C	0.283324	2.257943	1.084958
C	1.586592	1.709131	1.098040
C	2.031508	1.615124	-0.242985
C	0.995290	2.077023	-1.078584
C	-0.085269	2.474230	-0.256343
H	2.162730	1.454756	1.976739
H	-0.334982	2.450541	1.950435
H	3.000436	1.262864	-0.566539
H	1.021220	2.128337	-2.158641
H	-1.029119	2.869302	-0.603078
H	0.825269	-2.066415	2.323098
H	-0.990199	-2.899483	0.538019
H	-0.001800	-2.479496	-1.916515
H	2.441450	-1.388580	-1.649925
H	2.951951	-1.141359	0.973647
O	-1.822447	-0.055445	0.957737
C	-2.394036	-0.039643	-0.181093
C	-3.866723	-0.031757	-0.298026
H	-4.178992	-0.501791	-1.228851
H	-4.322691	-0.515040	0.563998
H	-4.206405	1.007599	-0.318752
O	-1.650744	-0.007273	-1.215557

(PO-^{i}Pr)PdMe$_2^-$
PCM(THF)

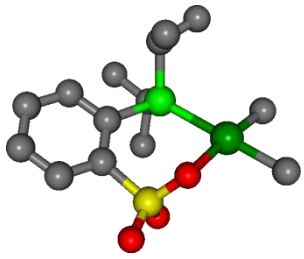

C	2.029658	-0.885056	-0.110647
C	3.358448	-1.275937	-0.267732
H	3.590036	-2.336612	-0.238258
C	4.358847	-0.333891	-0.470522
H	5.390747	-0.654400	-0.592199
C	4.026393	1.012867	-0.528608
C	2.700269	1.401920	-0.374827
H	2.464961	2.461498	-0.440240
C	1.671788	0.476075	-0.149682
C	-0.172442	2.372249	-1.294737
H	0.662172	3.079568	-1.182792
C	-0.061945	1.680189	-2.649081
H	-0.150469	2.412650	-3.461569
H	0.892775	1.154867	-2.768920
H	-0.866638	0.941689	-2.769630
C	-1.482635	3.143193	-1.188305
H	-2.338869	2.461583	-1.268008
H	-1.576812	3.689376	-0.241795
H	-1.554445	3.874971	-2.003012
C	-0.037745	2.033983	1.650338
H	-1.077896	2.389082	1.730907
C	0.219083	1.059363	2.794215
H	0.093099	1.564129	3.760393
H	-0.455620	0.197203	2.752606
H	1.244937	0.669055	2.750280
C	0.894035	3.233511	1.736986
H	1.944983	2.918638	1.726770
H	0.744907	3.954711	0.924194
H	0.725452	3.764822	2.682799
C	-3.360319	0.630506	0.546205
H	-3.976746	0.078259	1.266812
H	-2.991932	1.546121	1.029733
H	-4.003817	0.918555	-0.296678
C	-3.316980	-1.973829	-0.321876
H	-4.303045	-1.575686	-0.593007
H	-2.983726	-2.685675	-1.090112
H	-3.409248	-2.505849	0.636017
O	1.587605	-3.465783	-0.145647
O	-0.247332	-1.995016	-0.838052
O	0.409969	-2.102272	1.559844
P	-0.077602	1.076063	0.044525
Pd	-1.832480	-0.554827	-0.123668
S	0.852447	-2.228056	0.160257
H	4.793461	1.765142	-0.697082

(PO-^{i}Pr)PdMe(MeOCO)$^-$
TS S$_E$2, PCM(THF)

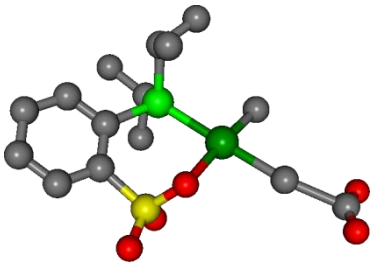

C	-2.008513	1.622059	-0.075397
C	-3.038326	2.548625	-0.224806
H	-2.794680	3.604894	-0.158147
C	-4.340511	2.131800	-0.469458
H	-5.133529	2.866501	-0.584396
C	-4.613533	0.775221	-0.578977
C	-3.585122	-0.148920	-0.433721
H	-3.826959	-1.203266	-0.538800
C	-2.265403	0.241163	-0.165132
C	-1.383184	-2.216605	-1.393532
H	-2.453094	-2.463552	-1.338585
C	-1.105208	-1.493682	-2.707211
H	-1.353154	-2.142333	-3.556406
H	-1.686763	-0.569603	-2.805486
H	-0.041100	-1.230371	-2.781939
C	-0.581891	-3.509382	-1.308383
H	0.494287	-3.304284	-1.359059
H	-0.776170	-4.071942	-0.387535
H	-0.839277	-4.158932	-2.154046
C	-1.447852	-1.979653	1.576692
H	-0.700381	-2.786474	1.622335
C	-1.230602	-1.058395	2.771481
H	-1.404355	-1.606378	3.705658
H	-0.215863	-0.645296	2.789862
H	-1.928533	-0.211287	2.743539
C	-2.834212	-2.607052	1.612376
H	-3.616950	-1.839569	1.645017
H	-3.031850	-3.264653	0.757157
H	-2.936027	-3.212319	2.521948
C	2.020979	-2.111048	0.576855
H	2.837776	-1.882253	1.271867
H	1.291063	-2.751324	1.084258
H	2.434615	-2.656446	-0.281638
C	3.336950	0.361900	-0.283764
H	3.580518	-0.553362	-0.817309
H	3.136654	1.266890	-0.846947
H	3.322901	0.407410	0.804479
O	-0.493739	3.757629	-0.038950
O	0.527848	1.648490	-0.758841
O	-0.049322	1.980334	1.637644
P	-0.968164	-1.073433	0.018117
Pd	1.243924	-0.334864	-0.078984
S	-0.377137	2.321000	0.243401
H	-5.623958	0.428882	-0.781877
C	5.347084	0.524223	-0.077639
O	5.685480	1.493549	-0.699884
O	5.701861	-0.396652	0.609633

(PO-^{i}Pr)PdMe(OAc)$^{-}$
σ-complex, PCM(THF)

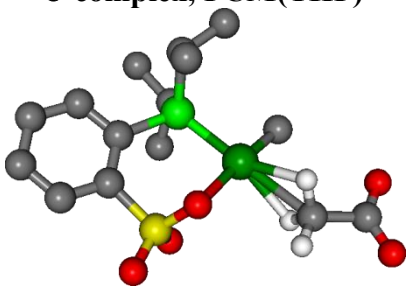

C	-2.074942	1.518273	-0.069776
C	-3.186293	2.350441	-0.179114
H	-3.032918	3.424501	-0.130184
C	-4.457311	1.820923	-0.363142
H	-5.314442	2.484048	-0.445874
C	-4.618061	0.445634	-0.454689
C	-3.509248	-0.386606	-0.351188
H	-3.664120	-1.458317	-0.442859
C	-2.218917	0.120180	-0.141626
C	-1.138183	-2.207766	-1.468263
H	-2.190841	-2.522554	-1.422750
C	-0.913717	-1.403632	-2.744314
H	-1.133662	-2.025542	-3.620068
H	-1.547398	-0.510718	-2.794094
H	0.133083	-1.079119	-2.814835
C	-0.255988	-3.448827	-1.447897
H	0.801727	-3.177145	-1.548619
H	-0.372804	-4.045263	-0.535276
H	-0.514216	-4.091130	-2.298143
C	-1.208669	-2.080861	1.541937
H	-0.337022	-2.747508	1.615182
C	-1.198496	-1.136125	2.739362
H	-1.273195	-1.713586	3.668210
H	-0.288493	-0.527300	2.780472
H	-2.055477	-0.450803	2.701535
C	-2.471616	-2.932260	1.525627
H	-3.373850	-2.310678	1.560655
H	-2.537356	-3.592655	0.653004
H	-2.484303	-3.567832	2.419294
C	2.021007	-1.829073	0.796401
H	3.094598	-1.716480	0.592591
H	1.818438	-1.756866	1.872892
H	1.643104	-2.780384	0.411614
C	3.494748	0.907760	-0.249376
H	3.042562	0.249016	-1.021355
H	3.390793	1.945596	-0.575832
H	3.004143	0.809734	0.739725
O	-0.738338	3.771063	-0.139558
O	0.418778	1.725953	-0.849064
O	-0.088355	2.073017	1.557086
P	-0.841687	-1.108103	0.000456
Pd	1.213697	-0.162804	-0.047797
S	-0.499329	2.358854	0.172588
H	-5.602409	0.012301	-0.611573
C	4.964404	0.422481	-0.076085
O	5.840685	1.296607	-0.208924
O	5.093011	-0.797352	0.181659

(PO-^{i}Pr)PdMe(OAc)$^{-}$
A, PCM(THF)

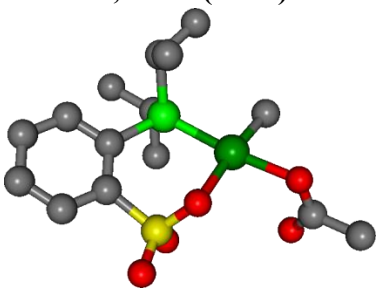

C	-1.807875	1.666817	-0.122248
C	-2.812884	2.621109	-0.267746
H	-2.526379	3.668182	-0.298827
C	-4.144590	2.243537	-0.380738
H	-4.916471	3.000612	-0.494498
C	-4.475037	0.895930	-0.355175
C	-3.472263	-0.056714	-0.217206
H	-3.763396	-1.103395	-0.213552
C	-2.120645	0.294696	-0.088142
C	-1.468691	-2.262357	-1.239537
H	-2.543848	-2.423987	-1.079447
C	-1.261237	-1.630926	-2.612343
H	-1.643839	-2.296738	-3.395663
H	-1.771600	-0.665437	-2.709167
H	-0.191652	-1.465630	-2.799555
C	-0.764049	-3.609590	-1.153802
H	0.315026	-3.499065	-1.313558
H	-0.917765	-4.109739	-0.190138
H	-1.151815	-4.273846	-1.936008
C	-1.213811	-1.862196	1.712299
H	-0.561164	-2.747801	1.693539
C	-0.726583	-0.935363	2.820722
H	-0.872381	-1.413401	3.797290
H	0.335698	-0.690514	2.705736
H	-1.282662	0.010898	2.819935
C	-2.642360	-2.324035	1.961723
H	-3.327273	-1.472141	2.050494
H	-3.020663	-2.991879	1.177903
H	-2.684394	-2.875228	2.909375
C	2.001712	-2.245290	0.381300
H	2.707497	-1.961685	1.171095
H	1.284610	-2.974122	0.770795
H	2.547214	-2.682818	-0.464019
O	-0.223182	3.745583	-0.298767
O	0.694060	1.565419	-0.932324
O	0.228824	2.055799	1.464959
P	-0.868894	-1.069698	0.061657
S	-0.140101	2.325173	0.067505
H	-5.510474	0.577513	-0.447154
Pd	1.286755	-0.457004	-0.260735
O	3.277851	-0.025814	-0.776059
C	4.012623	0.494294	0.143909
O	3.686060	0.697122	1.316887
C	5.402436	0.879246	-0.339206
H	6.029907	1.205310	0.493944
H	5.876515	0.036273	-0.852456
H	5.324208	1.693698	-1.067656

(PO-^{i}Pr)PdMe(OAc)$^{-}$
B, PCM(THF)

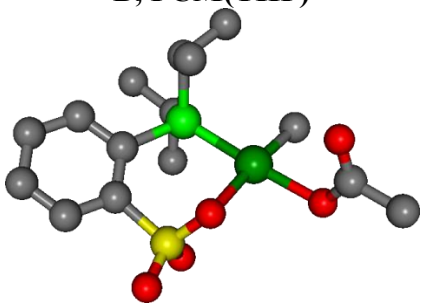

C	-2.020845	1.471860	-0.193700
C	-3.117120	2.277363	-0.495344
H	-3.010354	3.352867	-0.387757
C	-4.309118	1.721528	-0.941323
H	-5.155125	2.363774	-1.172910
C	-4.401084	0.346197	-1.104620
C	-3.306695	-0.457584	-0.806874
H	-3.403697	-1.528800	-0.960610
C	-2.100001	0.073078	-0.328460
C	-0.717993	-2.187804	-1.468909
H	-1.748678	-2.530214	-1.641117
C	-0.260558	-1.355355	-2.663217
H	-0.299471	-1.958699	-3.578512
H	-0.884589	-0.466652	-2.815760
H	0.775380	-1.017400	-2.521623
C	0.177945	-3.406077	-1.287645
H	1.216479	-3.101332	-1.109417
H	-0.137452	-4.048288	-0.456664
H	0.159370	-4.013430	-2.200905
C	-1.342340	-2.145559	1.456984
H	-0.537753	-2.885620	1.579594
C	-1.397523	-1.289192	2.716573
H	-1.669170	-1.907870	3.580627
H	-0.434684	-0.807048	2.920591
H	-2.153566	-0.498797	2.620240
C	-2.649792	-2.895373	1.243351
H	-3.502893	-2.207739	1.202747
H	-2.652780	-3.505452	0.331867
H	-2.819728	-3.571856	2.090311
C	2.142265	-1.839632	1.115450
H	2.638286	-1.486846	2.027544
H	1.471778	-2.669910	1.358316
H	2.896112	-2.172789	0.391526
O	-0.771665	3.762424	0.023987
O	0.570941	1.770963	-0.461818
O	-0.420347	2.067675	1.802921
P	-0.714221	-1.103621	0.045126
S	-0.547948	2.350899	0.364325
H	-5.319371	-0.108019	-1.468470
Pd	1.321130	-0.158269	0.328732
O	3.256174	0.657682	0.511458
C	3.970142	0.503269	-0.547231
O	3.629116	-0.086743	-1.579333
C	5.349184	1.135031	-0.452749
H	5.932252	0.936504	-1.355338
H	5.252120	2.217269	-0.315691
H	5.883509	0.750157	0.422216

[Li][(PO-^{i}Pr)PdMe$_2$]
A, PCM(THF)

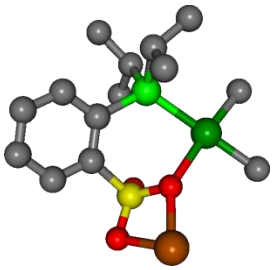

C	2.065640	-0.772851	-0.051506
C	3.403968	-1.137930	-0.188850
H	3.675597	-2.185739	-0.101883
C	4.371135	-0.173238	-0.440252
H	5.412887	-0.464147	-0.545391
C	3.991509	1.156175	-0.564168
C	2.654074	1.511671	-0.426458
H	2.387438	2.558965	-0.542145
C	1.653583	0.569476	-0.152542
C	-0.247488	2.356760	-1.375787
H	0.572526	3.085184	-1.300678
C	-0.131609	1.607947	-2.699137
H	-0.223599	2.305197	-3.541102
H	0.827091	1.084609	-2.797969
H	-0.934306	0.862694	-2.788929
C	-1.572786	3.104723	-1.294324
H	-2.416320	2.405093	-1.348240
H	-1.676052	3.685476	-0.369926
H	-1.658457	3.802972	-2.136128
C	-0.094441	2.149985	1.587399
H	-1.146610	2.467812	1.664459
C	0.213112	1.235161	2.767991
H	0.066830	1.774103	3.712054
H	-0.420264	0.340248	2.772538
H	1.257969	0.897952	2.735712
C	0.790220	3.387615	1.608586
H	1.853116	3.115846	1.600004
H	0.601811	4.065882	0.767655
H	0.609870	3.952227	2.532175
C	-3.388759	0.628451	0.526794
H	-4.035337	0.079791	1.221682
H	-3.028799	1.541413	1.019448
H	-3.987446	0.911538	-0.349291
C	-3.299387	-1.999592	-0.218812
H	-4.246819	-1.635627	-0.634916
H	-2.905075	-2.801458	-0.860774
H	-3.496409	-2.410907	0.780864
O	1.660086	-3.376916	-0.046824
O	-0.194318	-2.014572	-0.697002
O	0.522607	-2.004829	1.701583
P	-0.115097	1.129291	0.022545
Pd	-1.835083	-0.554284	-0.071747
S	0.938092	-2.121983	0.304819
H	4.733194	1.923703	-0.770333
Li	0.316107	-3.809654	-1.589820

[Li][(PO-^{i}Pr)PdMe$_2$]
B, PCM(THF)

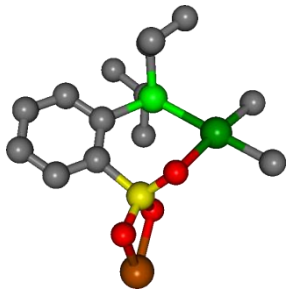

C	2.101976	-0.588225	-0.200771
C	3.461882	-0.827038	-0.393574
H	3.813909	-1.852918	-0.443190
C	4.346974	0.233128	-0.540497
H	5.405302	0.038763	-0.692582
C	3.863789	1.533721	-0.505544
C	2.504721	1.763675	-0.320554
H	2.155283	2.792792	-0.317375
C	1.584517	0.720363	-0.150953
C	-0.461120	2.422424	-1.237170
H	0.304281	3.202789	-1.117781
C	-0.301391	1.770674	-2.606742
H	-0.452761	2.511988	-3.401149
H	0.692214	1.327422	-2.743383
H	-1.045474	0.973415	-2.741772
C	-1.837534	3.062293	-1.101091
H	-2.627583	2.306856	-1.197144
H	-1.975728	3.574209	-0.141230
H	-1.982720	3.804111	-1.896196
C	-0.276848	2.029491	1.704557
H	-1.347286	2.277908	1.785651
C	0.067959	1.053563	2.824061
H	-0.098438	1.522491	3.801705
H	-0.533701	0.138889	2.767325
H	1.125337	0.759616	2.771165
C	0.528252	3.314182	1.832078
H	1.605603	3.108218	1.847104
H	0.326266	4.031183	1.027261
H	0.282279	3.808445	2.780585
C	-3.435584	0.302990	0.584798
H	-4.065246	-0.362415	1.186415
H	-3.136047	1.162230	1.199871
H	-4.031950	0.666849	-0.262797
C	-3.139478	-2.234784	-0.393950
H	-4.089349	-1.921392	-0.844788
H	-2.647102	-2.968904	-1.047682
H	-3.356949	-2.705165	0.574728
O	1.960283	-3.221246	-0.319544
O	-0.051904	-1.938653	-0.958623
O	0.692826	-2.135432	1.424010
P	-0.222399	1.117781	0.074161
Pd	-1.801748	-0.688159	-0.138398
S	1.086126	-2.056857	-0.012219
H	4.539847	2.376109	-0.628262
Li	1.706688	-3.917092	1.682768

[Li][(PO-^{i}Pr)PdMe$_2$]
C, PCM(THF)

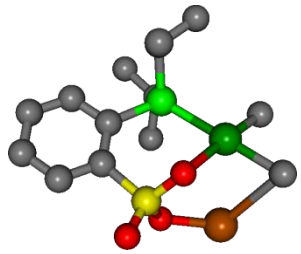

C	1.990058	-0.986776	-0.063621
C	3.301540	-1.456748	-0.116161
H	3.471523	-2.529279	-0.119838
C	4.368571	-0.570436	-0.183163
H	5.386325	-0.949432	-0.223602
C	4.119777	0.794640	-0.217395
C	2.810430	1.259089	-0.170059
H	2.644176	2.331871	-0.218442
C	1.712166	0.393583	-0.074240
C	0.080483	2.336818	-1.424888
H	0.969306	2.973225	-1.303970
C	0.200651	1.552632	-2.727237
H	0.234622	2.239682	-3.581672
H	1.103062	0.930791	-2.757322
H	-0.667195	0.891950	-2.859982
C	-1.160525	3.220851	-1.442133
H	-2.065284	2.614974	-1.580445
H	-1.281350	3.806635	-0.522774
H	-1.102265	3.927101	-2.279423
C	0.010135	2.163432	1.550572
H	-1.024469	2.542429	1.564262
C	0.192076	1.241793	2.752033
H	0.076388	1.806308	3.685309
H	-0.538344	0.424097	2.751656
H	1.195255	0.794386	2.754954
C	0.960919	3.349730	1.628129
H	2.001091	3.020832	1.738878
H	0.898494	4.009152	0.754291
H	0.720058	3.953376	2.512233
C	-3.201492	0.871761	0.696391
H	-3.012209	0.899129	1.779315
H	-3.071487	1.885281	0.296131
H	-4.235302	0.552186	0.527170
C	-3.412611	-1.734169	-0.300659
H	-4.051431	-1.393463	-1.126238
H	-3.016225	-2.727563	-0.565854
H	-4.056125	-1.818750	0.587583
O	1.398007	-3.524277	-0.380569
O	-0.336167	-1.882695	-0.975393
O	0.228402	-2.279110	1.404636
P	0.007315	1.130705	-0.006185
Pd	-1.836951	-0.392625	-0.141540
S	0.734376	-2.273959	-0.004226
H	4.940663	1.503881	-0.287198
Li	-1.678094	-2.444620	1.770466

[Li][(PO-^{i}Pr)PdMe$_2$]
D, PCM(THF)

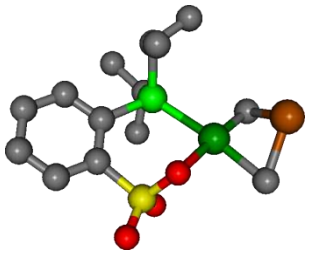

C	1.962458	-1.043086	-0.078162
C	3.244612	-1.568441	-0.206814
H	3.358436	-2.648906	-0.179374
C	4.337720	-0.728866	-0.380058
H	5.335197	-1.150332	-0.479237
C	4.147076	0.645394	-0.437752
C	2.865344	1.169856	-0.315871
H	2.738885	2.248378	-0.382502
C	1.749029	0.345586	-0.121706
C	0.095552	2.342930	-1.376418
H	0.990396	2.973455	-1.268622
C	0.175745	1.583855	-2.696714
H	0.172561	2.284685	-3.541020
H	1.079750	0.969175	-2.767097
H	-0.685351	0.910362	-2.807659
C	-1.136354	3.237636	-1.339828
H	-2.047938	2.639441	-1.470756
H	-1.234035	3.797618	-0.401636
H	-1.097870	3.965993	-2.159364
C	0.119949	2.095845	1.601835
H	-0.903158	2.502616	1.658838
C	0.323503	1.133141	2.768727
H	0.201436	1.664622	3.720531
H	-0.372021	0.287018	2.741555
H	1.335674	0.709195	2.747964
C	1.109401	3.250710	1.666918
H	2.142557	2.883270	1.681046
H	1.005863	3.956905	0.833791
H	0.956280	3.814232	2.596043
C	-3.116271	0.891732	0.770343
H	-4.164184	0.544834	0.891277
H	-2.759347	0.974539	1.804066
H	-3.138572	1.910125	0.353704
C	-3.208855	-1.938375	-0.191899
H	-2.758634	-2.643880	0.513760
H	-4.247764	-1.784243	0.168979
H	-3.219444	-2.438086	-1.173627
O	1.218640	-3.550152	-0.110709
O	-0.380426	-1.853796	-0.912759
O	0.106280	-1.992777	1.505208
P	0.073130	1.111329	0.020144
Pd	-1.753081	-0.421063	-0.089950
S	0.633135	-2.242045	0.154598
H	4.992064	1.314538	-0.582476
Li	-3.945187	-0.149192	-0.988590

[Li][(PO-^{i}Pr)PdMe$_2$(OCO)]
Li$^+$ assisted S$_E$2 TS, PCM(THF)

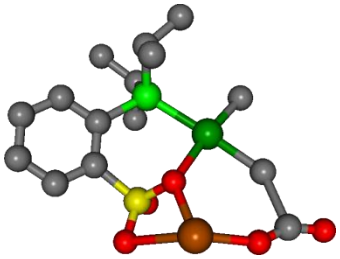

C	-1.357706	1.959094	-0.018609
C	-2.000874	3.182825	-0.187217
H	-1.436031	4.097652	-0.032901
C	-3.339536	3.227694	-0.555657
H	-3.834848	4.186054	-0.685597
C	-4.028191	2.041370	-0.764277
C	-3.379045	0.822411	-0.597542
H	-3.945179	-0.086297	-0.783460
C	-2.035478	0.737827	-0.208440
C	-1.900813	-1.814991	-1.555690
H	-2.994673	-1.712137	-1.589370
C	-1.296687	-1.149466	-2.787623
H	-1.660769	-1.639977	-3.698401
H	-1.549044	-0.084568	-2.853700
H	-0.201500	-1.237529	-2.771928
C	-1.551723	-3.297799	-1.517573
H	-0.465188	-3.441097	-1.463301
H	-2.007407	-3.820642	-0.668504
H	-1.908620	-3.783111	-2.433971
C	-2.144533	-1.722493	1.418068
H	-1.717284	-2.737192	1.434553
C	-1.718705	-1.006076	2.694505
H	-2.158401	-1.503424	3.567390
H	-0.628856	-0.995879	2.811643
H	-2.063106	0.036457	2.694054
C	-3.659167	-1.835818	1.325251
H	-4.135581	-0.849302	1.377296
H	-3.997717	-2.336112	0.410004
H	-4.032155	-2.420498	2.175136
C	1.220661	-2.905133	0.697122
H	0.252756	-3.392538	0.855100
H	1.791620	-3.467882	-0.051522
H	1.780048	-2.892577	1.640438
C	3.237034	-0.854864	0.083832
H	3.761533	-1.755664	0.387410
H	3.149439	-0.673419	-0.988771
H	3.131337	-0.066533	0.831293
O	0.813657	3.451232	0.259008
O	1.115066	1.188494	-0.501460
O	0.442747	1.585672	1.868986
P	-1.267636	-0.949932	-0.032661
Pd	1.069444	-0.970085	0.085721
S	0.357040	2.064540	0.487591
H	-5.073564	2.055658	-1.061457
Li	2.648322	2.426653	-0.985908
O	4.360276	1.466686	-0.718891
O	5.850718	-0.172702	-0.098466
C	4.862428	0.436386	-0.338121

[Li][(PO-^{i}Pr)PdMe(μ-OAc)]
σ-complex, PCM(THF)

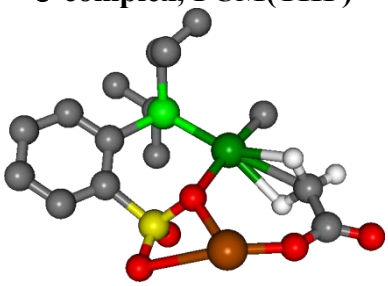

C	-1.462881	1.902111	-0.070789
C	-2.190652	3.070210	-0.275478
H	-1.695493	4.026029	-0.131426
C	-3.522925	3.009856	-0.665351
H	-4.084080	3.926678	-0.822778
C	-4.120940	1.773452	-0.858114
C	-3.388674	0.607898	-0.657739
H	-3.889190	-0.340816	-0.828544
C	-2.048245	0.633720	-0.249204
C	-1.739707	-1.959921	-1.510466
H	-2.835356	-1.888874	-1.555706
C	-1.145779	-1.315689	-2.758599
H	-1.507648	-1.837043	-3.652221
H	-1.413385	-0.257036	-2.853826
H	-0.050065	-1.390629	-2.746193
C	-1.357170	-3.431351	-1.421156
H	-0.268079	-3.556273	-1.403126
H	-1.778872	-3.932163	-0.542124
H	-1.734595	-3.952849	-2.308252
C	-1.989968	-1.758645	1.486960
H	-1.524316	-2.753256	1.537403
C	-1.587518	-0.971148	2.728483
H	-1.996990	-1.459622	3.620096
H	-0.499751	-0.901854	2.838449
H	-1.983131	0.051627	2.692879
C	-3.500651	-1.934738	1.406895
H	-4.016688	-0.967612	1.418031
H	-3.824418	-2.494465	0.521606
H	-3.838388	-2.493027	2.287818
C	1.230749	-2.725520	0.735198
H	0.326878	-3.328996	0.832435
H	1.918644	-3.211408	0.032181
H	1.702136	-2.602623	1.719257
C	3.630149	-0.755840	0.088257
H	4.073261	-1.702384	0.406989
H	3.016170	-0.950680	-0.815627
H	3.039401	-0.346643	0.931286
O	0.578087	3.549218	0.252557
O	1.052204	1.299434	-0.509846
O	0.322040	1.642739	1.842249
P	-1.200550	-0.998745	-0.014810
Pd	1.061710	-0.814667	0.081304
S	0.227971	2.137803	0.465773
H	-5.159858	1.704947	-1.168840
Li	2.720108	2.419618	-0.864652
O	4.227282	1.422126	-0.667735
O	5.872148	-0.038511	-0.224846
C	4.689455	0.297448	-0.299735

[Li][(PO-^{i}Pr)PdMe(μ-OAc)]
negative frequency present (-18 cm^{-1})
unless
grid=(-96023) is used

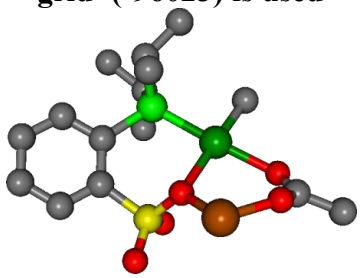

C	1.704055	1.756345	0.004676
C	2.621454	2.797505	0.124248
H	2.275136	3.816343	-0.023402
C	3.947512	2.537754	0.444765
H	4.654907	3.357660	0.534845
C	4.350603	1.228326	0.664109
C	3.431425	0.191547	0.547116
H	3.777635	-0.819682	0.741314
C	2.092696	0.417597	0.197793
C	1.370228	-1.982511	1.619090
H	2.462612	-2.087492	1.682625
C	0.879787	-1.151775	2.800843
H	1.127772	-1.656408	3.742094
H	1.328755	-0.151842	2.824034
H	-0.211573	-1.032774	2.758351
C	0.744871	-3.370982	1.637584
H	-0.349730	-3.306857	1.608302
H	1.074520	-4.000207	0.802397
H	1.023362	-3.883185	2.566248
C	1.695835	-2.033414	-1.378191
H	1.011239	-2.891496	-1.445379
C	1.553300	-1.207128	-2.652570
H	1.850757	-1.807608	-3.520278
H	0.524492	-0.862462	-2.806778
H	2.203242	-0.322731	-2.621242
C	3.116165	-2.559939	-1.222301
H	3.851594	-1.748325	-1.267536
H	3.272145	-3.119591	-0.292492
H	3.337368	-3.240017	-2.053759
C	-1.607265	-2.474055	-0.862505
H	-1.616726	-2.364176	-1.954930
H	-0.910063	-3.264119	-0.571490
H	-2.612920	-2.708075	-0.499853
O	-0.073001	3.689257	-0.094226
O	-0.831629	1.459480	0.548994
O	-0.205273	1.889187	-1.811469
P	0.987021	-1.066595	0.046629
S	0.034727	2.262058	-0.414180
H	5.379971	1.004685	0.931611
Pd	-1.225654	-0.611071	-0.164430
O	-3.311987	-0.311216	-0.467949
C	-4.086341	0.368241	0.270843
O	-3.756626	1.019250	1.291922
C	-5.545144	0.385051	-0.125596
H	-6.154363	0.048364	0.719333
H	-5.845970	1.414803	-0.345324
H	-5.741140	-0.244702	-0.995242
Li	-2.293608	2.134030	1.606723

[Li][(PO-^{i}Pr)PdMe$_2$(OCO)]
Li$^+$-assisted S$_E$2 TS, PCM(THF)

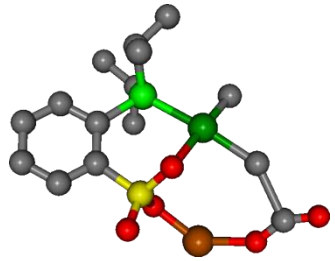

C	-1.410235	1.943181	-0.096214
C	-2.121113	3.142477	-0.090822
H	-1.571434	4.076032	-0.166237
C	-3.507635	3.143899	-0.015803
H	-4.049218	4.085919	-0.010253
C	-4.188710	1.935672	0.028043
C	-3.477591	0.741347	0.016555
H	-4.038912	-0.188877	0.032439
C	-2.076735	0.704665	-0.023292
C	-2.182924	-1.873166	-1.313810
H	-3.260062	-1.777119	-1.113582
C	-1.863402	-1.229367	-2.658722
H	-2.403661	-1.745770	-3.461246
H	-2.141697	-0.169576	-2.690934
H	-0.788685	-1.302279	-2.874045
C	-1.810047	-3.350374	-1.319906
H	-0.742447	-3.479051	-1.539320
H	-2.026201	-3.850410	-0.368156
H	-2.374568	-3.870552	-2.103060
C	-1.781449	-1.694238	1.653476
H	-1.220962	-2.641921	1.662075
C	-1.243460	-0.813716	2.777361
H	-1.401105	-1.301410	3.746773
H	-0.171630	-0.611530	2.662458
H	-1.766117	0.151830	2.801434
C	-3.257072	-2.006338	1.861088
H	-3.846891	-1.090885	1.987135
H	-3.693889	-2.590115	1.042190
H	-3.375900	-2.592699	2.780638
C	1.305989	-2.763639	0.630586
H	0.522300	-3.466990	0.327742
H	2.282672	-3.179688	0.363662
H	1.261023	-2.619644	1.718514
C	3.226570	-0.763505	-0.310385
H	3.695619	-1.637949	-0.750946
H	3.133929	0.124310	-0.934559
H	3.194688	-0.719082	0.779027
O	0.610739	3.492484	-0.749035
O	0.840274	1.084885	-1.195127
O	0.923016	1.926421	1.133462
P	-1.259400	-0.962973	0.019217
Pd	1.057252	-0.933987	-0.234175
S	0.371392	2.139494	-0.240079
H	-5.274774	1.914570	0.065612
Li	2.849269	2.140079	1.418893
C	4.955950	0.343120	0.199747
O	4.538612	1.311518	0.789344
O	5.889412	-0.255478	-0.218194

[Li][(PO-^{i}Pr)PdMe(μ-OAc)]
σ-complex, PCM(THF)

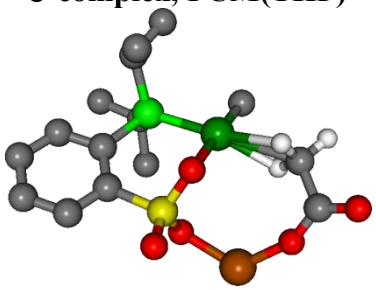

C	-1.238528	1.987067	-0.118289
C	-1.878501	3.221958	-0.183620
H	-1.272653	4.122913	-0.207698
C	-3.263910	3.298485	-0.244963
H	-3.751217	4.268168	-0.295249
C	-4.011366	2.129951	-0.266316
C	-3.371261	0.897193	-0.205147
H	-3.985012	0.001356	-0.240121
C	-1.976665	0.789006	-0.109323
C	-2.107780	-1.804050	-1.396105
H	-3.189186	-1.635398	-1.288632
C	-1.633397	-1.184431	-2.706667
H	-2.142186	-1.668561	-3.548106
H	-1.836974	-0.109199	-2.761942
H	-0.553120	-1.332767	-2.836652
C	-1.838164	-3.302634	-1.372771
H	-0.771362	-3.509721	-1.521713
H	-2.158725	-3.784672	-0.441838
H	-2.384258	-3.779142	-2.194948
C	-1.948610	-1.590614	1.626384
H	-1.484287	-2.585436	1.682880
C	-1.406597	-0.737354	2.769230
H	-1.687417	-1.184642	3.729478
H	-0.314534	-0.648119	2.736840
H	-1.828286	0.275670	2.736837
C	-3.459553	-1.756144	1.730418
H	-3.965586	-0.787220	1.806914
H	-3.894286	-2.312523	0.892099
H	-3.690712	-2.312593	2.646262
C	0.996036	-2.843794	0.722301
H	0.126385	-3.477563	0.534898
H	1.884595	-3.311680	0.279654
H	1.132507	-2.709782	1.802663
C	3.569904	-0.990409	-0.228032
H	4.055006	-1.961398	-0.362228
H	3.019291	-0.768957	-1.157192
H	2.916687	-1.047297	0.667083
O	0.925604	3.403807	-0.582677
O	1.008793	0.989086	-1.045014
O	0.978844	1.797643	1.297512
P	-1.292063	-0.924878	0.019397
Pd	0.963706	-0.989671	-0.104829
S	0.554583	2.072635	-0.104807
H	-5.094962	2.167961	-0.336808
Li	2.917466	2.049076	1.619885
C	4.583861	0.145900	0.003597
O	4.180044	1.100131	0.738397
O	5.681992	0.036645	-0.545495

[Li][(PO-^{i}Pr)PdMe(μ-OAc)]
PCM(THF)

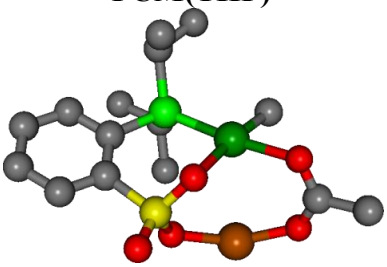

C	-1.802240	1.687246	-0.152976
C	-2.782627	2.665661	-0.298648
H	-2.476234	3.706363	-0.344365
C	-4.123037	2.315221	-0.396029
H	-4.878867	3.087540	-0.509678
C	-4.480486	0.975604	-0.358429
C	-3.498999	0.000563	-0.219778
H	-3.815293	-1.038301	-0.206506
C	-2.139313	0.320832	-0.102210
C	-1.547794	-2.283206	-1.207199
H	-2.628232	-2.408901	-1.052513
C	-1.309520	-1.691640	-2.592662
H	-1.713225	-2.362573	-3.360117
H	-1.784208	-0.711247	-2.717062
H	-0.233893	-1.572277	-2.779694
C	-0.881167	-3.646306	-1.075153
H	0.200958	-3.572900	-1.235230
H	-1.053794	-4.113891	-0.098679
H	-1.284899	-4.321222	-1.839122
C	-1.295636	-1.821100	1.741650
H	-0.664315	-2.721737	1.749577
C	-0.800263	-0.878414	2.832634
H	-0.989077	-1.318111	3.819122
H	0.275834	-0.689301	2.742108
H	-1.316758	0.089339	2.789179
C	-2.736406	-2.244432	1.992095
H	-3.401869	-1.376198	2.065497
H	-3.126745	-2.918170	1.220150
H	-2.791213	-2.777912	2.948615
C	1.918848	-2.291593	0.419220
H	2.671575	-2.002807	1.163279
H	1.193443	-2.973165	0.870904
H	2.409161	-2.780862	-0.430884
O	-0.165622	3.729411	-0.388945
O	0.690280	1.508915	-1.009053
O	0.289088	2.052285	1.374409
P	-0.933293	-1.079675	0.071836
S	-0.123800	2.311100	-0.035721
H	-5.522588	0.678610	-0.441530
Pd	1.237281	-0.518431	-0.289964
O	3.260697	-0.140231	-0.789246
C	4.033885	0.422359	0.043970
O	3.707030	0.817576	1.190030
C	5.461443	0.637764	-0.395894
H	6.143482	0.258604	0.371158
H	5.671285	0.155696	-1.352397
H	5.647049	1.713327	-0.486636
Li	2.060594	1.426811	1.848689

[Li(THF)$_2$][(PO-^{i}Pr)PdMe$_2$]

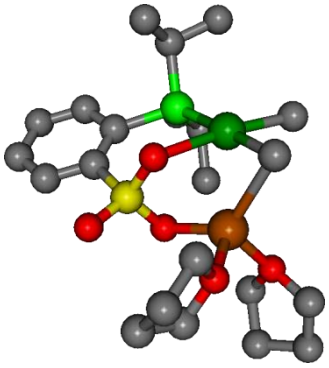

C	-1.410741	2.119263	0.576429
C	-1.565960	3.422916	1.042983
H	-0.723816	4.103702	0.959135
C	-2.774981	3.840489	1.583100
H	-2.885082	4.860520	1.942875
C	-3.838502	2.951274	1.644021
C	-3.680870	1.653302	1.172462
H	-4.534675	0.981885	1.217906
C	-2.469408	1.193470	0.638666
C	-3.979796	-0.752444	-0.874987
H	-4.810296	-0.456007	-0.217276
C	-3.957672	0.154760	-2.101043
H	-4.886131	0.043345	-2.675132
H	-3.848393	1.212372	-1.834546
H	-3.118383	-0.109853	-2.758602
C	-4.172403	-2.208124	-1.284223
H	-3.338472	-2.547303	-1.912391
H	-4.243977	-2.884649	-0.423911
H	-5.096359	-2.314223	-1.866427
C	-2.517672	-1.588023	1.575869
H	-2.547029	-2.610852	1.167715
C	-1.236465	-1.445092	2.390262
H	-1.251893	-2.129946	3.248188
H	-0.351623	-1.664600	1.779748
H	-1.125054	-0.422826	2.777100
C	-3.751514	-1.375425	2.439459
H	-3.738667	-0.386122	2.913499
H	-4.688387	-1.475400	1.876985
H	-3.773077	-2.120363	3.245436
C	-0.616191	-3.152225	-1.122256
H	0.349618	-3.573912	-0.818647
H	-1.377039	-3.441230	-0.386467
H	-0.888059	-3.566186	-2.101356
C	1.237178	-1.592067	-2.410174
H	0.957915	-2.285084	-3.211565
H	1.605806	-0.663003	-2.868039
H	2.054142	-2.083351	-1.853067
O	0.921828	3.030286	-0.203520
O	-0.011190	1.110289	-1.442316
O	0.848921	0.783346	0.839737
P	-2.359790	-0.558080	0.024913
Pd	-0.455661	-1.124616	-1.294985
S	0.214512	1.752508	-0.107370
H	-4.796743	3.263306	2.052935
Li	1.875371	-0.508980	-0.217654
O	3.445360	0.551084	-0.814257
C	3.983404	1.418910	0.199706
C	3.430215	1.237499	-2.082306
C	4.193228	2.767214	-0.470068
H	3.267591	1.466753	1.031684

[Li(THF)$_2$][(PO-^{i}Pr)PdMe$_2$(OCO)]
Li$^+$-assisted S$_E$2 TS

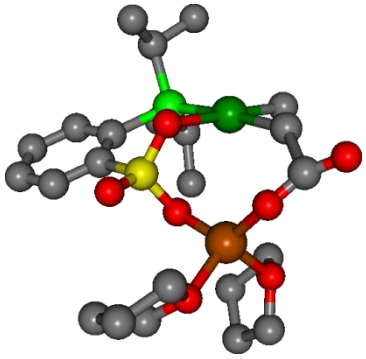

C	-0.872886	2.161537	-0.501635
C	-0.540246	3.512441	-0.577746
H	0.451790	3.781412	-0.931379
C	-1.466687	4.490114	-0.241056
H	-1.195028	5.540793	-0.305054
C	-2.744745	4.113739	0.147678
C	-3.074799	2.765558	0.220875
H	-4.088576	2.497800	0.507821
C	-2.150429	1.753877	-0.073935
C	-4.264608	-0.034320	-0.887311
H	-4.919881	0.774127	-0.527996
C	-3.915402	0.213612	-2.350937
H	-4.823182	0.178881	-2.965814
H	-3.437192	1.187297	-2.505975
H	-3.225035	-0.556470	-2.719535
C	-4.976812	-1.370893	-0.719547
H	-4.341807	-2.190521	-1.079518
H	-5.247616	-1.584431	0.321844
H	-5.900319	-1.379944	-1.311336
C	-3.209530	-0.152605	1.906375
H	-3.434598	-1.228398	1.981928
C	-1.993942	0.136645	2.780393
H	-2.216861	-0.081553	3.832438
H	-1.129066	-0.465385	2.477925
H	-1.701840	1.193519	2.712013
C	-4.426868	0.627208	2.384546
H	-4.207133	1.697458	2.474234
H	-5.300518	0.506282	1.732749
H	-4.714734	0.277298	3.384075
C	-1.898927	-3.078617	0.642129
H	-1.413134	-4.034253	0.425128
H	-1.714813	-2.810824	1.691738
H	-2.978734	-3.181258	0.479131
C	0.483629	-2.946794	-1.155890
H	0.150909	-3.964303	-1.330827
H	0.540714	-2.270237	-2.007812
H	0.894132	-2.722111	-0.170242
O	1.382212	1.838619	-1.807648
O	-0.252152	-0.012401	-1.856242
O	1.010622	0.470548	0.215789
P	-2.698905	-0.011516	0.116174
Pd	-1.132841	-1.602937	-0.536426
S	0.428769	1.037068	-1.038830
H	-3.492406	4.865609	0.388782
Li	2.618326	-0.611713	0.013429
O	4.096985	0.674355	-0.158063
C	3.921439	1.946236	0.485921
C	4.574646	0.871123	-1.504251
C	4.186418	2.996942	-0.580643
H	2.901585	1.992145	0.893209

H	4.930499	0.980638	0.555692
C	4.423280	2.370065	-1.924004
H	3.692311	0.510026	-2.858122
H	2.412449	1.612945	-2.270078
H	5.024087	3.326937	-0.029689
H	3.275180	3.359944	-0.384410
H	5.449028	2.006560	-2.073825
H	4.240274	3.185528	-2.629877
O	2.661249	-1.751057	1.080373
C	3.978475	-2.267815	0.828282
C	2.503939	-1.480141	2.478777
C	4.690952	-2.288217	2.177120
H	3.890183	-3.260772	0.370945
H	4.465818	-1.595456	0.107511
C	3.914543	-1.247754	2.979834
H	1.830509	-0.620907	2.575038
H	2.043501	-2.351962	2.970943
H	5.758069	-2.063607	2.087021
H	4.594712	-3.274109	2.649208
H	4.242906	-0.232349	2.720198
H	4.009947	-1.372607	4.062570
H	4.643558	2.013249	1.315638
C	5.156154	2.269863	-1.506695
H	5.293286	0.075730	-1.723559
H	3.724776	0.793041	-2.197428
H	4.587848	3.925578	-0.163242
H	3.256435	3.215346	-1.118783
H	6.170161	2.266937	-1.084482
H	5.202390	2.701247	-2.510920
O	2.756141	-1.431683	1.803013
C	3.799290	-0.974716	2.665380
C	1.570676	-1.470719	2.595423
C	3.135341	-0.019833	3.671295
H	4.249557	-1.841098	3.172338
H	4.559804	-0.505494	2.031524
C	1.629821	-0.184672	3.400999
H	0.715630	-1.540172	1.909955
H	1.593632	-2.363630	3.242120
H	3.457121	1.016595	3.523200
H	3.396556	-0.297271	4.698129
H	1.253107	0.636183	2.778829
H	1.030099	-0.227409	4.316118
C	2.473949	-3.041040	-1.604879
O	2.916648	-1.939856	-1.346752
O	2.703982	-4.130831	-2.012837

[Li][(κ^1-PO-^{i}Pr)PdMe$_2$(OCO)]
PCM(THF)

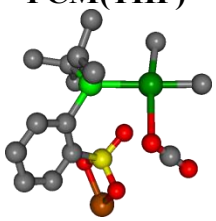

C	2.250580	0.014798	-0.242115
C	3.548501	0.009453	-0.762180
H	4.183591	-0.854248	-0.584768
C	4.030125	1.071968	-1.507712
H	5.040407	1.047071	-1.906990
C	3.199028	2.161099	-1.731594
C	1.909453	2.163050	-1.219137
H	1.296922	3.035326	-1.421299
C	1.380631	1.101872	-0.462806
C	-1.094068	2.602705	-0.949326
H	-0.440770	3.485502	-0.947295
C	-1.243295	2.075389	-2.373478
H	-1.664760	2.850783	-3.025436
H	-0.291172	1.749162	-2.808443
H	-1.927939	1.215241	-2.386052
C	-2.454036	3.037396	-0.409757
H	-3.144919	2.186454	-0.360710
H	-2.393513	3.485512	0.588875
H	-2.890441	3.787323	-1.081295
C	-0.170727	2.100697	1.792332
H	-1.209363	2.309752	2.093476
C	0.438272	1.153846	2.818563
H	0.433823	1.628151	3.808013
H	-0.104704	0.205083	2.879835
H	1.482795	0.919663	2.572495
C	0.600206	3.412179	1.740481
H	1.635189	3.247771	1.413424
H	0.145831	4.151094	1.070440
H	0.640320	3.858753	2.742239
C	-3.288394	0.017982	1.384426
H	-3.569795	-0.826083	2.022799
H	-2.818635	0.800679	1.992356
H	-4.187062	0.415212	0.899145
C	-3.336226	-2.124330	-0.291707
H	-4.377081	-1.828530	-0.119505
H	-3.243527	-2.477256	-1.331391
H	-3.090670	-2.949216	0.392042
O	2.415169	-2.602379	-0.081852
O	0.497260	-1.527983	1.068260
O	2.826008	-1.349318	1.933497
P	-0.389892	1.249789	0.136381
Pd	-1.960966	-0.608927	-0.034907
S	1.925049	-1.455709	0.744699
H	3.547562	3.014587	-2.307674
Li	3.750905	-3.134200	1.424145
O	-0.434662	-1.686038	-1.775432
C	-0.430617	-2.791693	-1.387492
O	-0.439943	-3.901597	-1.046084

[Li][(κ^1-PO-^{i}Pr)PdMe$_2$(OCO)]
1,2-insertion TS, PCM(THF)

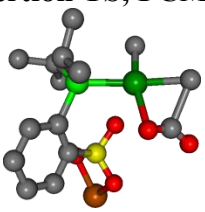

C	2.144054	-0.245817	-0.426994
C	3.318255	-0.430938	-1.159932
H	3.851130	-1.372843	-1.065066
C	3.799994	0.549648	-2.012521
H	4.712441	0.380835	-2.577827
C	3.102499	1.743499	-2.124750
C	1.921504	1.920351	-1.416541
H	1.396196	2.860603	-1.548960
C	1.392191	0.940380	-0.559510
C	-0.981946	2.670902	-0.827428
H	-0.262883	3.499351	-0.880119
C	-1.295440	2.173123	-2.235284
H	-1.680153	2.999661	-2.845203
H	-0.422778	1.751955	-2.746762
H	-2.066688	1.392065	-2.200345
C	-2.253914	3.200355	-0.169664
H	-3.009902	2.408896	-0.088049
H	-2.082385	3.615150	0.830272
H	-2.676564	4.000045	-0.789743
C	0.127542	2.118733	1.838309
H	-0.867279	2.326305	2.261389
C	0.874344	1.194040	2.790722
H	0.989445	1.691611	3.761383
H	0.361847	0.240035	2.942059
H	1.880058	0.965821	2.414858
C	0.887475	3.429578	1.670801
H	1.857794	3.262170	1.185116
H	0.338299	4.178672	1.090436
H	1.087953	3.863049	2.658328
C	-2.623506	0.029234	1.791232
H	-1.854302	-0.020914	2.569928
H	-3.060180	1.034334	1.762582
H	-3.408579	-0.707406	1.994659
C	-3.376999	-1.939846	-0.411468
H	-3.676056	-2.430805	-1.344206
H	-3.501266	-2.632378	0.423833
H	-4.052747	-1.076961	-0.311608
O	2.215781	-2.844757	0.030221
O	0.476509	-1.527914	1.231088
O	2.888297	-1.374899	1.813715
P	-0.268049	1.290864	0.210500
S	1.857973	-1.585837	0.747490
H	3.463607	2.538684	-2.771662
Li	3.734466	-3.214137	1.425237
Pd	-1.783830	-0.468623	0.000690
O	-1.065189	-1.519943	-1.840308
C	-1.525705	-2.446461	-1.178608
O	-1.419544	-3.607378	-0.929752

[Li][(PO-^{i}Pr)PdMe$_2$(OCO$_{trans\text{-to-}O}$)]
S_E2 TS, PCM(THF)

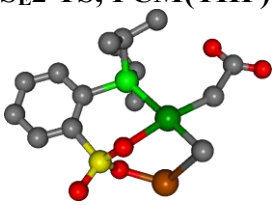

C	-2.679962	-0.152886	-0.151597
C	-4.069382	-0.070052	-0.211944
H	-4.644141	-0.982288	-0.340559
C	-4.704887	1.159376	-0.093951
H	-5.788930	1.215749	-0.142879
C	-3.945465	2.304470	0.102692
C	-2.559363	2.214286	0.169416
H	-1.992275	3.124287	0.346907
C	-1.885230	0.994129	0.029138
C	0.250542	2.006276	1.668695
H	-0.242550	2.978337	1.522073
C	-0.371601	1.307606	2.873023
H	-0.188804	1.892902	3.782435
H	-1.454456	1.175211	2.768831
H	0.077024	0.315177	3.020060
C	1.740199	2.241658	1.892162
H	2.236117	1.308107	2.191498
H	2.262631	2.624245	1.008176
H	1.882129	2.956914	2.711270
C	0.549414	2.011448	-1.297901
H	1.643330	1.979481	-1.167289
C	0.196710	1.295095	-2.597400
H	0.602545	1.847502	-3.453378
H	0.603799	0.277386	-2.627843
H	-0.891277	1.223168	-2.730088
C	0.105395	3.466617	-1.345767
H	-0.964604	3.554093	-1.570614
H	0.311439	4.009541	-0.415804
H	0.646563	3.981823	-2.149047
C	3.074567	-0.677208	-0.171544
H	3.629331	-1.606134	-0.116377
H	2.555519	-0.446065	-1.105220
H	2.898241	-0.128987	0.759532
C	1.769013	-3.089185	0.762072
H	2.497084	-2.997908	1.576494
H	0.915753	-3.700206	1.078856
H	2.269317	-3.541812	-0.103906
O	-3.131725	-2.741848	-0.184800
O	-1.010846	-1.988687	0.799186
O	-1.345492	-1.848229	-1.648772
P	-0.033710	0.978636	0.141166
Pd	0.996407	-1.224685	0.372748
S	-2.012583	-1.809633	-0.312754
H	-4.426789	3.272910	0.211824
Li	0.251390	-2.856640	-1.993414
C	4.380758	0.599075	-0.605449
O	5.447874	0.037255	-0.672405
O	3.862296	1.689305	-0.726263

[Li][(PO-^{i}Pr)PdMe$_2$(OCO$_{trans\text{-to-}O}$)]
S_E2 TS, PCM(THF)

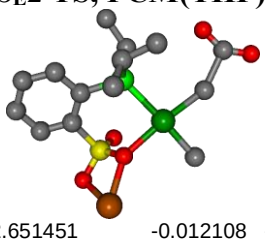

C	-2.651451	-0.012108	-0.194942
C	-4.036559	0.127440	-0.261926
H	-4.647105	-0.747725	-0.463183
C	-4.622722	1.371320	-0.065630
H	-5.702909	1.475759	-0.119530
C	-3.818750	2.469437	0.208450
C	-2.437595	2.320497	0.275208
H	-1.836280	3.195328	0.509307
C	-1.810213	1.085944	0.062563
C	0.385301	1.982412	1.696459
H	-0.042109	2.985892	1.557997
C	-0.275521	1.315806	2.898313
H	-0.029852	1.863398	3.816431
H	-1.367233	1.278758	2.809619
H	0.090913	0.285923	3.016221
C	1.887822	2.120443	1.917934
H	2.319810	1.158265	2.225326
H	2.433485	2.459456	1.029851
H	2.078282	2.832034	2.730403
C	0.645283	1.988262	-1.280004
H	1.738114	1.872736	-1.195789
C	0.181913	1.321013	-2.571472
H	0.659144	1.801856	-3.433773
H	0.419381	0.250755	-2.595681
H	-0.905358	1.418028	-2.695054
C	0.308539	3.471959	-1.281147
H	-0.766637	3.641042	-1.420337
H	0.625498	3.984297	-0.365071
H	0.821876	3.958398	-2.119993
C	3.076328	-0.784055	-0.175357
H	3.611831	-1.723766	-0.117938
H	2.597442	-0.526138	-1.123877
H	2.920423	-0.223822	0.750587
C	1.660973	-3.205730	0.441922
H	0.777112	-3.805167	0.692144
H	2.083919	-3.537921	-0.513068
H	2.419080	-3.294268	1.228503
O	-3.185999	-2.587870	-0.343265
O	-1.089914	-1.994477	0.648386
O	-1.387739	-1.673870	-1.815537
P	0.042071	0.977269	0.166002
Pd	0.976545	-1.280357	0.286114
S	-2.031342	-1.664199	-0.503428
H	-4.262069	3.447868	0.374500
Li	-2.386328	-3.591017	1.293463
C	4.450744	0.462296	-0.576601
O	5.500124	-0.132706	-0.581189
O	3.964406	1.561049	-0.735525

(PO-^{i}Pr)PdMe(THF)
PCM(THF)

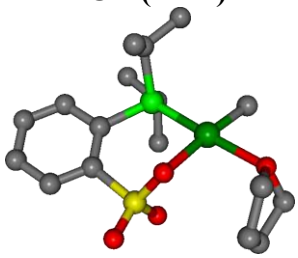

C	-1.415923	1.942081	-0.054022
C	-2.137466	3.129287	-0.144096
H	-1.592886	4.068863	-0.123574
C	-3.520459	3.110524	-0.275390
H	-4.071480	4.044552	-0.346170
C	-4.184928	1.893612	-0.328784
C	-3.463858	0.707735	-0.243554
H	-4.012856	-0.227980	-0.304675
C	-2.070342	0.696691	-0.091436
C	-2.011132	-1.873629	-1.407318
H	-3.100991	-1.786600	-1.291912
C	-1.595113	-1.205053	-2.713699
H	-2.084550	-1.703999	-3.558373
H	-1.863518	-0.143043	-2.745732
H	-0.509452	-1.284592	-2.859016
C	-1.639459	-3.350361	-1.412233
H	-0.563056	-3.481208	-1.576646
H	-1.911812	-3.866167	-0.483855
H	-2.163235	-3.852559	-2.234085
C	-1.855821	-1.709593	1.601330
H	-1.326876	-2.673461	1.631031
C	-1.375306	-0.855801	2.770479
H	-1.632977	-1.344877	3.717151
H	-0.292418	-0.691666	2.744926
H	-1.859360	0.129324	2.759082
C	-3.353101	-1.972652	1.695028
H	-3.918759	-1.037088	1.774086
H	-3.747312	-2.547640	0.849062
H	-3.556406	-2.549222	2.605366
C	1.180634	-2.724137	0.651080
H	1.235576	-2.595734	1.740694
H	0.395750	-3.446268	0.410284
H	2.140278	-3.087546	0.264076
O	0.682805	3.514861	-0.215443
O	0.933173	1.178259	-0.910719
O	0.683813	1.717653	1.503938
P	-1.243296	-0.957272	0.015385
Pd	1.000068	-0.863463	-0.138940
S	0.363464	2.125224	0.124796
H	-5.265148	1.857662	-0.442599
O	3.214643	-0.836050	-0.346860
C	3.944115	-0.610225	0.873092
C	3.744009	0.127297	-1.281508
C	4.007352	0.900664	0.999500
H	3.413080	-1.124236	1.679550
H	4.944561	-1.055489	0.759281
C	4.086758	1.374705	-0.463936
H	4.636822	-0.318842	-1.741897
H	2.983782	0.291318	-2.048501
H	4.860882	1.226016	1.601379
H	3.088448	1.271610	1.467997
H	5.084273	1.743747	-0.722512
H	3.365299	2.175249	-0.655194

(PO-^{i}Pr)PdMe(OCO)
PCM(THF)

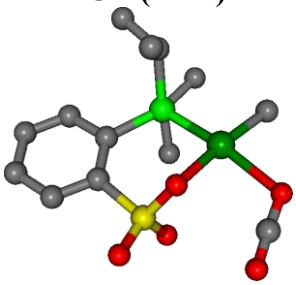

Pd	1.099785	-1.102788	-0.174784
P	-1.110053	-0.801921	0.010818
C	-1.556360	0.995533	0.037640
C	-0.661901	2.083197	0.049355
S	1.126572	1.937029	0.195023
O	1.512005	0.915711	-0.860034
O	1.390772	1.439905	1.554298
O	1.683573	3.251166	-0.128681
C	-1.138462	3.391663	0.039957
C	-2.502341	3.654552	0.026633
C	-3.400525	2.597798	0.038827
C	-2.927257	1.290590	0.046015
H	-0.417104	4.203448	0.043489
H	-2.856607	4.681743	0.016058
H	-3.656842	0.486175	0.065011
C	-1.907283	-1.529143	-1.505657
H	-1.572359	-2.576478	-1.449928
C	-1.988909	-1.427723	1.521451
H	-2.987295	-0.968040	1.473091
C	0.973439	-3.061210	0.300763
H	0.119508	-3.615771	-0.098953
H	1.898120	-3.429413	-0.166773
H	1.027524	-3.186200	1.388346
C	4.013667	-0.120072	-0.200000
O	4.584404	0.883984	-0.119446
O	3.476315	-1.161070	-0.275908
C	-1.273110	-0.904956	2.762163
C	-2.156331	-2.940926	1.566599
C	-3.429373	-1.509171	-1.586005
C	-1.287120	-0.888005	-2.743812
H	-1.687260	-1.363585	-3.646621
H	-1.529523	0.181589	-2.794684
H	-0.195174	-0.988752	-2.757360
H	-3.746481	-2.164993	-2.405313
H	-3.921519	-1.864764	-0.673311
H	-3.803905	-0.505680	-1.816616
H	-2.804161	-3.200470	2.411997
H	-2.616938	-3.352256	0.661189
H	-1.197802	-3.444976	1.722075
H	-1.830301	-1.195274	3.660295
H	-1.176397	0.186705	2.758734
H	-0.263637	-1.329126	2.836626
H	-4.471698	2.780396	0.044673

(PO-^{i}Pr)PdMe(OCO)
1,2-insertion TS, PCM(THF)

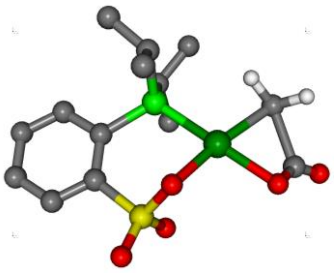

Pd	1.443937	-0.228567	0.386295
P	-0.364839	1.134854	0.043454
C	-1.944060	0.229417	-0.240789
C	-2.098709	-1.166298	-0.196843
S	-0.729666	-2.298767	0.023898
O	0.113515	-1.631379	1.117179
O	-0.014417	-2.348361	-1.255190
O	-1.284748	-3.550063	0.530867
C	-3.340032	-1.756886	-0.409483
C	-4.455586	-0.972237	-0.674234
C	-4.324034	0.408247	-0.732786
C	-3.082945	0.997737	-0.518577
H	-3.419777	-2.839166	-0.358212
H	-5.421935	-1.441279	-0.837080
H	-3.014450	2.080801	-0.573775
C	-0.584369	2.168064	1.570307
H	0.375155	2.706495	1.630929
C	-0.252354	2.239319	-1.441887
H	-1.269178	2.631725	-1.587579
C	3.131162	1.098152	-0.071551
H	3.240405	1.494745	-1.080125
H	2.454557	1.738782	0.525785
H	4.063540	1.194909	0.496598
C	3.747053	-0.698926	-0.298992
O	3.157354	-1.432138	0.504600
O	4.611699	-0.689927	-1.113969
C	0.116469	1.385466	-2.651279
C	0.694477	3.418443	-1.258858
C	-1.718641	3.184689	1.527093
C	-0.711528	1.254558	2.785781
H	-0.798209	1.863680	3.692546
H	-1.611005	0.629535	2.715774
H	0.151742	0.589932	2.900579
H	-2.694752	2.688988	1.576557
H	-1.641662	3.836998	2.404483
H	-1.696805	3.825530	0.638270
H	0.654195	4.047141	-2.155581
H	0.430886	4.050511	-0.404049
H	1.733597	3.096413	-1.138976
H	0.103197	2.000971	-3.557641
H	-0.581078	0.552378	-2.797278
H	1.123805	0.962916	-2.544088
H	-5.184707	1.036028	-0.946197

Trans-P,OAc-(PO-^{i}Pr)Pd(OAc)
PCM(THF)

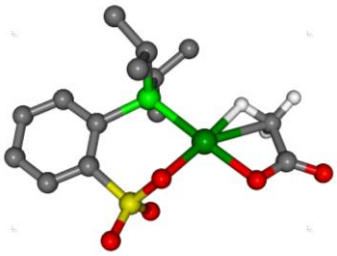

Pd	1.423950	-0.157704	0.235403
P	-0.469690	1.130437	0.034581
C	-2.032715	0.188509	-0.156538
C	-2.124182	-1.212305	-0.124599
S	-0.687635	-2.278348	-0.079819
O	0.231358	-1.622732	0.975210
O	-0.086657	-2.225677	-1.413992
O	-1.123432	-3.574656	0.425093
C	-3.353646	-1.852372	-0.235619
C	-4.517517	-1.107967	-0.389164
C	-4.446792	0.277488	-0.444180
C	-3.216871	0.916273	-0.327620
H	-3.387126	-2.937613	-0.197853
H	-5.475459	-1.613557	-0.472676
H	-3.190995	2.001886	-0.377786
C	-0.606307	2.129596	1.591040
H	0.372813	2.633239	1.632334
C	-0.446496	2.260502	-1.430260
H	-1.436022	2.741309	-1.450247
C	3.489365	0.855715	-0.549574
H	3.431008	0.853254	-1.641500
H	2.487075	1.262140	-0.152925
H	4.135597	1.676003	-0.221205
C	4.038561	-0.476453	-0.033452
O	3.133547	-1.263872	0.455735
O	5.227277	-0.713564	-0.132886
C	-0.276797	1.425278	-2.696181
C	0.617462	3.343774	-1.310628
C	-1.708692	3.181242	1.605490
C	-0.722501	1.187096	2.785609
H	-0.736094	1.771828	3.712079
H	-1.655283	0.610223	2.741685
H	0.110892	0.478405	2.840416
H	-2.698289	2.715368	1.674277
H	-1.585442	3.809847	2.494755
H	-1.692372	3.841960	0.731317
H	0.551289	4.010163	-2.177795
H	0.503419	3.959953	-0.412053
H	1.630344	2.922677	-1.311428
H	-0.326899	2.075383	-3.576573
H	-1.054683	0.659696	-2.794867
H	0.695526	0.915006	-2.711058
H	-5.347487	0.869998	-0.578264

Cis-P,OAc-(PO-^{i}Pr)Pd(OAc)THF PCM(THF)

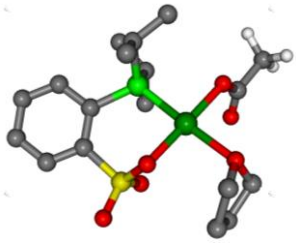

C	-2.22041	-1.57054	-0.24634
C	-3.29041	-2.44759	-0.38764
H	-3.08533	-3.49499	-0.58983
C	-4.59555	-1.98969	-0.25170
H	-5.42626	-2.68098	-0.36356
C	-4.82720	-0.65285	0.04120
C	-3.75599	0.22198	0.18860
H	-3.96816	1.26017	0.43112
C	-2.43218	-0.20940	0.03468
C	-1.53946	1.97462	1.74991
H	-2.59726	2.25756	1.64504
C	-1.38944	1.05206	2.95544
H	-1.73553	1.56625	3.85924
H	-1.96794	0.12661	2.85061
H	-0.33614	0.78045	3.10480
C	-0.70161	3.23858	1.90676
H	0.36471	2.99919	1.97435
H	-0.83397	3.94039	1.07503
H	-1.00164	3.75391	2.82658
C	-1.23085	2.17298	-1.24621
H	-0.38766	2.86308	-1.09227
C	-1.00374	1.38428	-2.53086
H	-0.98589	2.07635	-3.38073
H	-0.05696	0.83586	-2.51090
H	-1.81975	0.66956	-2.69916
C	-2.52753	2.97158	-1.30655
H	-3.38500	2.32100	-1.51543
H	-2.73432	3.53932	-0.39219
H	-2.45956	3.69035	-2.13145
O	-0.72217	-3.72720	-0.27436
O	0.19948	-1.70392	0.72858
O	-0.06731	-1.81684	-1.74321
P	-1.09474	1.04094	0.21391
Pd	0.97149	0.16591	0.42422
S	-0.58920	-2.28321	-0.45453
H	-5.84157	-0.28255	0.16167
O	2.99494	-0.63798	0.75195
C	3.74652	-0.90790	-0.45259
C	3.07781	-1.85466	1.52451
C	3.32537	-2.31198	-0.84172
H	3.49705	-0.12555	-1.17436
H	4.81527	-0.85586	-0.19488
C	3.09247	-3.00432	0.51436
H	4.00887	-1.80706	2.10586
H	2.22702	-1.86922	2.20980
H	4.08195	-2.81301	-1.45244
H	2.39245	-2.27021	-1.41649
H	3.88944	-3.71571	0.75273
H	2.14094	-3.54495	0.52100
O	1.74714	2.01641	0.28566
C	2.23593	2.36771	-0.87059
O	2.26068	1.66401	-1.87685
C	2.76711	3.78203	-0.86269
H	3.55327	3.88691	-0.10856
H	3.16109	4.04771	-1.84540
H	1.96342	4.47401	-0.58564

Trans-P,OAc-(PO-^{i}Pr)Pd(OAc)THF PCM(THF)

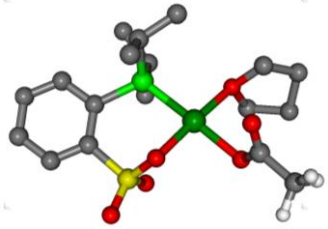

C	-2.790113	-1.043000	-0.242961
C	-4.070892	-1.577924	-0.335767
H	-4.184729	-2.627290	-0.592556
C	-5.181421	-0.782122	-0.080383
H	-6.178944	-1.206317	-0.154887
C	-5.008274	0.545711	0.287774
C	-3.726962	1.077080	0.387397
H	-3.615788	2.112594	0.700860
C	-2.594492	0.302896	0.106248
C	-0.967010	1.835960	1.955822
H	-1.831185	2.516066	1.995807
C	-1.140764	0.730686	2.993156
H	-1.176659	1.171358	3.995968
H	-2.060319	0.154428	2.843594
H	-0.293340	0.032910	2.962999
C	0.311286	2.623494	2.213320
H	1.174322	1.945574	2.246207
H	0.503728	3.395688	1.458720
H	0.246928	3.119766	3.188251
C	-0.855710	2.432456	-1.012781
H	0.190396	2.764606	-0.925508
C	-1.059382	1.813449	-2.393158
H	-0.856290	2.561795	-3.167688
H	-0.406744	0.949883	-2.567959
H	-2.095709	1.474395	-2.519338
C	-1.781567	3.622273	-0.796739
H	-2.830548	3.345389	-0.954046
H	-1.684580	4.071406	0.198061
H	-1.541279	4.399127	-1.532199
O	-1.949171	-3.518561	-0.412218
O	-0.410036	-1.859904	0.503780
O	-0.927274	-1.818086	-1.932262
P	-0.944579	1.090004	0.262982
Pd	0.828181	-0.318991	0.035593
S	-1.437972	-2.164564	-0.602629
H	-5.868305	1.172804	0.506384
O	2.130882	1.229937	-0.559443
C	2.676190	1.012881	-1.896758
C	3.217623	1.593258	0.352118
C	4.152039	0.785324	-1.675760
H	2.146739	0.167568	-2.345156
H	2.475206	1.922744	-2.479179
C	4.442604	1.747281	-0.529216
H	2.917780	2.515416	0.859929
H	3.319184	0.785000	1.085766
H	4.742666	0.988186	-2.573041
H	4.317355	-0.253448	-1.364829
H	4.523968	2.774333	-0.905321
H	5.361148	1.509512	0.013982
O	2.412373	-1.645702	-0.200058
C	3.013451	-1.863512	0.924499
O	2.746223	-1.289044	1.985873
C	4.123503	-2.885409	0.841088
H	4.890320	-2.543422	0.136946
H	4.575852	-3.045577	1.821952
H	3.734093	-3.831746	0.453541

(PO-^{i}Pr)PdMe(py)
Crystal structure coordinates

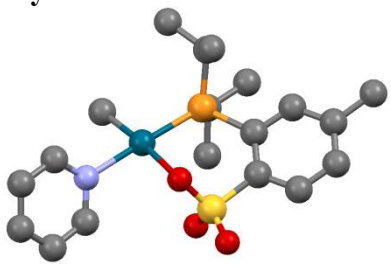

C	2.399308	5.602475	-0.262317
H	3.264178	5.471778	0.106176
C	2.041677	4.897448	-1.386535
H	2.661716	4.306552	-1.798748
C	0.772049	5.054837	-1.911325
H	0.498276	4.553219	-2.670016
C	-0.086464	5.949466	-1.317832
H	-0.960409	6.084764	-1.664466
C	0.345971	6.647129	-0.207824
H	-0.242205	7.277603	0.190492
C	4.298062	9.283154	3.993938
H	4.044123	10.022236	3.369529
C	5.438485	8.521063	3.330494
H	6.200751	9.122084	3.200896
H	5.140415	8.177754	2.462348
H	5.705511	7.771858	3.903532
C	4.758346	9.944002	5.293189
H	5.068250	9.256463	5.917755
H	4.011540	10.436416	5.691350
H	5.491751	10.564351	5.101136
C	1.523390	9.102756	5.053825
H	1.928184	9.451588	5.899018
C	0.389996	8.145540	5.422787
H	-0.363088	8.656362	5.785034
H	0.707239	7.508623	6.097317
H	0.099612	7.658648	4.623343
C	0.999753	10.290992	4.248604
H	0.598632	9.967932	3.414810
H	1.741809	10.896616	4.039375
H	0.324042	10.769600	4.773239
C	3.599325	5.536206	5.032590
C	3.342251	6.880910	5.343779
C	3.457710	7.261956	6.680036
H	3.271008	8.164868	6.910813
C	3.833994	6.383894	7.689021
C	4.088476	5.069563	7.351912
H	4.340847	4.449214	8.025662
C	3.975685	4.651702	6.035797
H	4.159678	3.746028	5.816263
C	3.952345	6.878149	9.106784
H	3.632079	6.185088	9.721356
H	3.410946	7.688101	9.217020
H	4.891277	7.081558	9.304459
C	2.235999	9.131288	1.252721
H	2.913176	9.103676	0.544933
H	2.474584	9.821588	1.906485
H	1.363724	9.340219	0.860338
N	1.561100	6.473173	0.333049
O	3.388976	3.411923	3.566579
O	4.441383	5.370534	2.569149
O	2.048771	5.328196	2.984797
P	2.828063	8.174533	4.128375
Pd	2.147872	7.319297	2.178967
S	3.386560	4.846182	3.404192

2.5. References and Notes

1 (a) Miyashita, A.; Yamamoto, A. *J. Organomet. Chem.* **1973**, *49*, C57. (b) Darensbourg, D. J.; Hanckel, R. K.; Bauch, C. G.; Pala, M.; Simmons, D.; White, J. N. *J. Am. Chem. Soc.* **1985**, *107*, 7463. (c) Darensbourg, D. J.; Groetsch, G.; Weigreffe, P.; Rheingold, A. L. *Inorg. Chem.* **1987**, *26*, 3827. (d) Arafa, I. M.; Shin, K.; Goff, H. M. *J. Am. Chem. Soc.* **1988**, *110*, 5228. (e) Allen, O. R.; Dalgarno, S. J.; Field, L. D.; Jensen, P.; Willis, A. C. *Organometallics* **2009**, *28*, 2385. (f) Darensbourg, D. J.; Grotsch, G. *J. Am. Chem. Soc.* **1985**, *107*, 7473. (g) Johnson, M. T.; Johansson, R.; Kondrashov, M. V.; Steyl, G.; Ahlquist, M.H.G.; Roodt, A.; Wendt, O. F. *Organometallics* **2010**, *29*, 3521. (h) Schmeier, T. J.; Hazari, N.; Incarvito, C. D.; Raskatov, J. A. *Chem. Commun.* **2011**, *47*, 1824. (i) Fan, T.; Chen, X.; Lin, Z. *Chem. Commun.* **2012**, *48*, 10808. (j) Ostapowicz, T. G.; Holscher, M.; Leitner, W. *Chem. Eur. J.* **2011**, *17*, 10329. (k) Aresta, M.; Dibenedetto, A. *Dalton Trans.* **2007**, 2975. (l) Correa, A.; Martin, R. *Angew. Chem. Int. Ed.* **2009**, *48*, 6201. (m) Schmeier, T. J.; Nova, A.; Hazari, N.; Maseras, F. *Chem. Eur. J.* **2012**, *18*, 6915. (n) Darensbourg, D. J.; Kyran, S. J.; Yeung, A. D.; Bengali, A. A. *Eur. J. Inorg. Chem.* **2013**, 4024. (o) Johansson, R.; Jarenmark, M.; Wendt, O. F. *Organometallics* **2005**, *24*, 4500. (p) Allen, O. R.; Dalgarno, S. J.; Field, L. D.; Jensen, P.; Turnbull, A. J.; Willis, A. C. *Organometallics* **2008**, *27*, 2092. (q) Kloppenburg, L.; Petersen, J. L. *Organometallics* **1996**, *15*, 7. (r) Johnston, R. F.; Cooper, J. C. *Organometallics* **1987**, *6*, 2448. (s) Luinstra, G. A.; Ten Cate, L. C.; Heeres, H. J.; Pattiasina, J. W.; Meetsma, A.; Teuben, J. H. *Organometallics* **1991**, *10*, 3227. (t) Cooper, R. T.; Chadwick, F. M.; Ashley, A. E.; O'Hare, D. *Chem. Commun.* **2015**, *51*, 11856. (u) Jonasson, K. J.; Wendt, O. *Chem. Eur. J.* **2014**, *20*, 11894.

2. Hill, M.; Wendt, O. *Organometallics* **2005**, *24*, 5772.

3. Janiak, C. *Coord. Chem. Rev.* **2006**, *250*, 66.

4. (a) $Li[MeB(C_6F_5)_3]$ reacts with CO_2 to yield $Li[B(C_6F_5)_3(OAc)]$. (b) Simona, M.; Baird, M. C. *Can. J. Chem.* **2006**, *84*, 225.

5. Wu, F.; Dash, A. K.; Jordan, R. F. *J. Am. Chem. Soc.* **2004**, *126*, 15360.

6. Castro-Rodriguez, I.; Nakai, H.; Zakharov, L.; Rheingold, A.L.; Meyer, K. *Science* **2004**, *305*, 1757.

7. (a) Wailes, P. C.; Weigold, H.; Bell, A. P. *J. Organomet. Chem.* **1972**, *34*, 155. (b) Gambarotta, S.; Strologo, S.; Floriani, C.; Chiesa-Villa, A.; Guastini, C. *Inorg. Chem.* **1985**, *24*, 654.

8. Suzuki, H.; Takiguchi, T.; Kawasaki, Y. *Bull. Chem. Soc. Jpn.* **1978**, *51*, 1764.

9. Batsanov, S. S. *Inorg. Mater.* **2001**, *37*, 871.

10. (a) Nakamura, A.; Anselment, T.; Claverie, J.; Goodall, B.; Jordan, R. F.; Mecking, S.; Rieger, B.; Sen, A.; van Leeuwen, P.; Nozaki. K. *Acc. Chem. Res.* **2013**, *46*, 1438. (b) Nakamura, A.; Ito, S.; Nozaki, K. *Chem. Rev.* **2009**, 109, 5215. (c) Berkefeld, A.; Mecking, S. *Angew. Chem., Int. Ed.* **2008**, 47, 2538. (d) Jian, Z.; Mecking, S. *Angew. Chem.* **2015**, *127*, 16071. (e) Lanzinger, D.; Giuman, M. M.; Anselment, T. M. J.; Rieger, B. *ACS Macro Lett.* **2014**, *3*, 931. (f) Ito, S.; Wang, W.; Nishimura, K.; Nozaki, K. *Macromolecules* **2015**, *48*, 1959. (g) Zhou, X.; Lau, K.-C.; Petro, B. J.; Jordan, R. F. *Organometallics* **2014**, *33*, 7209. (h) Contrella, N. D.; Jordan, R. F. *Organometallics* **2014**, *33*, 7199. (i) Feng, G.; Conley, M. P.; Jordan, R. F. *Organometallics* **2014**, *33*, 4486. (j) Rezabal, E.; Asua, J. M.; Ugalde, J. M. *Organometallics* **2015**, *34*, 373. (k) Ota, Y.; Ito, S.; Kuroda, J.; Okumura, Y.; Nozaki, K. *J. Am. Chem. Soc.* **2014**, *136*, 11898. (l) Wucher, P.; Schwaderer, J. B.; Mecking, S. *ACS Catal.* **2014**, *4*, 2672. (m) Wucher, P.; Goldbach, V.; Mecking, S. *Organometallics* **2013**, *32*, 4516. (n) Chen, M.; Yang, B.; Chen, C. *Angew. Chem. Int. Ed.* **2015**, *54*, 15520. (o) Gaikwad, S. R.; Deshmukh, S. S.; Gonnade, R. G.; Rajamohanan, P. R.; Chikkali, S. H. *ACS Macro Lett.* **2015**, *4*, 933.

11. Cai, Z.; Shen, Z.; Zhou, X.; Jordan, R. F. *ACS Catal.* **2012**, *2*, 1187.

12. (a) Pushkar, J.; Wendt, O. F. *Inorg. Chim. Acta.* **2004**, *357*, 1295. (b) Ariyananda, P. W. G.; Yap, G. P. A.; Rosenthal, J. *Dalton Trans.* **2012**, *41*, 7977.

13. Anionic metal hydrides exhibit enhanced reactivity with CO_2. (a) Darensbourg, M. Y.; Ludwig, M.; Riordan, C. G. *Inorg. Chem.* **1989**, *28*, 1630. (b) Schmeier, T. J.; Dobereiner, G. E.; Crabtree, R. H.; Hazari, N. *J. Am. Chem. Soc.* **2011**, *133*, 9274. (c) Suh, H.-W.; Schmeier, T. J.; Hazari, N.; Kemp, R. A,; Takase, M. K. *Organometallics* **2012**, *31*, 8225.

14. Reich, H. J.; Borst, J. P.; Dykstra, R. R.; Green, D. P. *J. Am. Chem. Soc.* **1993**, *115*, 8728.

15. Deacon, G. B.; Phillips, R. J. *Coord. Chem. Rev.* **1980**, *33*, 227.

16. Li^+ does not promote carboxylation of (PO)PdMe(L) species.

17. (a) Ziegler, K.; Zeiser, H. *Ber. dtsch. Chem. Ges. A/B* **1930**, *63*, 1847. (b) Scriven, E. F. V. In *Comprehensive Heterocyclic Chemistry: the structure, reactions, synthesis and uses of heterocyclic compounds*; Katritzky, A. R.; Rees, W., Eds.; Pergamon Press: California, 1984; Vol. 2, Chapter 2.05.

18. Camara, J. M.; Petros, R. A.; Norton, J. R. *J. Am. Chem. Soc.* **2011**, *133*, 52631.

19. (a) Graaf, W. D.; Boersma, J.; Smeets, W. J. J.; Spek, A. L.; Koten, G. V. *Organometallics* **1989**, *8*, 2907. (b) Biscoe, M. R.; Fors, B. P.; Buchwald, S. L. *J. Am. Chem. Soc.* **2008**, *130*, 6686.

20. Ruelke, R. E.; Ernsting, J. M.; Spek, A. L.; Elsevier, C. J.; van Leeuwen, P. W. N. M.; Vrieze, K. *Inorg. Chem.* **1993**, *32*, 5769.

21. Cai, Z.; Shen, Z.; Zhou, X.; Jordan, R. F. *ACS Catal.* **2012**, *2*, 1187.

22. (a) Calvin, G.; Coates, G. E. *J. Chem. Soc.* **1960**, 2008. (b) Foley, S. R.; Stockland, R. A. Jr; Shen, H.; Jordan, R. F. *J. Am. Chem. Soc.* **2003**, *125*, 4350.

23. Data for unidentified products: ^{1}H NMR (THF-d_8): δ 8.08 (br s, H^3 of E), 8.01 (br d, J = 8, 1 H, H^3 of B), 7.79 (d, J = 8, 1 H, H^3 of A), 7.73 (d, J = 8, 1 H, H^3 of D), 7.66 (br s, 1 H, H^6 of D), 7.50 (br s, 1 H, H^3 of C), 7.42 (s, 1 H, H^6 of B), 7.24 (d, J = 8, 1 H, H^4 of B), 7.11 (br d, 2 H, H^6 of C & H^4 of D), 6.96 (s, 1 H, H^6 of A), 6.90 (d, J = 8, 1 H, H^4 of A), 6.73 (d, J = 7, H^4 of E), 6.55 (d, J = 6, 1 H, H^4 of C), 6.49 (br s, H^6 of E), 2.61 (s, 3 H, CH_3–ArSO$_3$ of A), 2.46 (m, 2 H, CHMe$_2$ of B), 2.38 (s, 3 H, CH_3–ArSO$_3$ of B), 2.34 (s, 3 H, CH_3–ArSO$_3$ of D), 2.32 (s), 2.26 (s), 2.24 (s), 1.20 (m, 12 H, CHMe_2 of all species), 0.74 (d, J = 7), 0.70 (d, J = 8), 0.65 (d, J = 7). ^{31}P{^{1}H} NMR (THF-d_8): δ 32.7, 24.9, 21.5, 21.1, 16.3, 15.0.

24. (a) Massey, A. G.; Park, A. J. *J. Organomet. Chem.* **1964**, *2*, 245. (b) Vela, J.; Lief, G. R.; Shen, Z.; Jordan, R. F. *Organometallics* **2007**, *26*, 6624.

25. Simona, M.; Baird, M. C. *Can. J. Chem.* **2006**, *84*, 225. ESI-MS (THF/MeOH, negative ion mode): *m*/*z* 570.8 $(B(C_6F_5)_3(OAc))^-$.

26. Data for unidentified compounds: ^{1}H NMR (THF-d_8): δ 8.03 (d, J = 8), 7.62 (d, J = 8), 6.97 (d, J = 8), 2.31 (s), 0.75 (dd, J = 16, 8), 0.40 (s), 0.28 (t, J = 5). ^{31}P{^{1}H} NMR (THF-d_8): δ 32.1.

27. Stejskal, E. O.; Tanner, J. E. *J. Chem. Phys.* **1965**, *42*, 288.

28. Gaussian 09, Revision A.02, Frisch, M. J.; Trucks, G. W.; Schlegel, H. B.; Scuseria, G. E.; Robb, M. A.; Cheeseman, J. R.; Scalmani, G.; Barone, V.; Mennucci, B.; Petersson, G. A.; Nakatsuji, H.; Caricato, M.; Li, X.; Hratchian, H. P.; Izmaylov, A. F.; Bloino, J.; Zheng, G.; Sonnenberg, J. L.; Hada, M.; Ehara, M.; Toyota, K.; Fukuda, R.; Hasegawa, J.; Ishida, M.; Nakajima, T.; Honda, Y.; Kitao, O.; Nakai, H.; Vreven, T.; Montgomery, Jr., J. A.; Peralta, J. E.; Ogliaro, F.; Bearpark, M.; Heyd, J. J.; Brothers, E.; Kudin, K. N.; Staroverov, V. N.; Kobayashi, R.; Normand, J.; Raghavachari, K.; Rendell, A.; Burant, J. C.; Iyengar, S. S.; Tomasi, J.; Cossi, M.; Rega, N.; Millam, J. M.; Klene, M.; Knox, J. E.; Cross, J. B.; Bakken, V.; Adamo, C.; Jaramillo, J.; Gomperts, R.; Stratmann, R. E.; Yazyev, O.; Austin, A. J.; Cammi, R.; Pomelli, C.; Ochterski, J. W.; Martin, R. L.; Morokuma, K.; Zakrzewski, V. G.; Voth, G. A.; Salvador, P.; Dannenberg, J. J.; Dapprich, S.; Daniels, A. D.; Farkas, Ö .; Foresman, J. B.; Ortiz, J. V.; Cioslowski, J.; Fox, D. J. Gaussian, Inc., Wallingford CT, 2009.

29. Zhao, Y.; Truhlar, D. G. *Theor. Chem. Acc.* **2008**, *120*, 215.

30. Varetto, U. MOLEKEL, 5.4; Swiss National Supercomputing Centre: Lugano, Switzerland, 2009.

31. Weigand, F.; Ahlrichs, R. *Phys. Chem. Chem. Phys.* **2005**, *7*, 3297.

32. Andrae, D. Haeussermann, U.; Dolg, M.; Stoll, H.; Preuss, H. *Theor. Chim. Acta* **1990**, *77*, 123.

33. (a) Weigand, F.; Ahlrichs, R. *J. Chem. Phys.* **1992**, *97*, 2571. (b) Weigand, F.; Ahlrichs, R. *J. Chem. Phys.*, **1994**, *100*, 5829.

34. Rappoport, D.; Furche, F. *J. Chem. Phys.* **2010**, *133*, 134105.

35. Hunter, W. E.; Hrncir, D. C.; Vann Bynum, R.; Penttila, R. A.; Atwood, J. L. *Organometallics* **1983**, *2*, 750.

36. Erker, G.; Rosenfeldt, F. *J. Organomet. Chem.* **1980**, *188*, C1.

37. (a) Erker, G.; Dorf, U.; Lecht, R.; Ashby, M. T.; Aulbach, M.; Schlund, R.; Kruger, C.; Mynott, R. *Organometallics* **1989**, *8*, 2037. (b) Amor, J. I.; Burton, N. C.; Cuenca, T.; Gomez-Sal, P.; Royo, P. *J. Organomet. Chem.* **1995**, *485*, 153. (c) Perrotin, P.; El-Zoghbi, I.; Oguadinma, P. O.; Schaper, F. *Organometallics* **2009**, *28*, 4912. (d) Meyer zu Berstenhorst, B.; Erker, G.; Kehr, G.; Fröhlich, R. *Dalton Trans.* **2006**, 3200.

Chapter Three

Reactivity of Fe–Alkyl Complexes with Carbon Dioxide

3.1. Introduction

The previous chapter describes studies of the reactions of CO_2 with the olefin polymerization catalysts $[Cp_2ZrMe(ClC_6D_5)][B(C_6F_5)_4]$ and (PO-R)Pd(Me)L ($[PO\text{-}R]^-$ = 2−PR_2−4−Me−$C_6H_3SO_3^-$; R = 3,5–$^tBu_2$–C_6H_3, ^{i}Pr; L = pyridine, THF), along with the analogous dialkyl species Cp_2ZrMe_2, $\{[Li(THF)_2][(PO\text{-}^iPr)PdMe_2]\}_2$ and $[Li(Crypt211)][(PO\text{-}^iPr)PdMe_2]$ (Crypt 211 = 4,7,13,18–tetraoxa–1,10–diazabicyclo[8.5.5]eicosane). The carboxylation reactions of cationic $[Cp_2ZrMe(ClC_6D_5)][B(C_6F_5)_4]$ and neutral Cp_2ZrMe_2 proceed through insertion mechanisms, with the cationic complex exhibiting higher reactivity owing to a stronger Zr- - -*O*CO interaction. In contrast, CO_2 does not react with neutral (PO)Pd(Me)L complexes but reacts readily with anionic $(PO)PdMe_2^-$. The carboxylation reaction of the anionic $(PO)PdMe_2^-$ species proceeds via direct S_E2 attack of CO_2 at the back side of the carbon of the methyl group that is *trans* to the phosphine. Li^+ (if present) accelerates the S_E2 attack via Li- - -OCO interactions. The observation that M- - -*O*CO interactions play a dominant role in carboxylation reactions of early-metal alkyl complexes (group 4) while the nucleophilicity of the M–*R* group is a critical factor in the carboxylation reactions of late-metal alkyl complexes (group 10) raises the question of how these and other electronic and structural factors influence the carboxylation of other olefin polymerization catalysts. To address this question, the carboxylation reactions of the mid-transition-metal (group 8) olefin polymerization catalyst $(PDI)FeMe^+$ (PDI = 2,6−(2,6−$^iPr_2$−C_6H_3−N=CMe)$_2$−C_5H_3N), and two analogous complexes (PDI)FeMe and

(PDI)Fe(Me)PMe_3, were investigated. These three compounds differ in charge and coordination number and thus can provide insight to how these parameters influence the carboxylation reactivity of (PDI)Fe complexes.

3.2. Results and Discussion

Synthesis of (PDI)Fe Methyl Complexes. (PDI)FeMe (**1**) is a precursor to the olefin polymerization catalyst [(PDI)FeMe][BPh_4] (**2**). Complexes **1** and **2** were synthesized by literature procedures (Scheme 3.1).[1,2]

Scheme 3.1

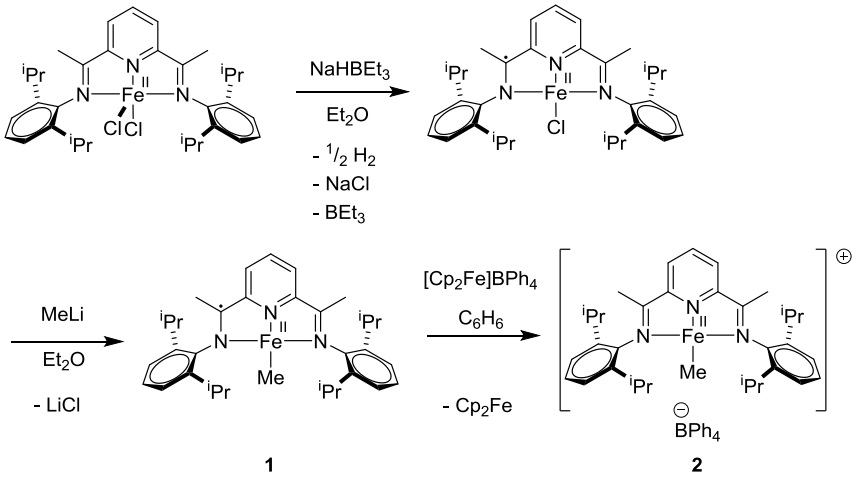

Previous studies by Chirik and co–workers have determined the electronic structure of complex **1** and **2**.[2] Mössbauer spectroscopy shows that the Fe atom in both **1** and **2** is high-spin Fe^{2+}. The PDI ligand is redox active and can be reduced by up to 2 electrons.[3a] Reduction causes

characteristic changes in bond lengths within the PDI ligand.[3b] The N_{imine}–C_{imine} (1.335(7) Å) and C_{imine}–C_{ipso} (1.437(8) Å) distances in **1** imply a $(PDI^{-})Fe^{II}$ electronic configuration in which the PDI ligand is reduced by one electron, while the corresponding bond distances in **2** (N_{imine}–C_{imine}: 1.290(4) Å; C_{imine}–C_{ipso}: 1.486(5) Å) imply a $(PDI^{0})Fe^{II}$ electronic configuration. These assignments are supported by magnetic measurements, which indicate that **1** has 3 unpaired electrons as a result of antiferromagnetic coupling between the PDI^{-} spin and the high-spin Fe^{2+} center, and **2** has 4 unpaired electrons consistent with a high-spin Fe^{2+} center. The molecular orbitals computed for the analogous complexes (PDI)Fe(CH_2CMe_3) and [(PDI)Fe(CH_2CMe_3)][BPh_4] are consistent with these experimentally determined electronic configurations, and indicate that there is significant spin density on the PDI ligand of (PDI)Fe(CH_2CMe_3) but not [(PDI)Fe(CH_2CMe_3)][BPh_4] (Figure 3.1).

Synthesis of (PDI)Fe(Me)PMe_3. The reaction of **1** with PMe_3 yields the corresponding PMe_3 adduct **1-PMe_3** (Scheme 3.2). **1-PMe_3** represents an unusual example of (PDI)FeXL species with anionic X (Me) and neutral L (PMe_3) ligands, the only other example being (PDI)Fe(Br)THF, and was therefore characterized by X-ray diffraction (Figure 3.2).[4] **1-PMe_3** has a square pyramidal geometry, with the PMe_3 ligand bound in the axial position. The Fe atom is displaced by 0.05(1) Å out of the plane formed by PDI ligand and the Fe–*Me* group toward the PMe_3 ligand (Fe1–N2–C1 angle = 3.1(6) º). The N_{imine}–C_{imine} (1.36(1) Å) and C_{imine}–C_{ipso} (1.42(1) Å) distances in **1-PMe_3** imply a $(PDI^{-})Fe^{II}$ electronic configuration in which the PDI ligand is reduced by one electron.

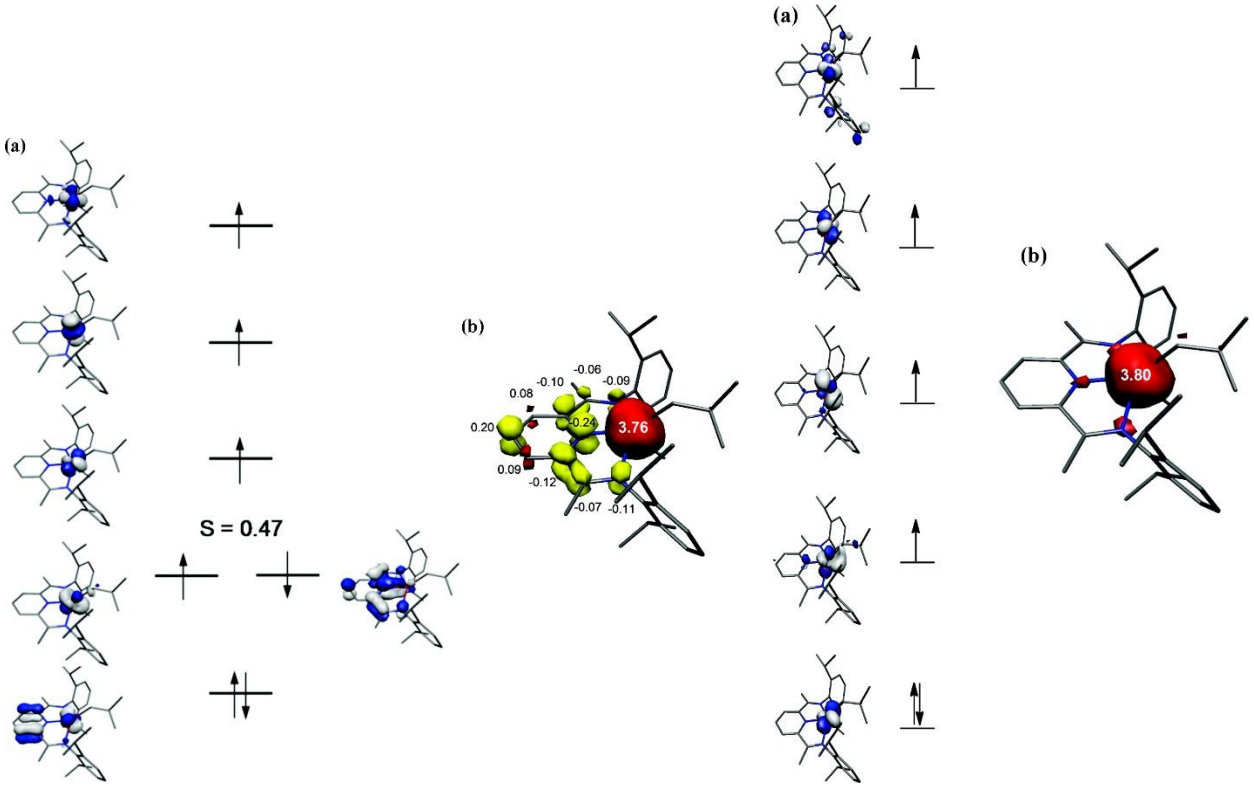

Figure 3.1. (a) Molecular orbital diagram, and (b) spin density plot for (PDI)Fe(CH_2CMe_3) (left) and [(PDI)Fe(CH_2CMe_3)][BPh_4] (right). S represents the spatial overlap of antiferromagnetically coupled magnetic orbitals. Reprinted with permission from Tondreau, A. M.; Milsmann, C.; Patrick, A. D.; Hoyt, H. M.; Lobkovsky, E.; Wieghardt, K.; Chirik, P. J. *J. Am. Chem. Soc.* **2010**, *132*, 15046. Copyright 2010 American Chemical Society.

Scheme 3.2

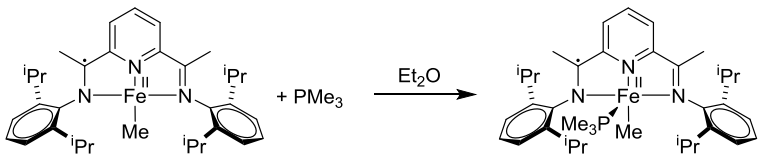

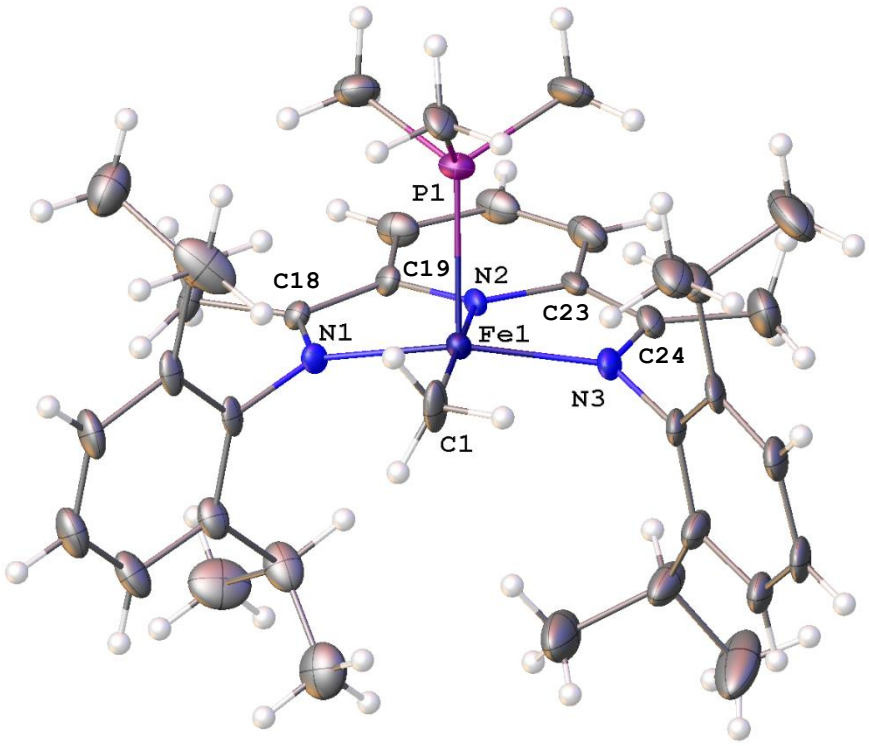

Figure 3.2. Molecular structure of (PDI)Fe(Me)PMe_3 (**1-PMe_3**). Selected bond lengths (Å) and angles (deg): Fe1–C1 2.00(4), Fe1–P1 2.359(8), Fe1–N1 1.962(9), Fe1–N2 1.874(10), Fe1–N3 1.955(10), N1–C18 1.356(11), C18–C19 1.414(11), N3–C24 1.354(13), C24–C23 1.423(11), C1–Fe1–P1 101.1(14), N2–Fe1–C1 174.2(15), N2–Fe1–P1 84.3(4), N2–Fe1–N1 80.1(4), N3–Fe1–C1 101.7(12).

SQUID measurements establish that **1-PMe_3** has an effective magnetic moment of μ_{eff} = 1.8 μ_B, consistent with the presence of one unpaired electron. The bond lengths determined from X-ray diffraction and the SQUID results together imply that the electronic configuration of **1-PMe_3** comprises a PDI^- radical anion that is antiferromagnetically coupled with an intermediate spin state (S = 1) Fe^{2+} center, or a PDI^- radical anion coordinating to a low-spin Fe^{2+} center.

The ^{1}H NMR spectrum of **1-PMe$_3$** in C_6D_6 exhibits concentration-dependent behavior. Upon dilution of the solution, the ^{1}H resonances for **1-PMe$_3$** shift towards resonances for base-free **1** and free PMe_3 (Figure 3.3). In addition, the ^{1}H NMR spectra of mixtures of **1** and **1-PMe$_3$** contain a single set of resonances at the mole-fraction-weighted average of the chemical shifts of **1** and **1-PMe$_3$** (Figure 3.4). Addition of excess PMe_3 to **1-PMe$_3$** shifts the ^{1}H resonances for **1-PMe$_3$** away from resonances for **1** but also broadens the resonances significantly. Collectively, these results show that **1-PMe$_3$** undergoes partial dissociation of PMe_3 to form **1**, and that **1** and **1-PMe$_3$** undergo rapid exchange relative to the NMR timescale (Scheme 3.3). The equilibrium constant for PMe_3 dissociation of **1-PMe$_3$** was determined to be K_{eq} = 1.8(9) × 10^{-3} M at 23 ºC by analysis of these data using the method of Rose and Drago.[5]

The ^{1}H NMR spectrum of the paramagnetic complex **1** has been assigned by Chirik by analysis of peak intensities and the ^{1}H and ^{2}H NMR spectra of ^{2}H-labelled samples.[1] The ^{1}H resonances for **1-PMe$_3$** were assigned by analysis of the ^{1}H NMR spectra in Figure 3.4, which show fast exchange between **1** and **1-PMe$_3$**. For example, the two CH*Me*$_2$ resonance of **1** at δ -21 and -11 (Figure 3.4a) move steadily to δ -5 and -3 as the **1-PMe$_3$**/**1** ratio increases, implying that the resonance at δ -5 and -3 can be assigned to the CH*Me*$_2$ groups of **1-PMe$_3$**. The resonance at δ 17 for **1-PMe$_3$** was assigned to the Fe–P*Me*$_3$ unit because this resonance is not correlated with any resonance for **1** and moves towards that for free PMe_3 (δ 0.8) as the solution of **1-PMe$_3$** is diluted (Figure 3.3a). The resonance at δ -198 for **1-PMe$_3$** was assigned to the Fe–*Me* unit based on the observation that this resonance disappears upon mixing **1-PMe$_3$** with **1** and the fact that the resonance of Fe–*Me* for **1** is not observable.

Scheme 3.3

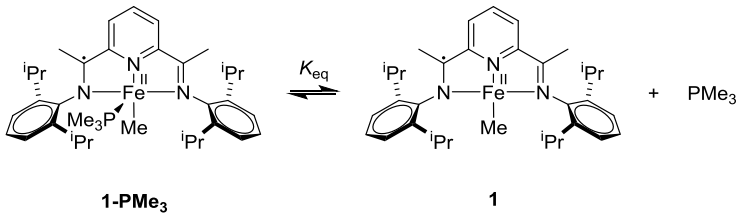

1-PMe$_3$ **1**

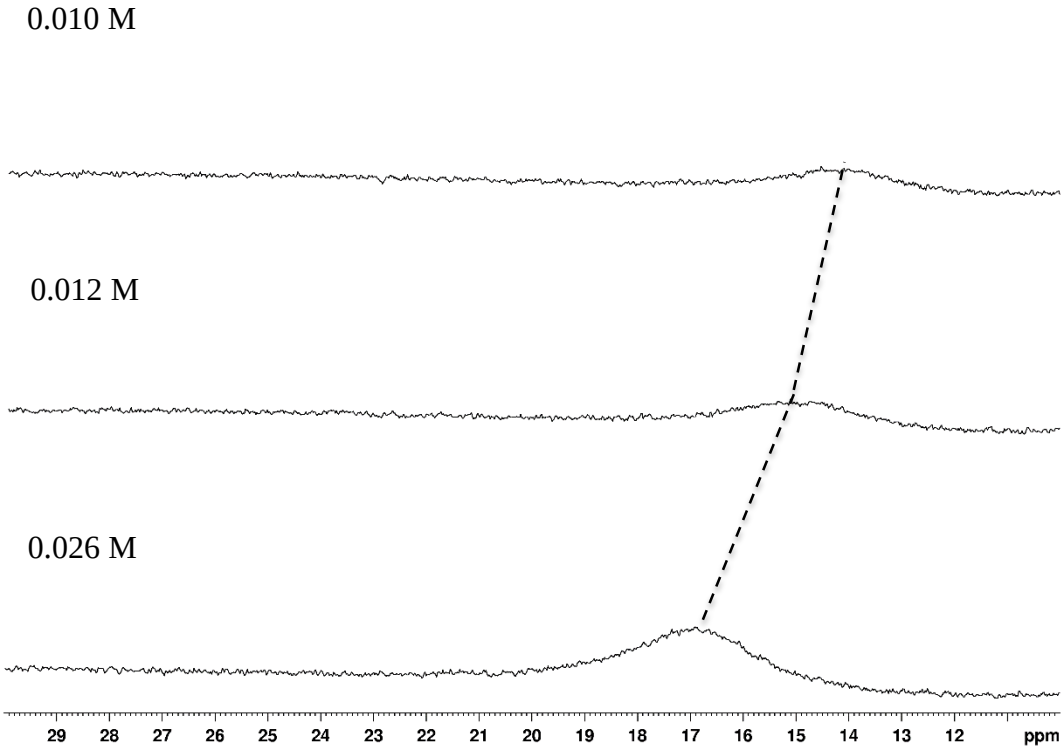

Figure 3.3a. ^{1}H NMR spectra of **1-PMe$_3$** in C_6D_6 at 23 ºC (δ 30 – 10). The shift and correlation of the ^{1}H resonances of **1-PMe$_3$** are indicated by dashed lines.

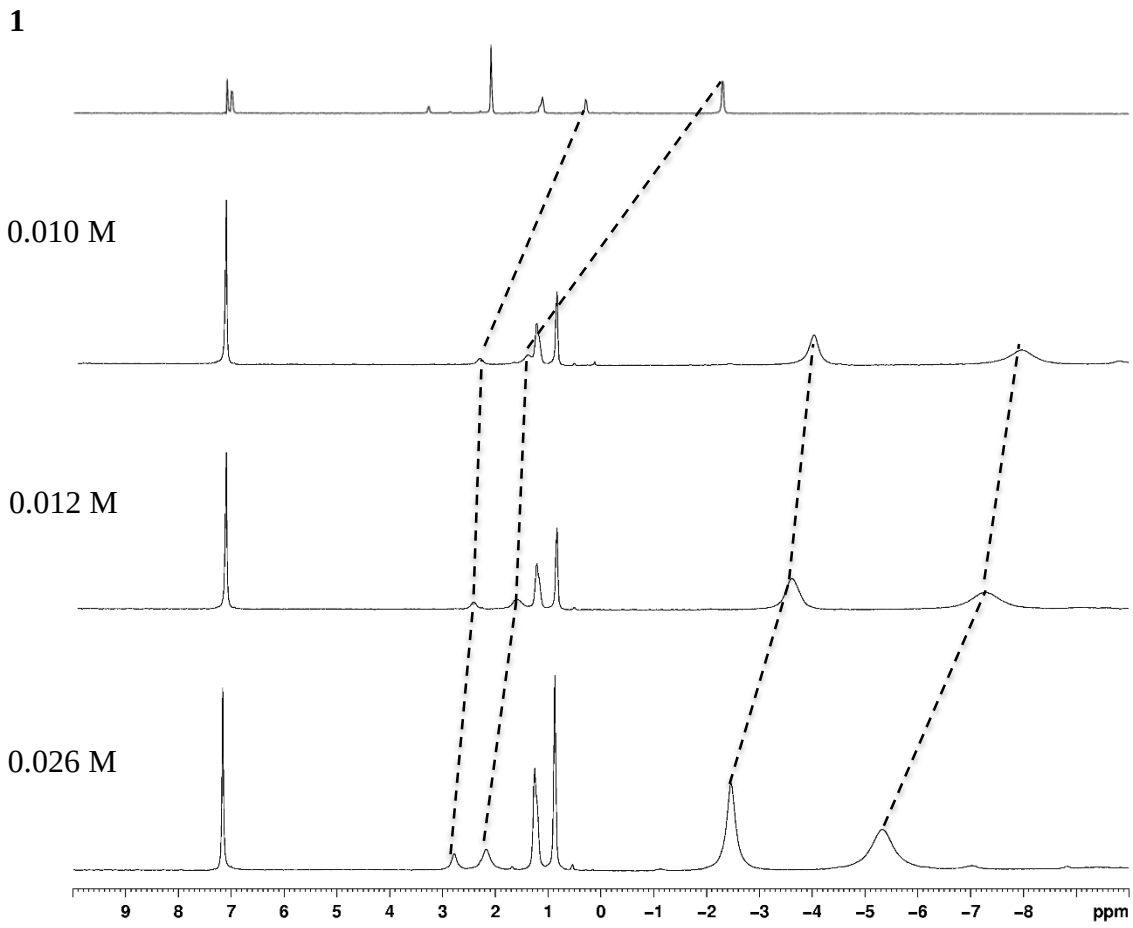

Figure 3.3b. ^{1}H NMR spectra of **1-PMe$_3$** in C_6D_6 (bottom three spectra) and **1** in toluene-d_8 (top) at 23 ºC (δ 10 – -10). The shift and correlation of the ^{1}H resonances of **1-PMe$_3$** and **1** are indicated by dashed lines. Other resonances: δ 1.3 (pentane), 0.9 (pentane).

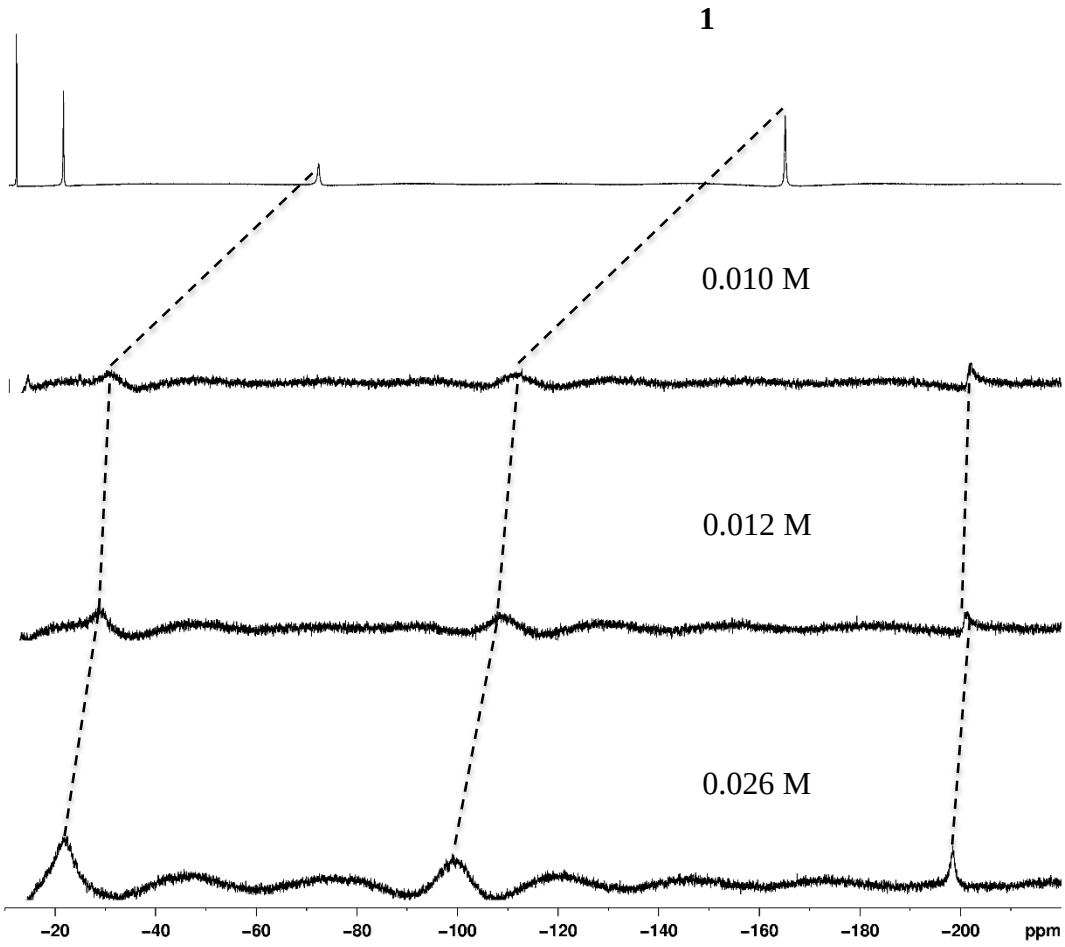

Figure 3.3c. ^{1}H NMR spectra of **1-PMe$_3$** in C_6D_6 (bottom three spectra) and **1** in toluene-d_8 (top) at 23 ºC (δ -10 – -220). The shift and correlation of the ^{1}H resonances of **1-PMe$_3$** and **1** are indicated by dashed lines. The resonances were identified from the baseline by comparison with the spectrum of blank C_6D_6 using the same spectral parameters.

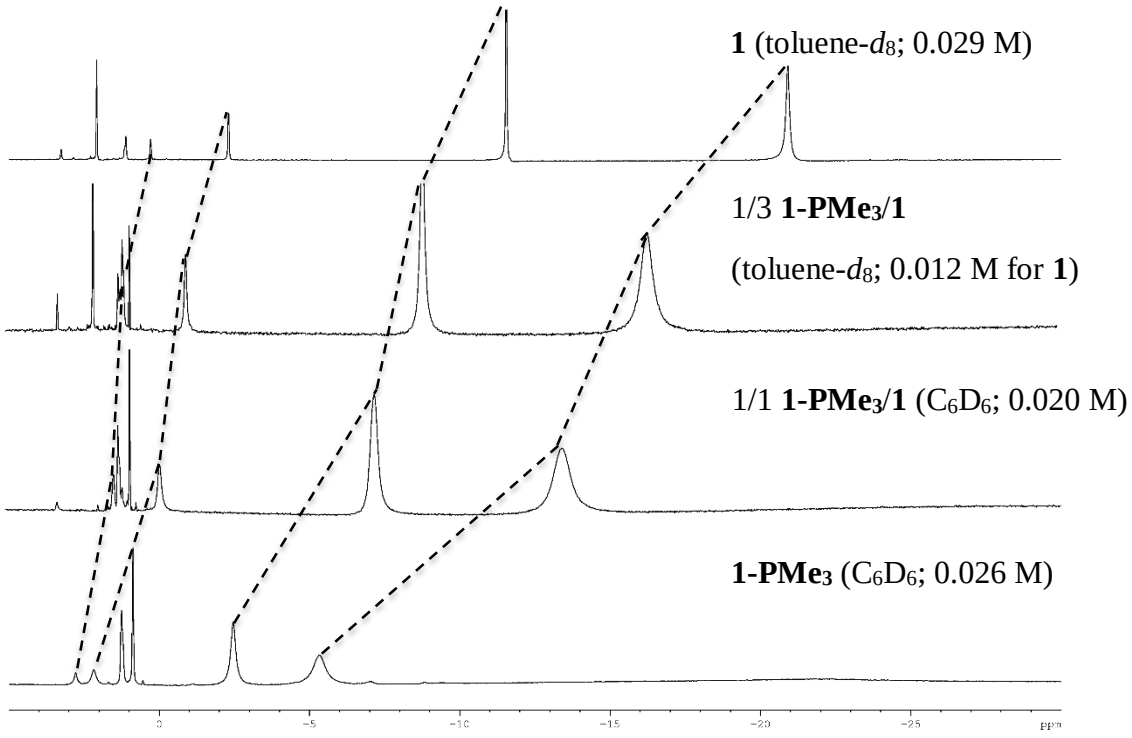

Figure 3.4a. ^{1}H NMR spectra of mixtures of **1-PMe$_3$** and **1** in toluene-d_8 C_6D_6 (top) and (bottom three spectra) at 23 ºC (δ 10 – -30). The shift and correlation of the ^{1}H resonances are indicated by dashed lines. Other resonances: δ 3.3 (Et_2O), 2.1 (toluene-d_7), 1.3 (pentane), 1.2 (Et_2O), 0.9 (pentane).

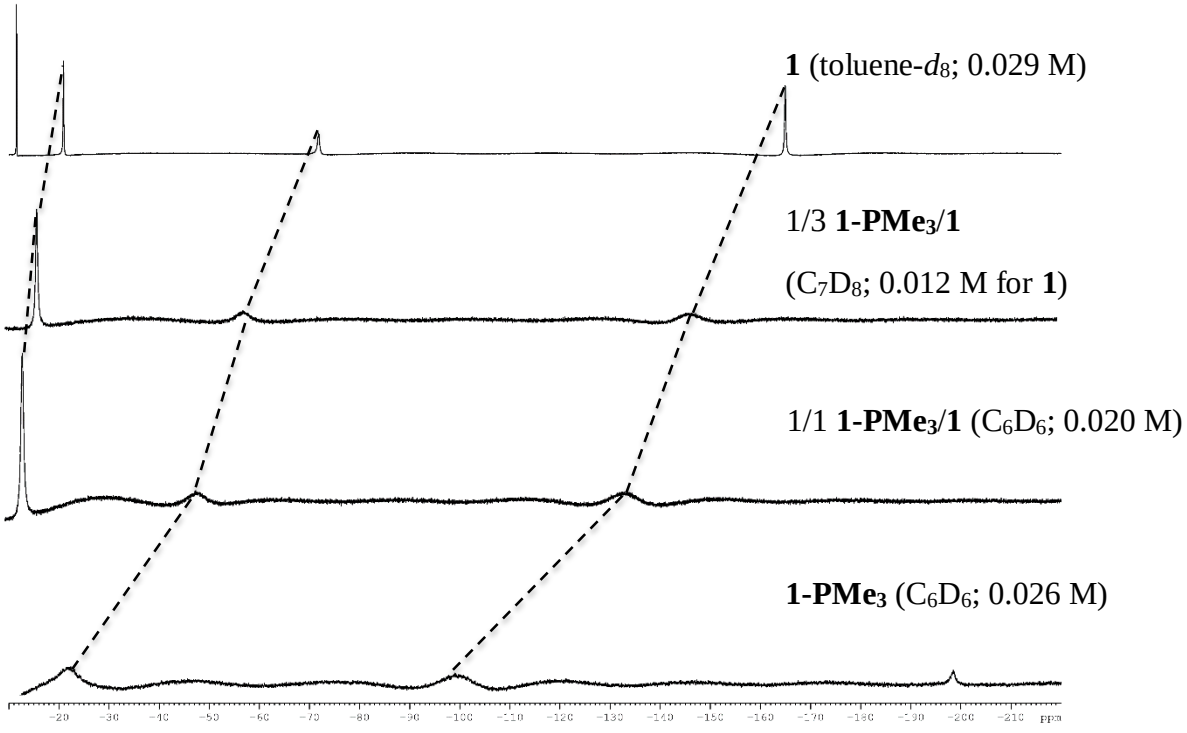

Figure 3.4b. ^{1}H NMR spectra of mixtures of **1-PMe$_3$** and **1** in toluene-d_8 C_6D_6 (top) and (bottom three spectra) at 23 ºC (δ -10 – -220). The shift and correlation of the ^{1}H resonances are indicated by dashed lines. Other resonances: δ -20.8 (CH*Me*$_2$, **1**), -198.4 (Fe–P*Me*$_3$, **1-PMe$_3$**).

Carboxylation of 1. Complex **1** reacts with CO_2 in C_6D_6 at room temperature to afford the known acetate complex (PDI)FeOAc (**3**; Scheme 3.4), which has been independently synthesized and characterized by Chirik and co–workers.[6] The kinetics of the reaction of **1** with CO_2 in toluene-d_8 were measured by ^{1}H NMR spectroscopy by monitoring the disappearance of the CH*Me*$_2$ resonance of **1** (Figure 3.5). The reaction is first order in **1** (Figure 3.6):

$$\text{rate} = k_{\mathbf{1},CO2}[\mathbf{1}],$$

where $k_{\mathbf{1},CO2}$ is the observed first-order rate constant.

Scheme 3.4

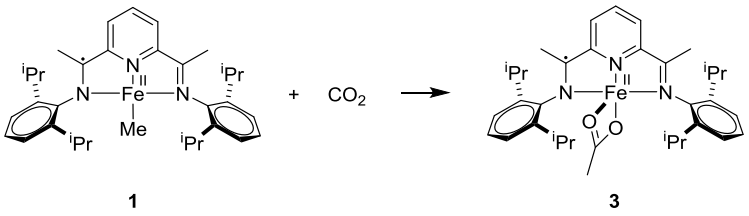

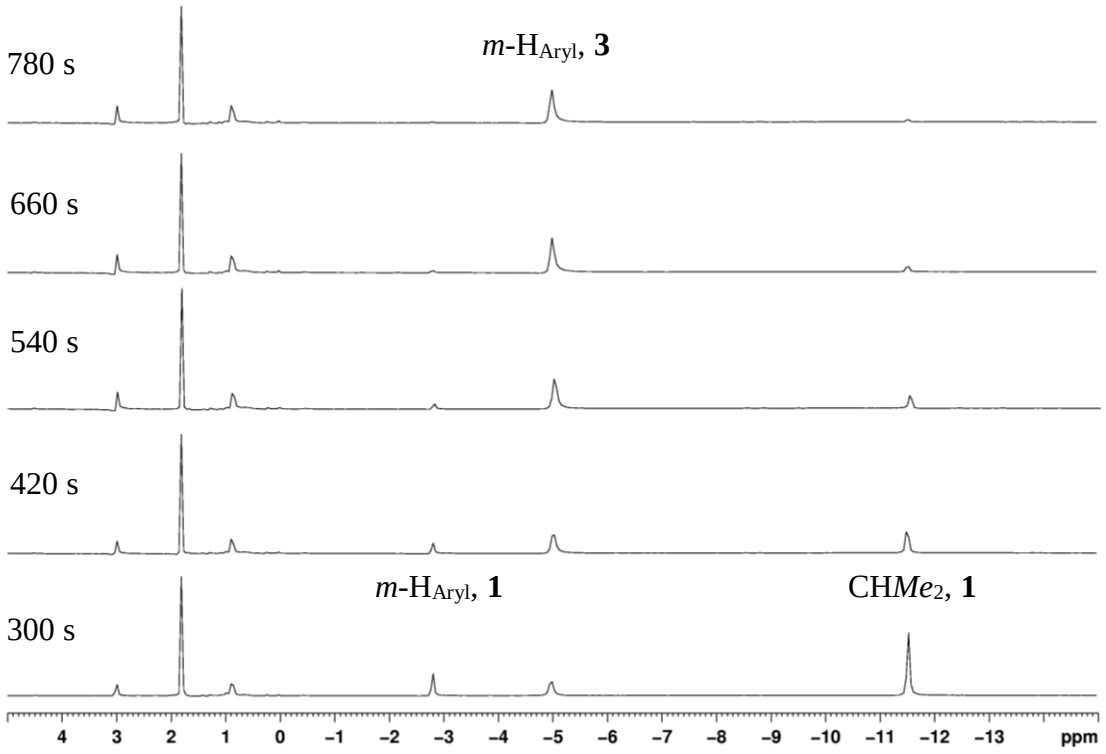

Figure 3.5. ^{1}H NMR monitoring of the reaction of CO_2 (1 atm) with **1** in toluene-d_8 at 0 ℃. Selected spectra are shown. These spectra show the disappearance of **1** and concomitant formation of **3**. Unlabeled resonances: δ 3.3 (Et_2O), 2.1 (toluene-d_7), 1.2 (Et_2O).

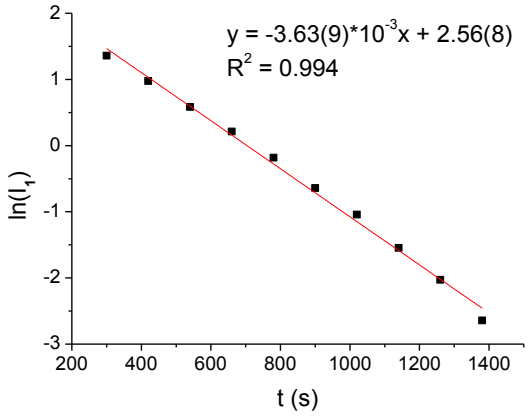

Figure 3.6. Representative first-order kinetic plot for the reaction of **1** with CO_2 (1 atm) in toluene-d_8 (0 ℃) shown in Figure 3.5. A plot for the disappearance of **1** is shown ($k_{\mathbf{1},CO2}$ = 3.63(9) × 10^{-3} s^{-1}). $I_{\mathbf{1}}$ = integral value for the CHMe_2 resonance of **1** at δ -11 relative to the integral value of the Et_2O resonance.

The observed first-order rate constant $k_{\mathbf{1},CO2}$ at 0 ℃ was determined to be 3.63(9) × 10^{-3} s^{-1}. $k_{\mathbf{1},CO2}$ values for the conversion of **1** to **3** were determined over the temperature range of 0 ℃ to -35 ℃ and an Eyring analysis provided the following activation parameters: $\Delta H^{‡}$ = +10.9(6) kcal/mol; $\Delta S^{‡}$ = -29(2) e.u.; $\Delta G^{‡}$ (23 ℃) = +20(1) kcal/mol (Figure 3.7). Extrapolation from the Eyring plot gave $k_{\mathbf{1},CO2}$ (23 ℃) = 2(4) × 10^{-2} s^{-1}.

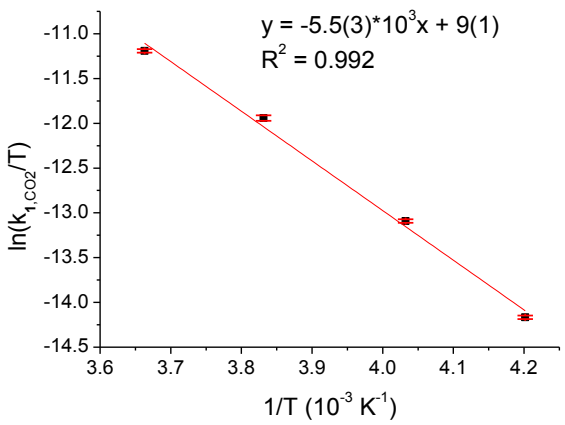

Figure 3.7. Eyring plot for the reaction of CO_2 (1 atm) with **1** in toluene-d_8. $\Delta H^{\ddagger}$ = +10.9(6) kcal/mol; $\Delta S^{\ddagger}$ = -29(2) e.u.; $\Delta G^{\ddagger}$ (23 ºC) = +20(1) kcal/mol.

Carboxylation of 1-PMe$_3$. As noted earlier in this thesis, carboxylation reactions of metal alkyl complexes that proceed by insertion mechanisms require a vacant site for CO_2 binding and therefore are expected to be inhibited or quenched by addition of competing ligands. In contrast, carboxylation reactions that proceed by S_E2 (or S_Ei or S_E2 (front)) mechanisms do not require a vacant site but do require a nucleophilic alkyl ligand, and these are expected to be unaffected or possibly accelerated by electron-donating ligands. Therefore, comparison of the carboxylation reactions of **1** and **1-PMe$_3$**, the PMe_3 adduct of **1**, may provide insights into the mechanism of the carboxylation of the former complex.

The reaction of **1-PMe$_3$** with CO_2 in C_6D_6 proceeds at room temperature to form an equilibrium mixture of the corresponding acetate complex (PDI)Fe(OAc)PMe_3 (**3-PMe$_3$**; Scheme 3.5) and its PMe_3-dissociated form **3**. **3-PMe$_3$** was independently synthesized by the reaction of **3** with PMe_3.

Scheme 3.5

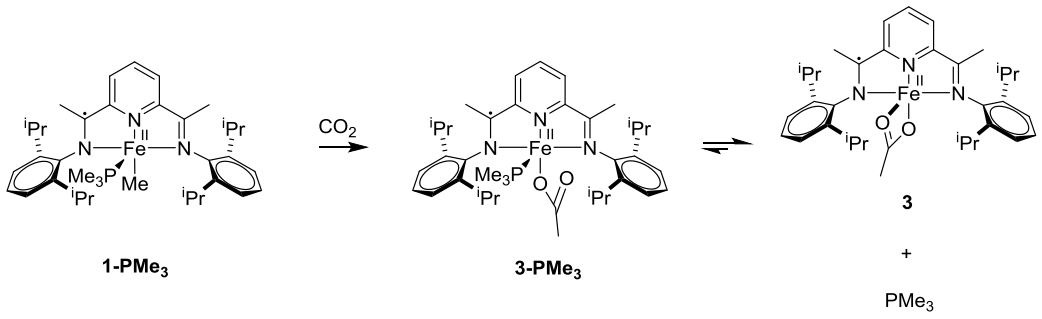

Vacuum transfer of the volatiles from a solution of **3-PMe$_3$** in C_6D_6 afforded 0.9 equivalent of PMe_3 in the volatile fraction and essentially pure **3** in the non-volatile fraction, as determined by ^{1}H NMR and ^{31}P NMR, indicating that the PMe_3 of **3-PMe$_3$** is quite labile. The ^{1}H NMR spectrum of **3-PMe$_3$** in C_6D_6 at room temperature is only slightly shifted from that of base-free **3** ($\Delta\delta$ < 1 – 2 ppm; Figure 3.8). No PMe_3 resonance is observed for **3-PMe$_3$** by ^{1}H and ^{31}P NMR. Collectively, these observations indicate that PMe_3 of **3-PMe$_3$** is very weakly coordinated and undergoes extensive dissociation and fast exchange. The differences in the observed ^{1}H NMR chemical shifts of **3** and **3-PMe$_3$** are too small to allow determination of K_{eq}. Attempts to shift the equilibrium to **3-PMe$_3$** by addition of excess PMe_3 to **3-PMe$_3$** shift the ^{1}H resonances for **3-PMe$_3$** away from resonances for **3** but also broaden the resonances significantly. **3-PMe$_3$** could not be isolated.

The ^{1}H NMR spectrum of the paramagnetic complex **3** has been assigned by Chirik by analysis of peak intensities and comparison of the ^{1}H and ^{2}H NMR spectra of the ^{2}H-labelled samples.[6] The ^{1}H resonances for **3-PMe**$_3$ were assigned by analysis of ^{1}H NMR spectra in Figure 3.8, following the same analysis for **1-PMe$_3$** (see above). As noted above, the Fe–P*Me*$_3$ resonance for **3-PMe$_3$** is not observable.

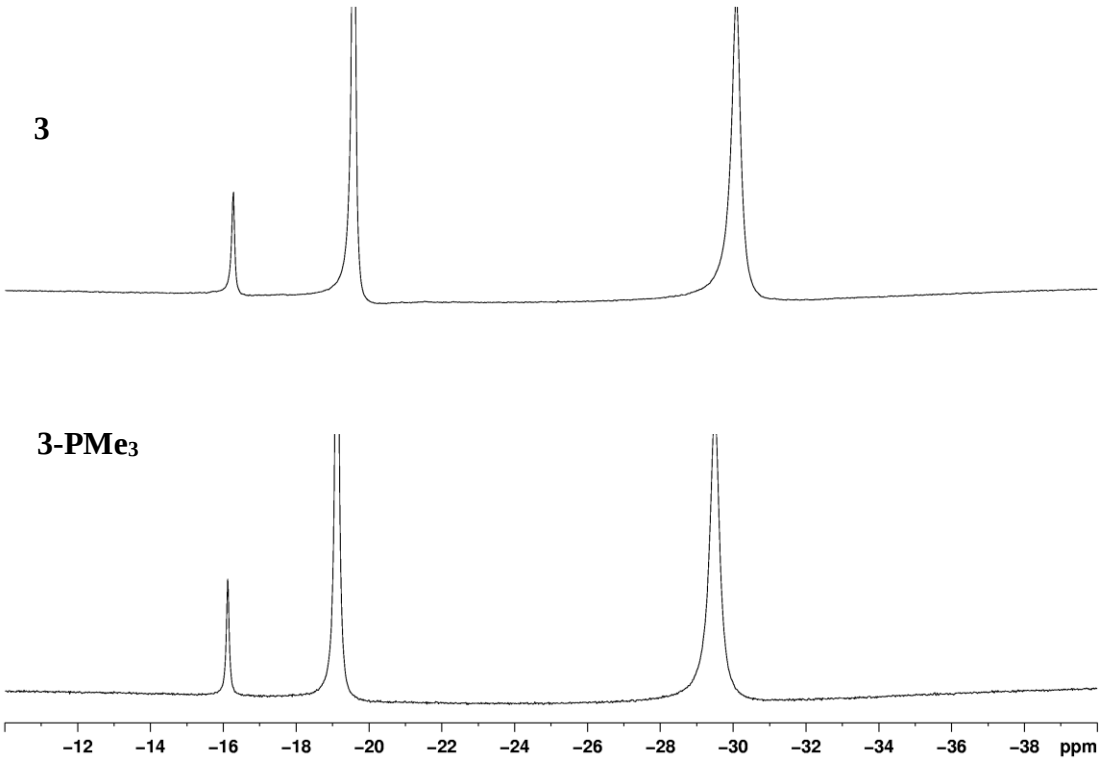

Figure 3.8a. ^{1}H NMR spectra of **3-PMe$_3$** and **3** in C_6D_6 at 23 ºC (δ -10 – -40).

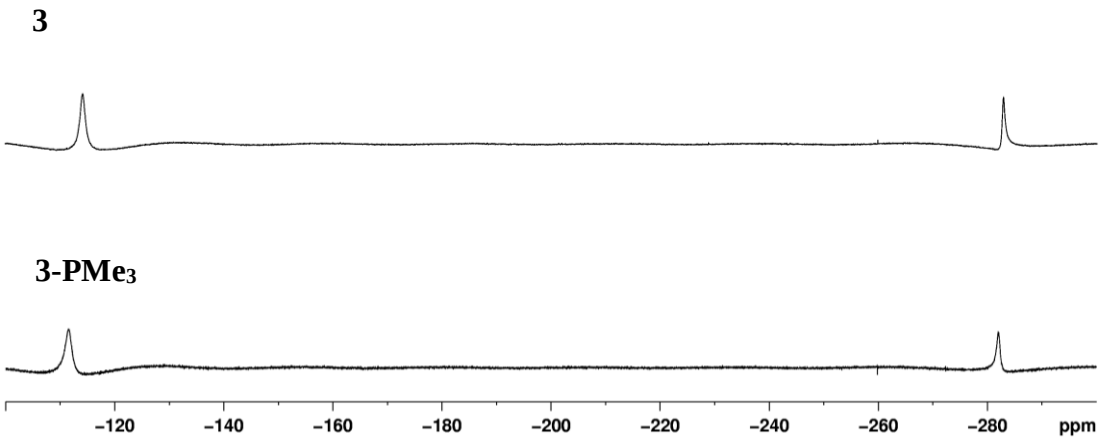

Figure 3.8b. ^{1}H NMR spectra of **3-PMe$_3$** and **3** in C_6D_6 at 23 ºC (δ -100 – -300).

Kinetics of Carboxylation of 1-PMe$_3$. The observation that **1-PMe$_3$** undergoes partial dissociation of PMe_3 to form base-free **1** and free PMe_3 raises the question of whether the observed reaction of **1-PMe$_3$** and CO_2 to form **3-PMe$_3$** proceeds by direct carboxylation of **1-PMe$_3$** or requires prior PMe_3 dissociation. Therefore, the kinetics of the reaction of **1-PMe$_3$** with CO_2 in the presence of excess PMe_3 were studied. Due to overlapping of resonances for the **1-PMe$_3$** and PMe_3, the kinetics were evaluated by analyzing the appearance of equilibrium mixture of **3-PMe$_3$** and **3** (Figure 3.9). The reaction is first order in $[Fe]_{total}$ = [**1-PMe$_3$**] + [**1**]:

$$\text{Rate} = k_{obs}([\textbf{1-PMe}_3] + [\textbf{1}]) = k_{obs}[Fe]_{total}$$

where k_{obs} = observed first-order rate constant; $[Fe]_{total}$ = [**1-PMe$_3$**] + [**1**]

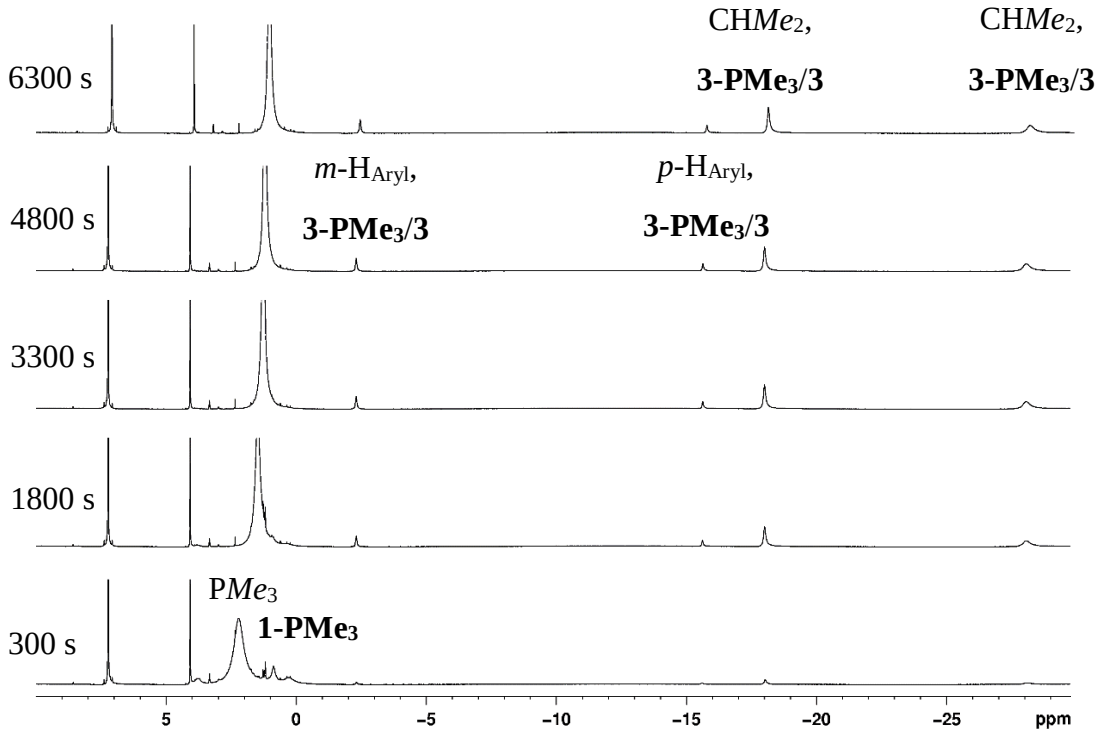

Figure 3.9a. ^{1}H NMR monitoring of the reaction of **1-PMe$_3$** and PMe_3 (total: 0.047 M) with CO_2 (1 atm) in C_6D_6 at 23 ℃. Other resonances: δ 7.2 (C_6D_5H), 4.0 (Cp_2Fe), 3.3 (q, Et_2O), 1.1 (q, Et_2O).

The first-order rate equation for the appearance of mixture of **3-PMe$_3$** and **3** (exponential form) is given by:

$$I_{Fe} = -I_{Fe,\infty} \exp(-k_{obs}t) + I_{Fe,\infty}$$

where I_{Fe} = integral value of the CH*Me*$_2$ resonance at δ -18 of mixture of **3-PMe$_3$** and **3** relative to the integral value of Cp_2Fe resonance at time = t; $I_{Fe,\infty}$ = integral value of the CH*Me*$_2$ resonance at δ -18 of mixture of **3-PMe$_3$** and **3** relative to the integral value of Cp_2Fe resonance at the end of the reaction

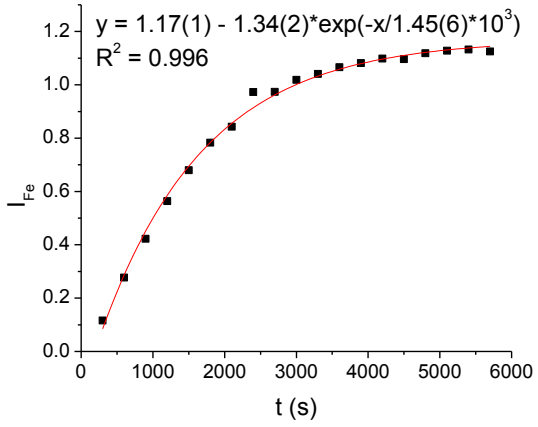

Figure 3.9b. Representative first-order kinetic plot for the formation of an equilibrium mixture of **3-PMe$_3$** and **3** from the reaction of **1-PMe$_3$** with CO_2 (1 atm) in C_6D_6 at 23 ℃ (total [PMe_3] = 0.047 M). k_{obs} = 6.9(3) × 10^{-4} s^{-1}.

The kinetic results show that the conversion of **1-PMe$_3$** to **3-PMe$_3$** is inhibited by increasing the concentration of PMe_3 (Figure 3.10).

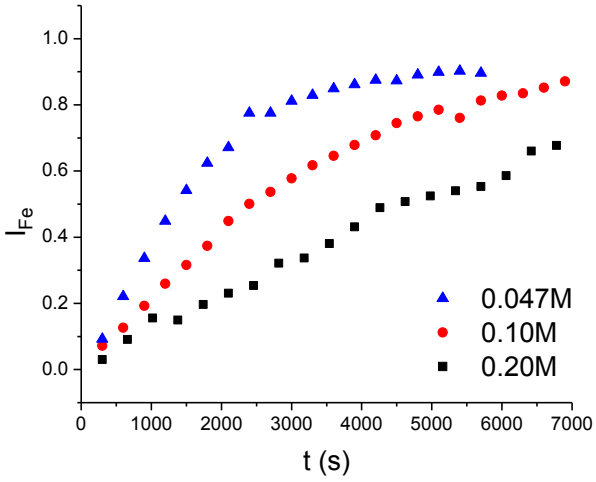

Figure 3.10. Representative plots for the formation of mixture of **3-PMe$_3$** and **3** from the reaction of **1-PMe$_3$** and excess PMe_3 (concentration range: 0.047 M – 0.20 M) and CO_2 (1 atm) in C_6D_6 at 23 ℃.

A fast pre-equilibrium reaction scheme consistent with these kinetic results and the known dissociation of PMe_3 from **1-PMe$_3$** is shown in Scheme 3.6. In Scheme 3.6, reversible dissociation of PMe_3 from **1-PMe$_3$** generates an equilibrium mixture of **1**, **1-PMe$_3$** and PMe_3. The base-free complex **1** reacts with CO_2 to form **3**, which, in the presence of PMe_3, gives an equilibrium mixture of **3**/**3-PMe$_3$**. **1-PMe$_3$** does not react directly with CO_2. The rate equation for this mechanism is:

$$\text{rate} = k_{obs}[\text{Fe}]_{total},$$

where $k_{obs} = \frac{k_{\mathbf{1},CO2}K_{eq}}{K_{eq}+[PMe_3]}$ and $[\text{Fe}]_{total}$ = [**1**+**PMe$_3$**] + [**1**]

Rearranging,

$$\frac{1}{k_{obs}} = \frac{1}{k_{\mathbf{1},CO2}K_{eq}}[PMe_3] + \frac{1}{k_{\mathbf{1},CO2}}$$

From this rate equation, a plot of $1/k_{obs}$ versus $[PMe_3]$ should be linear and gives $1/k_{\mathbf{1},CO2}$ and $1/(k_{\mathbf{1},CO2}K_{eq})$ as the y-intercept and slope, respectively.

Scheme 3.6

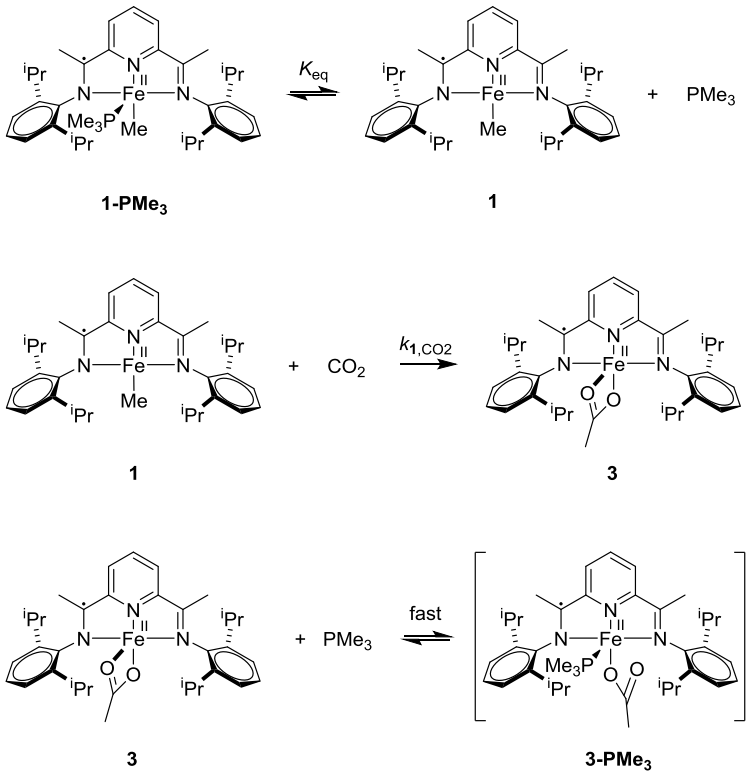

A plot of $1/k_{obs}$ versus $[PMe_3]$ over the range of $[PMe_3]$ = 0.05 to 0.20 M is shown in Figure 3.11. Consistent with Scheme 3.6, the plot is linear and gives $k_{\mathbf{1},CO2}$ (23 °C) = 2(4) × 10^{-2} s^{-1} and K_{eq} (23 °C) = 1(6) × 10^{-3} M. Importantly, these results are in excellent agreement with the values determined independently by the kinetic studies of **1** and ^{1}H NMR analysis of **1-PMe$_3$**

($k_{\mathbf{1},CO2}$ = 2(4) × 10^{-2} s^{-1} and K_{eq} = 1.8(9) × 10^{-3} M), which confirms the proposed mechanism in Scheme 3.6, and, in particular, that **1-PMe$_3$** does not react directly with CO_2 under those conditions.

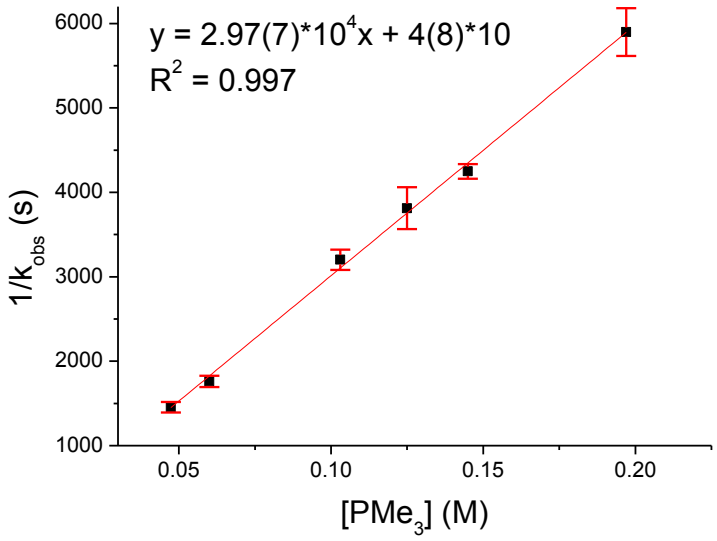

Figure 3.11. Plot of $1/k_{obs}$ versus the concentration of PMe_3 for the reaction of **1-PMe$_3$** with CO_2 (1 atm) to produce an equilibrium mixture of **3-PMe$_3$** and **3** in C_6D_6 at 23 ℃.

Mechanism of the reaction of 1 with CO_2. The kinetic analysis for the reaction of **1-PMe$_3$** with CO_2 to produce **3** shows that the addition of the donor ligand PMe_3 to **1** strongly inhibits, rather than accelerates the carboxylation reaction. In fact, **1-PMe$_3$** itself is unreactive with CO_2. This result strongly suggests that the carboxylation of **1** proceeds by initial coordination of CO_2 to the Fe center and subsequent insertion, a process which is blocked by the PMe_3 coordination. This proposal is supported by the large and negative $\Delta S^{\ddagger}$ value for the carboxylation of **1** which is consistent with a bimolecular transition state.

Carboxylation of 2 in a Non-Coordinating Solvent. With an understanding of the carboxylation reaction of **1** in hand, studies of the cationic analogue **2**, which is the form that is active in olefin polymerization, were initiated. The reaction of **2** with CO_2 in C_6D_5F at room temperature affords the monoacetate product [(PDI)FeOAc][BPh_4] (**4**; Scheme 3.7). Complex **4** was independently synthesized by the oxidation of **3** with [Cp_2Fe][BPh_4] and characterized by X-ray diffraction (Figure 3.12). The (PDI)Fe(OAc)$^+$ cation of **4** is structurally similar to the neutral analogue **3**.[3] The coordination geometry at Fe is trigonal bipyramidal. The acetate unit is bound to Fe in a κ^2- fashion and the plane of acetate unit is orthogonal to the (PDI)Fe chelate plane. The O atoms are nearly symmetrical about the plane formed by the (PDI)Fe chelate and the central C atom of the acetate unit (N2–Fe1–O1 angle = 143.44(9) º; N2–Fe1–O2 angle = 151.91(8) º). The C–O bond distances in the OAc unit of **4** are very similar (C–O2: 1.282(4) Å; C–O1: 1.258(4) Å) as are the Fe–O distances (Fe–O1: 2.087(2) Å; Fe–O2: 2.046(2) Å). The Fe–O bond distances in **4** are ca. 0.04 Å shorter than those in **3** (Fe–O1: 2.127(1) Å; Fe–O2: 2.084(2) Å), which is expected for stronger Fe–O bonding in cationic **4** versus neutral **3**.[6] The bond lengths within the PDI ligand of **4** are consistent with a neutral (non-reduced) PDI ligand (N_{imine}–C_{imine}: 1.279(3) Å; C_{imine}–C_{ipso}: 1.493(4) Å). A SQUID analysis gave μ_{eff} = 5.3 μ_B, consistent with 4 unpaired electrons for the compound. These results are consistent with an electronic configuration of a high-spin Fe^{2+} with neutral PDI ligand for **4**, (PDI^0)Fe^{II}.

Scheme 3.7

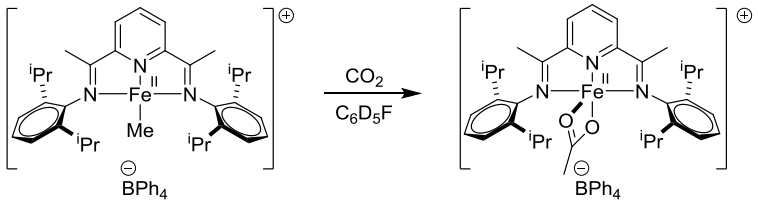

2 4

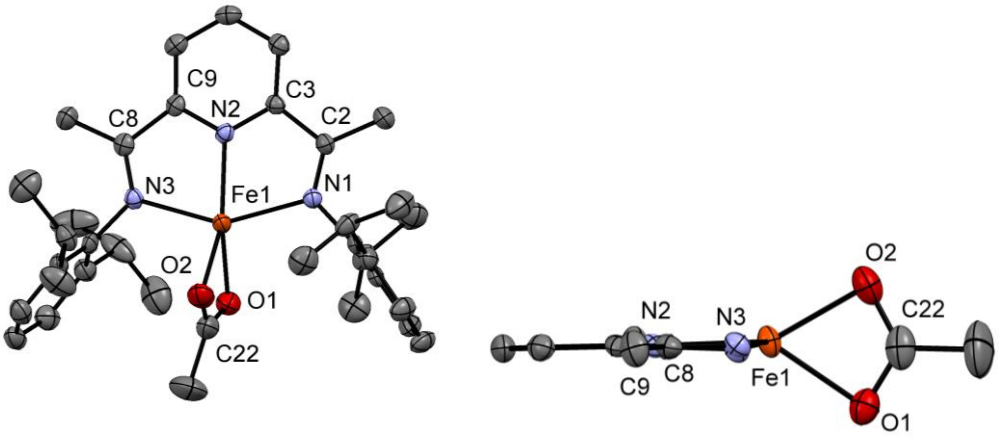

Figure 3.12. Molecular structure of [(PDI)FeOAc][BPh_4] (**4**). Top view is shown on the left and side view is shown on the right. The BPh_4^- anion and hydrogen atoms are omitted in both views and 2,6–^{i}Pr$_2$–C_6H_3 groups are omitted in the side view. Selected bond lengths (Å) and angles (deg): Fe1–O1 2.0869(19), Fe1–O2 2.0462(19), Fe1–N1 2.153(2), Fe1–N2 2.082(2), Fe1–N3 2.169(2), N1–C2 1.282(3), C8–C7 1.493(4), N3–C8 1.276(3), C2–C3 1.492(4), O2–Fe1–O1 63.94(9), N2–Fe1–O1 143.44(9), N2–Fe1–N1 74.36(8), N3–Fe1–O1 98.36(8).

The kinetics of the reaction of **2** with CO_2 were measured by ^{1}H NMR spectroscopy, monitoring the resonance at δ -25 of **2**. Typical NMR monitoring results and the corresponding

first-order kinetic plot are shown in Figure 3.13 and Figure 3.14. These results show that the reaction is first order in **2**:

rate = $k_{\mathbf{2},CO2}$[**2**],

where $k_{2,CO2}$ is the observed first-order rate constant.

$k_{\mathbf{2},CO2}$ at 0 ºC = 7.10(9) × 10^{-4} s^{-1}. Therefore, at 0 ºC, the conversion of the cationic complex **2** to **4** is 5-fold *slower* than the conversion of neutral complex **1** to **3** ($k_{\mathbf{1},CO2}$ (0 ºC) = 3.63(9) × 10^{-3} s^{-1}).

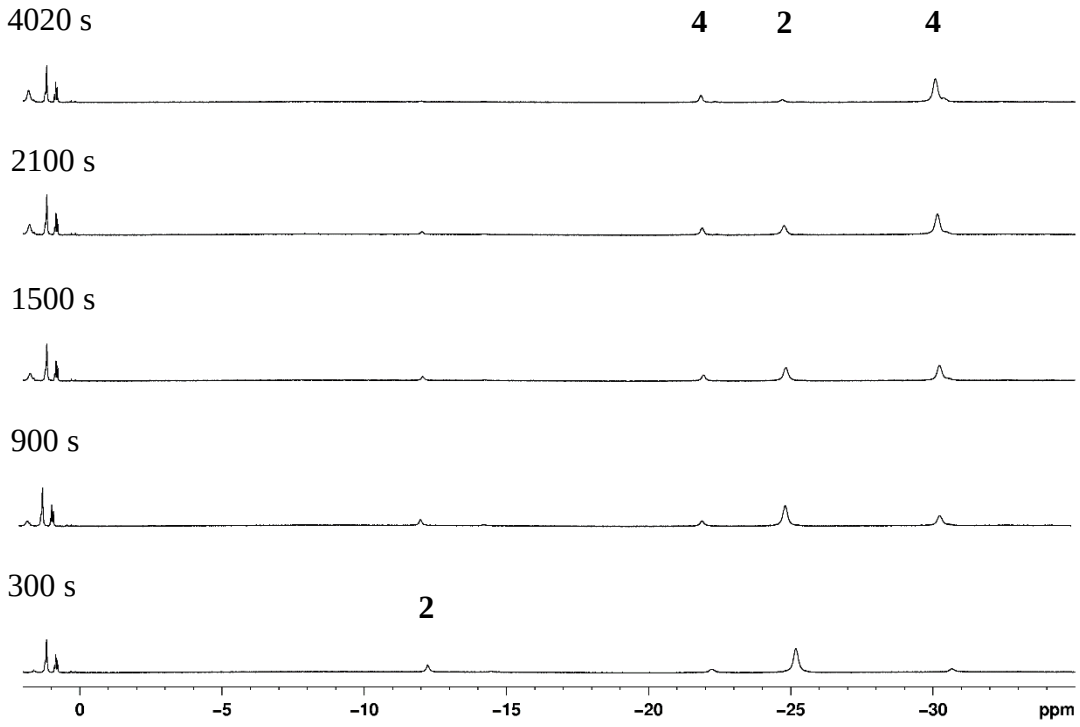

Figure 3.13. ^{1}H NMR monitoring of the reaction of **2** with CO_2 (1 atm) in C_6D_5F at 0 ºC. Other resonances: δ 1.2 (pentane), 0.9 (pentane).

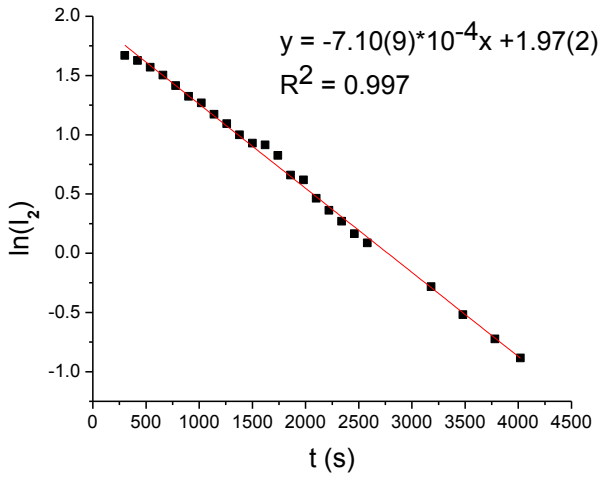

Figure 3.14. Representative first-order kinetic plot for the reaction of **2** with CO_2 (1 atm) in C_6D_5F (0 ºC) shown in Figure 3.13. A plot for the disappearance of **2** is shown. From the plot, $k_{\mathbf{2},CO2} = 7.10(9) \times 10^{-4}$ s^{-1}.

Carboxylation of 2 in a Coordinating Solvent. To probe whether CO_2 coordination is necessary for the carboxylation reaction of **2**, the reaction of **2** with CO_2 (1 atm) was carried out in the coordinating solvent THF-d_8 at room temperature. Several observations show that **2** binds THF to form, presumably, **2-THF**. First, the color of a solution of **2** in C_6D_5F changes from red to blue after the addition of THF, consistent with the color change for the conversion of analogous complexes [(PDI)FeR][BPh_4] to [(PDI)Fe(R)THF][BPh_4] (R = CH_2CMe_3, CH_2SiMe_3).[2,7] Second, the ^{1}H NMR spectrum of **2** in THF-d_8 is significantly shifted from that of **2** in C_6D_5F (Figure 3.15). These results confirm that the coordination of THF to **2** forms **2-THF**. ^{1}H NMR analysis shows that **2** did not react with CO_2 to produce **4** in THF-d_8 at room temperature but rather partially decomposed over time. The rate of decomposition is approximately the same as in the absence of CO_2. These results show that the coordination of THF to **2** quenches the carboxylation reaction.

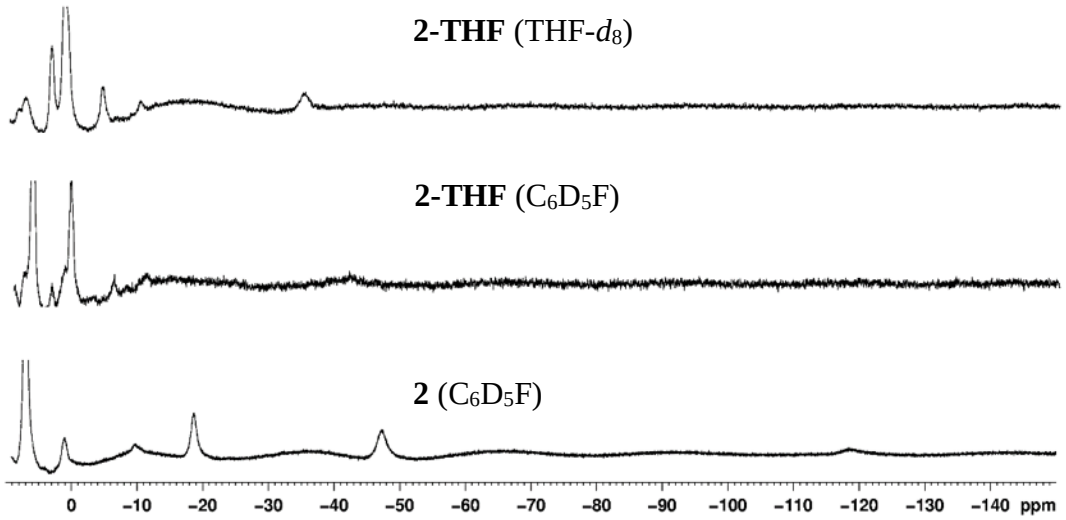

Figure 3.15. ^{1}H NMR spectra of **2** and **2-THF** in C_6D_5F and **2-THF** in THF-d_8 at 23 ℃.

Mechanism of the reaction of 2 with CO_2. These reactivity studies show that the coordination of a donor ligand (THF) quenches the reaction of **2** with CO_2 and imply that the carboxylation of **2** proceeds by initial coordination of CO_2 and subsequent insertion to form **4**, similar to the mechanism for the carboxylation proposed for **1**. The similarity in mechanisms proposed for **1** and **2** are consistent with the similar electronic structures and coordination environment of **1** and **2**, which indicate that both complexes **1** and **2** have a high-spin Fe^{II} center and square planar coordination geometry. Interestingly, CO_2 reacts 5-fold faster with neutral **1** than with cationic **2**. This suggests that the more electron-rich **1**, which results from the anionic PDI^{-} ligand versus a neutral PDI ligand for **2**, is more reactive with CO_2, presumably due to labilization and hence a higher nucleophilicity of the Fe–Me group by the anionic PDI^{-} ligand. However, complexes **1**, **2**, **3** and **4** all have a high-spin Fe^{II} center, and the conversions of **1** to **3**

and **2** to **4** experience no overall change in spin state. There is likely a change in spin state of Fe^{II} from high spin to intermediate or low spin upon the coordination of CO_2, which is observed for the coordination of PMe_3 to **1** to form **1-PMe$_3$**. This may affect the Fe---*O*CO interaction in the insertion transition state and cause the observed reactivity difference.

Carboxylation of Group 8 Metal Alkyls. The reactions of CO_2 with **1**, **1-PMe$_3$** and **2** represent unusual examples of carboxylation of group 8 metal alkyls. To the best of our knowledge, the only other reported examples of group 8 metal alkyls that react with CO_2 are (TPP)FeR ($[TPP]^{2-}$ = tetraphenylporphyrinato dianion),[8a] *cis*-/*trans*-$(dmpe)_2FeMe_2$ (dmpe = $Me_2PCH_2CH_2PMe_2$),[8b] *cis*-/*trans*-$(depe)_2FeMe_2$ (depe = $Et_2PCH_2CH_2PEt_2$),[8b] $Fe[(bpy)(pyea)]Me_2$ (bpy = 2,2'–bipyridine; pyea = 2–($H_2NCH_2CH_2$)–C_5H_4N),[8c] *cis*-/*trans*-$(dmpe)_2RuMe_2$,[8d,e] and *trans*-$(dmpe)_2Ru(Me)H$.[8d]

3.3. Conclusions

(PDI)FeMe (**1**), (PDI)Fe(Me)PMe_3 (**1-PMe$_3$**) and [(PDI)FeMe][BPh_4] (**2**) react with CO_2 to yield the corresponding monoacetate products (PDI)FeOAc (**3**), (PDI)Fe(OAc)PMe_3 (**3-PMe$_3$**) and [(PDI)FeOAc][BPh_4] (**4**). Donor ligands (PMe_3, THF) strongly inhibit these reactions, which is indicative of an insertion mechanism involving CO_2 pre-coordination to the Fe center. Eyring analysis is consistent with a bimolecular mechanism. The reaction of CO_2 with cationic complex **2** is 5-fold slower than the carboxylation of neutral complex **1**, suggesting that the nucleophilicity of Fe–Me group may control the reactivity of (PDI)Fe alkyl complexes with CO_2.

3.4. Experimental Section

General Procedures. All experiments were performed using dry box or Schlenk techniques under a nitrogen atmosphere. Nitrogen was purified by passage through activated molecular sieves and Q-5 oxygen scavenger. Deuterated solvents were purchased from Cambridge Isotope Laboratories. C_6D_5F and C_6H_5F were distilled from and stored over P_2O_5. C_6D_6, toluene-d_8 and THF-d_8 were distilled from Na/benzophenone. Pentane, hexanes and toluene were purified by passage through activated alumina and BASF R3-11 oxygen scavenger. THF, CH_2Cl_2, and Et_2O were purified by passage through activated alumina. CO_2 (99.999%) was purchased from Airgas and used as is. $[Cp_2Fe]BPh_4$,[9] (PDI)$FeCl_2$ (PDI = 2,6−(2,6−$^iPr_2$−C_6H_3−N=CMe)$_2$−C_5H_3N),[10] (PDI)$FeBr_2$,[11a] (PDI)FeMe (**1**)[1] and [(PDI)FeMe]BPh_4 (**2**)[2] were synthesized by literature procedures. NMR spectra were recorded on a Bruker DMX-500 spectrometer in Teflon-valved J. Young tubes at ambient temperature unless otherwise indicated. ^1H and $^{13}C\{^1H\}$ chemical shifts are reported relative to $SiMe_4$ and were determined by reference to the residual ^1H and ^{13}C solvent resonances. Mass spectrometry was performed on an Agilent 6224 TOF-MS instrument (high resolution) or an Agilent 6130 LCMS (low resolution). SQUID magnetization data were recorded with a SQUID magnetometer (Quantum Design). Values of the magnetic susceptibility were corrected for the underlying diamagnetic increment by using tabulated Pascal constants and the effect of the blank sample holders.

X-Ray Crystallography. Crystallographic data are summarized in Table 3.1. Data were collected on a Bruker Smart Apex diffractometer using Mo K_α radiation (0.71073 Å). Direct methods were used to locate many atoms from the E-map. Repeated difference Fourier maps allowed location of all expected non-hydrogen atoms. Following anisotropic refinement of all non-H atoms, ideal H-atom positions were calculated. Final refinement was anisotropic for all

non-H atoms, and isotropic-riding for H atoms. ORTEP diagrams are drawn with 40 % probability ellipsoids. Specific comments for each structure are as follows. **(PDI)Fe(Me)PMe$_3$ (1-PMe$_3$)**: Crystals of **1-PMe$_3$** were obtained by crystallization of a saturated solution of **1-PMe$_3$** in pentane at −35 ºC. Significant elongation of essentially all thermal ellipsoids was observed. This was modeled as a whole body disorder of two equivalent complexes sitting at almost the same location (ratio: 60/40). All atoms were refined with anisotropic thermal parameters utilizing constraints on thermal parameters (RIGU, SIMU, EADP). While geometric restraints were initially used to support the refinement, geometric parameters were not restrained during final refinement cycles except soft SADI restraints were imposed on all *i*-Pr groups. After modelling the disorder, the data to parameters ratio is about 9. **[(PDI)FeOAc][BPh$_4$] (4)**: Crystals of **4** were obtained by layering hexanes onto a solution of **4** in C_6H_5F at room temperature. No anomalous bond lengths or thermal parameters were noted.

Table 3.1. Summary of X-ray Diffraction Data for **1-PMe$_3$** and **4.**

	1-PMe$_3$	**4**
Formula	$C_{37}H_{55}FeN_3P$	$C_{59}H_{66}BFeN_3O_2$
Formula weight	628.66	915.80
Crystal system	Monoclinic	Monoclinic
Space group	$P2_1/c$	$P2_1/c$
a (Å)	17.2088(12)	12.5740(8)
b (Å)	12.6102(8)	12.6375(8)
c (Å)	16.3707(11)	31.6380(19)
β (deg)	100.567(2)	96.473(2)

Table 3.1. (Continued)

V (Å^3)	3492.3(4)	4995.4(5)
Z	4	4
T (K)	100	100
Crystal color, habit	green, block	red, brick
GOF on F^2	1.045	1.073
R indices ($I > 2\sigma(I)$)[a]	R_1 = 0.0751, wR_2 = 0.1483	R1 = 0.0530, wR2 = 0.0995
R indices (all data)[a]	R_1 = 0.0933, wR_2 = 0.1560	R1 = 0.0847, wR2 = 0.1084

[a]R1 = $\Sigma||F_o| - |F_c|| / \Sigma|F_o|$; wR2 = $[\Sigma[w(F_o^2 - F_c^2)^2] / \Sigma[w(F_o^2)^2]]^{1/2}$, where $w = q[\sigma^2(F_o^2) + (aP)^2 + bP]^{-1}$

Synthesis, Characterization and Reactions of Compounds

(PDI)FeOAc (3). This compound was previously synthesized by the reaction of (PDI)Fe(N_2)$_2$ with EtOAc, or with MeOAc and H_2.[6] In this work, **3** was prepared by carboxylation of **1**. A Schlenk flask was charged with **1** (210 mg, 0.379 mmol). The flask was evacuated and exposed to CO_2 (1 atm). Et_2O (10 mL) was added by syringe and the reaction was stirred for 15 min at room temperature under a CO_2 atmosphere. The volatiles were removed under vacuum to afford **3** as a green solid (212 mg, 0.354 mmol, 93 %). ^{1}H NMR data matched the literature data. IR (KBr; see below): 1514, 1459 cm^{-1}.

[**(PDI)FeOAc]BPh$_4$ (4).** **3** (61 mg, 0.10 mmol) and [Cp_2Fe]BPh$_4$ (45 mg, 0.089 mmol) were dissolved in benzene (5 mL) and the solution was stirred at room temperature for 45 min. Pentane (10 mL) was added and the mixture was stirred for 15 min to form an orange-red slurry.

The yellow supernatant was removed by pipette and the solid was washed with pentane until the washes were colorless. The solid was dried under vacuum to afford a light red powder (81 mg, 0.088 mmol, 99 %). A substoichiometric amount of $[Cp_2Fe]BPh_4$ was used to ensure that all of $[Cp_2Fe]BPh_4$, which is insoluble under reaction conditions, was fully consumed. Residual **3** dissolved in the supernatant and was washed away by pentane. ^{1}H NMR (C_6D_5F): δ 273.3, 167.5, 17.7, 16.2, 10.9, 3.8, -18.1, -23.9, -35.1, -146.3. IR (KBr; see below): 1582, 1466 cm^{-1}. HR-ESI-MS (C_6H_5F, positive ion mode) *m*/*z* 596.2949 ($[M - BPh_4^-]^+$, calcd. for $C_{59}H_{66}BFeN_3O_2$: 596.2934). ESI-MS (C_6H_5F, negative ion mode) *m*/*z* 319.2 ($[BPh_4]^-$). μ_{eff} (SQUID, 27 ºC): 5.3 μ_B. Multiple elemental analyses of crystalline samples of **4** failed to give reproducible results for C but gave accurate results for H and N. Anal. Calcd. for $C_{59}H_{66}BFeN_3O_2$: C, 77.38; H, 7.26; N, 4.59. Found: C, 74.92; H, 7.54; N, 4.43.

Addition of THF (0.01 mmol) to a solution of **4** (9.1 mg, 0.0099 mmol) in C_6D_5F via syringe generated [(PDI)Fe(OAc)THF][BPh_4] (**4-THF**). The formation of **4-THF** is supported by the analysis of ^{1}H NMR spectra of mixtures of **4** and THF, which show that the observed ^{1}H NMR resonances for the mixtures appear at the mole-fraction-weighted average of chemical shifts of **4** and **4-THF**. These results imply that **4-THF** is formed and exchanges with **4** rapidly relative to the NMR timescale (Figure 3.16a). ^{1}H NMR (C_6D_5F): δ 199.2, 112.9, 12.4, 9.3, 4.3, 2.9, 2.4, 1.2, -1.3, -11.8, -13.7, -16.0, -78.9. ^{1}H NMR (THF-d_8): δ 156.8, 78.7, 13.9, 8.7, 7.8, 7.3, -4.5, -11.1, -13.5, -35.1.

^{1}H NMR of **4** (C_6D_5F). The full spectrum and expansion of key regions are shown below.

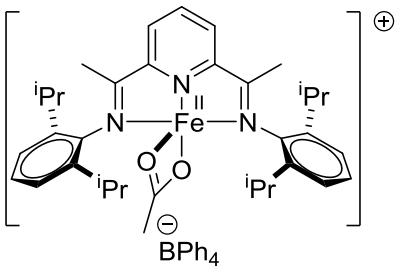

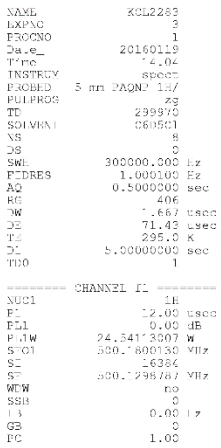

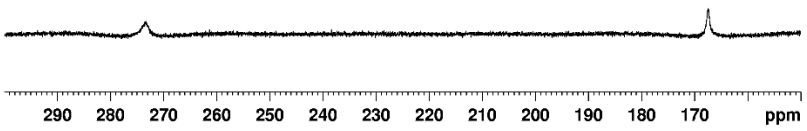

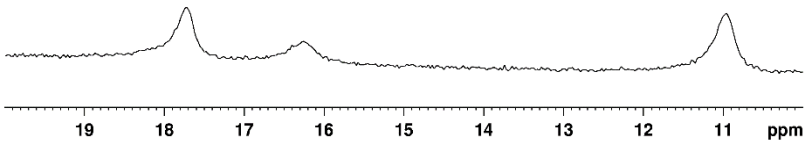

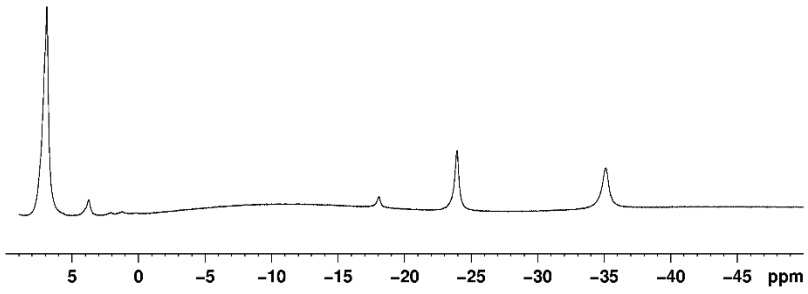

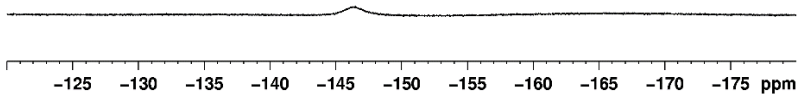

^{1}H NMR of **4-THF** (C_6D_5F). The full spectrum and expansion of key regions are shown below.

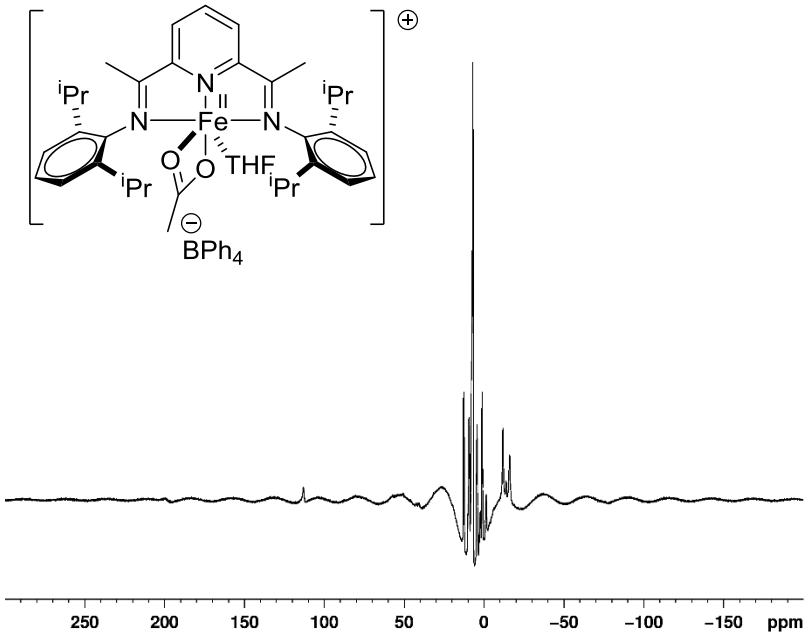


```
NAME                XCL2283
EXPNO                     9
PROCNO                    1
Date_              20160119
Time                  14.32
INSTRUM                spect
PROBHD    5 mm PAQNP 1H/
PULPROG                zg
TD                    289970
SOLVENT               C6D5Cl
NS                        8
DS                        0
SWH               300000.000 Hz
FIDRES              1.034130 Hz
AQ                  0.5000000 sec
RG                      287
DW                    1.667 usec
DE                    71.43 usec
TE                    294.8 K
D1                  5.00000000 sec
TD0                       1

======== CHANNEL f1 ========
NUC1                      1H
P1                    12.00 usec
PL1                    0.00 dB
PL1W            24.54113007 W
SFO1            500.1800130 MHz
SI                    16384
SF              500.1298979 MHz
WDW                      no
SSB                       0
LB                     0.00 Hz
GB                        0
PC                     1.00
```

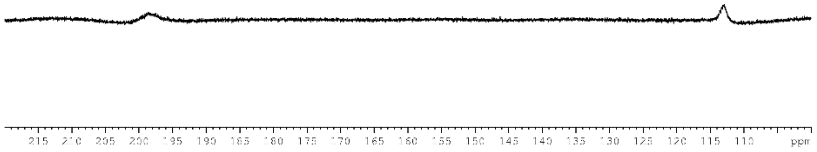

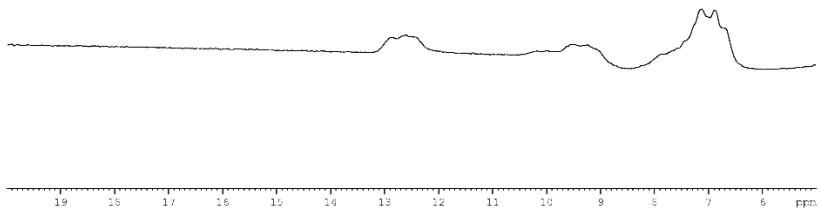
19 18 17 16 15 14 13 12 11 10 9 8 7 6 ppm

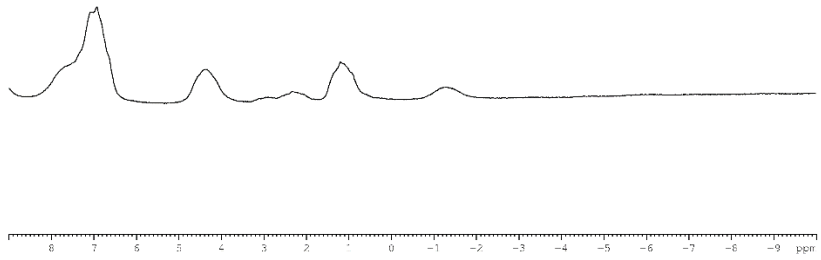
8 7 6 5 4 3 2 1 0 −1 −2 −3 −4 −5 −6 −7 −8 −9 ppm

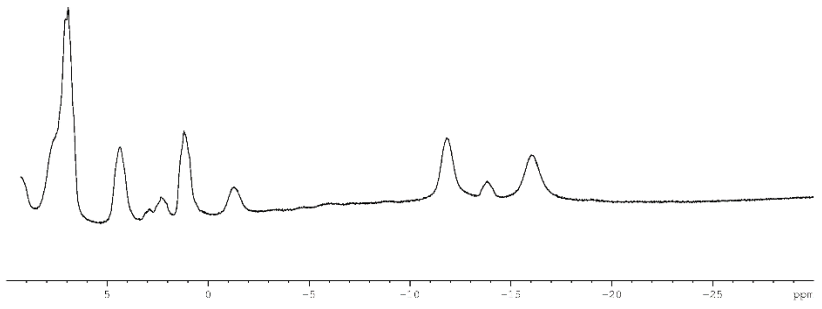
5 0 −5 −10 −15 −20 −25 ppm

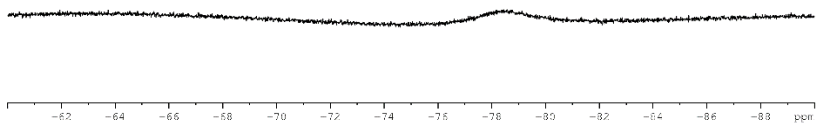
−62 −64 −66 −68 −70 −72 −74 −76 −78 −80 −82 −84 −86 −88 ppm

^{1}H NMR of **4-THF-d_8** (THF-d_8). The full spectrum and expansion of key regions are shown below.

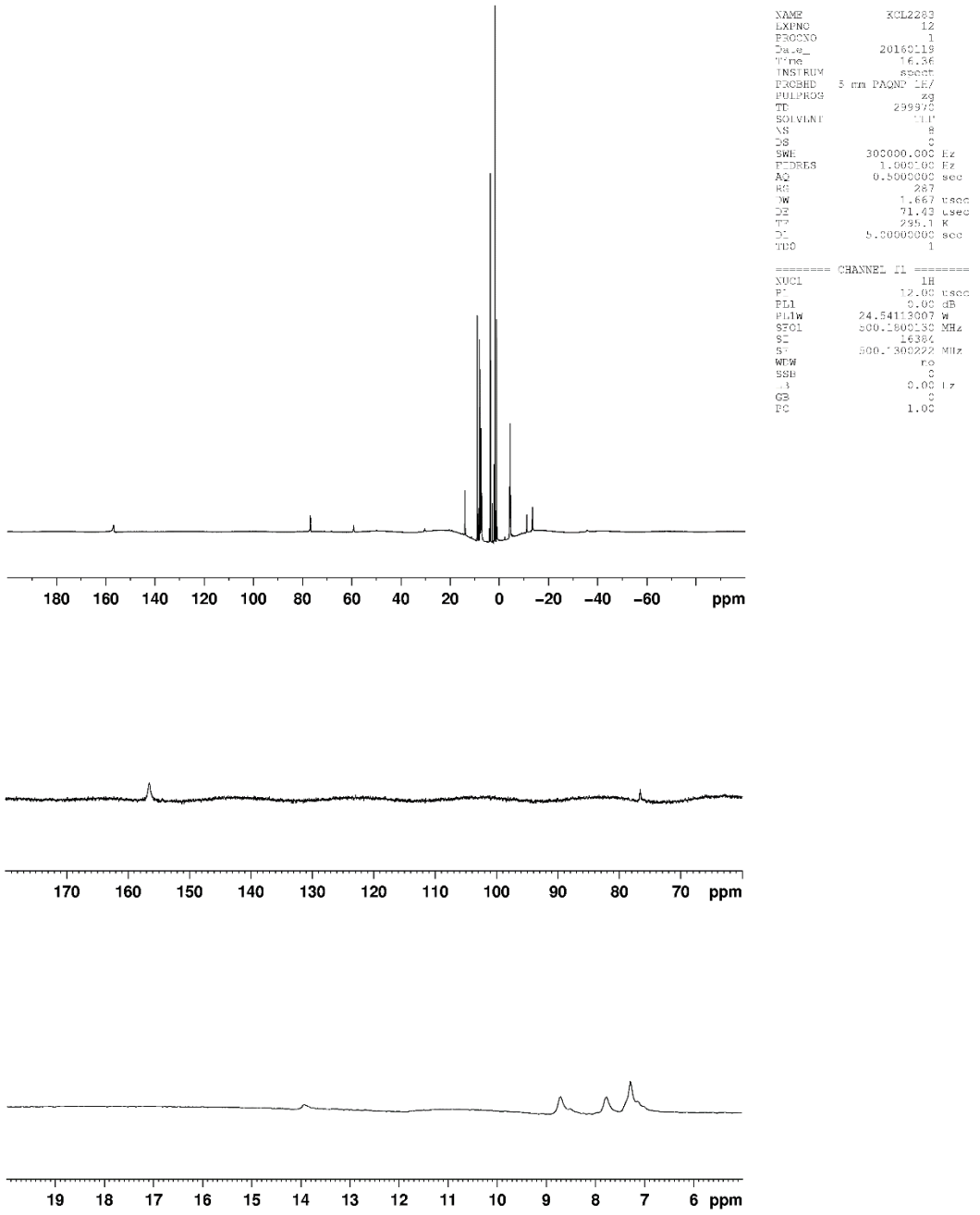

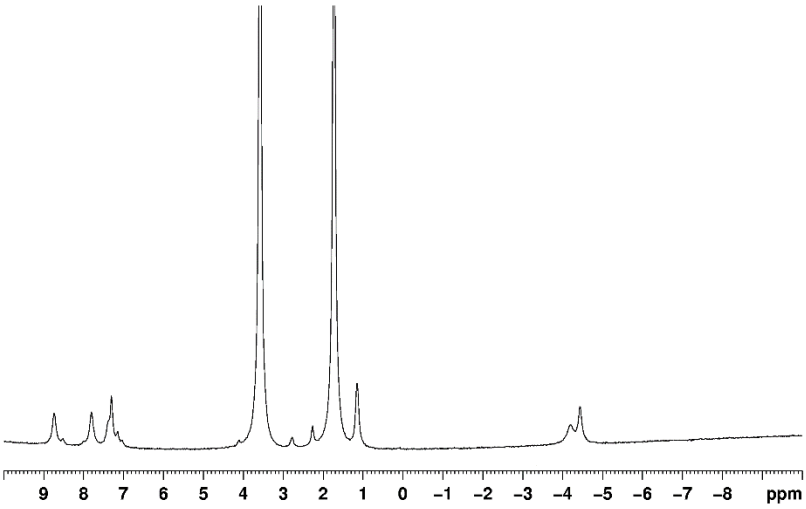
9 8 7 6 5 4 3 2 1 0 −1 −2 −3 −4 −5 −6 −7 −8 ppm

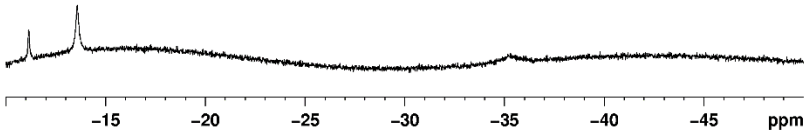
−15 −20 −25 −30 −35 −40 −45 ppm

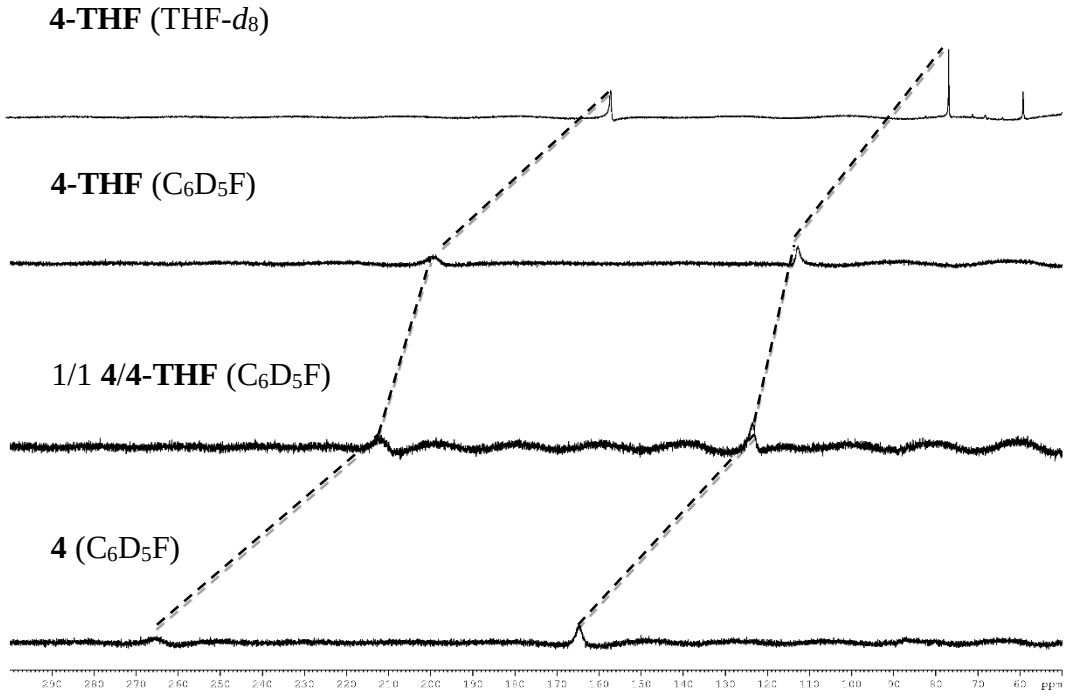

Figure 3.16a. ^{1}H NMR spectra of mixtures of **4** and **4-THF** at 23 °C (δ 300 – 50). The shift and correlation of the ^{1}H resonances are indicated by dashed lines.

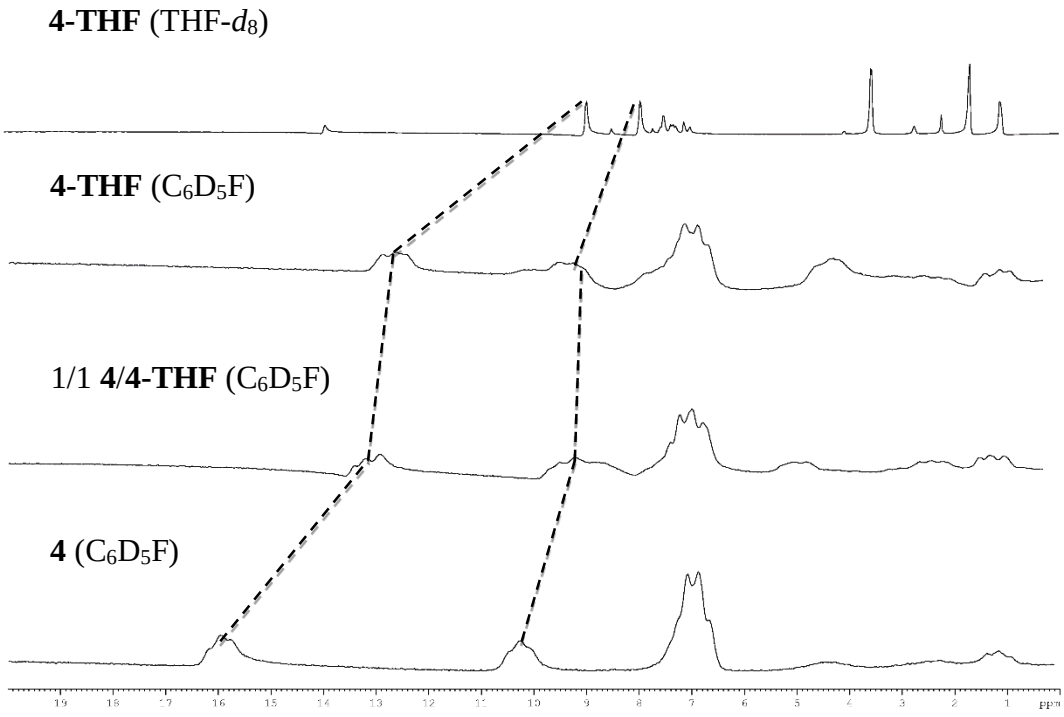

Figure 3.16b. ^{1}H NMR spectra of mixtures of **4** and **4-THF** at 23 $^\circ$C (δ 20 – 0). The shift and correlation of the ^{1}H resonances are indicated by dashed lines.

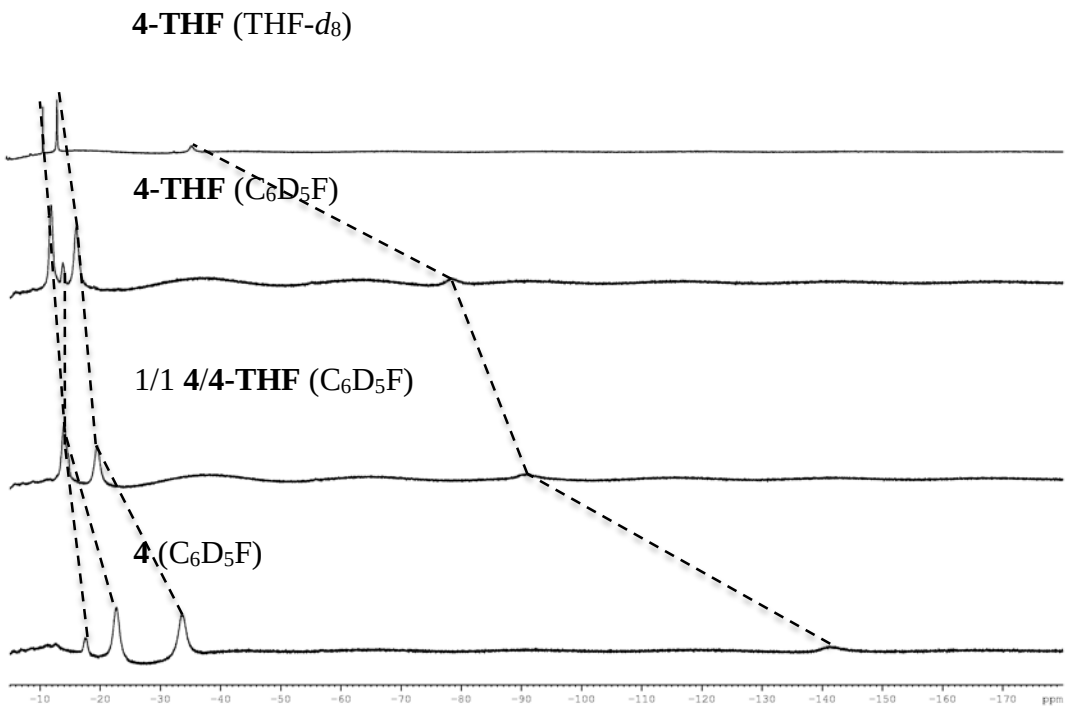

Figure 3.16c. ^{1}H NMR spectra of mixtures of **4** and **4-THF** at 23 °C (δ -5 – -180). The shift and correlation of the ^{1}H resonances are indicated by dashed lines.

(PDI)Fe(Me)PMe$_3$ (1-PMe$_3$). A solution of PMe_3 in Et_2O (0.098 M, 1.15 mL, 0.11 mmol) was added to a solution of **1** in Et_2O (0.054 M, 2.0 mL, 0.11 mmol) and the mixture was stirred at room temperature for 5 min. ^{1}H NMR analysis showed that an equilibrium mixture of **1-PMe$_3$** and **1** had formed. The volatiles were removed under vacuum to afford a brown solid. Recrystallization of the solid from a saturated pentane solution at −35 ºC afforded dark green crystals that were identified by ^{1}H NMR and X-ray diffraction to be **1-PMe$_3$** (45 mg, 0.072 mmol, 66 %). ^{1}H NMR (C_6D_6, 0.027 M): δ 16.9 (Fe–P*Me*$_3$), 2.8 (*p*–Ar), 2.2 (*m*–Ar), -2.7 (CH*Me*$_2$), -5.3 (CH*Me*$_2$), -22.1 (C*H*Me$_2$), -100.2 (N=C*Me*), -198.4 (Fe–*Me*). μ_{eff} (SQUID, 27 ºC): 1.8 μ_B. Multiple elemental analyses of crystalline samples of **1-PMe$_3$** failed to give

reproducible results for C but gave accurate results for H, N and P. Anal. Calcd. for $C_{37}H_{55}FeN_3P$: C, 70.69; H, 8.82; N, 6.68; P, 4.93. Found: C, 69.81; H, 9.21; N, 6.49; P, 4.88.

^{1}H NMR of **1-PMe$_3$** in C_6D_6 (0.027 M). The full spectrum and expansion of key regions are shown below.

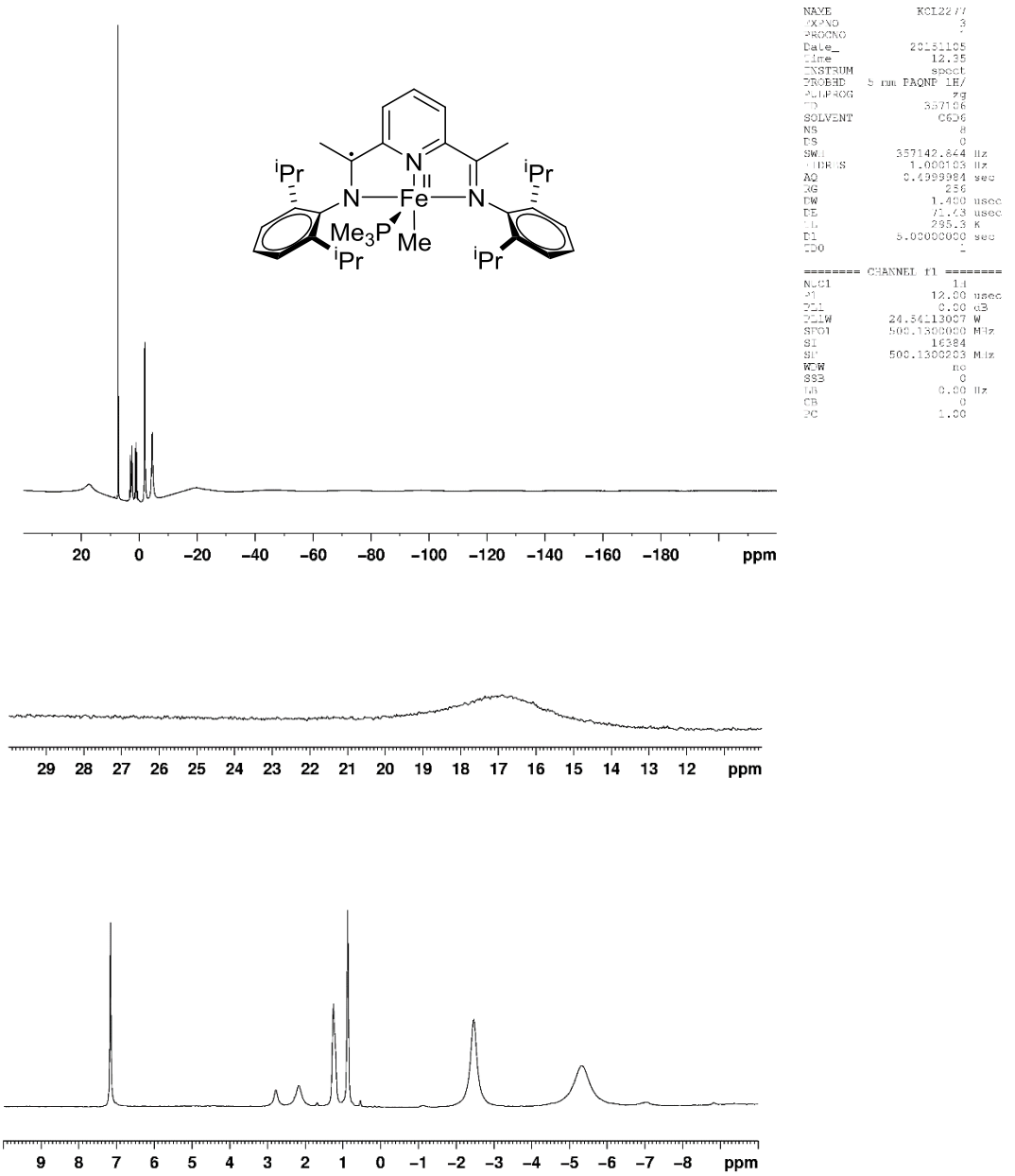


```
NAME                 KCL2277
EXPNO                      3
PROCNO                     1
Date_               20151105
Time                   12.35
INSTRUM                spect
PROBHD     5 mm PAQNP 1H/
PULPROG                   zg
TD                    557106
SOLVENT                 C6D6
NS                         8
DS                         0
SWH                357142.844 Hz
FIDRES               1.000103 Hz
AQ                   0.4999984 sec
RG                         256
DW                       1.400 usec
DE                       7.43 usec
TE                      295.3 K
D1                 5.00000000 sec
TD0                        1

======== CHANNEL f1 ========
NUC1                      1H
P1                     12.00 usec
PCPD1                   0.00 dB
PLW1             24.56113027 W
SFO1             500.1300000 MHz
SI                       16384
SF               500.1300203 MHz
WDW                       no
SSB                        0
LB                      0.00 Hz
GB                         0
PC                      1.00
```

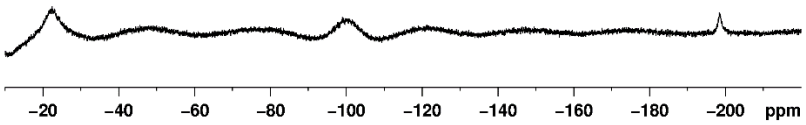

Reversible Dissociation of PMe_3 from 1-PMe_3. A valved J. Young NMR tube was charged with **1-PMe_3** (8.0 mg, 0.013 mmol). C_6D_6 (0.5 mL) was added by vacuum transfer at −196 °C. The mixture was thawed at room temperature. This solution was serially diluted by C_6D_6 and ^1H NMR spectra were recorded at each concentration. Upon dilution, the ^1H NMR resonances for **1-PMe_3** shifted towards resonances for base-free **1** and free PMe_3. These results are consistent with partial dissociation of PMe_3 to form **1**, and rapid exchange between **1-PMe_3** and **1** relative to the NMR timescale (See Figure 3.3).

The fast exchange between **1-PMe_3** and **1** was confirmed by ^1H NMR spectra of mixtures of **1-PMe_3** and **1** (See Figure 3.4 and Figure 3.17). The observed ^1H NMR resonances for mixtures of **1-PMe_3** and **1** appear at the mole-fraction-weighted-averaged chemical shifts of corresponding chemical shifts of **1-PMe_3** and **1**, as expected for fast exchange between **1-PMe_3** and **1**.

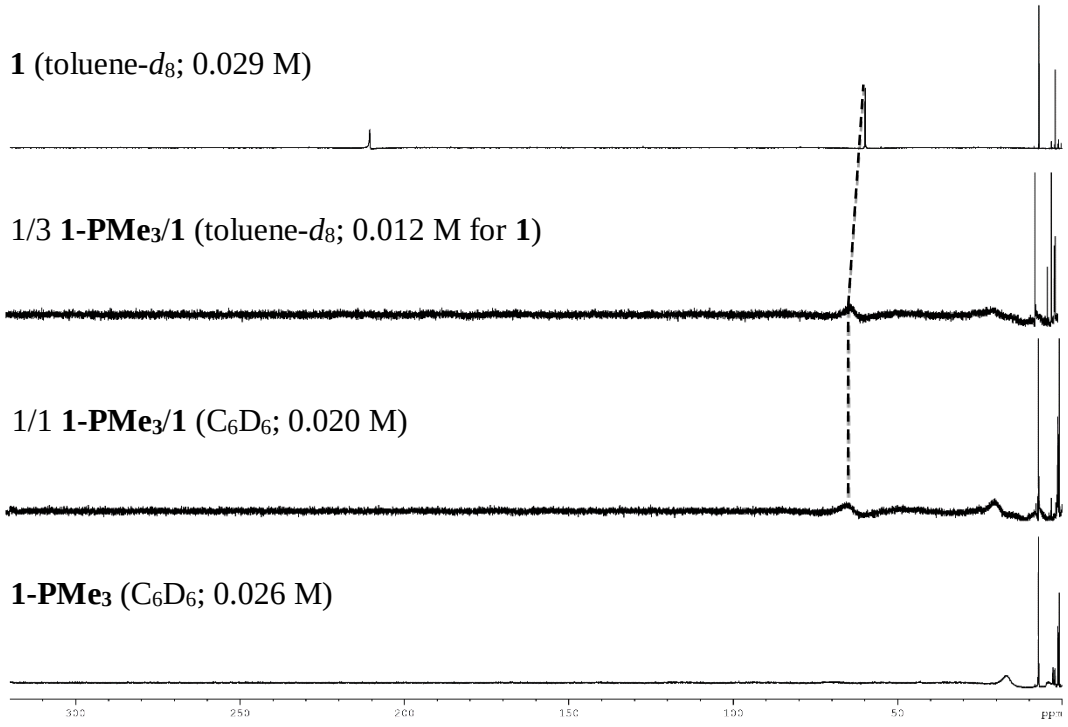

Figure 3.17. ^{1}H NMR spectra of mixtures of **1-PMe$_3$** and **1** at 23 °C (δ 320 – 0). The shift and correlation of the ^{1}H resonances are indicated by dashed lines. No resonances for **1-PMe$_3$** > δ 20 were observed presumably due to significantly broadened signals.

Determination of Dissociation Equilibrium Constant for 1-PMe$_3$. The equilibrium constant (K_{eq}) for dissociation of PMe_3 from **1-PMe$_3$** (Scheme 3.3) is defined by eq 1:

$$K_{eq} = \frac{[\mathbf{1}][PMe_3]}{[\mathbf{1}\text{-}\boldsymbol{PMe_3}]} \qquad (1)$$

The observed chemical shifts are mole-fraction-weighted averages of the chemical shifts of the two compounds and are given by eq 2:

$$\delta_{obs} = \chi_{\mathbf{1}}\delta_{\mathbf{1}} + \chi_{\mathbf{1\text{-}PMe3}}\delta_{\mathbf{1\text{-}PMe3}} \qquad (2)$$

where δ_{obs} = observed chemical shift; $\delta_{\mathbf{1}}$ = chemical shift for **1**; $\delta_{\mathbf{1\text{-}PMe3}}$ = chemical shift for **1-**

PMe$_3$; $\chi_{\mathbf{1}}$ and $\chi_{\mathbf{1\text{-}PMe_3}}$ are the mole fractions of **1** and **1-PMe$_3$**.

Combining eq 1 and 2,

$$[\text{Fe}]_{\text{total}}\delta_{\text{obs}} = [\mathbf{1}]\delta_{\mathbf{1}} + [\mathbf{1\text{-}PMe_3}]\delta_{\mathbf{1\text{-}PMe_3}} = ([\text{Fe}]_{\text{total}} - [\mathbf{1\text{-}PMe_3}])\delta_{\mathbf{1}} + [\mathbf{1\text{-}PMe_3}]\delta_{\mathbf{1\text{-}PMe_3}}$$

where $[\text{Fe}]_{\text{total}} = [\mathbf{1}] + [\mathbf{1\text{-}PMe_3}]$

Rearranging,

$$[\text{Fe}]_{\text{total}}(\delta_{\text{obs}} - \delta_{\mathbf{1}}) = [\mathbf{1\text{-}PMe_3}](\delta_{\mathbf{1\text{-}PMe_3}} - \delta_{\mathbf{1}})$$

Defining $\Delta\delta_{\text{obs}} = \delta_{\text{obs}} - \delta_{\mathbf{1}}$ and $\Delta\delta_{\mathbf{1\text{-}PMe_3}} = \delta_{\mathbf{1\text{-}PMe_3}} - \delta_{\mathbf{1}}$,

$$[\mathbf{1\text{-}PMe_3}] = \frac{[Fe]_{total}\Delta\delta_{obs}}{\Delta\delta_{\mathbf{1-PMe3}}}$$

$$[\mathbf{1}] = [\text{Fe}]_{\text{total}} - [\mathbf{1\text{-}PMe_3}] = \frac{[Fe]_{total}(\Delta\delta_{\mathbf{1-PMe3}} - \Delta\delta_{obs})}{\Delta\delta_{\mathbf{1-PMe3}}}$$

Therefore, without externally added PMe_3, K_{eq} is given by eq 3.[5a]

$$K_{eq} = \frac{[Fe]_{total}(\Delta\delta_{\mathbf{1-PMe_3}} - \Delta\delta_{obs})^2}{\Delta\delta_{\mathbf{1-PMe_3}}\Delta\delta_{obs}} \qquad (3)$$

Eq 3 contains K_{eq} and $\Delta\delta_{\mathbf{1\text{-}PMe_3}}$ as unknowns, and $[\text{Fe}]_{\text{total}}$ and $\Delta\delta_{\text{obs}}$ as experimentally determined variables. K_{eq} was determined using the graphical method described by Rose and Drago.[5b] To determine K_{eq}, a series of $\Delta\delta_{\text{obs}}$ values were measured over a series of $[\text{Fe}]_{\text{total}}$ values. For each set of $[\text{Fe}]_{\text{total}}$ and $\Delta\delta_{\text{obs}}$ values, K_{eq} was calculated for a range of $\Delta\delta_{\mathbf{1\text{-}PMe_3}}$ values, and plots of K_{eq} vs $\Delta\delta_{\mathbf{1\text{-}PMe_3}}$ were generated according to eq 3. Since K_{eq} and $\Delta\delta_{\mathbf{1\text{-}PMe_3}}$ are independent of $[\text{Fe}]_{\text{total}}$, simulated curves of K_{eq} vs $\Delta\delta_{\mathbf{1\text{-}PMe_3}}$ at different $[\text{Fe}]_{\text{total}}$ (and corresponding $\Delta\delta_{\text{obs}}$) values should intersect at two points (K_{eq}, $\Delta\delta_{\mathbf{1\text{-}PMe_3}}$), corresponding to the two solutions of eq 3. As shown in Figure 3.18, this result was indeed observed for **1-PMe$_3$**. One of the two solutions corresponds to an unreasonable value for $\delta_{\mathbf{1\text{-}PMe_3}}$ (eg $K_{eq} = 2.5 \times 10^{-3}$ M at $\Delta\delta_{\mathbf{1\text{-}PMe_3}} = 21.5$; Figure 3.18) and was rejected. The other intersection point provided values for K_{eq} and $\Delta\delta_{\mathbf{1\text{-}PMe_3}}$.

From plots of K_{eq} vs $\Delta\delta_{\mathbf{1\text{-}PMe_3}}$ for different resonances, it was determined that K_{eq} (23 ºC) for **1-PMe$_3$** = 1.8(9) × 10^{-3} M.

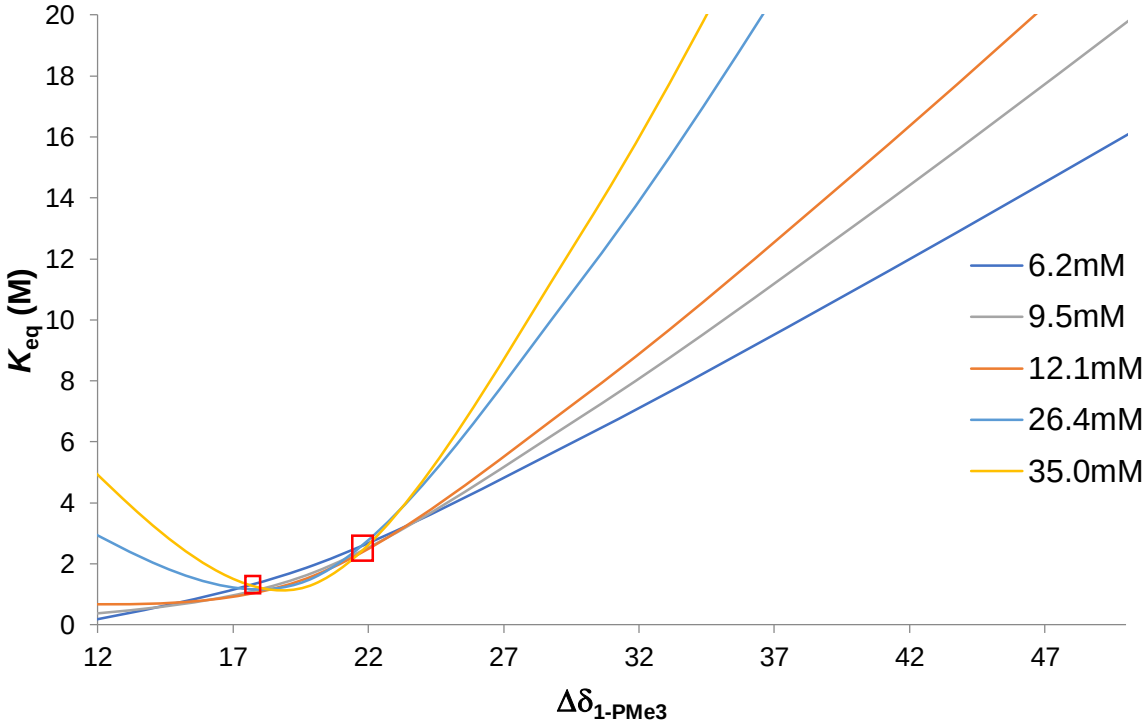

Figure 3.18. Representative plot of K_{eq} vs $\Delta\delta_{\mathbf{1\text{-}PMe_3}}$ for the CH*Me*$_2$ resonance of a solution of **1-PMe$_3$** in C_6D_6. The two solutions to eq 3 are the intersection points on this plot: K_{eq} = 1.3(2) × 10^{-3} M, $\Delta\delta_{\mathbf{1\text{-}PMe_3}}$ = 17.8(3) and K_{eq} = 2.5(5) × 10^{-3} M, $\Delta\delta_{\mathbf{1\text{-}PMe_3}}$ = 21.5(6). Error bars are indicated by the red boxes. The latter solution was rejected as it gave an unreasonable $\delta_{\mathbf{1\text{-}PMe_3}}$ value.

Generation of (PDI)Fe(OAc)PMe$_3$ (3-PMe$_3$). (a) A valved J. Young NMR tube was charged with **1-PMe$_3$** (5.2 mg, 0.0083 mmol). Toluene-d_8 (0.6 mL) was added by vacuum transfer at −196 °C. The mixture was thawed and exposed to CO_2 (1 atm, 12 equiv) at room temperature. The tube was agitated for 15 min at room temperature. ^{1}H NMR analysis showed

that an equilibrium mixture of **3-PMe$_3$** and **3** had formed. These species exchange rapidly on the NMR timescale in toluene-d_8 (see below). ^{1}H NMR (toluene-d_8, 0.017 M): δ 184.5 (OC(O)*Me*), 118.9 (*m*−py), -2.9 (*m*−Ar), -16.2 (*p*−Ar), -19.3 (CH*Me*$_2$), -29.7 (CH*Me*$_2$), -112.2 (C*H*Me$_2$), -282.4 (N=C*Me*). (b) A valved J. Young NMR tube was charged with **3** (10.7 mg, 0.0179 mmol) and a solution of PMe_3 in C_6D_6 (0.036 M, 0.5 mL, 0.018 mmol) was added. The tube was agitated at room temperature for 5 min. ^{1}H NMR analysis showed that an equilibrium mixture of **3-PMe$_3$** and **3** had formed.

^{1}H NMR of **3-PMe$_3$** in toluene-d_8 (0.017 M). The full spectrum and expansion of key regions are shown below.

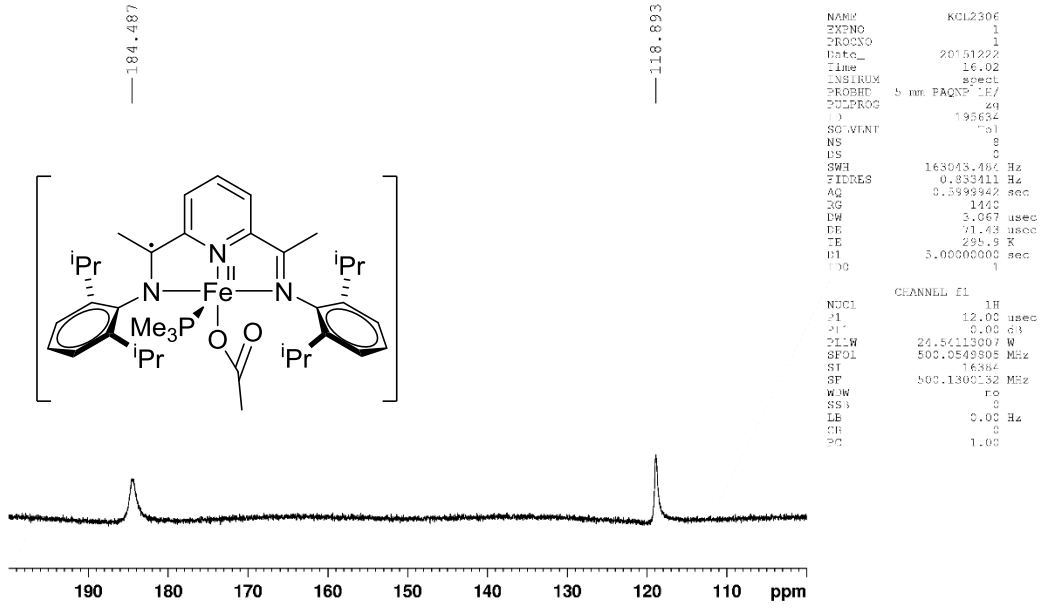

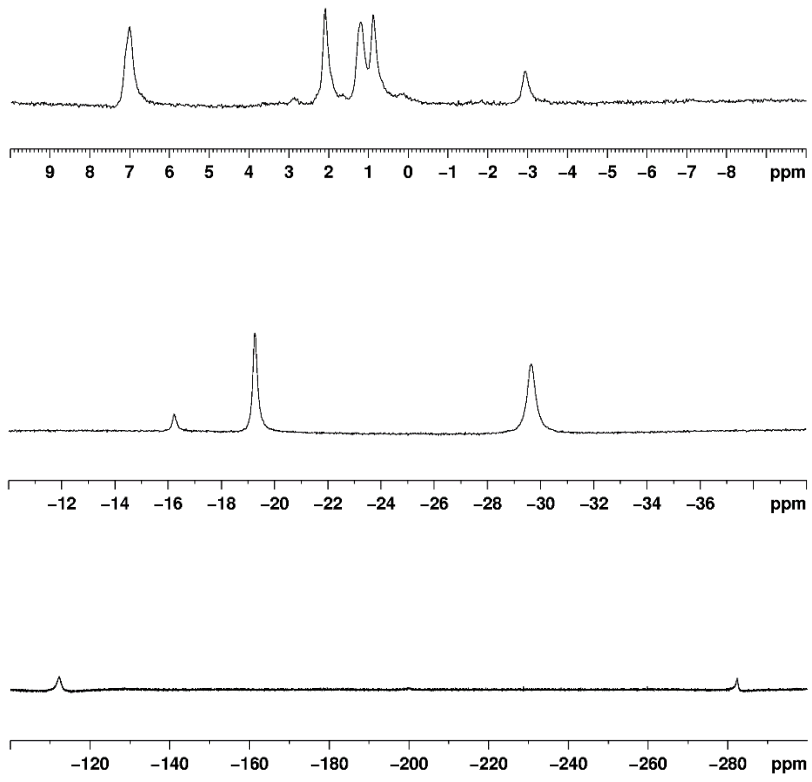

Generation of [(PDI)Fe(Me)THF][BPh$_4$] (2-THF). A valved J. Young NMR tube was charged with **2** (8.7 mg, 0.010 mmol). C_6D_5F (0.5 mL) was added by vacuum transfer at −196 °C to produce a red solution. The mixture was thawed at room temperature and THF (0.010 mmol) was added via syringe to afford a blue solution. The formation of **2-THF** is supported by several observations as discussed in the text (Figure 3.15 and 3.19). ^{1}H NMR (THF-d_8): δ 82.37, 78.79, 11.52, 8.70, 7.66, -4.17, -9.95, -34.84. ^{1}H NMR (C_6D_5F): δ 85.58, 81.26, 9.54, 8.18, 4.40, 2.35, 1.17, -5.67, -10.46, -42.71. **2-THF** is thermally unstable in THF-d_8 or C_6D_5F at room temperature and decomposed over 1 d to give a black precipitate.

^{1}H NMR of **2-THF** in C_6D_5F. The full spectrum and expansion of key regions are shown below.

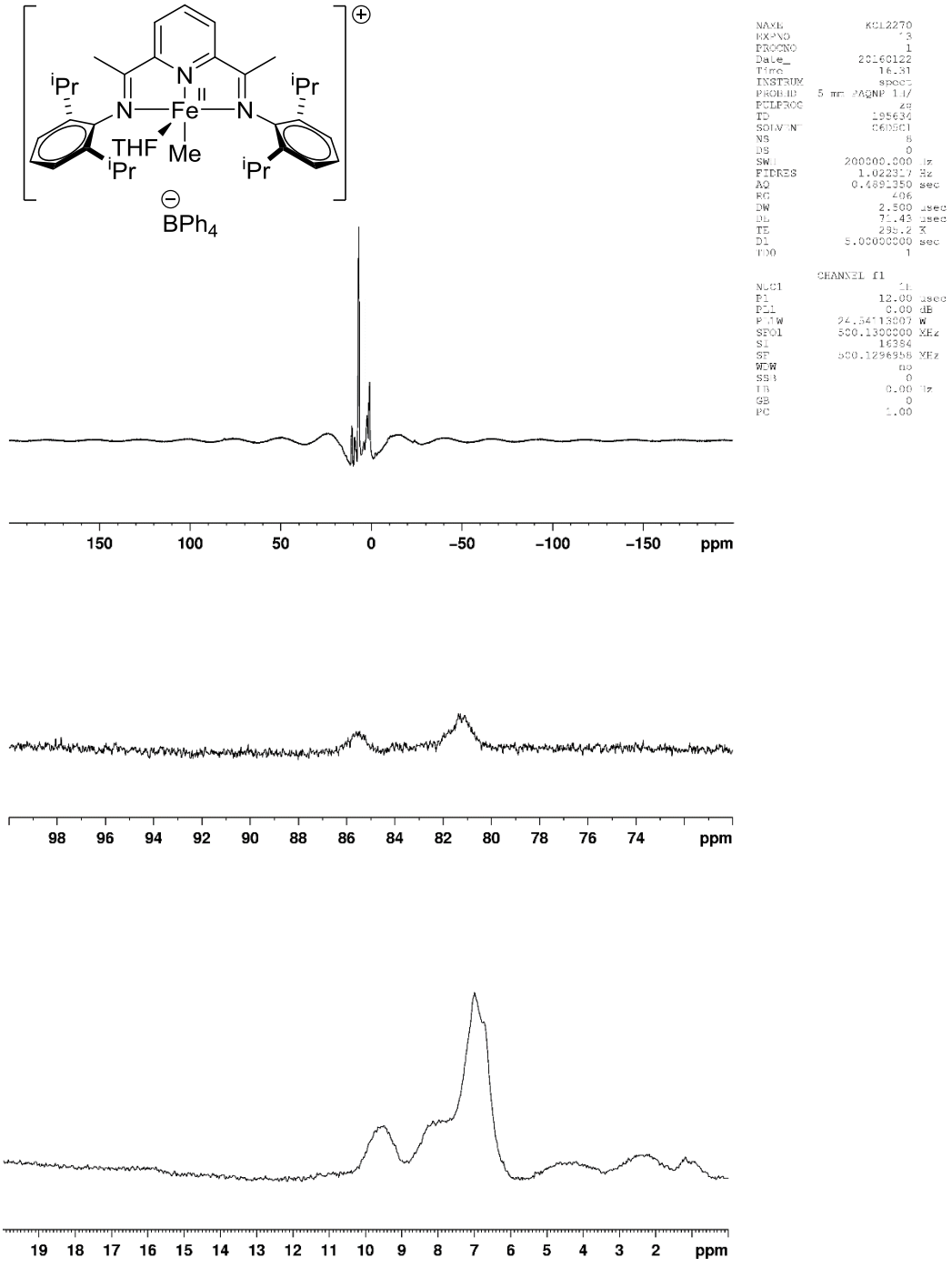

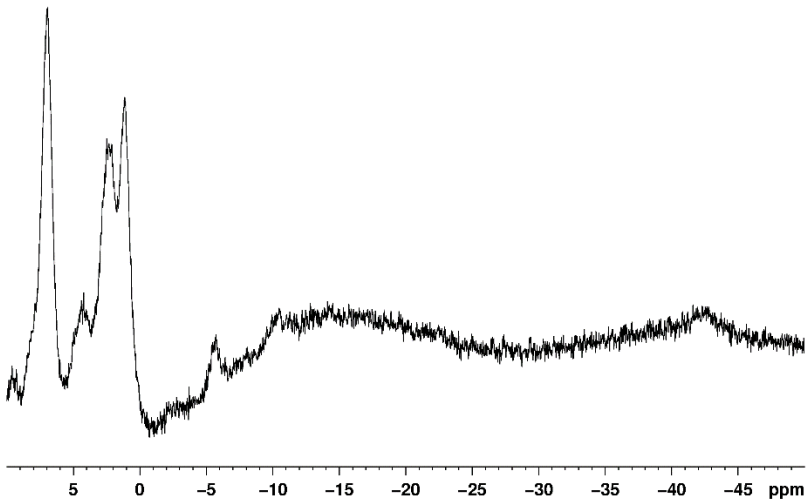

^{1}H NMR of **2-THF** in THF-d_8. The full spectrum and expansions of key regions are shown below.

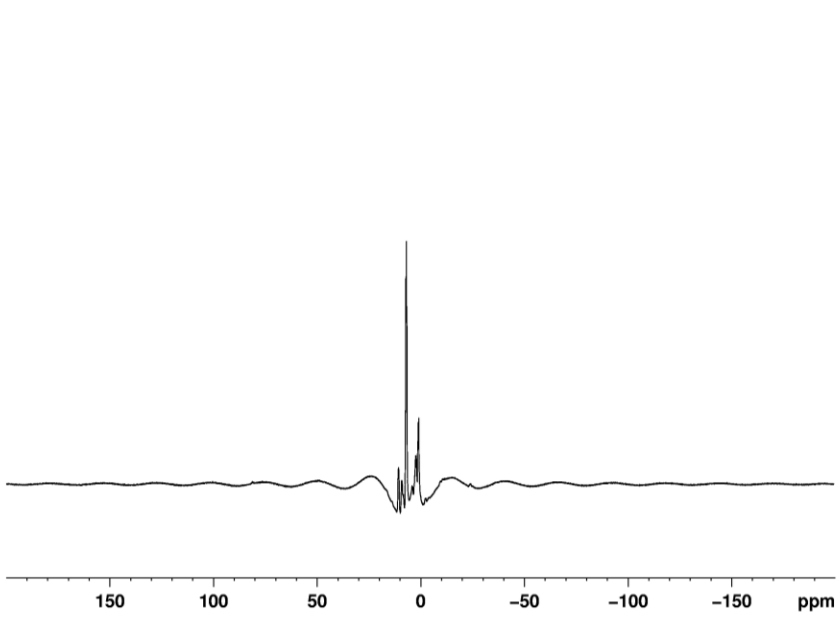

NAME	KCL2270	
EXPNO	13	
PROCNO	1	
Date_	20160122	
Time	16.31	
INSTRUM	spect	
PROBHD	5 mm PAQNP 1H/	
PULPROG	zg	
TD	195634	
SOLVENT	C6D5Cl	
NS	8	
DS	0	
SWH	200000.000	Hz
FIDRES	1.022317	Hz
AQ	0.4891350	sec
RG	406	
DW	2.500	usec
DE	71.43	usec
TE	295.2	K
D1	5.00000000	sec
TD0	1	
======== CHANNEL f1 ========		
NUC1	1H	
P1	12.00	usec
PL1	0.00	dB
PL1W	24.54113007	W
SFO1	500.1300000	MHz
SI	16384	
SF	500.1296958	MHz
WDW	no	
SSB	0	
LB	0.00	Hz
GB	0	
PC	1.00	

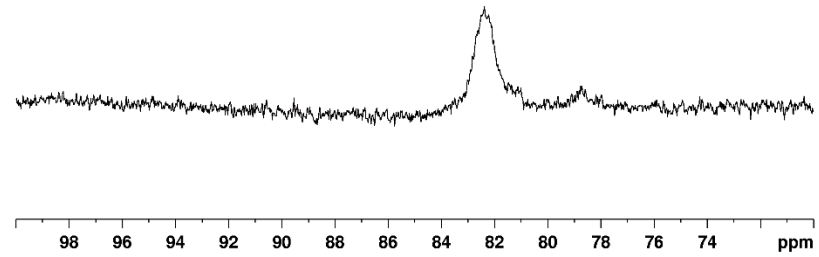
98 96 94 92 90 88 86 84 82 80 78 76 74 ppm

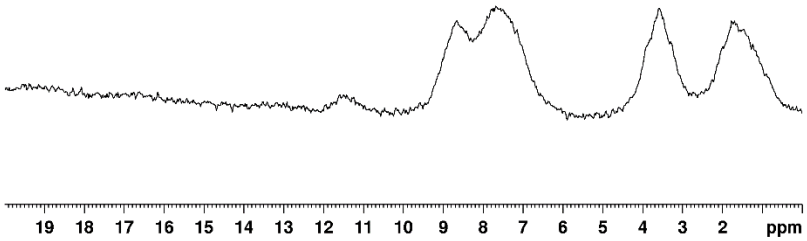
19 18 17 16 15 14 13 12 11 10 9 8 7 6 5 4 3 2 ppm

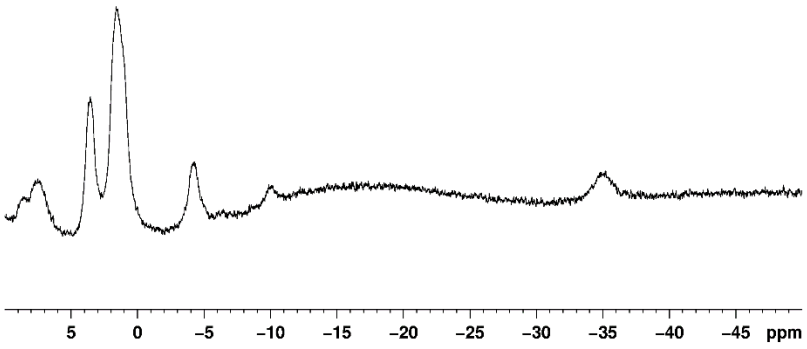
5 0 −5 −10 −15 −20 −25 −30 −35 −40 −45 ppm

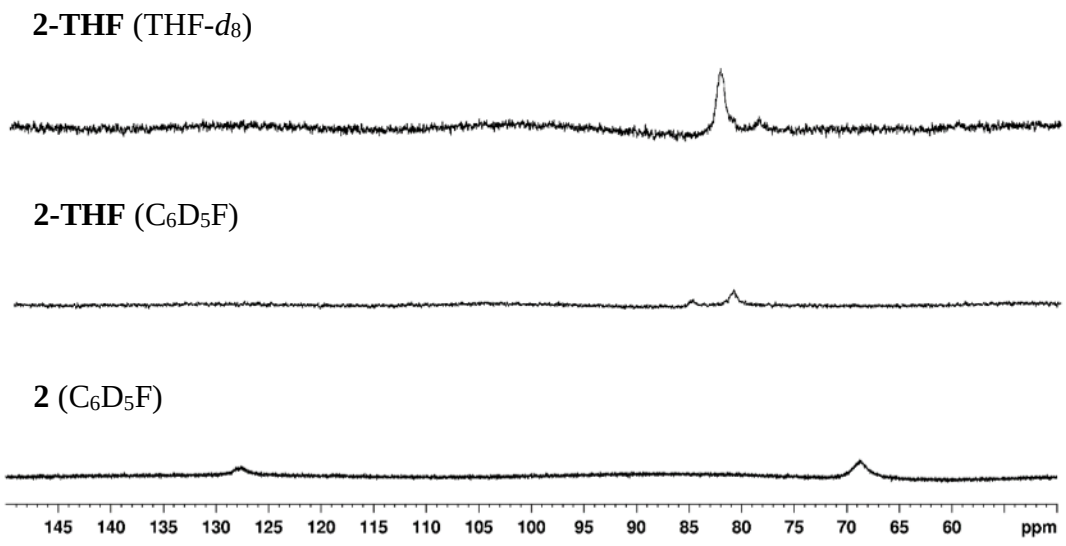

Figure 3.19a. ^{1}H NMR spectra of mixtures of **2** and **2-THF** at 23 °C (δ 150 – 50).

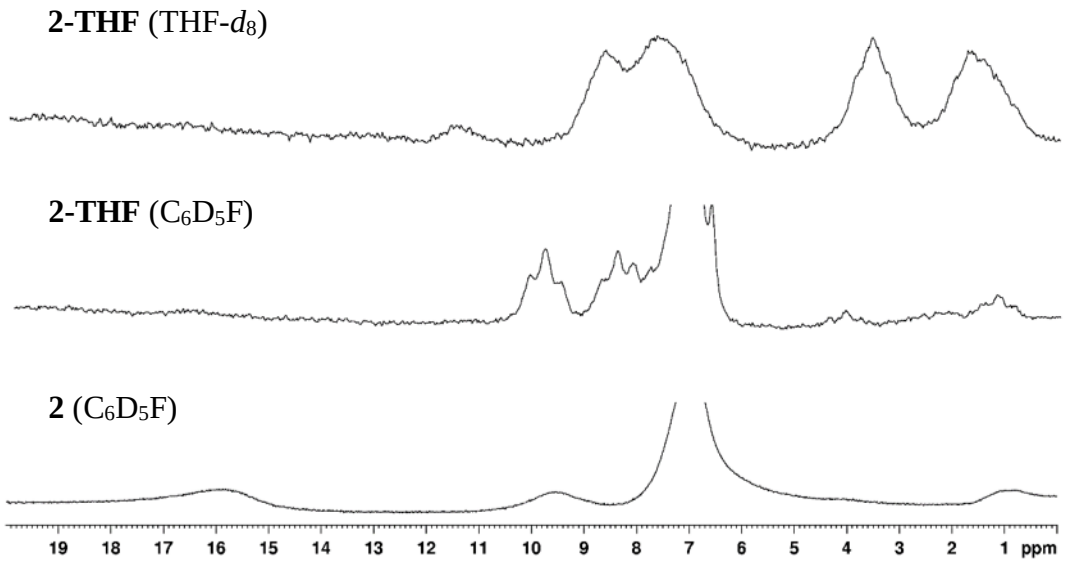

Figure 3.19b. ^{1}H NMR spectra of mixtures of **2** and **2-THF** at 23 °C (δ 20 – 0).

Representative Kinetics of the Reaction of 1 with CO_2. A valved J. Young NMR tube was charged with **1** (5.8 mg, 0.010 mmol). Toluene-d_8 (0.5 mL) was added by vacuum transfer at −196 ºC. The mixture was thawed at 0 ºC and exposed to CO_2 (1 atm, 10 equiv). The tube was then rapidly inserted into an NMR probe that had been pre-cooled at 0 ºC. ^{1}H NMR spectra were recorded periodically. Representative spectra are shown in Figure 3.5.

The rate equation for the conversion of **1** to **3** is given by eq 4. The effect of pressure of CO_2 was not studied and the rate equation was assumed to be first order with respect to the pressure of CO_2 (1 atm).

$$\text{Rate} = k_{\mathbf{1},CO2}[\mathbf{1}] \qquad (4)$$

where $k_{\mathbf{1},CO2}$ = observed first-order rate constant.

The logarithmic form of first-order rate equation for the disappearance of **1** is given by eq 5.

$$\ln(I_{\mathbf{1}}) = -k_{\mathbf{1},CO2}t + \ln(I_{\mathbf{1},0}) \qquad (5)$$

where $I_{\mathbf{1}}$ = integral value of the CHMe_2 resonance of **1** at δ -11 relative to the integral value of Et_2O resonance at time = t; $I_{\mathbf{1},0}$ = integral value of the CHMe_2 resonance of **1** at δ -11 relative to the integral value of Et_2O resonance at the start of the reaction

The integral value for **1** was determined by integration of the CHMe_2 resonance of PDI ligand at δ -11 relative to the integral value of Et_2O resonance. The first-order kinetic plots were generated using the program Origin 8 and are shown in Figure 3.20. The first-order kinetic plot

for the disappearance of **1** is shown in Figure 3.6. From the plot, $k_{\mathbf{1},CO2}$ (0 ℃) = 3.63(9) × 10^{-3} s^{-1}. The logarithmic form of first-order rate equation for the appearance of **3** is given by eq 6.

$$\ln(I_{\mathbf{3},\infty} - I_{\mathbf{3}}) = -k_{\mathbf{1},CO2}t + \ln(I_{\mathbf{3},\infty}) \qquad (6)$$

where $I_{\mathbf{3},\infty}$ = integral value of the *m*–Ar resonance of **3** relative to the integral value of Et_2O resonance at the end of reaction. $I_{\mathbf{3}}$ = integral value of the *m*–Ar resonance of **3** relative to residual Et_2O resonance at time = t

The integral value for **3** was determined by integration of the *m*–Ar resonance of PDI ligand relative to the integral value of Et_2O resonance. The first-order plot for the appearance of **3** is shown Figure 3.20. From the plot, $k_{\mathbf{1},CO2}$ (0 ℃) = 3.5(2) × 10^{-3} s^{-1}, which is in good agreement with the $k_{\mathbf{1},CO2}$ value for the disappearance of **1**.

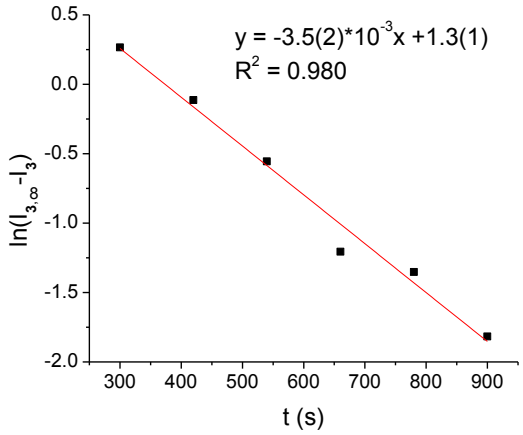

Figure 3.20. Representative first-order kinetic plot for the reaction of **1** with CO_2 (1 atm) in toluene-d_8 (0 ℃). A plot for the appearance of **3** is shown ($k_{\mathbf{1},CO2}$ = 3.5(2) × 10^{-3} s^{-1}).

The first-order rate constants for the conversion of **1** to **3** were obtained over the temperature range of -35 ℃ – 0 ℃. The Eyring plot for the conversion of **1** to **3** is shown in Figure 3.7.

Representative Kinetics of Reaction of 1-PMe_3 with CO_2. A valved J. Young NMR tube was charged with **1** (4.5 mg, 0.0081 mmol), Cp_2Fe (0.8 mg, 0.004 mmol, internal standard) and a solution of PMe_3 in C_6D_6 (0.047 M, 0.5 mL, 0.024 mmol). ^{1}H NMR spectroscopy showed that an equilibrium mixture of **1-PMe_3** and **1** had formed. The mixture was degassed and exposed to CO_2 (1 atm, 13 equiv). The J. Young tube was then inserted into an NMR probe that was equilibrated at 23 ℃. ^{1}H NMR spectra were recorded periodically. Representative spectra are shown in Figure 3.9.

The rate equation for the conversion of **1-PMe_3** to **3-PMe_3**/**3** is given by eq 7. The effect of pressure of CO_2 was not studied and the rate equation was assumed to be first order with respect to the pressure of CO_2 (1 atm).

$$\text{Rate} = k_{obs}([\textbf{1-PMe}_3] + [\textbf{1}]) = k_{obs}[Fe]_{total} \qquad (7)$$

where k_{obs} = observed first-order rate constant; $[Fe]_{total}$ = [**1-PMe_3**] + [**1**]

Due to overlapping of resonances for the **1-PMe_3** and PMe_3, the kinetics were evaluated by analyzing the appearance of equilibrium mixture of **3-PMe_3** and **3**. The total integral value for the **3-PMe_3**/**3** mixture was determined by integration of the CH*Me*$_2$ resonance at δ -18 of PDI ligand relative to the integral value of the internal standard resonance. The first-order rate equation for the appearance of **3-PMe_3**/**3** mixture (exponential form) is given by eq 8 The first-

order kinetic plots were generated using the program Origin 8 and are shown in Figure 3.9b. k_{obs} (23 ℃) = 6.9(3) × 10^{-4} s^{-1}.

$$I_{Fe} = -I_{Fe,\infty} \exp(-k_{obs}t) + I_{Fe,\infty} \quad (8)$$

where I_{Fe} = integral value of the CH*Me*$_2$ resonance at δ -18 of **3-PMe$_3$/3** mixture relative to the integral value of Cp_2Fe resonance at time = t; $I_{Fe,\infty}$ = integral value of the CH*Me*$_2$ resonance at δ -18 of **3-PMe$_3$/3** mixture relative to the integral value of Cp_2Fe resonance at the end of the reaction

The first-order rate constants for the conversion of **1-PMe$_3$** to **3-PMe$_3$/3** mixture were obtained over the PMe_3 concentration range of 0.047 M – 0.20 M, and the representative first-order kinetic plots are shown in Figure 3.10.

The kinetic results show that the conversion of **1-PMe$_3$** to **3-PMe$_3$/3** is inhibited by PMe_3. A fast pre-equilibrium reaction scheme that is consistent with these kinetic results and the known reversible dissociation of PMe_3 from **1-PMe$_3$** is shown in Scheme 3.6. In Scheme 3.6, base-free **1** reacts with CO_2 to form **3**, which, in the presence of PMe_3, gives an equilibrium mixture of **3-PMe$_3$/3**, while **1-PMe$_3$** does not react directly with CO_2.

The rate law for this scheme is derived below and given by eq 9.

$$\text{Rate} = k_{obs}[\text{Fe}] = k_{\mathbf{1},CO2}[\mathbf{1}],$$

where $[\text{Fe}]_{total} = [\mathbf{1\text{-}PMe_3}] + [\mathbf{1}]$

$$\text{Since } K_{eq} = \frac{[\mathbf{1}][PMe_3]}{[\mathbf{1\text{-}PMe_3}]}$$

$$[\mathbf{1\text{-}PMe_3}] = \frac{[\mathbf{1}][PMe_3]}{K_{eq}}$$

Therefore,

$$[\text{Fe}]_{total} = [\mathbf{1\text{-}PMe_3}] + [\mathbf{1}] = \frac{[\mathbf{1}][PMe_3]}{K_{eq}} + [\mathbf{1}]$$

$$= \frac{K_{eq} + [PMe_3]}{K_{eq}}[\mathbf{1}]$$

Rearranging,

$$[\mathbf{1}] = \frac{K_{eq}}{K_{eq} + [PMe_3]}[\mathbf{Fe}]_{total}$$

$$\text{And rate} = k_{\mathbf{1},CO2}[\mathbf{1}] = k_{\mathbf{1},CO2}\frac{K_{eq}}{K_{eq} + [PMe_3]}[\text{Fe}]_{total} = k_{obs}[\text{Fe}]_{total}, \quad (9)$$

$$\text{where } k_{obs} = \frac{k_{\mathbf{1},CO2}K_{eq}}{K_{eq} + [PMe_3]}$$

Therefore,

$$\frac{1}{k_{obs}} = \frac{1}{k_{\mathbf{1},CO2}K_{eq}}[PMe_3] + \frac{1}{k_{\mathbf{1},CO2}} \quad (10)$$

A plot of $1/k_{obs}$ vs $[PMe_3]$ is shown in Figure 3.11. From Figure 3.11 and eq 10 , the y-intercept = $1/(k_{\mathbf{1},CO2})$ = 4(8) × 10 s. $k_{\mathbf{1},CO2}$ (23 ℃) = 2(4) × 10^{-2} s^{-1} And the slope = $1/(k_{\mathbf{1},CO2}K_{eq})$ = 2.97(7) × 10^4 sM^{-1}. K_{eq} (23 ℃) = 1(6) × 10^{-3} M. These values are in good agreement with the

independently determined $k_{\mathbf{1},CO2}$ and K_{eq} values determined by the studies of **1** discussed above: $k_{\mathbf{1},CO2} = 2(4) \times 10^{-2}$ s^{-1} and $K_{eq} = 1.8(9) \times 10^{-3}$ M.

Representative Kinetics of Reaction of 2 with CO_2. A valved J. Young NMR tube was charged with **2** (8.7 mg, 0.010 mmol). C_6D_5F (0.5 mL) was added by vacuum transfer at −196 ºC. The mixture was thawed at 0 ºC and exposed to CO_2 (1 atm, 11 equiv). The tube was then rapidly inserted into an NMR probe that had been pre-cooled at 0 ºC. ^{1}H NMR spectra were recorded periodically. Representative spectra are shown in Figure 3.13.

The rate equation for the conversion of **2** to **4** is given by eq 11. The effect of pressure of CO_2 was not studied and the rate equation was assumed to be first order with respect to the pressure of CO_2 (1 atm).

$$\text{Rate} = k_{\mathbf{2},CO2}[\mathbf{2}] \qquad (11)$$

where $k_{\mathbf{2},CO2}$ = observed first-order rate constant.

The logarithmic form of the first-order rate equation for the disappearance of **2** is given by eq 12.

$$\ln(I_{\mathbf{2}}) = -k_{\mathbf{2},CO2}t + \ln(I_{\mathbf{2},0}) \qquad (12)$$

where $I_{\mathbf{2}}$ = integral value of the resonance of **2** at δ -25.0 relative to residual Et_2O resonance at time = t; $I_{\mathbf{2},0}$ = integral value of the resonance of **2** at δ -25.0 relative to residual Et_2O resonance at the start of the reaction

The integral value for **2** was determined by integration of the resonance at δ -25.0 relative to the integral value of Et_2O resonance. The first-order kinetic plots were generated

using the program Origin 8 and are shown in Figure 3.14. $k_{\mathbf{2},CO2}$ (0 ℃) = 7.10(9) × 10^{-4} s^{-1}. The first-order rate equation for the appearance of **4** (logarithmic form) is given by eq 13. The integral value for **4** was determined by integration of the resonance at δ -30.5 relative to residual Et_2O resonance. The first-order plot for the appearance of **4** is shown Figure 3.21. The rate constant, $k_{\mathbf{2},CO2}$ (0 ℃) = 8.3(3) × 10^{-4} s^{-1}, is in good agreement with the one for the disappearance of **2**.

$$\ln(I_{\mathbf{4},\infty} - I_{\mathbf{4}}) = -k_{\mathbf{2},CO2}t + \ln(I_{\mathbf{4},\infty}) \qquad (13)$$

where $I_{\mathbf{4},\infty}$ = integral value of the resonance of **4** at δ -30.5 relative to residual Et_2O resonance at the end of reaction. $I_{\mathbf{4}}$ = integral value of the resonance of **4** at δ -30.5 relative to residual Et_2O resonance at time = t

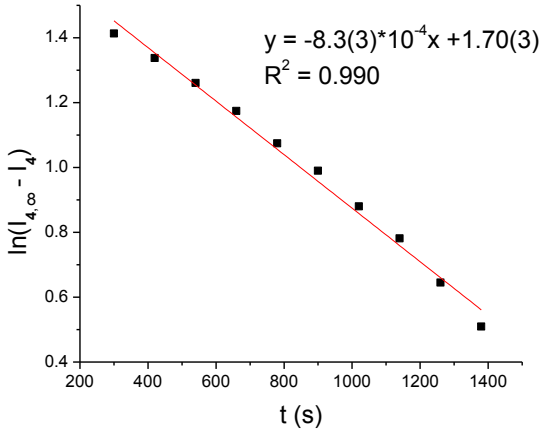

Figure 3.21. Representative first-order kinetic plot for the reaction of **2** with CO_2 (1 atm) in C_6D_5F (0 ℃). A plot for the appearance of **4** is shown ($k_{\mathbf{2},CO2}$ = 8.3(3) × 10^{-4} s^{-1}).

Attempted Reaction of 2-THF-d_8 with CO_2. A valved J. Young NMR tube was charged with **2** (4.8 mg, 0.0055 mmol). THF-d_8 (0.5 mL) was added by vacuum transfer at −196 °C. The mixture was thawed at room temperature, exposed to CO_2 (1 atm, 19 equiv) and allowed to stand at room temperature for 2 d. ^{1}H NMR spectra were recorded and showed that **2-THF-d_8** had partially decomposed to the same unidentified products at approximately the same rate as in the absence of CO_2. There was no evidence for the formation of **4-THF-d_8**.

IR Assignments

The ν_{CO} bands for **3-$^{13}C_1$**, which was synthesized from **3** + $^{13}CO_2$, and **3** are assigned by comparing IR bands of these complexes and (PDI)FeCl. Calculated ν_{CO} bands for **3-$^{13}C_1$** from isotopic shift of ν_{CO} bands for **3** are in good agreement with the assignment (Calcd. $\nu_{CO,asym}$ = 1479 cm^{-1}; $\nu_{CO,asym}$ = 1425 cm^{-1}). However, these assignments are inconclusive due to significant overlap with bands for the PDI ligand.

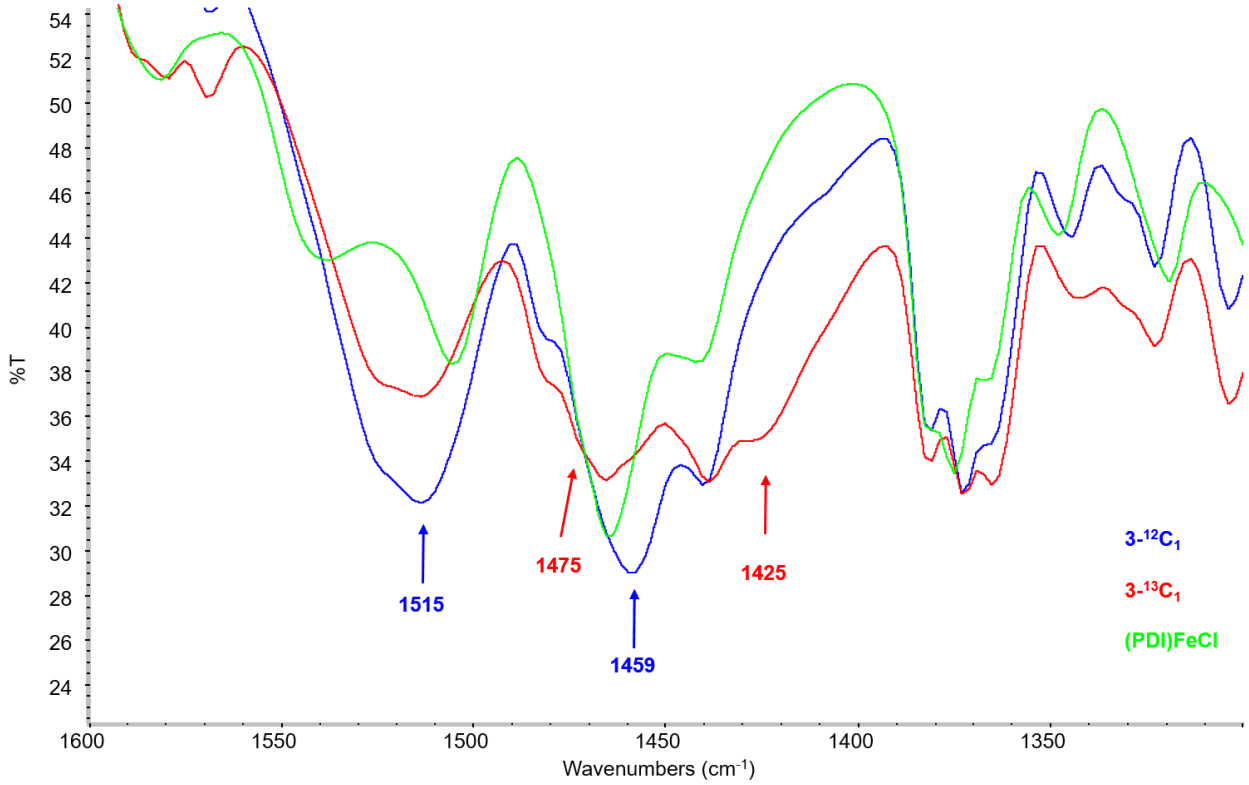

Figure 3.22. IR spectra of **3**, **3-$^{13}C_1$** and (PDI)FeCl in KBr pellet.

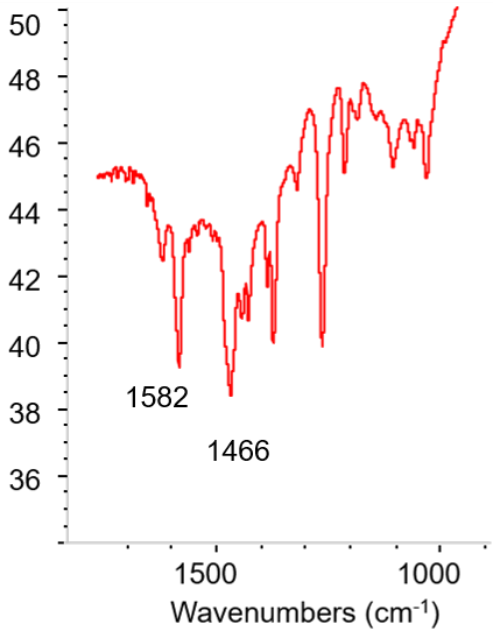

Figure 3.23. IR spectrum of **4** in KBr pellet.

Temperature-Dependent SQUID Magnetization Data

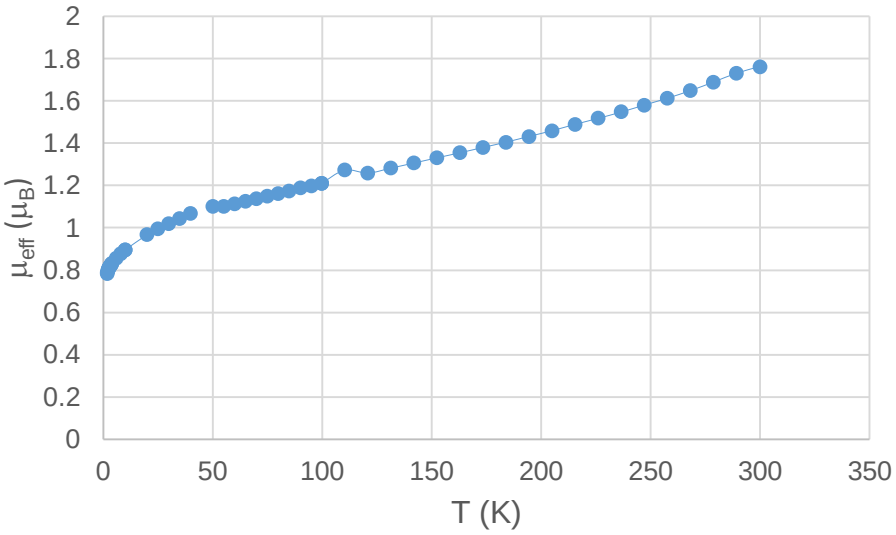

Figure 3.24. SQUID data of **1-PMe$_3$**.

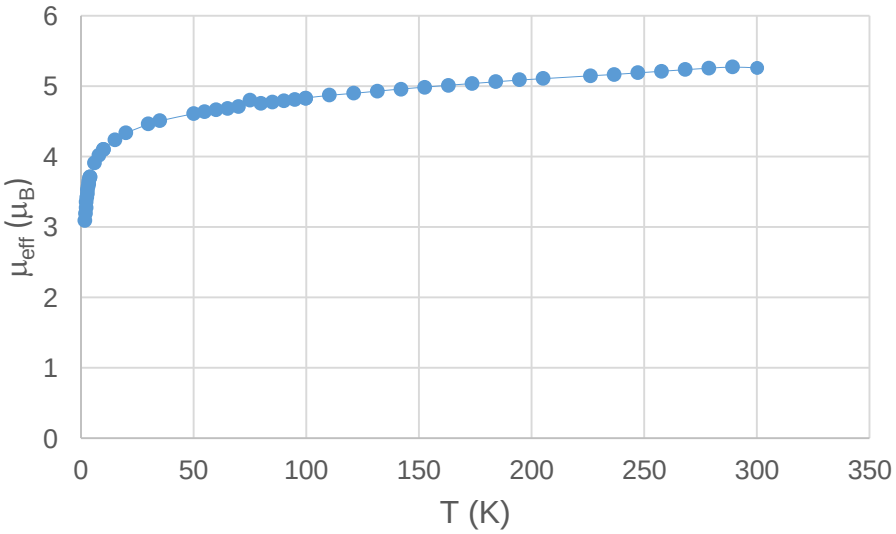

Figure 3.25. SQUID data of **4**.

3.5. References

1. Bouwkamp, M. W.; Bart, S. C.; Hawrelak, E. J.; Trovitch, R. J.; Lobkovsky, E.; Chirik, P. J. *Chem. Commun.* **2005**, 3406.

2. Tondreau, A. M.; Milsmann, C.; Patrick, A. D.; Hoyt, H. M.; Lobkovsky, E.; Wieghardt, K.; Chirik, P. J. *J. Am. Chem. Soc.* **2010**, 132, 15046.

3. (a) Tondreau, A. M.; Milsmann, C.; Lobkovsky, E.; Chirik, P. J. *Inorg. Chem.* **2011**, *50*, 9888. (b) Bart, S. C.; Chlopek, K.; Bill, E.; Bouwkamp, M. W.; Lobkovsky, E.; Neese, F.; Wieghardt, K.; Chirik, P. J. *J. Am. Chem. Soc.* **2006**, *128*, 13901.

4. Trovitch, R. J.; Lobkovsky, E.; Chirik, P. J. *J. Am. Chem. Soc.* **2008**, *130*, 11631.

5. (a) Slejko, F. L.; Drago, R. S.; Brown, D. G. *J. Am. Chem. Soc.* **1972**, *94*, 9210. (b) Rose, N. J.; Drago, R. S. *J. Am. Chem. Soc.* **1959**, *81*, 6138.

6. Trovitch, R. J.; Lobkovsky, E.; Bouwkamp, M. W.; Chirik, P. J. *Organometallics* **2008**, *27*, 6264.

7. Bouwkamp, M. W.; Lobkovsky, E; Chirik, P. J. *J. Am. Chem. Soc.* **2005**, *127*, 9660.

8. (a) Arafa, I. M.; Shin, K.; Goff, H. M. *J. Am. Chem. Soc.* **1988**, *110*, 5228. (b) Allen, O. R.; Dalgarno, S. J.; Field, L. D.; Jensen, P.; Turnbull, A. J.; Willis, A. C. *Organometallics* **2008**, *27*, 2092. (c) Roth, C. E.; Dibenedetto, A.; Aresta, M. *Eur. J. Inorg. Chem.* **2015**, *30*, 5066. (d) Allen, O. R.; Dalgarno, S. J.; Field, L. D.; Jensen, P.; Willis, A. C. *Organometallics* **2009**, *28*, 2385. (e) Darensbourg, D. J.; Kyran, S. J.; Yeung, A. D.; Bengali, A. A. *Eur. J. Inorg. Chem.* **2013**, 4024.

9. (a) Jolly, W. L. *The Synthesis and Characterization of Inorganic Compounds*; Prentice-Halls: Englewood Cliffs, NJ, 1970, p 487. (b) Jordan, R. F.; LaPointe, R. E.; Bajgur, C. S.; Echols, S. F.; Willett, R. *J. Am. Chem. Soc.* **1987**, *109*, 4111.

10. (a) Small, B. L.; Brookhart, M.; Bennet, A. M. A. *J. Am. Chem. Soc.* **1998**, *120*, 4049. (b) Britovsek, G. J. P.; Gibson, V. C.; Kimberley, B. S.; Maddox, P. J.; McTavish, S. J.; Solan, G. A.; White, A. J. P.; Williams, D. J. *Chem. Commun.* **1998**, 849.